

Anne Charlotte Wold

# Modified dolomite-based pellets synthesized by one-pot method for high-temperature CO<sub>2</sub> capture

February 2021





Norwegian University of  
Science and Technology

# Modified dolomite-based pellets synthesized by one-pot method for high- temperature CO<sub>2</sub> capture

**Anne Charlotte Wold**

Industriell kjemi og bioteknologi

Submission date: February 2021

Supervisor: De Chen

Co-supervisor: Kumar Ranjan Rout  
Ainara Moral

Norwegian University of Science and Technology  
Department of Chemical Engineering





# Preface

This thesis is written as the finish of a five-year integrated master's degree at the Norwegian University of Science and Technology (NTNU). The work has been done in the Catalysis group at the Department of Chemical Engineering to continue the specialization project written in spring 2020. The master is a part of the *Moving Bed Carbonate Looping (MBCL) Technology for Post-combustion CO<sub>2</sub> capture*. A project which is done in collaboration between Gassanova and NTNU.

First, I would like to thank my supervisor and co-supervisors for the project. Professor De Chen has regularly guided me through the project and has extensive knowledge. Also, Dr. Kumar Rout has supported me through the whole project. I am immensely grateful for the daily support of Dr. Ainara Moral Larrasoana. Her guidance has been impeccable.

Further, I would also like to thank the lab-engineers at the catalysis group for their outstanding effort in keeping it possible to perform close to normal work at the lab during the challenging period of COVID 19.

Last, I would like to thank my friends and family. The support and collaboration of my friends have been crucial, and my family's encouragement has been neverending.

I declare this as an independent work following the Norwegian University of Science and Technology exam regulations.



---

Anne Charlotte Wold  
12.02.2021  
Trondheim, Norway

# Abstract

The release of CO<sub>2</sub> by human activity into the atmosphere is one of the main challenges the world is facing today. This master thesis is a part of a project where a Moving Bed Carbonate Looping (MBCL) technology has been developed. In the technology, CaO-based sorbents are used to capture CO<sub>2</sub> at high temperatures. While circulating between two reactors, the sorbents are continuously exposed to cyclic carbonation-regeneration and should, therefore, stay stable for a long time.

Previous research has found dolomite (CaCO<sub>3</sub>·MgCO<sub>3</sub>) to be a good choice as a CaO-based sorbent. However, the sorbents suffer from deactivation through cycles, mainly attributed to sintering and attrition. Pellets with mechanical strength should be made to reduce attrition, and for this, a suitable binder is required. Sintering can be reduced using a stabilizer. Based on earlier research, the main objective of this project was to find the optimal combination of two additives; ZrO<sub>2</sub> or CeO<sub>2</sub> expected to work as a stabilizer, and cement to work as both a stabilizer and a binder.

Furthermore, it was intended to prepare sorbents for an easy industrial-scale up the "one-pot method" was applied - hence mixing everything at once. However, adding the additives was explored in two different sequences: mixing all compounds at once (one-step method) or adding cement after impregnation (two-step method). It was found that preparing the sorbents by the two-step method gave higher capturing capacity and slightly better stability. This was attributed to the better dispersion of ZrO<sub>2</sub>, detected from Energy Dispersive X-ray Spectroscopy.

The sorbents cyclic stability was tested in both dry and wet conditions in Thermogravimetric analyzers. Wet conditions refer to steam present during the carbonation. In addition, a higher temperature and partial pressure of CO<sub>2</sub> were applied - conditions closer to reality. Also, two sorbents were tested in a microbalance fixed bed reactor - where it is possible to test in even more realistic conditions. The modified sorbents were able to keep stable over several cycles in all the set-ups.

It was found that a higher amount of both cement and ZrO<sub>2</sub> reduced the capturing capacity but increased the stability. This was attributed to the formation of the two stabilizing phases CaZrO<sub>3</sub> and Ca<sub>12</sub>Al<sub>14</sub>O<sub>33</sub>. CeO<sub>2</sub> did not improve the stability of the sorbents in the studied conditions. The best sorbent was found to be 2S(5.5Zr,10Al), consisting of 5.5 wt % Zirconium and 10 wt % Aluminium from cement. The sorbent had a capacity loss of 15.7 % from cycle 3-60 in wet conditions.

Sorbents were characterized through X-ray diffraction (XRD), Scanning electron microscopy (SEM), and Nitrogen-adsorption desorption, both before and after testing the cyclic stability. No significant changes were observed through XRD. In the two other techniques, small changes in the pore-structure were revealed, which was attributed to being due to sintering. It was found that, in order to reduce the deactivation of the sorbents further, the pore-

structure of the sorbents should be improved.

## Sammendrag

Utslipp av CO<sub>2</sub> grunnet menneskelig aktivitet er en av de største utfordringene verden står ovenfor i dag. Denne masteroppgaven er en del av et prosjekt hvor en MBCL (Moving Bed Carbonate Looping)-reaktor har blitt utviklet. I teknologien brukes CaO-baserte sorbenter til å fange CO<sub>2</sub> ved høy temperaturer. Sorbentene sirkulerer mellom to reaktorer hvor de er kontinuerlig utsatt for sykluser av karbonatisering og regenerering, og bør derfor klare å holde seg stabile over lengre tid

Tidligere forskning har funnet dolomitt (CaCO<sub>3</sub>·MgCO<sub>3</sub>) til å være et godt valg av sorbent. Desverre blir dolomitt utsatt for deaktivering etter sykluser. Dette skyldes i hovedsak sintering og slitasje av materialet. Grunnet slitasje, bør det lages pellets med god mekanisk styrke – dette kan oppnås ved å bruke et bindemiddel. Sintering kan bli redusert ved å bruke en stabilisator. ZrO<sub>2</sub>, CeO<sub>2</sub> og sement har i tidligere forskning vist seg å være et godt valg for å forbedre CaO-baserte sorbenter. Hovedformålet med denne oppgaven vært å finne den optimale kombinasjonen av dolomitt, stabilisator og bindemiddel. Både ZrO<sub>2</sub> og CeO<sub>2</sub> har blitt testet som stabilisator. Sement har blitt tilsatt med hensikt å virke som både stabilisator og bindemiddel.

Videre var det ønskelig å lage sorbenter som det vil være lett for industrien å produsere. For å oppnå dette ble «one-pot»-metoden brukt. I motsetning til typiske syntetiseringsmetoder var det ingen kalsinering mellom tilsetning av de forskjellige stoffene til dolomitt. Tilsetninger av stoffer ble undersøkt på to ulike måter; enten var alle stoffene blandet samtidig (et-steps metoden) eller så var sement tilsatt etter impregnering (to-steps metoden). Det ble funnet at sorbenter laget med to-steps metoden klarte å fange mer CO<sub>2</sub> og ga en noe bedre stabilitet. Trolig var dette grunnet bedre spredning av ZrO<sub>2</sub> i sorbenten, som ble oppdaget gjennom kartlegging av elementer.

Den sykliske stabiliteten til sorbentene var testet både i våte og tørre reaksjonsbetingelser i termogravimetrisk analysatorer. Våte reaksjonsbetingelser vil si at det er vanddamp til stedet i karboneringen. I disse betingelsene var det også høyere temperatur og partialtrykk av CO<sub>2</sub>-betingelser mer likt de som er i reelle prosesser. I tillegg var to sorbenter testet i en «microbalance fixed bed»-reaktor, hvor enda mer reelle reaksjonsbetingelser er mulig. De modifiserte sorbentene klarte å holde seg stabile gjennom flere sykluser under alle betingelsene.

Det ble funnet at en økt mengde av både sement og ZrO<sub>2</sub> reduserte kapasiteten til å fange CO<sub>2</sub>, men økte stabiliteten. Dette ble begrunnet med formasjonen av to stabiliserende faser; CaZrO<sub>3</sub> og Ca<sub>12</sub>Al<sub>14</sub>O<sub>33</sub>. CeO<sub>2</sub> påvirket ikke stabiliteten i de testede reaksjonsbetingelsene. Den beste sorbenten ble funnet til å være 2Sa(5.5Zr,10Al), som besto av 5.5 wt% Zirkonium og 10 wt% Aluminium fra sement. Sorbenten hadde et kapasitetstap på 15.7 % fra syklus 3-60 i våte reaksjonsbetingelser.

Sorbentene var karakterisert gjennom X-ray diffraksjon (XRD), Skanning elektron mikroskopi

(SEM) og Nitrogen adsorpsjon-desorpsjon, både før og etter syklisk testing. Ingen merkbare forskjeller ble funnet gjennom XRD. Derimot ble det observert en liten forskjell i porestrukturen gjennom de to andre teknikkene. Dette var trolig grunnet en hvis grad av sintering. Det ble funnet at for å videre redusere deaktiveringen i sorbentene, bør porestrukturen forbedres.

# Contents

|  |           |
|--|-----------|
| Preface  | i         |
| Abstract   | ii        |
| Sammendrag                                       | iv        |
| List of abbreviations                            | xvi       |
| Glossary   | xvii      |
| <b>1 Introduction</b>                            | <b>1</b>  |
| 1.1 Ca-looping . . . . .                         | 2         |
| 1.2 Moving Bed Carbonate Looping . . . . .       | 4         |
| 1.3 The Carbonation reaction . . . . .           | 6         |
| 1.4 CaO as a sorbent . . . . .                   | 7         |
| 1.4.1 Dolomite . . . . .                         | 9         |
| 1.4.2 Stabilizers to improve stability . . . . . | 10        |
| 1.4.3 Calcium Aluminate Cement . . . . .         | 12        |
| 1.4.4 The pore structure . . . . .               | 13        |
| 1.4.5 Synthesis method . . . . .                 | 15        |
| 1.5 Experimental conditions . . . . .            | 16        |
| 1.5.1 Presence of steam . . . . .                | 16        |
| <b>2 Objective</b>                               | <b>19</b> |
| <b>3 Experimental Techniques</b>                 | <b>20</b> |
| 3.1 Synthesis by the one-pot method . . . . .    | 20        |
| 3.2 Testing cyclic performance . . . . .         | 21        |
| 3.2.1 Thermogravimetric Analysis (TGA) . . . . . | 21        |
| 3.2.2 Instrumental Limitations . . . . .         | 22        |

|          |  |           |
|----------|--|-----------|
| 3.2.3    | Microbalance Fixed Bed Reactor . . . . .                 | 23        |
| 3.3      | Characterization . . . . .                               | 25        |
| 3.3.1    | X-ray Fluorescence (XRF) . . . . .                       | 25        |
| 3.3.2    | X-ray Diffraction (XRD) . . . . .                        | 25        |
| 3.3.3    | Nitrogen Adsorption-Desorption at 77 K . . . . .         | 26        |
| 3.3.4    | Electron Microscopy . . . . .                            | 29        |
| <b>4</b> | <b>Experimental Procedure</b>                            | <b>31</b> |
| 4.1      | Synthesis of the sorbent by the one-pot method . . . . . | 31        |
| 4.1.1    | Material preparation . . . . .                           | 31        |
| 4.1.2    | One-pot process . . . . .                                | 31        |
| 4.1.3    | Calcination conditions . . . . .                         | 34        |
| 4.2      | Testing of cyclic performance . . . . .                  | 35        |
| 4.2.1    | TGA TA . . . . .   | 36        |
| 4.2.2    | TGA Linseis . . . . .                                    | 37        |
| 4.2.3    | Microbalance Fixed Bed Reactor . . . . .                 | 38        |
| 4.3      | Characterization . . . . .                               | 39        |
| 4.3.1    | X-Ray Fluorescence Spectroscopy (XRF) . . . . .          | 39        |
| 4.3.2    | X-ray Diffraction (XRD) . . . . .                        | 39        |
| 4.3.3    | Nitrogen Adsorption-Desorption at 77 K . . . . .         | 39        |
| 4.3.4    | Scanning Electron Microscopy (SEM) . . . . .             | 40        |
| 4.3.5    | Energy Dispersive X-ray Spectroscopy (EDS) . . . . .     | 40        |
| <b>5</b> | <b>Results and Discussion</b>                            | <b>41</b> |
| 5.1      | Cyclic testing . . . . .                                 | 41        |
| 5.1.1    | Dry conditions . . . . .                                 | 41        |
| 5.1.2    | Wet conditions . . . . .                                 | 47        |
| 5.2      | Characterization . . . . .                               | 65        |
| 5.2.1    | X-Ray Fluorescence Spectroscopy (XRF) . . . . .          | 65        |
| 5.2.2    | X-Ray Diffraction (XRD) . . . . .                        | 66        |

|          |  |            |
|----------|--|------------|
| 5.2.3    | Nitrogen Adsorption-Desorption at 77 K . . . . .     | 77         |
| 5.2.4    | Scanning Electron Microscopy (SEM) . . . . .         | 84         |
| 5.2.5    | Energy Dispersive X-ray Spectroscopy (EDS) . . . . . | 89         |
| <b>6</b> | <b>Conclusion</b>                                    | <b>98</b>  |
| <b>7</b> | <b>Future Work</b>                                   | <b>100</b> |
|          | <b>Appendices</b>                                    | <b>112</b> |
| <b>A</b> | <b>Composition calculation</b>                       | <b>112</b> |
| <b>B</b> | <b>Incipient Wetness method</b>                      | <b>114</b> |
| <b>C</b> | <b>XRF calculation</b>                               | <b>115</b> |
| <b>D</b> | <b>XRD</b>   | <b>117</b> |
| <b>E</b> | <b>Nitrogen Adsorption-Desorption</b>                | <b>121</b> |
| <b>F</b> | <b>Matlab codes for calculating capacity</b>         | <b>138</b> |
| F.1      | Capacities TGA TA . . . . .                          | 138        |
| F.2      | Capacities TGA Linseis . . . . .                     | 143        |



# List of Tables

|     |  |    |
|-----|--|----|
| 1.1 | List of the lines used in the process flow diagram shown in figure 3.3. . . . .  | 5  |
| 1.2 | Tamann temperature and melting temperature of different compounds [36, 41]   | 8  |
| 1.3 | Research where the formation of $\text{CaZrO}_3$ led to increased stability. All experiments performed in TGA. . . . .   | 11 |
| 1.4 | Research where incorporation of $\text{CeO}_2$ to CaO-based sorbents led to increased cyclic behavior. All experiments performed in TGA. . . . .   | 12 |
| 1.5 | Overview over reserach where calcium aluminate cement was used as support for CaO-based sorbents. All experiments performed in TGA. . . . .  | 13 |
| 1.6 | Different preparation-methods, capacity and cost for CaO-based sorbents [77].  | 15 |
| 1.7 | Experiments with steam present during the carbonation [78, 80]. . . . .  | 18 |
| 4.1 | The weight percentages (wt%) of Zirconium, Cerium and Aluminium in the sorbents and the method used to create them. . . . .  | 34 |
| 5.1 | The capacity in different cycles ( $c_i$ ), and capacity loss ( $c_{i-j}$ ) for ZrAl-based sorbents. Calcined dolomite is included for comparison. Ads: 5% $\text{CO}_2$ , 600°C, 30 min. Des: % $\text{N}_2$ , 900°C . . . . .  | 44 |
| 5.2 | The capacity in different cycles ( $c_i$ ) and capacity loss ( $c_{i-j}$ ) for 2S(5.5Zr,10Al) as pellets (500-850 $\mu\text{m}$ ) and crushed. Ads: 5 % $\text{CO}_2$ , 600 °C, 30 min. Des: % $\text{N}_2$ , 900 °C . . . . .   | 45 |
| 5.3 | The capacity in different cycles ( $c_i$ ) and capacity loss ( $c_{i-j}$ ) for identical pairs of ZrAl-based sorbents prepaered in two batches. Ads: 5 % $\text{CO}_2$ , 600 °C, 30 min. Des: $\text{N}_2$ , 900 °C . . . . .  | 47 |
| 5.4 | The capacity in different cycles ( $c_i$ ), and capacity loss ( $c_{i-j}$ ) for a selection of ZrAl-based sorbents and calacined dolomite in wet and dry conditions. Dry conditions: Ads: 5 % $\text{CO}_2$ , 600 °C, 30 min. Des: % $\text{N}_2$ , 900 °C. Wet conditions: Ads: 5 % $\text{CO}_2$ , 8 % $\text{H}_2\text{O}$ , 600 °C, 30 min. Des: 80 % $\text{CO}_2$ , 950 °C | 48 |
| 5.5 | The capacity in different cycles ( $c_i$ ) and capacity loss ( $c_{i-j}$ ) for sorbents modified with cement and $\text{ZrO}_2$ . Calcined dolomite is included for comparison. Ads: 5 % $\text{CO}_2$ , 8 % $\text{H}_2\text{O}$ , 600 °C, 30 min. Des: 80 % $\text{CO}_2$ , 950 °C . . . . .   | 50 |
| 5.6 | The capacity in different cycles ( $c_i$ ) and capacity loss ( $c_{i-j}$ ) for ZrAl-based sorbents prepared in by the two-step method. Calcined dolomite is included for comparison. Ads: 5 % $\text{CO}_2$ , 8 % $\text{H}_2\text{O}$ , 600 °C, 30 min. Des: 80 % $\text{CO}_2$ , 950 °C . . . . .  | 52 |

|      |  |    |
|------|--|----|
| 5.7  | Comparison of one-step method vs. two step method for ZrAl-based sorbents. The capacity in different cycles ( $c_i$ ) and capacity loss ( $c_{i-j}$ ) are presented Ads: 5 % CO <sub>2</sub> , 8 % H <sub>2</sub> O, 600 °C, 30 min. Des: 80 % CO <sub>2</sub> , 950 °C . . . . .                        | 54 |
| 5.8  | The capacity in different cycles ( $c_i$ ) and capacity loss ( $c_{i-j}$ ) Sa(5.5Zr,10Al), 2Sa(5.5Zr,10Al), 1Sa(5.Ce,10Al), 2Sa(5.5Ce,10Al), 15Al, 11Al and calcined dolomite. Ads: 5 % CO <sub>2</sub> , 8 % H <sub>2</sub> O, 600 °C, 30 min. Des: 80 % CO <sub>2</sub> , 950 °C.                      | 57 |
| 5.9  | The capacity in different cycles ( $c_i$ ) and capacity loss ( $c_{i-j}$ ) for 2SInter(5.5Zr,10Al) and(2Sa(5.5Zr,10Al). Ads: 5 % CO <sub>2</sub> , 600 °C, 30 min. Des: 100 % N <sub>2</sub> , 900 °C  | 60 |
| 5.10 | The capacity in different cycles ( $c_i$ ) and capacity loss ( $c_{i-j}$ ) for 1Sa(5.5Zr,10Al) and 2Sa(5.5Zr,10Al). Total cycles: 60. Ads: 5 % CO <sub>2</sub> , 8 % H <sub>2</sub> O, 600 °C, 30 min. Des: 80 % CO <sub>2</sub> , 950 °C . . . . .  | 61 |
| 5.11 | The maximum theoretical capacity, capacity in different cycles ( $c_i$ ) and capacity loss ( $c_{i-j}$ ) for the best sorbents modified with cement and ZrO <sub>2</sub> . Total cycles: 60. Ads: 5 % CO <sub>2</sub> , 8 % H <sub>2</sub> O, 600 °C, 6 min. Des: 100 % CO <sub>2</sub> , 950 °C         | 64 |
| 5.12 | Composition of oxides obtained through XRF for Cement Fondu, calcined dolomite, 1Sa(5.5Zr,10Al) and 2Sa(5.5Zr,10Al) compared to their theoretical value. For Cement Fondu the specification ranges are included. . . . .   | 65 |
| 5.13 | Crystal sizes (CS) of CaO at $2\theta \approx 37^\circ$ found from the Scherrer equation (3.2).  | 72 |
| 5.14 | Crystal sizes (CS) of CaO at $2\theta \approx 37^\circ$ found from the Scherrer equation (3.2). Sizes presented are for sorbents prepared without ZrO <sub>2</sub> compared to the best ZrAl-based sorbents and calcined dolomite. . . . .   | 74 |
| 5.15 | Crystal sizes (CS) of CaO at $2\theta \approx 37^\circ$ found from the Scherrer equation (3.2) for calcined dolomite, 1Sa(5.5Zr,10Al), 2Sa(5.5Zr,10Al), 1SUncalc(5.5Zr,10Al) and 2SInter(5.5Zr,10Al). . . . .  | 75 |
| 5.16 | The crystal sizes of CaO and MgO for fresh and spent sorbents compared to calcined dolomite. Experiments spent (TGA / microbalance reactor*) : (Ads: 5 % CO <sub>2</sub> , 8 % H <sub>2</sub> O, 600 °C, 6 / 30min. Des: 80 / 100 % CO <sub>2</sub> , 950 °C) . . .                                      | 77 |
| 5.17 | BET surface area ( $S_{BET}$ ) for a selection of fresh sorbents compared to calcined dolomite. Obtained from Nitrogen adsorption-desorption at 77 K. . . . .  | 79 |
| 5.18 | BET surface area ( $S_{BET}$ ) of 2Sa(5.5Zr,10Al), 1SUncalc(5.5Zr,10Al), 2Sinter(5.5Zr,10Al). Obtained from Nitrogen adsorption-desorption at 77 K. . . .  | 82 |
| 5.19 | The Surface area ( $S_{BET}$ ) of 1Sa(5.5Zr,10Al): fresh, spent spent after 3 cycles and spent after 20 cycles in the microbalance reactor. (Ads: 5 % CO <sub>2</sub> , 8 % H <sub>2</sub> O, 600 °C, 6 min. Des: 100 % CO <sub>2</sub> .) Obtained from Nitrogen adsorption-desorption at 77 K. . . . . | 83 |

- A.1 Unknown values needed in order to find the right amount of precursor for a sorbent consisting of 11.5g dolomite with 13.4 wt % of Al and 1.3wt % Zr. . . 113
- D.1 Crystal sizes (CS) of CaO, MgO and the stabilizing phase (CaZrO<sub>3</sub> or (CeO<sub>2</sub>)). 119
- D.2 The crystal sizes of CaO and MgO for fresh and spent sorbents compared to calcined dolomite. Experiments spent (TGA / microbalance reactor\*) : (Ads: 5 % CO<sub>2</sub>, 8 % H<sub>2</sub>O, 600 °C, 6 / 30min. Des: 80 / 100 % CO<sub>2</sub>, 950 °C) . . . 120

# List of Figures

|     |   |    |
|-----|---|----|
| 1.1 | Ca-looping for Post combustion CO <sub>2</sub> -capture. . . . .  | 3  |
| 1.2 | The equilibrium pressure of CO <sub>2</sub> vs temperature [20]. . . . .  | 4  |
| 1.3 | Process flow diagram for the MBCL-technology [22]. . . . .  | 5  |
| 1.4 | Conversion of CaO from the reaction controlled (1) to the diffusional controlled (2) regime [24] . . . . .  | 6  |
| 1.5 | Sintering during cycles of a CaO-based sorbent. dark grey: CaCO <sub>3</sub> , light grey: CaO [40]. . . . .  | 7  |
| 1.6 | CaO particles before and during sintering (a) and prevention of sintering by inert metal oxides (b). . . . .  | 9  |
| 1.7 | Pore-size distribution of a CaO based particle, before and after cycles. (Calcination 100 % N <sub>2</sub> , 850 °C . Carbonation 100 % CO <sub>2</sub> , 850 °C) [71] . . . . .  | 14 |
| 2.1 | The ideal sorbent distribution. . . . .   | 19 |
| 3.1 | Typical sorbent preparation (a) compared to the one-pot processing (b). . .   | 21 |
| 3.2 | The direction of gas flow on the samples [93]. . . . .  | 23 |
| 3.3 | Schematics of the fixed-bed microbalance reactor [22]. . . . .  | 24 |
| 3.4 | Illustration of the stainless steel reactor [22]. . . . .   | 24 |
| 3.5 | Diffraction fulfilling Braggs Law [95]. . . . .   | 25 |
| 3.6 | Adsorption-desorption isotherms [96]. . . . .   | 27 |
| 3.7 | The figure shows the most common processes happening in electronmicroscopy.   | 29 |
| 4.1 | Illustration of the preparation of a two step sorbent with ZrO <sub>2</sub> as the stabilizer.  | 32 |
| 4.2 | Calcination procedure for all the sorbents. . . . .   | 35 |
| 4.3 | The setup of the different instruments used to test the cyclic performance of the sorbents [22, 99] . . . . .   | 36 |
| 4.4 | Simplified scheme of the Program used in TGA Linseis. . . . .   | 38 |
| 5.1 | The capturing capacity of calcined dolomite and all ZrAl-based sorbents tested in dry conditions (1S(1.3Zr,13Al), 1S(2.6Zr,13Al), 1S(3.8Zr,13Al), 1Sb(5.0Zr,13Al), 1Sa(5.5Zr,10Al), 1Sa(1.5Zr,10Al), 1Sa(1.8Zr,6Al), 2Sa(1.3Zr,13Al), 2Sa(5.5Zr,10Al)). Ads: 5 % CO <sub>2</sub> , 600 °C, 30 min. Des: N <sub>2</sub> , 900 °C . . . . . | 43 |

|      |   |    |
|------|---|----|
| 5.2  | Comparison of the capturing capacity in cycle 3 for similar sorbents varying the Al (a) or Zr (b) content. (1S(1.8Zr,6Al), 1S(5.5Zr,10Al), 1S(1.3Zr,13Al). 1S(2.6Zr,13Al), 1S(3.8Zr,13Al), 1S(5.0Zr,13Al) Ads: 5 % CO <sub>2</sub> , 600 °C, 30 min. Des: N <sub>2</sub> , 900 °C . . . . .                     | 44 |
| 5.3  | The capturing capacity of 2S(5.5Zr,10Al) as pellets (500-850 μm) and crushed. Ads: 5 % CO <sub>2</sub> , 600 °C, 30 min. Des: N <sub>2</sub> , 900 °C . . . . .   | 45 |
| 5.4  | Comparing the capturing capacity of identical sorbents prepared in two batches. (1Sa(5.0Zr,13Al), 1Sb(5.0Zr,13Al), 1Sa(5.5Zr,10Al), 1Sb(5.5Zr,10Al), 2Sa(1.3Zr,13Al), 2Sb(1.3Zr,13Al), 2Sa(5.5Zr,10Al), 2Sb(5.5Zr,10Al)) Ads: 5 % CO <sub>2</sub> , 600 °C, 30 min. Des: N <sub>2</sub> , 900 °C . . . . .      | 46 |
| 5.5  | The capturing capacity of calcined dolomite and all the ZrAl-based sorbents prepared in one step. (1S(2.6Zr,10Al), 1S(3.8Zr,10Al), 1Sb(5.0Zr,13Al), 1S(5.5Zr,10Al), 1S(6.0Zr,9Al), 1S(1.8Zr,6Al)) Ads: 5 % CO <sub>2</sub> , 8 % H <sub>2</sub> O, 600 °C, 30 min. Des: 80 % CO <sub>2</sub> , 950 °C . . . . . | 50 |
| 5.6  | The capturing capacity of calcined dolomite and ZrAl-based sorbents prepared by the two step method. (2S(2.6Zr,10Al), 2Sa(5.0Zr,13Al), 2Sa(5.5Zr,10Al), 2S(6.0Zr,9Al)) Ads: 5 % CO <sub>2</sub> , 8 % H <sub>2</sub> O, 600 °C, 30 min. Des: 80 % CO <sub>2</sub> , 950 °C . . . . .                            | 51 |
| 5.7  | Comparison of the cyclic capacity of one step method vs. two-step method for different compositions of Aluminium and Zirconium . Ads: 5 % CO <sub>2</sub> , 8 % H <sub>2</sub> O, 600 °C, 30 min. Des: 80 % CO <sub>2</sub> , 950 °C . . . . .  | 53 |
| 5.8  | Comparison of the capacity loss of one-step method vs. two-step method for different compositions of Aluminium and Zirconium . Ads: 5 % CO <sub>2</sub> , 8 % H <sub>2</sub> O, 600 °C, 30 min. Des: 80 % CO <sub>2</sub> , 950 °C . . . . .  | 54 |
| 5.9  | The capturing capacity of 1Sa(5.5Zr,10Al), 2Sa(5.5Zr,10Al), 1Sa(5.Ce,10Al), 2Sa(5.5Ce,10Al), 11Al, 15Al and calcined dolomite. Ads: 5 % CO <sub>2</sub> , 8 % H <sub>2</sub> O, 600 °C, 30 min. Des: 80 % CO <sub>2</sub> , 950 °C. . . . .   | 56 |
| 5.10 | The capacity loss of 1Sa(5.5Zr,10Al), 2Sa(5.5Zr,10Al), 1S(5.Ce,10Al), 2S(5.5Ce,10Al) and 11Al. Ads: 5 % CO <sub>2</sub> , 8 % H <sub>2</sub> O, 600 °C, 30 min. Des: 80 % CO <sub>2</sub> , 950 °C  | 57 |
| 5.11 | Repeatability of 2Sa(5.5Zr,10Al). Ads: 5 % CO <sub>2</sub> , 8 % H <sub>2</sub> O 600 °C, 30 min. Des: 80 % CO <sub>2</sub> , 950 °C . . . . .  | 58 |
| 5.12 | Capturing capacity of 2SInter(5.5Zr,10Al) and 2Sa(5.5Zr,10Al). Ads: 5 % CO <sub>2</sub> , 600 °C, 30 min. Des: N <sub>2</sub> , 900 °C . . . . .  | 59 |
| 5.13 | The capturing capacity of 1Sa(5.5Zr,10Al) and 2Sa(5.5Zr,10Al) during 60 regeneration-cycles. Ads: 5 % CO <sub>2</sub> , 8 % H <sub>2</sub> O, 600 °C, 30 min. Des: 80 % CO <sub>2</sub> , 950 °C . . . . .  | 61 |

|      |  |    |
|------|--|----|
| 5.14 | Bar plots showing the capacity loss between different cycles for 1Sa(5.5Zr,10Al) and 2Sa(5.5Zr,10Al). Ads: 5 % CO <sub>2</sub> , 8 % H <sub>2</sub> O, 600 °C, 30 min. Des: 80 % CO <sub>2</sub> , 950 °C. . . . .   | 62 |
| 5.15 | Comparison of the increase in capacities vs. time for 1Sa(5.5Zr,10Al) and 2Sa(5.5Zr,10Al). Ads: 5 % CO <sub>2</sub> , 8 % H <sub>2</sub> O, 600 °C, 30 min. Des: 80 % CO <sub>2</sub> , 950 °C. . . . .  | 63 |
| 5.16 | The capturing capacity of 1Sa(5.5Zr,10Al) and 2Sa(5.5Zr,10Al) during 40 regeneration-cycles tested in the microbalance-reactor. Ads: 5 % CO <sub>2</sub> , 8 % H <sub>2</sub> O, 600 °C, 6min. Des: 100 % CO <sub>2</sub> , 950 °C . . . . .               | 64 |
| 5.17 | Diffraction diagram of calcined dolomite and dried cement. In $2\theta$ range from 15° to 75°. . . . .   | 67 |
| 5.18 | Diffraction diagram of different steps until the calcination of 2S(6.0Zr, 9Al). In $2\theta$ range from 15° to 75°. . . . .  | 68 |
| 5.19 | Diffraction diagram of 1S(5.0Zr,13Al), 1S(3.8Zr,13Al) and 1S(1.3Zr,13Al). In $2\theta$ range from 15° to 75°. . . . .  | 69 |
| 5.20 | Diffraction diagram of 1S(1.8Zr,6Al), 1S(1.5Zr,10Al) and 1S(1.3Zr,13Al). In $2\theta$ range from 15° to 75°. . . . .   | 70 |
| 5.21 | Diffraction diagram comparing one-step and two-step sorbents. In $2\theta$ range from 15° to 75°. . . . .  | 71 |
| 5.22 | Diffraction diagram of 15Al, 11Al, 2S(5.5Ce,10Al) and 1S(5.5Ce,10Al). In $2\theta$ range from 15° to 75°. . . . .  | 73 |
| 5.23 | Diffraction diagram of 1Sa(5.5Zr,10Al), 2SInter(5.5Zr,10Al) and 1SUncalc(5.5Zr,10Al). In $2\theta$ range from 15° to 75°. . . . .  | 74 |
| 5.24 | Diffraction diagram of fresh and spent 1Sa(5.5Zr,10Al) and 2Sa(5.5Zr,10Al). In $2\theta$ range from 15° to 75°. Experiments spent: (Ads: 5 % CO <sub>2</sub> , 8 % H <sub>2</sub> O, 600 °C, 6min. Des: 100 % CO <sub>2</sub> , 950 °C) . . . . .          | 76 |
| 5.25 | The adsorption-desorption isotherm of 2Sa(5.5Zr,10Al) obtained from Nitrogen adsorption-desorption at 77 K. . . . .  | 78 |
| 5.26 | Pore volume distribution of calcined dolomite, 1Sa(5.5Zr,10Al) and 2Sa(5.5Zr,10Al) found from the desorption . . . . .   | 80 |
| 5.27 | Pore volume distribution of 2Sa(5.5Zr,10Al), 2SInter(5.5Zr,10Al) and 1SUncalc(5.5Zr,10Al) found from the desorption. . . . .   | 81 |
| 5.28 | Pore volume distribution of 1Sa(5.5Zr,10Al) found from the desorption; fresh, spent after 3 cycles and spent after 20 cycles in the microbalance reactor. Ads: 5% CO <sub>2</sub> , 8% H <sub>2</sub> O, 600°C, 6 min. Des: 100% CO <sub>2</sub> . . . . . | 83 |

|      |  |     |
|------|--|-----|
| 5.29 | SEM pictures of a selection of fresh samples: 1Sa(5.5Zr,10Al), 2Sa(5.5Zr,10Al), 1S(1.8Zr,6Al), 2SInter(5.5Zr,10Al). Magnification: 65.000 for 1Sa(5.5Zr,10Al), 50.000 for the rest. . . . .  | 85  |
| 5.30 | SEM pictures of 1S(5.5Zr,10Al) at 5000 Magnification. Microbalance conditions: Ads: 5 % CO <sub>2</sub> , 8 % H <sub>2</sub> O, 600 °C, 6min. Des: 100 % CO <sub>2</sub> , 950 °C . . .  | 86  |
| 5.31 | SEM pictures of fresh and spent 1Sa(5.5Zr,10Al). Fresh and 20 cycles at 65.000 magnification. 40 cycles at 50.000 Magnification. Experimental conditions: Ads: 5 % CO <sub>2</sub> , 8 % H <sub>2</sub> O, 600 °C, 6min. Des: 100 % CO <sub>2</sub> , 950 °C . . . . . | 88  |
| 5.32 | SEM pictures of fresh and spent 2Sa(5.5Zr,10Al) at 50.000 magnification. Experimental conditions: Ads: 5 % CO <sub>2</sub> , 8 % H <sub>2</sub> O, 600 °C, 6min. Des: 100 % CO <sub>2</sub> , 950 °C . . . . .   | 88  |
| 5.33 | EDS mapping of calcined dolomite at magnification 3000. . . . .  | 89  |
| 5.34 | EDS mapping of cement Fondu at magnification 3000. . . . .   | 90  |
| 5.35 | Illustration of an ideal sorbent distribution compared to a distribution close to the real sorbent distribution. . . . .   | 92  |
| 5.36 | EDS mapping of 1S(5.5Zr,10Al) fresh at magnification 3000. . . . .   | 93  |
| 5.37 | EDS mapping of 2S(5.5Zr,10Al) fresh at magnification 3000. . . . .   | 94  |
| 5.38 | EDS mapping of 2SInter(5.5Zr,10Al) fresh at magnification 3000. Experimental conditions: (Ads: 5 % CO <sub>2</sub> , 8 % H <sub>2</sub> O, 600 °C, 6 min. Des: 100 % CO <sub>2</sub> , 950 °C) . . . . .   | 95  |
| 5.39 | EDS mapping off 1S(5.5Zr,10Al) after 20 regeneration-cycles at magnification 3000 ≈ 10 mm. Experimental conditions: (Ads: 5 % CO <sub>2</sub> , 8 % H <sub>2</sub> O, 600 °C, 6 min. Des: 100 % CO <sub>2</sub> , 950 °C) . . . . .                                    | 96  |
| 5.40 | EDS mapping of 2Sa(5.5Zr,10Al) after 40 regeneration-cycles at magnification 3000. Experimental conditions: (Ads: 5 % CO <sub>2</sub> , 8 % H <sub>2</sub> O, 600 °C, 6 min. Des: 100 % CO <sub>2</sub> , 950 °C) . . . . .  | 97  |
| D.1  | Crystal phases of a selection of fresh vs. spent sorbent. In 2θ range from 15° to 75°. . . . .   | 117 |
| D.2  | Crystal pattern obtained from the software DIFFRA.EVA v5.1 . . . . .   | 118 |
| E.1  | Some obtained hysteresis loops. . . . .  | 121 |

## List of abbreviations

|               |   |
|---------------|---|
| <b>IPCC</b>   | Intergovernmental Panel on Climate Change |
| <b>CCS</b>    | Carbon Capture and Storage                |
| <b>PCCC</b>   | Post-Combustion CO <sub>2</sub> Capture   |
| <b>NGCC</b>   | Natural Gas Combined Cycles               |
| <b>MEA</b>    | Monoethanolamine                          |
| <b>MBCL</b>   | Moving Bed Carbonate Looping              |
| <b>HRS</b>    | Heat Recovery Steam Generator             |
| <b>CAC</b>    | Calcium Aluminate Cements                 |
| <b>TGA</b>    | Thermogravimetric Analyzer                |
| <b>FBR</b>    | Fluidized Bed Reactor                     |
| <b>HP TGA</b> | High Pressure Thermogravimetric Analyzer  |
| <b>BFB</b>    | Bubbling Fluidized Bed                    |
| <b>MFC</b>    | Mass Flow Controller                      |
| <b>BET</b>    | Brunauer-Emmet-Teller                     |
| <b>BJH</b>    | Barnett-Joyner-Halenda                    |
| <b>XRD</b>    | X-ray Diffraction                         |
| <b>XRF</b>    | X-ray Fluorescenc                         |
| <b>SEM</b>    | Scanning Electron Microscope              |
| <b>TEM</b>    | Transmission Electron Microscopy          |
| <b>BET</b>    | Brunauer-Emmet-Teller                     |
| <b>BJH</b>    | Barnett-Joyner-Halenda                    |
| <b>SEM</b>    | Scanning Electron Microscope              |
| <b>TEM</b>    | Transmission Electron Microscopy          |
| <b>EDS</b>    | Energy-dispersive X-ray spectroscopy      |



# Glossary

**TGA TA** Thermogravimetric analyzer TGA TA Q500

**TGA Linseis** Linseis ThermalAnalysis STA PT1600

**One pot process** Synthesis method where all compounds are mixed at once, without any intermediate calcination

**One-step method** One-pot method where all additives are mixed at once

**Two-step method** One-pot method, but the binder is added after drying

**1S-sorbents** Dolomite-based sorbents prepared by the one-pot method

**2S-sorbents** Dolomite-based sorbents prepared by the two-step method

**ZrAl-based sorbents** Dolomite-based sorbents modified with cement and  $ZrO_2$

**CeAl-based sorbents** Dolomite-based sorbents modified with cement and  $CeO_2$

**Dry conditions** Testing of the capturing capacity of CaO-based sorbents without steam present in the carbonation

**Wet Conditions** Testing of the capturing capacity of CaO-based sorbents with steam present during the carbonation.

**Fresh sorbents** Sorbents before they have been exposed to cyclic carbonation-regeneration

**Spent sorbents** Sorbents before they have been exposed to cyclic carbonation-regeneration

**Cyclic testing** Test the reactivity of CaO-based sorbend during cyclic carbonation-regeneration

**Pre-calcination** Calcination of fresh sorbents before cyclic testing

# 1 Introduction

This master thesis is a continuation of the specialization project 2020 [1]. Parts of the introduction are reused.

One of the worst environmental challenges the world is facing today is global warming. The greenhouse  $\text{CO}_2$  are a large contributor. This paper is part of the research trying to find efficient ways to capture the gas.

Likely, fossil fuel will be the main contributor to energy-sources until 2050. At the same time, the EU has a vision of a climate-neutral economy before 2050 [2]. Based on the Paris agreement in 2015, the global temperature increase due to global warming needs to stay below  $2^\circ\text{C}$  and limit climate changes, preferably below  $1.5^\circ\text{C}$ . EU has determined that to reach the goal of the Paris agreement, the reduction of greenhouse gas emissions into the atmosphere needs to be reduced by 40 % from 1990 to 2030.

About 70 % of the total greenhouse gas emission in the US from 1970 - 2010 came from  $\text{CO}_2$  from industrial processes and fossil fuel combustion. Thus, capturing the  $\text{CO}_2$  is vital to reach the goal of zero-emission before 2050. A report released by IPCC at the end of 2018 emphasized the importance of using Carbon Capture and Storage (CCS) to beat climate changes [3]. To reach zero emissions in 2050, CCS is the only existing technology able to reduce emissions from the cement and steel industry sectors.

The interest in CCS is already promising. The first power station using CCS-technology was the Boundary Dam Power Station in Canada in 2014 [4]. At the end of 2019, there were 48 commercial CCS-facilities worldwide; at the end of 2020, the number had increased to 65 [5]. Of them, 26 were in operational mode, able to capture over 40 MtPa in a year. At the end of 2020, the Norwegian government decided to finalize the project of capturing  $\text{CO}_2$  from the cement plant "Norcem" in Norway. The facility can be up running already from 2024.

In CCS-technology, the goal is to remove  $\text{CO}_2$  from industry and other energy-demanding sources and further hindering the gas from entering the atmosphere [6]. After the  $\text{CO}_2$  is separated from the source, the gas is transport to a place where it is long-term stored and isolated. Important points for capturing  $\text{CO}_2$  in an efficient way are a high adsorption-capacity, good kinetics of the adsorption and desorption at desirable temperatures, and high cyclic stability [7].

Most studies so far on CCS have been done on coal-fired power plants [8]. The use of natural gas as an energy-source is growing fast and is thought to reach coal by 2030. Combustion of natural gas emits about the half amount of  $\text{CO}_2$  combustion of coal. Flue gas from natural gas combined cycles (NGCC) contain less  $\text{CO}_2$  than coal-fired power plants (3.8 % vs. 15 %); the oxygen content is, on the other hand, higher. As follows, capturing  $\text{CO}_2$  from gas combined cycles (NGCC) plants are more challenging than coal-fired power plants.

Separation of  $\text{CO}_2$  can be done in three different ways; namely, Pre-combustion capture, Post-

combustion capture, and Oxy-fuel combustion [9]. In Pre-combustion, the fuel is separated into CO<sub>2</sub> and H<sub>2</sub> before the combustion, while in post-combustion after. The post-combustion technology is the easiest to integrate with existing technology [10]. However, its challenge lies in separating CO<sub>2</sub>, with a relatively low partial pressure, from flue gas [10].

Common ways to separate CO<sub>2</sub> from flue-gas is either by the use of scrubbing solutions, solid sorbents, or the membranes [11]. Today’s leading PCCC technology is a technology where liquid solvents are used; chemical absorption by monoethanolamine (MEA). MEA reacts strongly and fast with CO<sub>2</sub>; It can capture a high amount even at low concentrations (as in flue gas). Though there are several drawbacks with the technology, for instance, amines are corrosive, leading to fouling of the process equipment. The disadvantage is even worse when capturing CO<sub>2</sub> in flue gas from NGCC, than from coal-fired power plants, due to the higher oxygen content. Furthermore, the regeneration energy in the amine-technology is high as a large amount of steam is needed.

Solid sorbents are a good alternative to those in liquid; they can work in a higher temperature range (ambient-700 °C), produce less waste during cycles, and can be disposed of without causing harm to the environment [11]. Solid sorbents can be classified into chemisorbents, physisorbents, organic and inorganic adsorbents [7]. Chemisorbents are chosen over physisorbents due to better selectivity and higher adsorption capacity. Depending on the temperature, solid sorbents can be classified into low (< 200 °C), intermediate (200-400 °C), and high (> 400 °C) temperature sorbents. CaO-based sorbents, which are high-temperature solid sorbents, are of big interest due to a high sorption capacity. They are also readily available at a low cost, especially the naturally occurring limestone and dolomite [7].

## 1.1 Ca-looping

An alternative to the MEA-technology in PCCC can be the use of CaO based sorbents in Ca-looping; several researchers have investigated the possibility of integrating Ca-looping with NGCC-power plants [12, 13, 14, 15, 16]. Several pilot plants exist today, with the first one (1.7 MWth) developed in 2013, in Spain [17]. The technology has a great opportunity to be integrated with, for instance, the cement industry.

In the technology, CaO is exposed to multicyclic reactions where CaO capture CO<sub>2</sub> following the carbonation reaction;



And is regenerated following the reversed reaction, being the calcination reaction[13].

Figure 1.1 shows a simplified scheme of Ca-looping for PCCC. Flue gas containing 4-15 vol % CO<sub>2</sub> enters the first reactor (carbonator) [17]. Fresh sorbents enter the other reactor (calciner), where it is exposed to the calcination reaction before it enters the carbonator. There, the solid sorbents (CaO) capture CO<sub>2</sub> following the carbonation reaction. The decarbonized flue gas leaves the carbonator. The CO<sub>2</sub> released during the calcination reaction leaves the

calciner, ready for compression, drying, and storage [14]. Fuel is applied to add heat to the calciner. To avoid Nitrogen contamination in the captured  $\text{CO}_2$ , pure Oxygen is used when fuel is burned [13, 14].

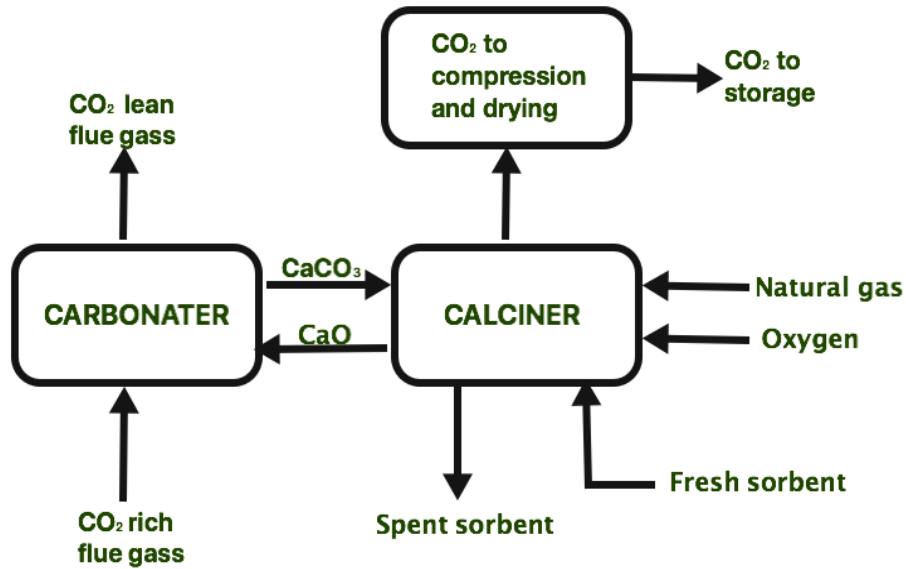


Figure 1.1: Ca-looping for Post combustion  $\text{CO}_2$ -capture.

The calcination reaction is endothermic, hence higher temperatures and a lower partial pressure are favoured compared to the forward reaction [18, 19]. The carbonation-reaction is, on the other hand, exothermic and favored at lower temperatures and a higher partial pressure.

The driving forces for the two reactions are the difference in the partial pressure of  $\text{CO}_2$  in the reactor, and the equilibrium pressure of  $\text{CO}_2$  [18]. Figure 1.2 illustrates the relationship between the  $\text{CO}_2$  equilibrium pressure and temperature [20]. At a given partial pressure, the carbonation temperature needs to be low enough to favor the forward reaction, but at the same time high enough to obtain sufficient kinetics, driving the reaction forward [14].

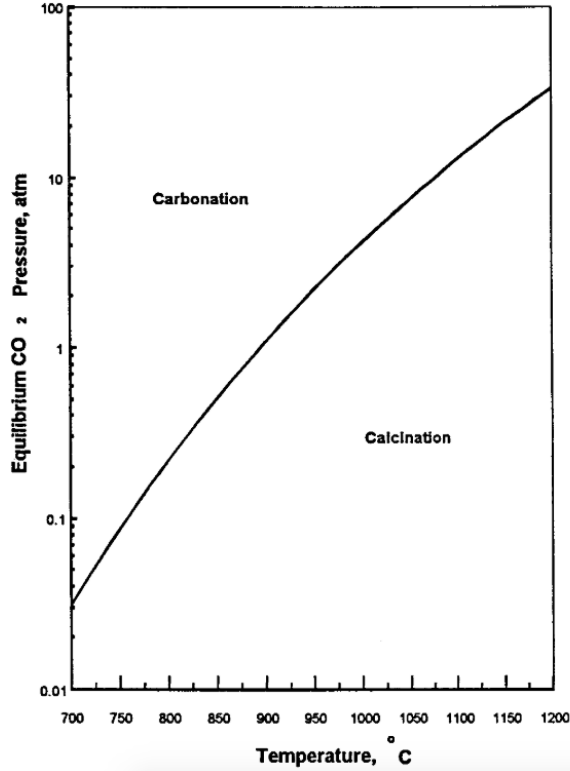


Figure 1.2: The equilibrium pressure of CO<sub>2</sub> vs temperature [20].

## 1.2 Moving Bed Carbonate Looping

Simulations have shown a certain decrease in the net electric efficiency (0.8-1.3 % with dolomite as sorbent) with needed for capturing CO<sub>2</sub> in Ca-looping compared to the MEA technology [15]. Most of which, the use of fluidized beds have been studied. Even so, their economic benefit is not considerably higher than the MEA-technology. For commercialization the technology, it is crucial to have a process design with a high enough economic and energetic benefit compared to the MEA technology [21].

Since 2017, NTNU/SINTEF/FTG has been working on a project in order to design a Moving Bed Carbonate Looping (MBCL) technology for PCCC [21]. By using cheap sorbents, optimizing the process design and making a compact reactor, the goal is to reduce cost, energy and size.

The project looks at the possibility of using solid sorbents in moving bed reactors to integrate CO<sub>2</sub> capture with NGCC [22]. A MBCL-technology has been designed, with both the carbonator and calciner being, as the name implies, moving beds. For the calcination also a fixed bed catalytic combustion is included. Figure 3.3 shows the Process flow diagram of Ca-looping in PCCC used in a NGCC.

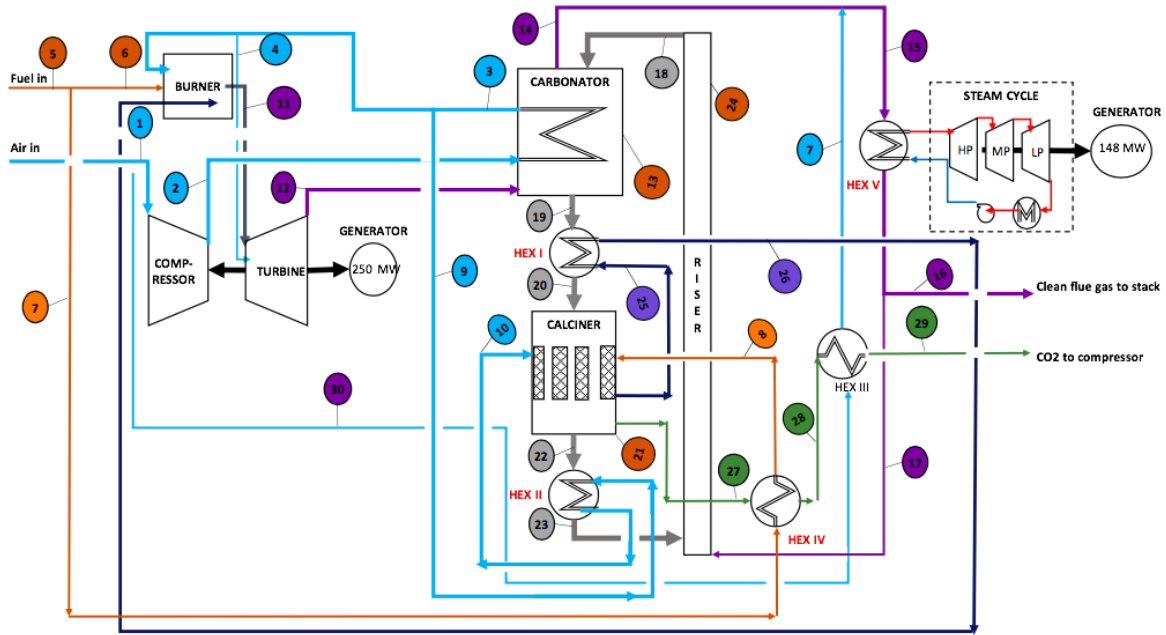


Figure 1.3: Process flow diagram for the MBCL-technology [22].

Table 1.1: List of the lines used in the process flow diagram shown in figure 3.3.

| 1                            | 2                                      | 3                                 | 4                          | 5                             | 6                           | 7                           | 8                     |
|------------------------------|--|-----------------------------------|----------------------------|-------------------------------|-----------------------------|-----------------------------|-----------------------|
| Inlet air                    | carbonator cooling air                 | hot air from carbonator           | Hot air from to burner     | Fuel in                       | Fuel to burner              | Fuel to catalytic combustor | Hot fuel to combustor |
| 9                            | 10                                     | 11                                | 12                         | 13                            | 14                          | 15                          | 16                    |
| Compressed Air to HEX II     | Hot Compressed air to combustor burner | flue gas                          | turbine flue gas           | Carbonator                    | Carbonator clean FG         | FG to HEX V                 | FG to stack           |
| 17                           | 18                                     | 19                                | 20                         | 21                            | 22                          | 23                          | 24                    |
| FG to riser                  | Solids to carbonator                   | Solids from carbonator            | Solids to calciner         | Calciner                      | Solids from calciner        | Solids to carbonator        | Riser                 |
| 25                           | 26                                     | 27                                | 28                         | 29                            | 30                          |                             |                       |
| Combustion flue gas to HEX I | Cold combustion flue gas to burner     | Hot CO <sub>2</sub> from calciner | CO <sub>2</sub> to HEX III | CO <sub>2</sub> to compressor | CO <sub>2</sub> cooling air |                             |                       |

In the process, fuel and air are combusted in the burner and sent to the gas turbine [22]. The carbonator is placed directly downstream of the gas turbine, post to combustion. Exhaust gas from the gas turbine, containing CO<sub>2</sub>, enters to the carbonator at 600 °C. This gas consists of 5 % CO<sub>2</sub> and 8 % H<sub>2</sub>O. Here the CaO-based sorbent capture the CO<sub>2</sub> according to the carbonation reaction (equation 1.1), forming CaCO<sub>3</sub>. Solid and gas move countercurrent. The lean flue gas is sent to the first heat recovery steam generator (HRSG) and further into the atmosphere.

In the calciner CaO is regenerated through the calcination reaction, at 950 °C [22]. CaO and CO<sub>2</sub> moves co-current and are separated in a gas-solid separation unit. The regenerated CaO is sent back to the carbonator through a riser, while the CO<sub>2</sub> is cooled down in two steps before compression and storage. As the calcination reaction is endothermic, fuel is burned in a fixed bed catalytic combustor in order to add heat to the reaction.

Exhaust gas from the catalytic combustion is sent to the second HRSG and mixed with exhaust gas from the turbine, which is then sent further to the carbonator [22]. The sorbents use only a few minutes from top to bottom, implying the importance of the sorbents staying stable over several cycles.

This master is a part of the MBCL-project, with focus on optimizing the CaO-based-sorbents.

### 1.3 The Carbonation reaction

The adsorption of CO<sub>2</sub> through the carbonation has a reaction-controlled regime and a diffusional controlled regime [23]. The stages are often referred to as the fast carbonation stage and the slow carbonation stage.

In the first stage, the reaction is controlled by the kinetics, hence temperature and partial pressure of CO<sub>2</sub> affect the reaction rate. The reaction happens fast; it only takes a few minutes under typical carbonation reactions (600 °C, 10-15 % CO<sub>2</sub>) [24].

Through the reaction a product-layer of CaCO<sub>3</sub> will form [18]. At a specific thickness of the product-layer, diffusion through the product layer will start to control the reaction. Alvarez et al. [25] found this value to be about 49 nm. In the slow reaction stage, the CO<sub>2</sub> needs to diffuse through the layer of CaCO<sub>3</sub> to reach the free surface of CaO. The diffusional regime is much slower than the first [26].

Figure 1.4 illustrates the conversion of CaO from the fast reaction stage (1) to the critical product layer of CaCO<sub>3</sub> is formed (2), to the slow reaction stage (3).

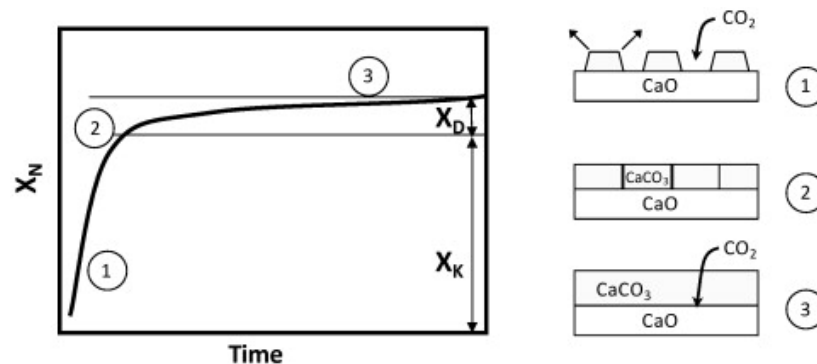


Figure 1.4: Conversion of CaO from the reaction controlled (1) to the diffusional controlled (2) regime [24]

## 1.4 CaO as a sorbent

One of the main disadvantages of using CaO as a sorbent for capturing CO<sub>2</sub> is the loss of activity with an increasing number of carbonation-calcination cycles [18, 27, 28]. The desired sorbent should have a sufficient capacity, but just as important is the ability to remain stable over several cycles. Reduction in sorption capacity leads to more inactive material.

Much research has been done to increase the activity and reduce the capacity-loss of CaO-based sorbents [28, 29, 30, 31, 32, 33, 34, 35]. Some methods investigated are the chemical pretreatment of the sorbent and introducing modifiers with high Tamann temperature [36]. The last has been widely investigated both on natural and synthetic CaO-based material. Chemical pretreatment is less studied as it has shown to only improve the cyclic stability for a short period and has a high cost.

Two main phenomena that cause deactivation in CaO based sorbents are attrition and sintering [37]. The degree of attrition can be dependent on the experimental set-up and conditions. Thermal stress, high pressure of CO<sub>2</sub> and mechanical stress can cause fragmentation of pellets. Sintering causes coalescence of particles. The phenomenon is considered as the main contributor to the loss of activity in CaO-based sorbents [28]. It is found that sintering mainly happens during the calcination but can also be related to the closure of pores during the carbonation.

Sintering causes a reduction in porosity and surface area, which again reduce the reaction rate and gives a decrease in the conversion of CO<sub>2</sub> and CaO to CaCO<sub>3</sub> [18, 28, 38]. Blocking of pores at the surface and increase of CaO crystal size can prevent diffusion of CO<sub>2</sub> into the particles, and hence decrease the cyclic stability [39]. Lysikov et al. [40] presented a sintering mechanism for CaO-based sorbents that are illustrated in figure 1.5.

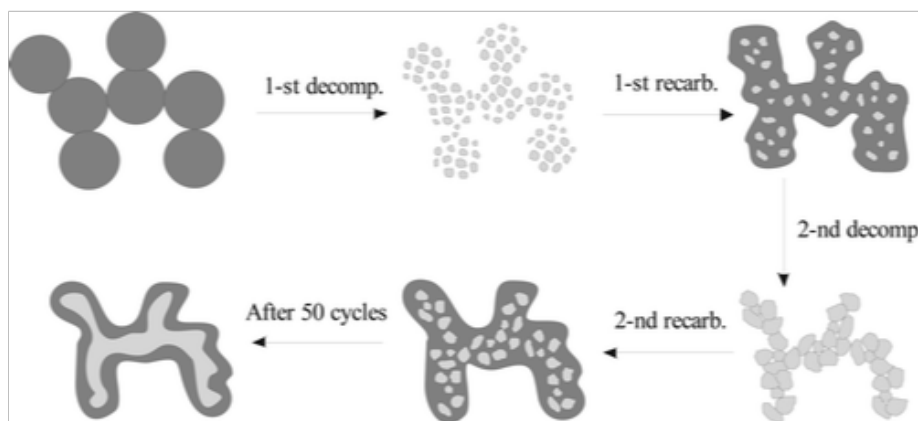


Figure 1.5: Sintering during cycles of a CaO-based sorbent. dark grey: CaCO<sub>3</sub>, light grey: CaO [40].



The dark gray area in the figure represents  $\text{CaCO}_3$  and the light gray  $\text{CaO}$ . First, the  $\text{CaCO}_3$  is calcined, leaving good dispersion of  $\text{CaO}$ -particles with adequate space between them. However, the next carbonation is incomplete, leaving some  $\text{CaO}$  in its calcined form. So, in the next decomposition,  $\text{CaO}$  particles will start to agglomerate. The agglomeration can continue until  $\text{CaO}$ -particles are connected in a skeleton, as shown in the last step (after 50 cycles). The skeleton created of  $\text{CaO}$ -particles will prevent further sintering. At the inner part of the framework, the  $\text{CaO}$  will keep its calcined form during cycles, and the carbonation will only occur on its outer layer.

Sintering typically occurs over the Tamann temperature, being 0.52 times the melting temperature. As presented in table 1.2, the Tamann temperature of  $\text{CaCO}_3$  is lower than the typical carbonation/decarbonation temperature typically used in Ca-looping ( $\sim 600$  °C).

Table 1.2: Tamann temperature and melting temperature of different compounds [36, 41]

| <b>Compound</b>           | <b>Melting temperature [°C]</b> | <b>Tamann temperature [°C]</b> |
|---------------------------|---------------------------------|--------------------------------|
| CaO                       | 2898                            | 1313                           |
| $\text{CaCO}_3$           | 1344                            | 533                            |
| $\text{ZrO}_2$            | 2709                            | 1218                           |
| $\text{Al}_2\text{O}_3$   | 1995                            | 1007                           |
| $\text{CeO}_2$            | 2400                            | 1064                           |
| MgO                       | 2800                            | 1400                           |
| $\text{CaZrO}_3$          | 2550                            | 1275                           |
| $\text{CaAl}_2\text{O}_4$ | 1600                            | 700                            |

A way to avoid sintering is by creating a barrier of small inert metal oxides, with a higher Tamann temperature than  $\text{CaCO}_3$  between the  $\text{CaO}$ -particles. The inert metal oxides prevents  $\text{CaO}$  particles from fusing. As a result a more stable pore structure can be obtained. Figure 1.6 illustrates the phenomena.

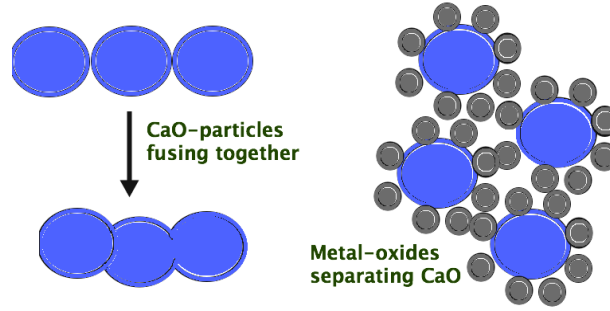


Figure 1.6: CaO particles before and during sintering (a) and prevention of sintering by inert metal oxides (b).

The modifiers might ( $\text{ZrO}_2$ ,  $\text{Al}_2\text{O}_3$ ,  $\text{SiO}_2$ ) or might not ( $\text{MgO}$ ,  $\text{CeO}_2$ ,  $\text{Y}_2\text{O}_3$ ) form mixed oxides with CaO, depending on the strength of the interactions [36]. In the mixed oxides, CaO active sites are consumed, which reduces the possible capturing capacity. Considerations need to be done between keeping a sufficient capacity and increase stability.

The creation of a well-dispersed phase with a high Tamann temperature and a large specific surface area is considered as the main benefits of the dopants affecting the performance of the sorbent [34].

#### 1.4.1 Dolomite

Limestone and dolomite have low cost and are readily available raw materials, making them among the most interesting CaO-based sorbents. Dolomite have proved an advantage in the regeneration-cycles compared to limestone [27, 28, 38]. Even though limestone ( $\text{CaCO}_3$ ) with a higher ratio of CaO than dolomite ( $\text{CaMg}(\text{CO}_3)_2$ ), has a higher initial capacity, the stability of dolomite appear to be better.

Calcination of  $\text{CaCO}_3$  and  $\text{MgCO}_3$  in dolomite leads towards two reactions. The first, "half-calcination reaction" decompose  $\text{MgCO}_3$ :



A lower molar volume in MgO compared to  $\text{MgCO}_3$  results in extra pore volume in dolomite. By further increasing the temperature, full calcination happens;



This stage gives the highest pore volume and surface area in dolomite. At which temperature each of the reactions happens, depends on the partial pressure of  $\text{CO}_2$  [42].

Equation 1.3 revealed the presence of MgO and CaO after calcination. MgO reacts with  $\text{CO}_2$  at lower temperatures than CaO. As follows, MgO will not react with  $\text{CO}_2$ , but act as

an inert during the carbonation reaction; calcined dolomite will react following equation 1.3 backwards. And owing to the higher Tamann temperature compared to  $\text{CaCO}_3$ , as shown in table 1.2, MgO function as a physical barrier which helps to keep the pore structure of the sorbent during several cycles. Hence, increasing the resistance towards sintering [43].

#### 1.4.2 Stabilizers to improve stability

Even though dolomite has better stability than limestone, it still suffers from loss in the activity. Modification of the natural-based CaO-based sorbents is expected to cost less than producing new sorbents [28]. Stabilizers are chemicals added to a compound to avoid degradation. Doping the CaO-based sorbents with metal-oxides can reduce degradation by making a barrier as illustrated in figure 1.6. For example, investigations have been done on oxides of Al-, Mg-, Ti-, Zr-, Si-, Y-, Ce-, La- [34, 36].

Doping sorbents with Zirconium oxide has been considered a smart choice and have been widely investigated [30, 32, 33, 35, 44, 45, 46, 47, 48, 49, 50, 51, 52]. The doped sorbents have shown remarkable stability over several cycles, attributed to the formation of the thermally resistant  $\text{CaZrO}_3$  when CaO reacts with  $\text{ZrO}_2$  according to the following reaction;



and in that way help prevent sintering [30, 32, 47].

Table 1.3, adapted from Chen et al. [36] presents an overview of some experiments where doping CaO-based sorbents with Zr have shown the best performance. The method used to prepare them, starting material, calcination and carbonation conditions, number of cycles, capacity in the first and last cycle, and the weight-percentage of  $\text{CaZrO}_3$  in the sorbent are given.

Arstad et al.[31] impregnated calcined dolomite with Ti nanoparticles -, Zr- and Al- in a breakthrough apparatus (Calcination at 850 °C in pure  $\text{N}_2$  and carbonation at 600 °C in 10 %  $\text{CO}_2$ ). The sample doped with Zr turned out to be the one with the best performance.

The best properties of the sorbent can be obtained by optimizing the ratio of Ca-Zr. Hamid et al. [30] found that, if the amount of Zr was too low, sintering was not prevented. On the other hand, an increase in Zirconium reduced the maximum possible capacity. Additionally, Zirconium is expensive. They concluded that a too high amount of the compound impacts the cost more than the stability. For them, the optimal Zr/Ca ratio was found to be 0.303.

Table 1.3: Research where the formation of  $\text{CaZrO}_3$  led to increased stability. All experiments performed in TGA.

| Name                      | Method   | Calcination                             | Carbonation                                 | Capacity [%] |       |      | $\text{CaZrO}_3$<br>[wt %] |
|---------------------------|--|---|---|--------------|-------|------|----------------------------|
|                           |  |   |   | cycles       | first | last |                            |
| Hashemi et al.[44]        | solution combustion synthesis                  | 950 °C, $\text{CO}_2$ , 10 min          | 675 °C, 20 % $\text{CO}_2$ , 20 min         | 50           | 53    | 29   | 20                         |
| Antzara et al.[32]        | sol-gel auto combustion route                  | 850 °C, $\text{N}_2$ , 5 min            | 650 °C, 15 % $\text{CO}_2$ , 30 min         | 50           | 48    | 46   | 34                         |
| Sultana et al.[45]        | thermal decomposition, then coating by sol-gel | 900-200 °C, Ar , 5 min                  | 200 til 900 °C, 80 % $\text{CO}_2$ , 30 min | 20           | 65    | 65   | 26                         |
| Broda et al.[46]          | sol-gel  | 800 °C, $\text{N}_2$ , 15 min           | 650 °C, 50 % $\text{CO}_2$ , 5 min          | 90           | 45    | 34   | 29                         |
| Koirala et al.[33]        | flame spray pyrolysis                          | 700 °C, 50 vol % $\text{CO}_2$ , 30 min | 650 °C, 50 vol % $\text{CO}_2$ , 30 min     | 1200         | 11    | 11   | 76                         |
| Radfarina et al.[30]      | surfactant template -ultrasound synthesis      | 750 °C, Ar , 30 min                     | 600 °C, $\text{CO}_2$ , 30 min              | 15           | 19    | 13   | 58                         |
| Soleimanisalim et al.[47] | wet impregnation                               | 850 °C, $\text{N}_2$ , 10 min           | 675 °C, % $\text{CO}_2$ , 10 min            | 21           | 45    | 36   | NA                         |
| Guo et al.[48]            | sol-gel  | 900 °C, $\text{N}_2$ , 5 min            | 600 °C, 50 vol % $\text{CO}_2$ , 45 min     | 18           | 67    | 64   | 10                         |
| Hong et al. [49]          | flame spray pyrolysis                          | 700 °C, He, 30 min                      | 700 °C, 30 vol % $\text{CO}_2$ , 30 min     | 100          | 21    | 21   | 58                         |
| Yoon et al.[50]           | citrate sol-gel                                | 780 °C, $\text{N}_2$ , 60 min           | 650 °C, % $\text{CO}_2$ , 60 min            | 10           | 71    | 69   | 10                         |
| He et al.[35]             | sol-gel  | 900 °C, $\text{N}_2$ , 5 min            | 650 °C, 15 vol % $\text{CO}_2$ , 10 min     | 30           | 44    | 45   | 29                         |
| He et al.[35]             | sol-gel  | 1000 °C,80 vol % $\text{CO}_2$ , 5 min  | 650 °C, 15 vol % $\text{CO}_2$ , 20 min     | 50           | 40    | 16   | 29                         |
| Zhaoe et al.[51]          | spray drying                                   | 950 °C,90 vol % $\text{CO}_2$ , 0 min   | 650 °C, 90 vol % $\text{CO}_2$ , 10 min     | 100          | 60    | 44   | 20                         |
| Zhaoe et al.[51]          | spray drying                                   | 950 °C,90 vol % $\text{CO}_2$ , 0 min   | 650 °C, 90 vol % $\text{CO}_2$ , 10 min     | 100          | 60    | 44   | 20                         |

Another type of oxide with the possibility to work as a stabilizer is Cerium oxide [36, 49, 53, 54]. It has a high Tamann temperature (1064 °C).  $\text{CeO}_2$  can work as a physical barrier, as explained in figure 1.6 and help to prevent sintering of the CaO particles. However, in contrast to, for instance,  $\text{ZrO}_2$ ,  $\text{CeO}_2$  do not form a mixed oxide with CaO. Hence, the oxide will not occupy any of the active sites of CaO and reduce its capturing capacity. Nevertheless, the total fraction of active material in the sorbent can be reduced due to the reduced fraction of CaO in the sorbent.

The carbonation reaction can be divided into two steps;

1.  $\text{CO}_{2(\text{ads})} + \text{O}^{2-} \rightarrow \text{CO}_3^{2-}$
2.  $\text{CO}_3^{2-} + \text{CaO} \rightarrow \text{CaCO}_3 + \text{O}^{2-}$

In order to capture  $\text{CO}_2$ , the mobility of  $\text{O}^{2-}$  is important.  $\text{CeO}_2$  can generate vacancy when incorporated into  $\text{CaO}$ . Hence  $\text{CeO}_2$  is able to help facilitate the diffusion of  $\text{O}^{2-}$  [36, 55].

Table 1.4 presents experiments where the use of Cerium have shown a positive effect on the carbonation reaction. The method used to prepare them, starting material, calcination and carbonation conditions, number of cycles, capacity in the last cycle, and the weight percentage of  $\text{CeO}_2$  in the sorbent are presented.

Table 1.4: Research where incorporation of  $\text{CeO}_2$  to  $\text{CaO}$ -based sorbents led to increased cyclic behavior. All experiments performed in TGA.

| Name             | Method                         | Calcination                            | Carbonation  | Capacity [%] |       | $\text{CeO}_2$<br>[wt %] |
|------------------|--------------------------------|--|--|--------------|-------|--------------------------|
|                  |                                |  |  | cycles       | first |                          |
| Wang et al. [54] | solgel<br>combustion<br>method | 700 °C, $\text{N}_2$ , 20 min          | 600 °C, 50 % $\text{CO}_2$ ,<br>50 % $\text{N}_2$ 45 min | 18           | 59    | 59                       |
| Lu et al. [56]   | Flame spray<br>pyrolysis (FSP) | 700 °C, 100 % $\text{N}_2$ ,<br>20 min | 700 °C, 30 % $\text{CO}_2$ ,<br>30 min                   | 100          | 19    | 23.5                     |

### 1.4.3 Calcium Aluminate Cement

Attrition can lead to loss of sorbent during the regeneration-cycles [14]. Manovic et al.[29] found that it is possible to reduce attrition significantly by preparing pellets. In order to form pellets, binders are needed. For the task, calcium aluminate cement (CAC) have proven to be good candidates, which in itself are inert towards the carbonation/calcination reaction. They are resistant to corrosion, have a low cost, and good refractory properties—making it able to work at high temperature [57]. However, their most significant advantage is probably that, in addition to work as binders, they also have shown good qualities as stabilizers [29].

Calcium aluminates are composed of  $\text{Al}_2\text{O}_3$ ,  $\text{CaO}$  and smaller amount of  $\text{SiO}_2$  and  $\text{Fe}_2\text{O}_3$  [58]. The reaction between  $\text{CaO}$  and  $\text{Al}_2\text{O}_3$  can lead to the formation of mayenite, ( $\text{Ca}_{12}\text{Al}_{14}\text{O}_{33}$ ) [38] ;



Depending on the  $\text{Al}_2\text{O}_3$ -content in cement, additional  $\text{CaO}$ -base might be required to convert all to mayenite [29]. Mayenite has a high Tamann temperature. As explained in section 1.4 a high Tamann temperature is an essential property of inert phases added to stabilize  $\text{CaO}$ -based sorbents.

Manovic et al. [29] attributed the improved performance of prepared sorbents (limestone + CAC) to be due to a uniform dispersion of Mayenite. They described that Mayenite created

a stable framework, hindering sintering among active CaO-sites.

Apart from cement, also many studies have been conducted on CaO-based sorbents modified with aluminates. Several researchers reported a stabilizing effect when due to the formation of Mayenite [59, 36, 60, 61, 62]

Table 1.5 gives an overview of research where calcium-aluminate cement has been used to support CaO-based sorbents. The method used to prepare them, starting material, calcination and carbonation conditions, number of cycles, capacity in the first and last cycle, and the weight-percentage of cement in the sorbent are given.

Table 1.5: Overview over reserach where calcium aluminate cement was used as support for CaO-based sorbents. All experiments performed in TGA.

| Name                | Method                        | Calcination                      | Carbonation                           | Capacity [%] |       |      | cement<br>[wt %] |
|---------------------|-------------------------------|----------------------------------|---------------------------------------|--------------|-------|------|------------------|
|                     |                               |                                  |                                       | cycles       | first | last |                  |
| Manovic et al. [63] | solution combustion synthesis | 800 °C, N <sub>2</sub> , 10 min  | 800 °C, 50 % CO <sub>2</sub> , 10 min | 1000         | 58    | 18   | 10               |
| Duan et al. [64]    | wet granulation method        | 850 °C, N <sub>2</sub> , 10 min  | 650 °C, 15 % CO <sub>2</sub> , 10 min | 20           | 45    | 13   | 10               |
| Erans et al. [65]   | wet granulation method        | 950 °C, CO <sub>2</sub> , 10 min | 650 °C, 15 % CO <sub>2</sub> , 20 min | 20           | 45    | 13   | 10               |
| Wei et al. [66]     | wet mixing and extrusion      | 850 °C, N <sub>2</sub> , 10 min  | 650 °C, 15 % CO <sub>2</sub> , 30 min | 15           | 49    | 20   | 15               |
| Li et al. [67]      | Wet mixing method             | 850 °C, N <sub>2</sub> , 10 min  | 650 °C, 15 % CO <sub>2</sub> , 25 min | 20           | 20    | 20   | 56               |

#### 1.4.4 The pore structure

An important factor affecting the diffusion of CO<sub>2</sub> into the CaO-based sorbents is their pore-structure. As mentioned, sintering and pore collapse leads to deactivation in CaO-based sorbents. The phenomena can significantly impact their pore size distribution and specific surface areas [68].

Li et al. [69] developed a rate equation-theory to explain the changes to explain the pore-size distribution of calcined CaCO<sub>3</sub>. A shrinkage-core model was used, and the calcination process was divided into three steps: 1. Decomposition of CaCO<sub>3</sub> at the surface of CaCO<sub>3</sub>-CaO. 2. Diffusion of CaO through a layer of CaO. 3. Formation of pores and sintering. The formation of pores and release of CO<sub>2</sub> will lead to a significant increase in the surface area and pore volume. Though, if sintering occurs, the surface area will be reduced and the pore-size distribution changed - which again can lead to reduced reactivity of the CaO-based sorbents. The researchers found the calcined CaCO<sub>3</sub> to have a bimodal pore-size distribution with average pore sizes of about 2.8 nm and 50 nm.

Smaller pore sizes have been reported to contribute most to the carbonation reaction [70]. Those are the pores contributing most to the surface area. Sintering can cause a decrease in the smaller pores while an increase in the larger pores. Figure 1.7 shows a pore-size distribution of CaO-based sorbents of fresh samples and after cycles, obtained by Quiao et al. [71]. In their case, a bimodal distribution is starting to form after cycles. The volume of the smaller pores decreases with cycles, while the higher volume increases - which they attributed to being due to sintering.

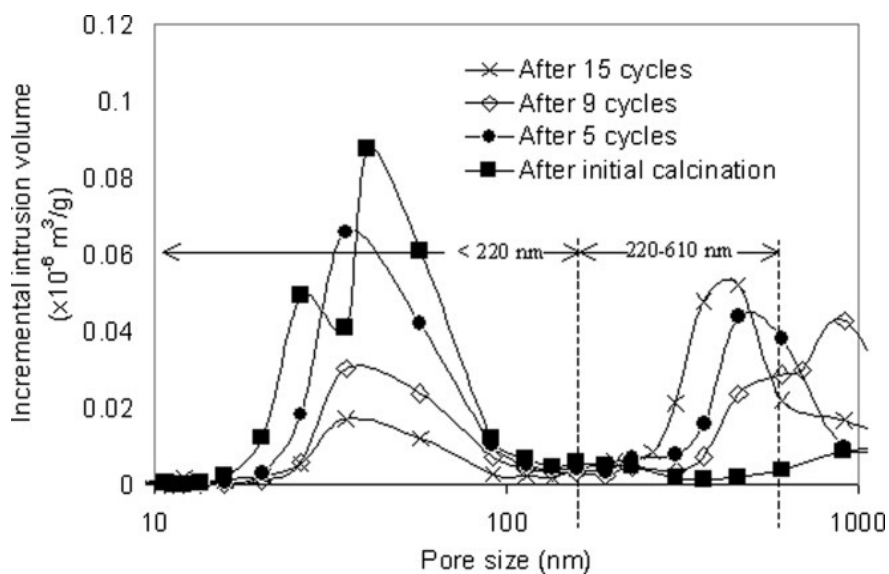


Figure 1.7: Pore-size distribution of a CaO based particle, before and after cycles. (Calcination 100 % N<sub>2</sub>, 850 °C . Carbonation 100 % CO<sub>2</sub>, 850 °C) [71]

Generally, a higher pore volume can make it easier to achieve a higher capturing capacity. However, Chen et al. [72] observed a decrease in the attrition resistance of CaO-based sorbents when the mesopores volume and surface area increased. They emphasized the importance of finding a balance between a high pore volume, and at the same time, obtaining a good attrition resistance.

Chen et al. [73] found that the distribution of the pore size was more critical than the surface area and pore volume. They emphasized that there is a necessity for enough pores larger than 50 nm in order to avoid pore blockage. They did not find any effect on the surface area if it exceeded 10 m<sup>2</sup>/g.

Different pore sizes have been found to affect the carbonation reaction differently. Wei et al. [68] a relation between small mesopores (2-10) and the reaction controlled stage. They found a linear relation between the CO<sub>2</sub> uptake and pore volume in this range. Pores of larger size, 10-100 nm, had a positive effect in the diffusional regime. While larger pores (> 400 nm) did not have any special promoting effect on the carbonation reaction.

Doping with additives with higher Tamann temperature can limit changes in the pore-

structure. For instance, Borda et al. [46] observed a loss of pore-size of pure limestone after cycles, while sorbents doped with Zirconium kept their pore sizes (less than 100 nm). They attributed it to the formation of  $\text{CaZrO}_3$ . Manovich et al. [63] observed a significant reduction in the BJH desorption pore volume distribution of limestone after 300 regeneration-cycles in a tube furnace. When the sorbents were supported with Calcium-aluminates, the change was much less pronounced. The improvement in the pore-structure was also observed through Scanning electron microscopy. They attributed the stable morphology due to Mayenite ( $\text{Ca}_{12}\text{Al}_{14}\text{O}_{33}$ ) present in the CaO structure.

### 1.4.5 Synthesis method

The composition of the sorbents and the way they are synthesized impacts their performance; Preparation methods have a big impact on properties like surface area, crystal sizes, phases present, and sorption capacity.

As might have been noticed in table 1.3, 1.4 and 1.5 diverse methods have been employed for preparation. Typical methods include, for instance coprecipitation [74], sol-gel method [32, 35, 44, 46], flame spray [49], dry [75] and wet [47] mixing.

Synthesis methods have resulted in a varying degree of stability and capacity. Unfortunately, most have caused disadvantages associated with expensive and challenging preparation methods. Consequently making scale-up difficult [76]. Cost of raw materials and preparation methods are crucial in determining if the sorbent is financially competitive or not [36].

A cost analysis conducted by Xu et al.[77] is reproduced in table 1.6. Different preparation methods, together with their respective costs, are given.

Table 1.6: Different preparation-methods, capacity and cost for CaO-based sorbents [77].

| Method                                    | Raw Material  | Number of Cycles | CO <sub>2</sub> capture capacity (g CO <sub>2</sub> /g sorbent) | cost (USD/ton of CaO sorbent) |
|---|---|------------------|---|-------------------------------|
| wet chemistry                             | CaO Al(NO <sub>3</sub> ) <sub>3</sub> , and 2-propanol    | 13               | 0.45  | ~4600                         |
| sol-gel                                   | Ca(NO <sub>3</sub> ) <sub>3</sub> and citric acid         | 20               | 0.37  | ~ 2800                        |
| PCC(precipitated calcium carbonated)      | Ca(OH) <sub>2</sub> and Al(NO <sub>3</sub> ) <sub>3</sub> | 30               | 0.23  | ~ 400                         |
| flame spray                               | Ca-naphthenate and xylene                                 | 20               | 0.46  | ~ 12000                       |
| SHI (simeltaneous hydration impregnation) | lime and sea salt   | 40               | 0.31  | ~ 80                          |
| limestone                                 | limestone (powder)  | 20               | 0.09  | ~ 62                          |

The continuous circulation of sorbents in the MBCL-process lead to a considerable quantity being consumed, making a low price and easy scale up a necessity [22]. With this in mind, NTNU/SINTEF/FTG has developed and patented a process *Pellets by one-pot method for removal of carbon dioxide from the gas stream at high temperatures* (Patent application number: GB1810620.3, 15 August 2018, Journal 6743) [76], which in this paper will be referred to as the one-pot method.

In the method, two additives are added at once, avoiding several intermediate steps usual in typical sorbent preparation [76]. As a result, the need for energy, synthesis material, and



time will be reduced. In opposition to other methods, there is no intermediate calcination. The method is an easy and effective way of producing sorbents for CO<sub>2</sub>-capture at high temperatures at a low cost. The method will be explained more in detail in section 3.1

## 1.5 Experimental conditions

The conditions of the carbonation and calcination reaction have a considerable impact on the performance of the sorbent and should be given a thought during testing. Not only variations in temperature and partial pressure of CO<sub>2</sub> affect the calcination and carbonation performance of the sorbent during testing. Other important factors are, for instance, the time of the carbonation and calcination and the presence of steam [78, 79]. The occurrence of sintering increases both with the partial pressure of CO<sub>2</sub> and H<sub>2</sub>O [28]. Concluding, experiments should be performed as close to realistic conditions as possible.

A lot of experiments so far have been done in mild calcination conditions (750-850 °C, pure N<sub>2</sub>) [36]. In realistic conditions, 80-90 % of CO<sub>2</sub> is present during the calcination; increasing the partial pressure means that the equilibrium pressure should be increased in order to enhance calcination. As illustrated in figure 1.2 temperature needs to be increased to increase the equilibrium pressure, which is why typical calcination temperatures in realistic conditions are 950 °C [27]. Which, in turn, can lead to a faster loss in capturing capacity compared to mild conditions due to enhanced sintering.

The transition between calcination and carbonation should ideally be as fast as possible, so the heating rates should be high. In real pilot plants, the effective heating rates are over 50 °C/min[79]. Though lower rates are used when testing in TG analyzers, due to limitations in the instrument[27]. A slow heating rate can, in the case of CO<sub>2</sub> still present in the stream, lead to an extra carbonation phase. Hence an additional amount of CO<sub>2</sub> will be absorbed until the partial pressure of CO<sub>2</sub> raises above the equilibrium pressure.

Donat et al.[78] performed experiments in a Thermogravimetric analyzer (TGA) using natural limestone as sorbent. Under realistic conditions for Ca-looping (carbonation at 650 °C in 15 vol % CO<sub>2</sub>, calcination at 950 °C in 80 vol % CO<sub>2</sub>) the heating rate was varied. Higher gave better cyclic stability, argued to be due to shorter exposure of high temperatures for the carbonation phase, and in that way preventing sintering.

### 1.5.1 Presence of steam

Some researchers have looked at the influence of steam during the carbonation (and calcination), with conflicting results [80]. An overview of some obtained results and explanations so far can be seen in table 1.7. The material used, the instrument, the carbonation and calcination conditions, together with a comment of the observations, are given.

Some researchers found a positive effect regarding the kinetics due to a decrease in diffusion-

limitations when steam is present during the carbonation reaction [78, 81, 82]. Dunstan et al.[81] observed a more homogeneous distribution of the formation of  $\text{CaCO}_3$  through the pellet [78]. Manovic et al. [82] found this effect more pronounced for sintered samples and reactions at lower temperatures. Steam greatly enhanced the carbonation at around 600 °C; typical for carbonation in Ca-looping. Results have indicated a small effect of steam during the kinetically controlled regime [26, 82].

Table 1.7: Experiments with steam present during the carbonation [78, 80].

| Name                | Material  | Instrument                       | Carbonation   | Calcination  | Comment   |
|---------------------|---|----------------------------------|---|--|---|
| Dunstant et al.[81] | CaO pellet ( $\approx 33$ mm) of nanopowders and calcined limestone   | FBR                              | 15 % CO <sub>2</sub> , 1023 K 0 or 2 % steam  |  | Steam during carbonation as function of time and particle size. Steam improve kinetic and homogeneity; Formation of CaCO <sub>3</sub> throughout the pellet (2 min).  |
| Li et al.[83]       | CaCO <sub>3</sub> -samples (28-45 $\mu$ m)/ limestone (0.35-0.355 mm) | TGA (calc) / FBR (carb) / HP TGA | 923 K 3 L/min CO <sub>2</sub> / 1L/min steam, 2 L/min CO <sub>2</sub> / 20 min, 923 K, 15 % CO <sub>2</sub> in N <sub>2</sub> | variation in steam, N <sub>2</sub> , CO <sub>2</sub> 1123 K / 10 min, 1993 K, pure CO <sub>2</sub> | Steam enhanced CaCO <sub>3</sub> decomposition rate during calcination giving lower sintering, higher reactivity. Doubled carbonation reactivity, formation of OH <sup>-</sup> steam higher effect in calcination than carbonation. |
| Donat et al.[78]    | 4 types of limestone  | BFB                              | 15 % CO <sub>2</sub> , 0-20 % steam, N <sub>2</sub> 650 °C  | 900 °C 0-20 % steam, N <sub>2</sub> , 15 %CO <sub>2</sub>  | Calcination: sintering, giving large pores, more stable. Carbonation: reduction in diffusion resistance. Synergetic effect when present during both reactions.  |
| Manovic et al.[82]  | 7 Limesones (250-425 $\mu$ m)   | TGA                              | 350-800 °C. 10/20 % steam, 20 % CO <sub>2</sub>   | 800 °C N <sub>2</sub> , 900 °C CO <sub>2</sub> )   | Steam promotes the carb.reaction (lower T and sintered samples. esp. 600 °C;). Effect in diffusional regime, limited in kinetically.  |
| Arias et al.[26]    |   |                                  | 650 °C, p <sub>CO2</sub> = 20/10 kPa, p <sub>H2O</sub> = 20 kPa 20/5 min  | 800/900 °C, 10/5 min in N <sub>2</sub>   | No influence of reaction rate constant using steam  |
| Lu et al.[84]       | Synthetic sorbent from calcium acetate (< 10 $\mu$ m)                 | TGA                              | 10 % steam, 30 %CO <sub>2</sub> , 60 % He, 700 °C   | He   | Steam negative effect on the capacity   |
| Dou et al.[85]      | commercial CaO (450-1000 $\mu$ m)                                     | FBR                              | 550 °C 5/10 % steam   | 900 °C in N <sub>2</sub>   | Improved capacity due to CaO to Ca(OH) <sub>2</sub> reacting with CO <sub>2</sub>   |
| Yang et al.[86]     | commercial CaO (150-250 $\mu$ m)                                      | TGA                              | p <sub>CO2</sub> =0.5 MPa, p <sub>H2O</sub> =0,0.3,0.5 MPa 823/923 K, p <sub>tot</sub> = 3 / 1.5 MPa                          | 1173 K, 3h in N <sub>2</sub>   | Big improvement of conversion in carbonation w/steam; catalytic effect of steam.  |
| Symonds et al.[87]  | limestone (250-425 $\mu$ m)   | FBR                              | 620 °C 17 % steam, simulated syngas   |  | Better reactivity in long term, increase in reaction rate. Believed to be due to increase in macro-porosity.  |
| He et al.[88]       | carbide slag (<0.125.mm)  | DFBR                             | 650 °C 0 %, 20 % , 40 % or 60 % steam, 120 % CO <sub>2</sub>  | 950 °C 100 % CO <sub>2</sub>   | Higher carbonation conversion with more steam at short carbonation time. It was not so big effect on the pore structure.  |

## 2 Objective

This master continued the work of the specialization project started during spring 2020 [1]. The aim was to optimize dolomite-based sorbents for the MBCL-project. The sorbents should keep stable during many carbonation-regeneration cycles and have a capacity over 10 %. This, in as realistic conditions as possible, with steam present during the carbonation and calcination at a temperature of 950 °C in pure CO<sub>2</sub>.

In order to improve the stability of the natural sorbents, the optimal compositions of additives were investigated; with ZrO<sub>2</sub> or CeO<sub>2</sub> as a stabilizer, and cement both as a binder and stabilizer. The stabilizing effect of cement was also studied. ZrO<sub>2</sub> was expected to react with the active sites of CaO to form the mixed oxide CaZrO<sub>3</sub>, while CeO<sub>2</sub> was intended to have a stabilizing effect without forming a mixed oxide.

Further, pellets were made by an easy synthesis method aiming to make industrial scale-up easy. For this, the one-pot method was followed, where, compared with the typical preparation method, the intermediated calcination step was avoided. The best sequence to prepare the sorbents was investigated to obtain a deposition of additives resulting in the best cyclic stability.

It was desirable to obtain a good dispersion of the additives. Figure 2.1 illustrates the desired distribution of the dolomite (CaO·MgO) and the additives (ZrO<sub>2</sub> and cement). CaZrO<sub>3</sub> particles are evenly distributed around the CaO-particles and hinder them from fusing under exposure to higher temperatures. Further, cement is meant to settle between the particles, both to help avoid CaO-particles from merging, and at the same time, strengthen the pellets.

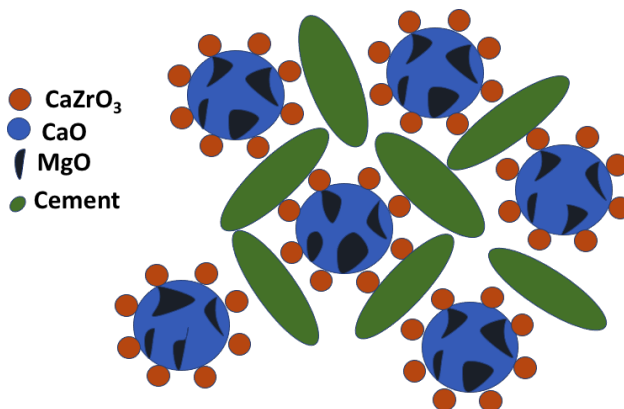


Figure 2.1: The ideal sorbent distribution.

In-depth characterization was performed before and after cyclic testing to get more knowledge about the sorbent. Then, it was possible to understand more about the cause of deactivation and how to prevent it.

### 3 Experimental Techniques

This section will start with a description of the one-pot method. In this project, two Thermo-gravimetric analyzers and one microbalance fixed bed reactor were used for the cyclic testing - the differences between the instruments will be explained. In the end, the theory of the methods used to characterize the sorbents will be reviewed. Some sections (3.1, 3.2, 3.3.2, 3.3.3) are adapted from the specialization project [1].

#### 3.1 Synthesis by the one-pot method

The one-pot method is a simple way to produce sorbents for CO<sub>2</sub> capture consisting of fewer steps than typical preparation methods [76]. Typical processing can be seen in figure 3.1a. An additive for improving the cyclic capacity of the sorbent, a stabilizer, is mixed with a CaO base material and water before it is dried and milled. Then the mixture is calcined again, so called intermediate calcination. An additive for granulation, a binder, is then typically added in order to form wet aggregates; pellets, granules, extrudes and so on. In the end, the sorbents are calcined. In the one-pot method, on the other hand, at least two additives are, together with water, simultaneously added to the base-material forming spherical pellets. No intermediate calcination is necessary, saving time and energy.

Figure 3.1b illustrates the one-pot processing, with the main steps being;

1. Pre-treatment making a solid base material
2. The one-pot processing: addition of minimum two additives and water to the base-material forming pellets of desired size and composition
3. Calcination of the sorbents

The components of the sorbents will consist of CaO from the base-material, together with inert metal oxides from the base-material and additives [76]. CaO acts as the active component, reacting with CO<sub>2</sub> at temperatures above 500 °C. The additives are meant to improve the sorbent in several ways; binding the material to form a pellet, having a stabilizing effect and better its morphology. The material should be continuously mixed. Mixing promotes the formation of aggregates with the compounds evenly distributed, which, again enhance the stability of the sorbents.

Natural dolomite has been considered to be a good base-material, due to its mentioned benefits as low cost, easy availability, and, the presence of MgO enhancing the stability [76, 18]. Calcination of dolomite (CaCO<sub>3</sub>·MgCO<sub>3</sub>) is necessary in order to obtain MgO and CaO and crushed to a size less than 100 μm before it can be used as a base material.

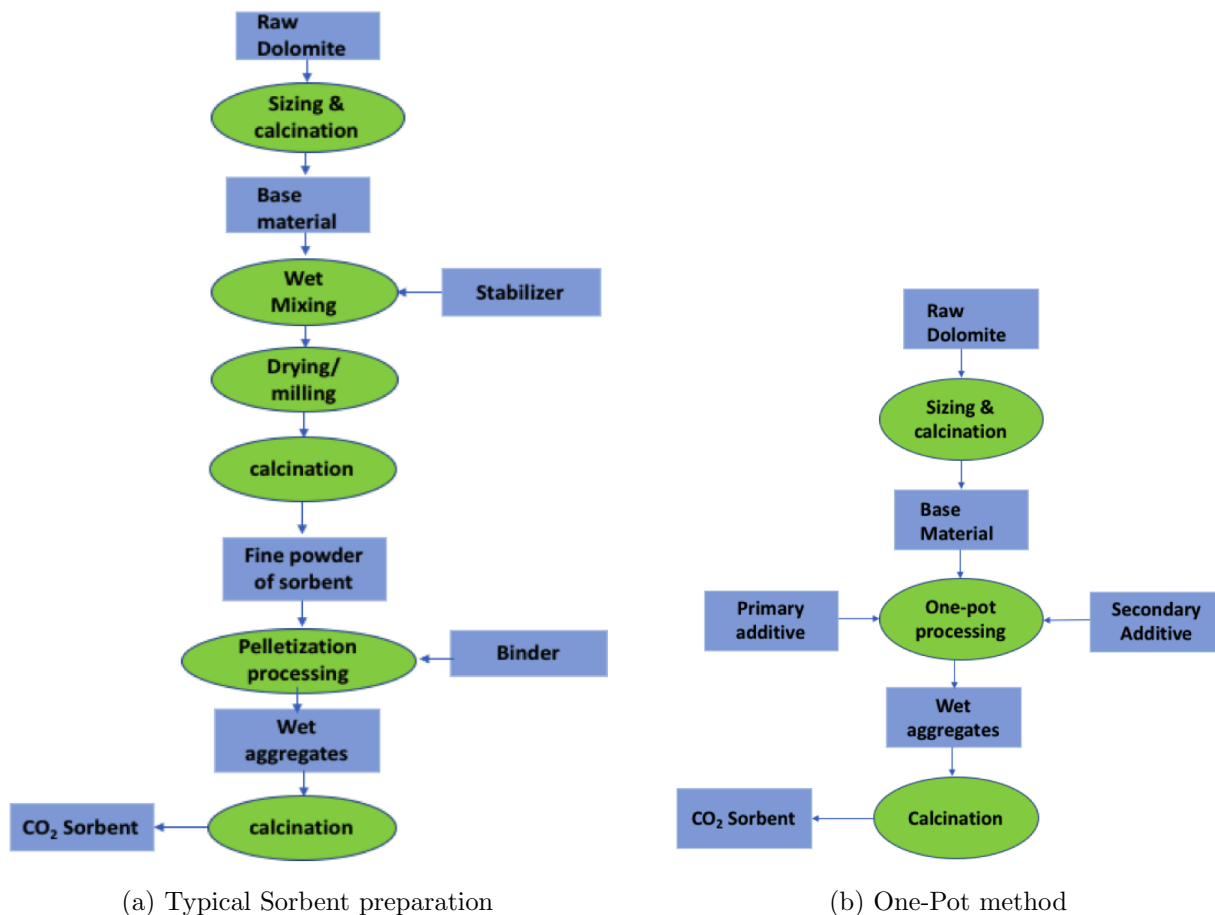


Figure 3.1: Typical sorbent preparation (a) compared to the one-pot processing (b).

## 3.2 Testing cyclic performance

### 3.2.1 Thermogravimetric Analysis (TGA)

Thermogravimetric analysis is a kind of thermal analysis. Thermal analyzes measure the chemical or physical properties of a material as a function of temperature. The temperature can increase linearly over time and include isothermal periods [89]. In the TGA, changes in mass are measured as a function of time and temperature. Reactions that lead to either a gain or loss in mass are studied. Typical reactions that lead to a gain in mass are oxidation, adsorption, and wetting, while reactions typically desorption reduction and drying. The type of measurement is beneficial for gas-solid reactions.

The samples are added to crucibles connected to a microbalance. They are then inserted into a furnace programmed to give the desired atmosphere, and temperature rise [89]. An increase in the loaded sample mass or the scanning rate might impact the temperature-

therefore, these factors should be equal when comparing results. The atmosphere can either be inert, oxidizing, or reducing. It might vary through the experiment. The purge gas is used to control the environment and might either be an inert or reactive gas [90, 91]. Three major factors that might cause an error in the TGA measurements are the atmosphere, possible secondary reactions, and electrical error [92].

The balance is a crucial element of the thermogravimeter. Asymmetrical balances only consist of one crucible. On the other hand, symmetric balances consist of two crucibles, one empty, a reference, and the other containing the sample. This can reduce external errors [89]. During the experiment, the weight of the crucibles might vary. For this reason, a correction file should be made before the experiment, using empty crucibles. Then, the actual weight-change during the experiment can be obtained.

Two TGAs for testing the cyclic performance of the sorbents were used in this project; TGA Instruments TGA TA Q500 and Linseis Thermal Analysis STA PT1600. The instruments will be referred to as TGA TA and TGA Linseis, respectively.

### 3.2.2 Instrumental Limitations

The two TGAs suffer from different limitations. Experiments in TGA TA can only be performed in dry conditions; that is, steam can not be introduced during the carbonation, which is the case for the MBCL-technology. In TGA Linseis, on the other hand, it is possible to introduce steam during the reaction (wet conditions), and experiments can be performed in more realistic conditions, however as will be explained in the next paragraphs, it suffers from diffusional limitations.

In TGA TA, the sample holder is shallow, without any high edges. The gas flow inlet is modified to be similar to in a fixed bed reactor; the sample gas is entering from the bottom, as shown in figure 3.2a. In TGA Linseis, on the other hand, there is a certain height on the edges of the sample holders. The sample-gas only enters from above, as shown in figure 3.2b.

Due to the different configurations of the sample holders and the different entering of the sample gas, mass transfer limitations are more pronounced in TGA Linseis than TGA TA [93]. The depth of the sample holder in the TGA Linseis reduces the accessibility of the sample gas during sorption, and a significant bypass is expected. As it can be seen, bypass can be expected for the gas when it flows through the sample holder. However, if a thin layer of the sorbent is used together with a sufficient amount of CO<sub>2</sub>, kinetical studies can be executed in TGA TA. Nevertheless, using an instrument that causes a negligible amount of mass transfer limitations is preferred. Bypasses can be avoided if gas enters the bottom, through a bed of sorbents, and then flows through the sample as illustrated in figure 3.2. Something which is the case for the microbalance fixed-bed reactor. The reactor will be described in the next section.

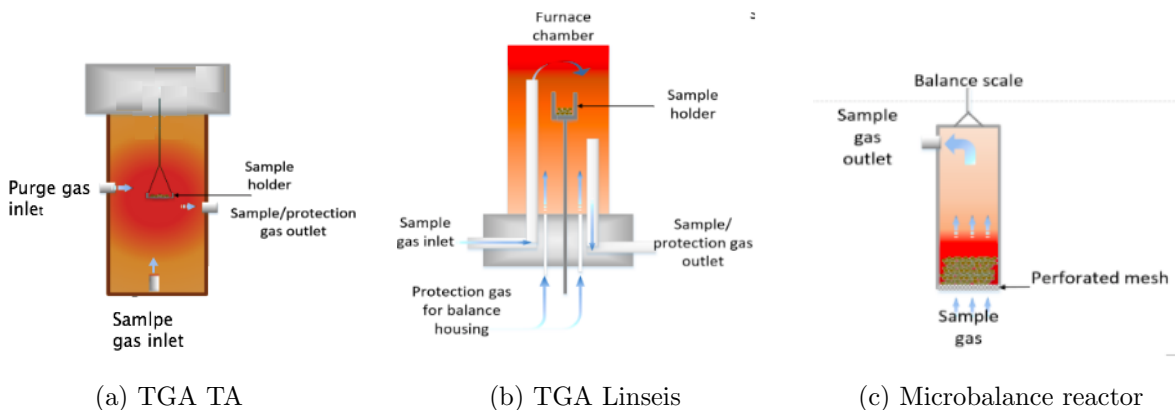


Figure 3.2: The direction of gas flow on the samples [93].

### 3.2.3 Microbalance Fixed Bed Reactor

Due to the drawbacks of experimental conditions, bypass and diffusion gradient in the TGAs discussed in the previous section, and a microbalance fixed bed reactor is preferable to obtain more realistic results. In contrast to TGA, the contact between the gas and reliable acceptors are well-controlled [22]. The microbalance fixed bed reactor will sometimes be referred to as the microbalance reactor.

The microbalance reactor is a gravimetric system where it is possible to measure weight-changes between gas and solid [22]. Figure 3.3 illustrates the connection between the flow of all the gasses, the reactor and the computer. The gasses that can be fed to the reactor are steam,  $\text{CO}_2$  and  $\text{N}_2$ .  $\text{N}_2$  is fed through three different lines; MFC1, where the gas goes directly to the evaporator. In the evaporator, the gas is mixed with the other gasses and sent to the reactor. MFC2, where it goes via a switch, the 4-way valve; depending on the position, the gas either flows to the vent or evaporator. With  $\text{CO}_2$  from MFC4 going to the vent when  $\text{N}_2$  goes to the evaporator, and vice versa. Hence  $\text{N}_2$  work as a balance gas and weight- changes are avoided when switching to the reactant gas,  $\text{CO}_2$ . MFC3, where the  $\text{N}_2$  work as a carrier-gas for the steam. A total of 800 mL/min can be fed to the reactor. The gas leaving the reactor is cooled down with a steam condenser. The dried gas ( $\text{N}_2$  and  $\text{CO}_2$ ) are analyzed with the mass spectrometer (MS) and a micro-chromatograph (GC).

The reactor is a stainless-steel fixed bed reactor, as shown in figure 3.4 [22]. The reactor is placed inside an oven ceramic tube. The gas enters at the top of the reactor, where it circulates between two concentric tubes. At the bottom, there is an open section in the middle. Here, the solid can be deposited on a support, which holes have a diameter of 0.5 mm. The gas flows through the bed of solids and enters at the top of the reactor. A hook is used to connect the microbalance and the reactor. The solids can weigh about 0.1-15 g. A thermocouple is used to control the temperature.



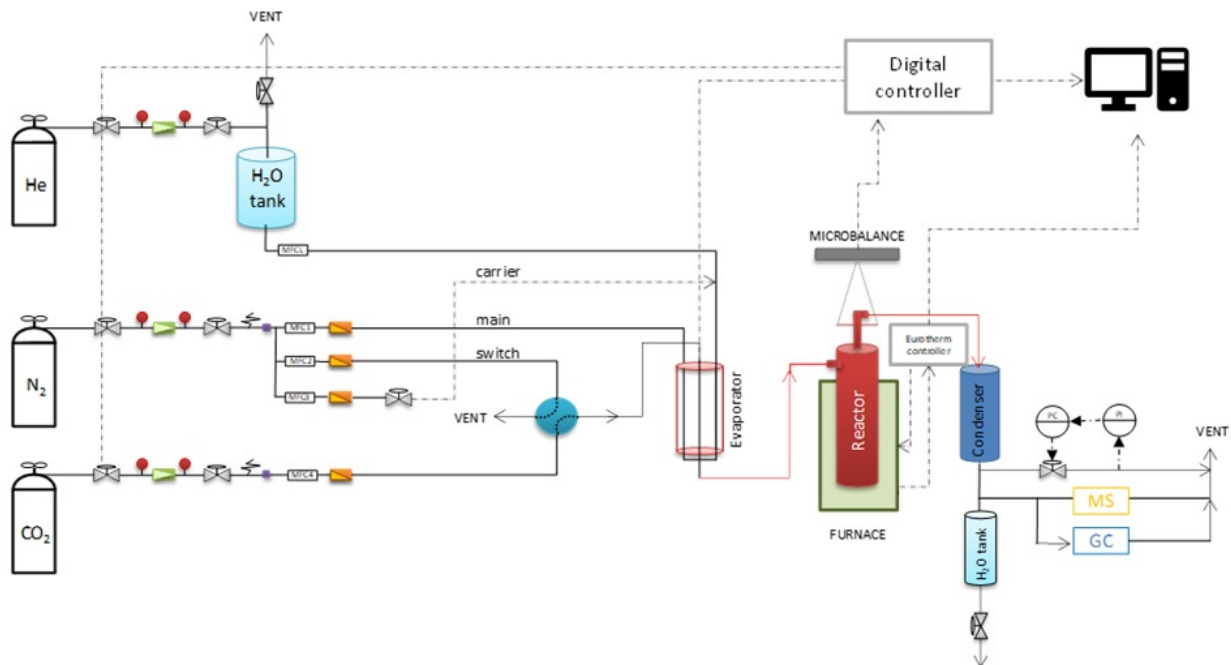


Figure 3.3: Schematics of the fixed-bed microbalance reactor [22].

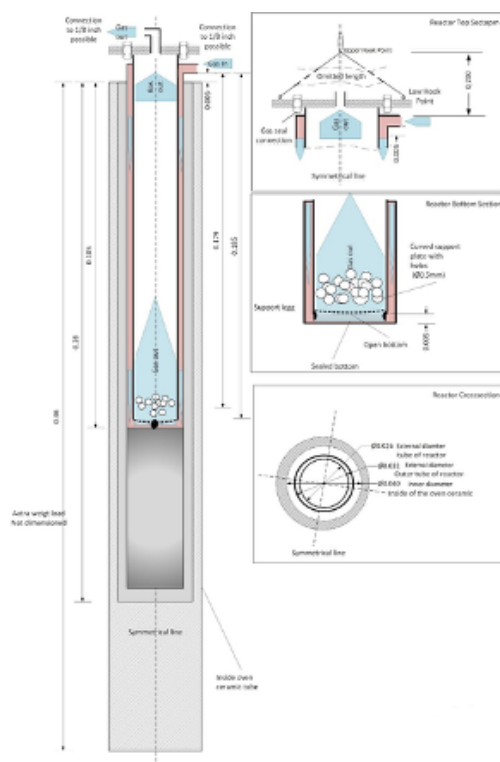


Figure 3.4: Illustration of the stainless steel reactor [22].

### 3.3 Characterization

#### 3.3.1 X-ray Fluorescence (XRF)

X-ray fluorescence is a fingerprint technique where secondary (fluorescent) X-rays are detected. The emission of X-rays is unique for all elements, making it possible to determine the composition in a sample [94].

When the primary X-rays hit an atom with sufficient energy, electrons from an inner orbital-shell can be ejected - this makes the atom unstable. To regain stability, an electron from a higher energy shell drops down to fill the hole. When the electron drops down, energy is released. The phenomenon is called X-ray fluorescence; the energy released is what is detected. From the spectrums obtained, it is possible to determine different elements. The intensity of peaks can determine the amount of the elements present.

#### 3.3.2 X-ray Diffraction (XRD)

X-ray diffraction (XRD) is a method used to find the composition of a compound. Further, the structure and particle size can be investigated. In the method, X-ray beams hit the lattice of a crystal-plane in a certain direction before it will be diffracted. A crystalline material follow Braggs law given as

$$n\lambda = 2d \sin \theta, \quad (3.1)$$

where  $\lambda$  is the wavelength of the X-rays,  $n$  an integer,  $d$  the distance between two crystal planes and  $\theta$  the angle between the crystal plane and the incoming wave [95].  $2d \sin \theta$  describes the path-difference. Figure 3.5 displays diffraction satisfying the law.

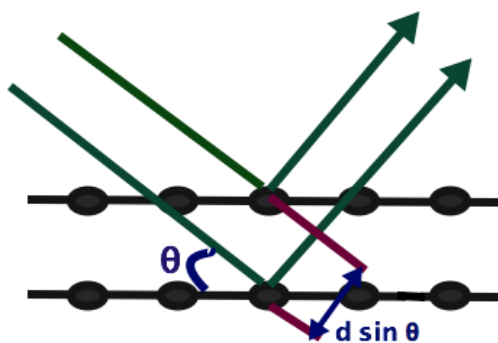


Figure 3.5: Diffraction fulfilling Braggs Law [95].

All compounds have their unique diffraction pattern [95]. In XRD analysis, this pattern will appear as a spectrum. The intensity of the diffraction is given as a function of the diffraction

angle,  $2\theta$ . If the compound is crystalline and the particles have the right orientation of the incident beam, constructive interference will happen, which is the case in figure 3.5.

The clarity of the patterns depends on the crystallinity of the particles [95]. Fully crystalline particles give patterns with narrow lines, while defects or disorder lead to more diffuse scattering. Imperfect crystals and nano-particles cause broadening of the peaks.

Crystal sizes can be estimated by using the Scherrer equation:

$$\langle L \rangle = \frac{K\lambda}{\beta \cos\theta} \quad (3.2)$$

where  $\langle L \rangle$  gives a measure of the size of the particle perpendicular to the plane reflected,  $\beta$  the breadth at half the height of the peak and  $K$  a constant [95]. For spherical particles the value is close to 0.9.

### 3.3.3 Nitrogen Adsorption-Desorption at 77 K

Textural properties of catalysts such as specific surface area ( $\text{m}^2/\text{g}$ ), pore size (nm), and pore volume ( $\text{m}^3/\text{g}$ ) are essential parameters in a catalyst. Pores of different sizes can be classified in three categories depending on the pore size: micropores ( $< 2$  nm), mesopores (2-50 nm), and macropores ( $> 50$  nm) [95]. A way to measure the properties is with Nitrogen adsorption-desorption at 77 K. From the relationship between the adsorbed gas and the relative pressure, different adsorption isotherms can be obtained.

The isotherms are classified into six different types, shown in figure 3.6 [96]. The volume of the pores restricts micropores; they will obtain an isotherm similar to type I. Macropores and nonporous material can reach an unrestricted number of multilayers; they give type II. Uniform nonporous material might give a type VI isotherm. Type III and V can occur if the adsorbate-adsorbent interactions are weak, but they are not common.

Mesoporous material will first follow a type II isotherm, where the pores will be filled until monolayer at low pressure. At point B, a multilayer will form until capillary condensation happens and gas starts to leave the pores. The gas will leave the pores at a lower pressure than it entered, known as the hysteresis effect, leading to a type IV isotherm [95, 96].

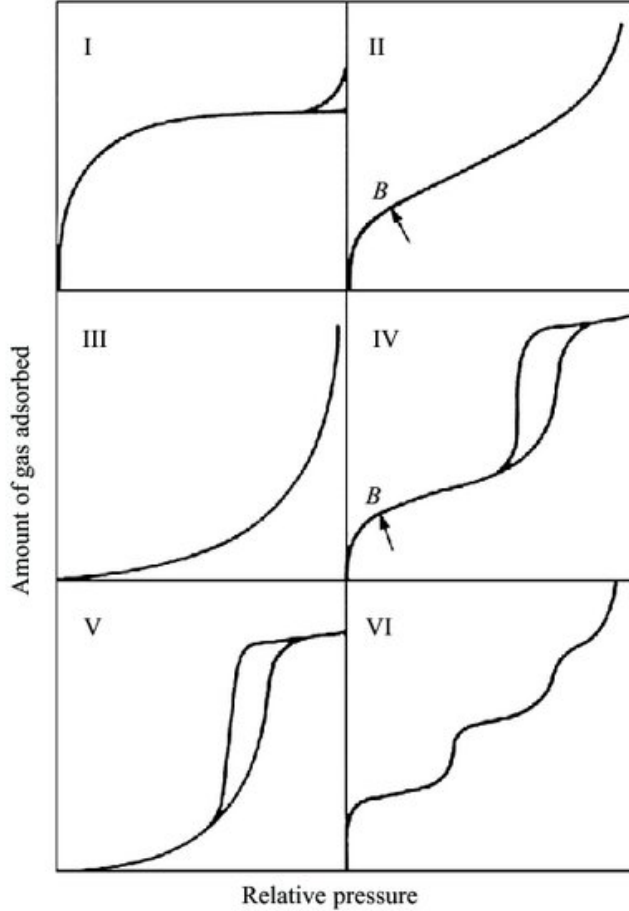


Figure 3.6: Adsorption-desorption isotherms [96].

The internal surface area is a vital aspect of catalysts; if larger, it allows a higher active area to be achieved [95, 97]. The surface area can be found from the BET-method. In the method, it is assumed that the gas is formed in layers on the surface. The specific surface area is found from the amount of gas required to form a monolayer. The method is only valid for isotherms of type II and IV. From the Brunauer-Emmet-Teller (BET)-isotherm, the relationship between  $N_2$  adsorbed at standard pressure and monolayer coverage can be found. The equation is given as

$$\frac{P}{V(P_0 - P)} = \frac{1}{V_m C} + \frac{(C - 1)P}{(V_m C)P_0} = \eta + \alpha \frac{P}{P_0} \quad (3.3)$$

where  $P$  represent the partial pressure of  $N_2$ ,  $P_0$  the saturation pressure at experimental temperature (750 mbar at 75 K for  $N_2$ ),  $V$  the volume adsorbed at  $P$ ,  $V_m$  volume adsorbed at mono-layer coverage and  $C$  a constant.

Plotting  $\frac{P}{V(P_0 - P)}$  against  $\frac{P}{P_0}$ , makes it possible to find the volume adsorbed, which further

can be used to find the surface area,  $S_{BET}$  [95, 97].  $\alpha$  represent the slope and  $\eta$  where it crosses the y-axis.

$$V_m = \frac{1}{\alpha + \eta} \quad \text{and} \quad N_0 = \frac{PV_m}{k_B T} \quad \text{and} \quad S_{BET} = N_0 A_0 \quad (3.4)$$

here  $N_0$  represent the number of molecules adsorbed,  $k_B$  is Boltzmann's constant.  $A_0$  is the area one single Nitrogen molecule occupies, assumed to be 0.162 nm<sup>2</sup> for Nitrogen at 77 K. For supported catalysts, the calculated surface area includes both the active material, as well as the support. To obtain a reliable result, the value of  $\frac{P}{P_0}$  should lay between 0.05 and 0.3.

The BET method is valid under the following assumptions:

- A dynamic equilibrium between adsorption and desorption
- Adsorption of one molecule in each site in the first layer
- No interaction between adsorbents
- From the second layer the conditions for adsorption between the layers are equal
- Adsorption energy = condensation energy for all layers, except the first
- $P = P_0$  gives a multi-layer growing to infinity

The pore-size distribution of mesopores can be found by following the BJH (Barnett, Joyner, and Halenda)-theory, assuming a spherical shape and no blocking of the pores. The most common is to calculate the desorption isotherm by following the Kelvin equation, as lower pressure is required for desorption than adsorption [96]. The equation is related to the occurrence of capillary condensation in the pores and given as

$$\ln \frac{P}{P_0} = \frac{2\sigma V \cos\theta}{r_k R T} \quad (3.5)$$

with  $\sigma$  as the surface tension of liquid Nitrogen,  $\theta$  is the contact angle,  $V$  is the molar volume of liquid Nitrogen,  $r_k$  is the radius of the pore,  $R$  the gas constant,  $T$  the absolute temperature,  $P$  the measured pressure a  $P_0$  saturation pressure [95].

The pores are full when the relative pressure  $P/P_0 = \approx 1$ . In the pore-size distribution, the pore volume is plotted against the pore size.

It is essential to note that the results obtained in Nitrogen adsorption-desorption are not accurate but can be used to obtain a relative comparison between different samples.

### 3.3.4 Electron Microscopy

Electron microscopy is a technique where primary electrons (less than 1 Å, 100-400 KeV) hits a sample and induce different signals [95]. The most common processes are shown in figure 3.7.

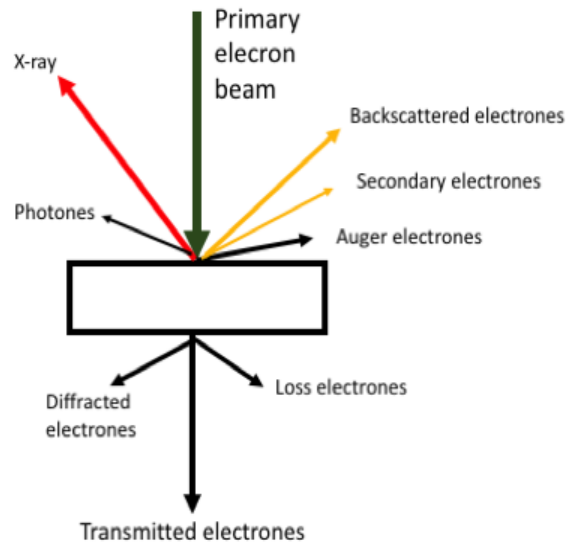


Figure 3.7: The figure shows the most common processes happening in electronmicroscopy.

#### 3.3.4.1 Scanning Electron Microscopy (SEM)

Scanning electron microscopy gives information about the topography of the surface [95]. The microscope detects the secondary or backscattered electrons. If the top of the surface points towards the detector, it becomes brighter than parts of the surface pointing in other directions. The secondary electrons have low energy (5-50 eV) and only gives information about the surface, while backscattered beams have a higher intensity and can give information about the composition of the sample. Heavier metals correspond to a brighter image. The resolution of SEM instruments is usually about 5 nm [95].

When working with SEM, it is important to consider the voltage, current, and working distance applied [98]. The voltage determines the energy of the electrons that are emitted. Decreasing the voltage generally gives a better resolution of the pictures. Low voltage is best when investigating the topography, while going further into the particle requires a higher voltage. The working distance is the distance between the lens and the specimen. A shorter working distance decreases the depth of field but increases the resolution.

### 3.3.4.2 Energy Dispersive X-ray Spectroscopy (EDS)

In similarity with XRD, crystal phases can also be detected an electron microscope [95]. energy dispersive X-ray spectroscopy (EDS) determines the unique elemental patterns from emitted X-rays. In EDS, it is possible to perform elemental mapping of the surface of the samples. Different charts can be generated, showing the location of different elements.

## 4 Experimental Procedure

In this section, the way the sorbents were prepared is described, followed by the procedure used for testing and characterizing them. The section is partly taken from the specialization project during spring 2020, as many of the experiments were similar [1].

### 4.1 Synthesis of the sorbent by the one-pot method

In the project, a total of 23 sorbents were prepared. They were prepared according to the one-pot method, described in section 3.1.

The CaO-based base material and additives were calcined dolomite ( $\text{CaO} \cdot \text{MgO}$ ), Calcium aluminate cement and Zirconium dioxide ( $\text{ZrO}_2$ ) or Cerium dioxide ( $\text{CeO}_2$ ). As previously described, employing Zr or Ce as a stabilizer, and cement both as a stabilizer and a binder. A 35 wt % Zirconyl solution was used as a precursor for  $\text{ZrO}_2$ , and a  $\geq 99\%$  Cerium(III) nitrate hexahydrate in solid form for  $\text{CeO}_2$ , both supplied by Sigma Aldrich. The dolomite was from Franzefoss Miljøkalk and the cement of type Fondu by Kerneos.

#### 4.1.1 Material preparation

Dolomite was calcined in air at a ramp of  $5\text{ }^\circ\text{C}/\text{min}$  up to  $800\text{ }^\circ\text{C}$  before the temperature was kept constant for 6 hours. It was then cooled down to room temperature before it was milled to a diameter of less than  $90\text{ }\mu\text{m}$ . The cement was dried in an oven overnight at  $120\text{ }^\circ\text{C}$ .

Water was added to the Zirconium solution to a total amount close to the pore volume of dolomite. The calculations are given in appendix B. Sorbents prepared with Cerium were mixed with water corresponding to the pore-volume of dolomite in an Erlenmeyer flask. In advance of the experiment, it was checked if the amount of water was enough to solve the Cerium. The solution was mixed using a spatula before it was placed in an ultrasonic bath for some minutes in order to ensure homogeneity. The solutions of Zirconium or Cerium mixed with water will sometimes be referred to as the prepared stabilizer solution in the next part of this section.

11.5 g of dolomite together with desired weight-percentages of the additives were used. Detailed calculations are given in the appendix A.

#### 4.1.2 One-pot process

The compounds were mixed in two different ways following the one-pot method, which will be referred to as the one-step method and two-step method.



**One-step method:** Dolomite and cement were mixed and milled homogeneously using a mortar and spatial. The obtained powder was transferred to a plate before the prepared stabilizer solution was added dropwise, under continuous mixing by using a spatial and a mortar, and gently shake the plate.

**Two-step method:** Dolomite was milled homogeneously using a mortar and spatial in order to get a fine powder. The prepared stabilizer solution was then added dropwise by incipient wetness impregnation, under continuous mixing by using spatial and mortar. The mixture was then dried for three-four hours. The dry material was milled in order to get a fine powder before it was mixed with cement, again using a mortar and a spatial, before the mixture was transferred to a plate.

After some time, while continuing mixing, water was sprayed on until dark grey pellets were formed. It was crucial not to add the water to slow in order to avoid evaporation. It was also important to make pellets of small sizes, as the desired size for testing was 500-850  $\mu\text{m}$ . In the end, the pellets were dried at room temperature for three days before calcination, following the procedure described in section 4.1.3. The pellets were then sieved in order to separate those under, between, and over 500-850  $\mu\text{m}$ . Milling was done to obtain an adequate amount of sample with the medium size for cyclic testing. In figure 4.1 the evolution of sorbent with  $\text{ZrO}_2$ , prepared by the two-step method is illustrated. The process presented is from mixing the prepared Zirconium solution with calcined dolomite to separating the final sorbents into the desired sizes.

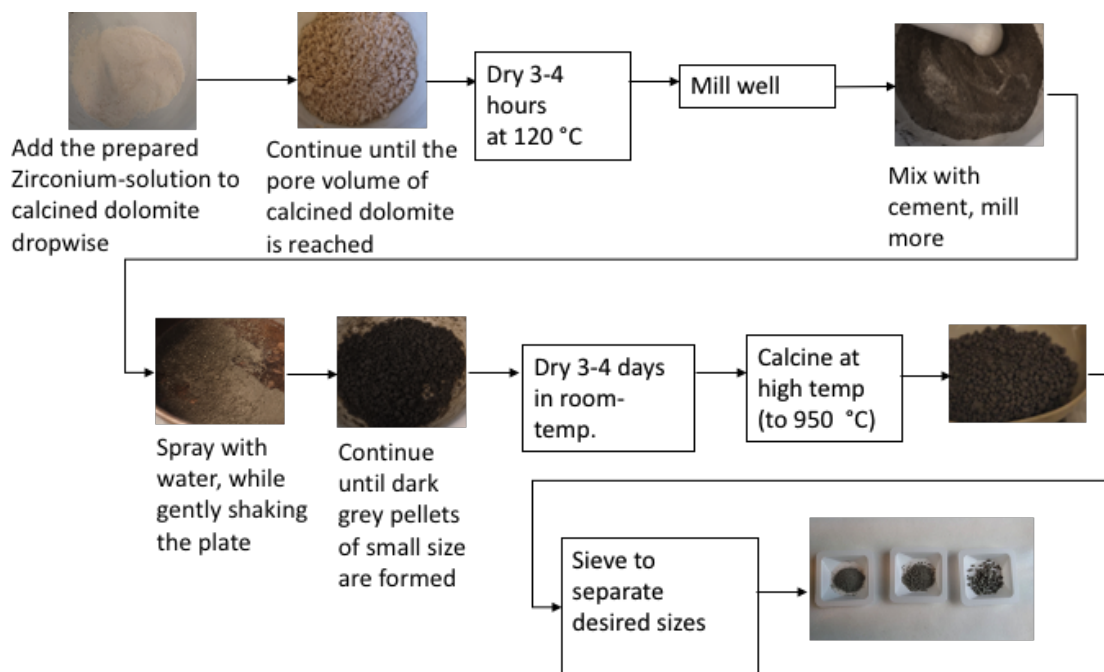


Figure 4.1: Illustration of the preparation of a two step sorbent with  $\text{ZrO}_2$  as the stabilizer.

In addition, two sorbents were made by only mixing cement and dolomite; they were made by the one-step method but without the addition of any prepared stabilizer solution. In this way, it was possible to understand the stabilizing effect of cement on its own.

It was desirable to see the effect of calcining the dolomite; therefore, one sorbent was prepared with uncalcined dolomite instead of calcined. It was also desired to see if there were any differences between drying the mixture of dolomite and the Zirconium solution compared to performing intermediate calcination. For that reason, one sorbent was made in two steps, but with intermediate calcination before adding cement. The calcination was in an atmosphere of air at a ramp of 5 °C/min up to 800 °C before the temperature was kept constant for 6 hours.

Table 4.1 gives a summary of sorbents synthesized, including the name of the sample, the method used to prepare them, and the weight percentages (wt%) of Zirconium, Cerium, and Aluminium. The total weight of the sorbents were assumed to be the dolomite, cement, and  $ZrO_2$  or  $CeO_2$ .

The sample names mainly consist of three parts; the method used to create them, the weight percentage of Zr or Ce, and the weight percentage of Aluminium in the sorbents. After the number representing the weight-percentages of the elements, their chemical symbols are given. For instance, 1S(1.3Zr,13Al) is made in one step, consist of 1.3 wt% of Zirconium and 13 wt% weight-percentages of Aluminium from Cement. 2S(5.5Ce,10Al) is made by the two-step method and consists of 5.5 wt% of Zirconium and 10 wt% of Aluminium. 11Al and 15Al are the sorbents only made with cement and dolomite, consisting of 11 wt% and 15% Aluminium from cement, respectively. 1SUncalc(5.5Zr,10Al) and 2SInter(5.5Zr,10Al) refers to the sorbents made with uncalcined dolomite and intermediate calcination, respectively.

Sorbents with similar compositions were prepared in two different batches. In this way, the reproducibility could be tested. Their names will consist of "a" or "b" after the 1S, for instance, 1Sa(5.5Zr,10Al) and 1Sb(5.5Zr,10Al), where a is produced in the first batch and b in the second.

Table 4.1: The weight percentages (wt%) of Zirconium, Cerium and Aluminium in the sorbents and the method used to create them.

| Sample               | Method | Zr [wt %] | Ce [wt %] | Al [wt %] |
|----------------------|--------|-----------|-----------|-----------|
| 1S(1.3Zr,13Al)       | 1-step | 1.3       | -         | 13.4      |
| 2S(1.3Zr,13Al)       | 2-step | 1.3       | -         | 13.4      |
| 1S(2.6Zr,13Al)       | 1-step | 2.6       | -         | 13.3      |
| 2S(2.6Zr, 13Al)      | 2-step | 2.6       | -         | 13.1      |
| 1S(3.8Zr,13Al)       | 1-step | 3.8       | -         | 12.9      |
| 1S(5.0Zr,13Al)       | 1-step | 5.0       | -         | 12.7      |
| 2S(5.0Zr,13Al)       | 2-step | 5.0       | -         | 12.7      |
| 1S(5.5Zr,10Al)       | 1-step | 5.5       | -         | 10.0      |
| 1SUncalc(5.5Zr,10Al) | 1-step | 5.5       | -         | 10.0      |
| 2S(5.5Zr,10Al)       | 2-step | 5.5       | -         | 10.0      |
| 2SInter(5.5Zr,10Al)  | 2-step | 5.5       | -         | 10.0      |
| 1S(1.5Zr,10Al)       | 1-step | 1.5       | -         | 10.3      |
| 1S(6.0Zr,9Al)        | 1-step | 6.0       | -         | 9.0       |
| 2S(6.0Zr,9Al)        | 2-step | 6.0       | -         | 9.0       |
| 1S(1.8Zr,6Al)        | 1-step | 1.8       | -         | 6.05      |
| 1S(5.5Ce,10Al)       | 1-step | -         | 5.5       | 10.0      |
| 2S(5.5Ce,10Al)       | 2-step | -         | 5.5       | 10.0      |
| 15Al                 | -      | -         | -         | 15.0      |
| 11Al                 | -      | -         | -         | 10.8      |

During the whole text, sorbents containing Zirconium and Aluminium will sometimes be referred to as the ZrAl-based sorbents. The ones made of Cerium and Aluminium as the CeAl-based sorbents. Sorbents prepared by the one-step method will be referred to as 1S-sorbents and sorbents prepared by the two-step method as 2S-sorbents.

#### 4.1.3 Calcination conditions

The dry sorbents were calcined in an atmosphere of air - this calcination will later in the text be referred to as the pre-calcination. The procedure was as follows;

**Step 1** Increase the temperature from room-temperature with 1 °C/min to 400 °C (6hours).

**Step 2** Keep isothermal for 2 hours.

**Step 3** Increase the temperature with a ramp of 1.4 °C/min to 650 °C.

**Step 4** Keep isothermal for 1 hour.

**Step 5** Increase the temperature with a ramp of 2 °C/min to 950 °C.

**Step 6** Keep isothermal for 6 hours.

**Step 7** Cool down to room temperature.

A scheme of the procedure is shown in figure 4.2. The y-axis gives the temperature in °C and the x-axis the time in hours.

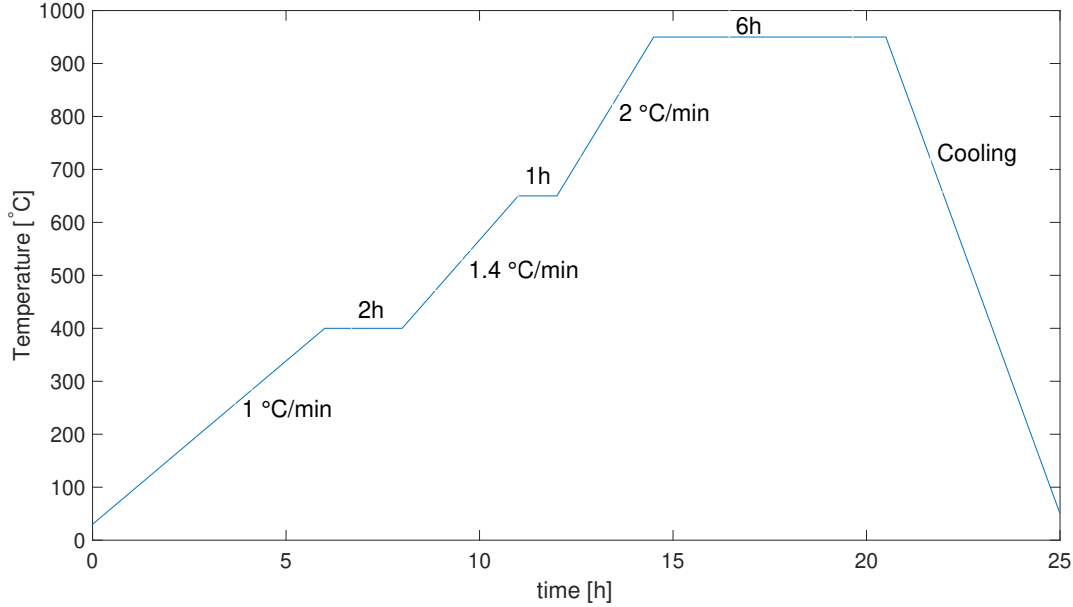


Figure 4.2: Calcination procedure for all the sorbents.

## 4.2 Testing of cyclic performance

Analysis were performed on the pre-calcined pellets in order to find the CO<sub>2</sub> capturing capacity, and most importantly the ability to stay stable over several regeneration-cycles. Mass-changes were assumed to only be due to adsorption and desorption of CO<sub>2</sub>. The increase in weight with time in each cycle  $m_{\text{increase},j,t}$ , was measured to be

$$m_{\text{increase},j,t} = m_{j,t} - m_{j,0}. \quad (4.1)$$

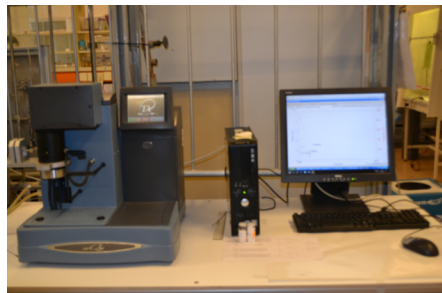
Here  $m_{j,t}$  refers to the mass of the sorbent in cycle  $j$  at time  $t$  and  $m_{j,0}$  the first mass measured in cycle  $j$ .

From this the capturing capacity,  $C_{j,t}$  in cycle  $j$  at time  $t$  was calculated to be

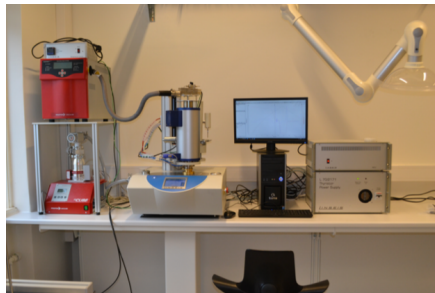
$$C_{j,t} = \frac{m_{\text{increase},j,t}}{m_{\text{original}}} \cdot 100\%. \quad (4.2)$$

with  $m_{\text{original}}$  referring to the weight of the loaded sample. The capacities in each cycle were found using Matlab; both the increase in capacity with time and the highest capacity achieved after a certain time of adsorption. The scripts are given in appendix F.

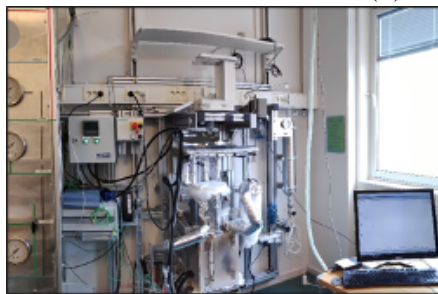
The experiments were performed in two different conditions; wet- and dry carbonation conditions. It is understood in the presence of steam and not. In the wet, the experiments were more close to realistic conditions. Two different TGAs were applied. The experiment in dry conditions was performed in TGA Instruments TGA TA Q500 and the experiment in wet conditions in Linseis Thermal Analysis STA PT1600, which, as mentioned, will be referred to as TGA TA and TGA Linseis. Furthermore, for the sorbents showing the best performance, experiments were performed in the micro-balance reactor, where more realistic conditions are possible. Figure 4.3 shows the set-up of the three instruments.



(a) TGA TA



(b) TGA Linseis



(c) Microbalance reactor

Figure 4.3: The setup of the different instruments used to test the cyclic performance of the sorbents [22, 99]

#### 4.2.1 TGA TA

In order to check the stability in dry conditions, analyzes were run in TGA TA. About 10-15 mg of the samples with a diameter of 500-850  $\mu\text{m}$  were loaded on to the sample holder.

The analyzes started with increasing the temperature to the desorption-temperature in order to make sure samples free of impurities like  $\text{CO}_2$  or water vapor after exposure to air. The adsorption was at 600  $^\circ\text{C}$  in a total of 30 minutes in an atmosphere consisting of Nitrogen and 5 %  $\text{CO}_2$ . The desorption was at 900  $^\circ\text{C}$  in pure Nitrogen. The total flow was 146 ml/min.

The procedures are given below.

**Step 1** Increase the temperature with 10 °C/min to 900 °C in pure N<sub>2</sub>. Keep isothermal for 15 minutes.

**Step 2** Decrease the temperature with 20 °C/min to 600 °C. Stabilize for 10 minutes.

**Step 3** Introduce 5 % CO<sub>2</sub>. Keep for 30 minutes.

**Step 4** Repeat step 1-3 for ten times.

#### 4.2.2 TGA Linseis

In the TGA Linseis, the experiments were conducted in wet conditions, which means that water vapor was introduced. Argon 5.0 was used as a purge gas. The rest of the atmosphere consisted of air and CO<sub>2</sub> 5.2. Due to set-up requirements, the flow of the purge was never lower than 60 ml/min. Prior to the experiment, a correction-file was made by running an experiment using empty, pre-weighed crucibles. The possible effect the crucibles have on the experiment was then eliminated, as well as the weight change due to the different total flows.

About 10 mg of the sample (500-850 μm) was weighted in one of the crucibles before loaded into the micro-balance. As in TGA TA, the program started with increasing the temperature to the desorption-temperature. A total of 15 cycles were chosen. The adsorption was at 600 °C in 5 % CO<sub>2</sub> and 8 % H<sub>2</sub>O. The adsorption-time was set to a total of 30 minutes. At 730 °C, the flow of water was removed, and the atmosphere consisted of about 80 % CO<sub>2</sub>. The desorption temperature was 950 °C. More closely, the analysis run according to the following procedure:

**Step 1** Increase the temperature from ambient to 850 °C with a ramp of 7.5 °C/min in 50 % purge and 50 % Nitrogen, with a flow of 200 ml/min. Keep isothermal for 5 minutes.

**Step 2** Decrease the temperature with a ramp of 6.25 °C/min to 600 °C in the same atmosphere as step 1.

**Step 3** Introduce water steam, being 8 % of a total flow of 400 ml/min. Keep constant for 25 minutes.

**Step 4** Introduce 5 % CO<sub>2</sub>, remaining the same total flow of 400 ml/min. Keep for 30 minutes. This is when the adsorption will happen.

**Step 5** Remove the flow of water, giving a flow of 5 % CO<sub>2</sub> and 45 % Nitrogen, with a total flow of 400 ml/min. Increase the temperature to 730 °C with a ramp of 7.5 °C/min.

**Step 6** Change the flow to consist of 200 ml/min of CO<sub>2</sub> with only the necessary amount of purge, to a total flow of 260 ml/min. With a ramp of 7.5 °C/min, increase the temperature to the one for desorption, 950 °C.

**Step 7** Keep constant for 6 minutes.

**Step 8** Repeat step 2-7 15 times.

**Step 9** Decrease the temperature to 600 °C in 1.2 hours.

**Step 10** Keep the temperature constant for 20 minutes before cooling down to 200 °C in 1 hour.

**Step 10** Reduce the flow to the half and cool down to 100 °C in 30 minutes.

**Step 11** Cool down to room temperature

For the sorbents showing the highest stability, the whole program was repeated more times. A simplified scheme is shown in figure 4.4. The changes in temperature, as well as flow of CO<sub>2</sub> and water, are plotted against time.

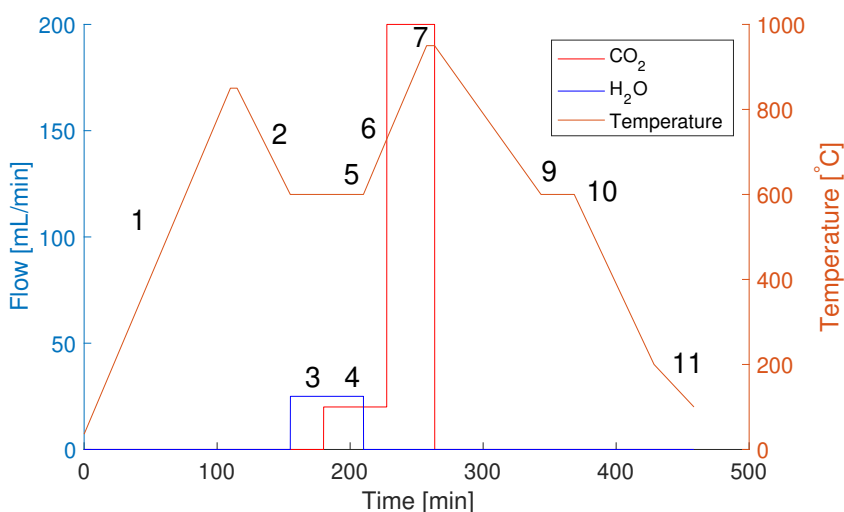


Figure 4.4: Simplified scheme of the Program used in TGA Linseis.

### 4.2.3 Microbalance Fixed Bed Reactor

Around 1 g of the middle-sized sorbent (500-850  $\mu\text{m}$ ) was placed on the support and inserted into the reactor. The testing was performed similarly to the experiments in TGA Linseis, 4.2.2. Though with some small differences: Instead of Argon and air, Nitrogen was used as the inert gas. The total flow was 800 mL/min. At a temperature of 870 °C, after stabilization, the 4-wave-valve was switched, and the gas entering the evaporator was changed from N<sub>2</sub> to CO<sub>2</sub>. The capacity was found after six minutes of adsorption. The desorption was in 100 % CO<sub>2</sub>. The number of cycles varied - the exact-values will be given in the results section.

## 4.3 Characterization

### 4.3.1 X-Ray Fluorescence Spectroscopy (XRF)

The composition of dolomite, cement, and two of the sorbents was obtained through X-Ray Fluorescence Spectroscopy.

About 3 g of the binder  $\text{H}_3\text{BO}_3$  and 200 mg of the sample were weighted. The accuracy of the measurement was crucial; it was important to use equipment that did not cause any loss of sample or contamination and to notice the exact weights. The acid and sample were mixed and milled thoroughly for at least ten minutes to get a homogeneous mixture.

Then, the mixture was transferred to a pellets form. A plastic straw was used in order to lose as little powder as possible. The mixed sample was pressed in the pressing-machine at ten tons, following instructions for the machine. After ten minutes, the pressure was released slowly. The obtained pellets were carefully placed in a solid sample holder with plastic under it. A sample retainer was used to press the pellets down carefully. It was important not to ruin the pellet.

In the end, the sample was transferred to the XRF analyzer, Rigaku Supermini200, where EZ analysis was performed.

### 4.3.2 X-ray Diffraction (XRD)

XRD was performed on fresh sorbents and a selection of spent sorbents. The approach was similar for all the samples, with a small difference for the spent.

Fresh, calcined pellets less than 0.5 mm were milled in order to obtain a fine powder before transferring it to a sample holder. A smooth surface was ensured. In the case of spent samples, pellets were milled into a fine powder before mixed with droplets of ethanol and transferred to sample holders of the type "Si-flat."

The diffractometer D8-Focus was used for the analyzes, where a  $2\theta$ -range of 5-105 ° and a step size of 0.020 were chosen. The total time was 30 minutes, and the divergence slit opening 0.6 mm. The X-ray wavelength was 1.54 Å.

The results were saved in the software DIFFRA.EVA v5.1 and the phases could be identified using the Crystallography Open Database (REV212673 2018.12.20). Crystal sizes were calculated according to Scherrer equation, equation 3.2. A value of  $K = 0.89$  was used.

### 4.3.3 Nitrogen Adsorption-Desorption at 77 K

The surface area and pore size distribution of a selection of fresh and spent sorbents were found by nitrogen adsorption-desorption at 77 K. About 1 g of sorbents with size 500-800



$\mu\text{m}$  were put into already weighted sample holders. A VacPrep 061 was used to degass the samples. After one hour in the cooling station, they were transferred to the heating station where they stayed at  $300\text{ }^{\circ}\text{C}$  overnight in order to reach a pressure of less than 100 mTorr in the degas-unit.

The measurements were done in the BET machine, Micromeritics TriStar II 3020 Surface Area and Porosity Analyzer. The weight of the sample holders with the sample after degassing and after the BET was recorded. The first weight was used when creating the file and the last when creating the report. BET/BJH was chosen as the method. The obtained data gave the BET-surface area according to the BET isotherm (equation 3.3 and 3.4), with relative pressures ranging from 0.1-0.3. The pore size distribution was found until a relative pressure of Nitrogen adsorbed equal to 0.995.

#### **4.3.4 Scanning Electron Microscopy (SEM)**

Investigation of the morphology was performed on a selection of fresh and spent sorbents using SEM APREO. The instrument is located in ISO 6 cleanroom.

Samples of size 500-850  $\mu\text{m}$  were attached to carbon tape on a metal holder and placed into the chamber. The instrument was started following the procedure placed by the instrument. Pictures were taken at different magnifications. For the magnification of 120, pictures were taken with the ETD-detector at a working distance of about 10 mm, 5 kV voltage, and 0.4 nA current. The other pictures were taken by using a T2-detector in immersion mode, with a working distance of about 4 mm, Voltage of 2 KV, and current of 12 pA. In all cases, there were  $0^{\circ}$  rotation and  $0^{\circ}$  tilt.

#### **4.3.5 Energy Dispersive X-ray Spectroscopy (EDS)**

Elemental mapping was performed on a selection of samples using the EDS detector in SEM APREO. Calcined dolomite and Cement Fondu were also included as references.

Sorbents of size 500-850  $\mu\text{m}$  were attached to carbon tape on a metal holder and placed into the chamber. Calcined dolomite less than  $90\mu\text{m}$  and cement were added in their powder form. The instrument was started following the procedure placed by the instrument.

The elemental mapping was performed at 3500 magnification with a working distance of about 10 mm, a current of around 1.6 nA, and a voltage of 10 kV. The most important was to keep the output count-rate relatively high. The dwell time was chosen in order to give a mapping taking about 3 minutes. In addition, reference pictures were taken at the same place using the ETD detector lowering the current and voltage. In all cases, there were  $0^{\circ}$  rotation and  $0^{\circ}$  tilt.

## 5 Results and Discussion

In the following section, all the results obtained through characterization and cyclic testing will be presented, together with a discussion. Some sorbents were prepared during the specialization project in spring 2020 [1]. This accounts for the following sorbents: 1Sa(1.3Zr,13Al), 1Sb(1.3Zr,13Al), 1S(2.6Zr,13Al), 1S(3.8Zr,13Al), 1Sa(5.0Zr,13Al), 1S(1.5Zr,10Al) and 1S(1.8Zr,6Al). Much of the characterization was done during the work of the master-project.

### 5.1 Cyclic testing

As described in section 4.2, the cyclic stability of the sorbents was tested both in wet and dry conditions. This section will discuss the sorbents tested in dry conditions in TGA TA and sorbents tested in wet conditions in TGA Linseis. Several factors will be considered, including the method used to create them, reproducibility, repeatability, the effect of calcination, and diffusional limitations in the set up used. In the end, the cyclic stability for two sorbents tested in the microbalance fixed bed reactor will be presented.

The capacities were calculated as explained in section 4.2. Appendix F gives examples of Matlab codes created to calculate the capacities in the different conditions. In all the plots presenting the capturing capacities during cycles, the x-axis will represent the number of cycles, while the y-axis the capturing capacity in percentage.

#### 5.1.1 Dry conditions

The cyclic performance of several of the prepared sorbents was, as explained in section 4.2.1 tested in dry conditions in TGA TA, hence in the absence of steam. The adsorption took place at a temperature of 600 °C in an atmosphere consisting of 5 % CO<sub>2</sub> in N<sub>2</sub> and the desorption in pure Nitrogen at 900 °C.

##### 5.1.1.1 ZrAl-based sorbents

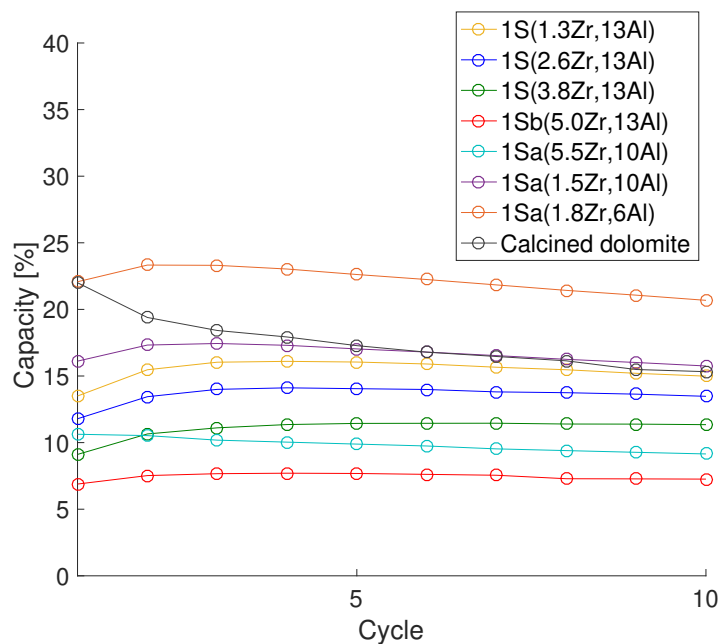
Figure 5.1 shows the capturing capacities during 10 cycles for ZrAl-sorbents tested after 30 minutes of adsorption. Figure 5.1a presents sorbents prepared in one step compared to calcined dolomite. Furthermore, in order to see differences between the sorbents prepared in one (circle) or two (star) steps in dry conditions, the capacity vs. cycle for four sorbents are also represented in figure 5.1b. The capacities in cycle 1, 3, and 10 and the capacity losses from cycle 3-10 are represented in table 5.1. Besides, the influence of varying the content of Aluminium and Zirconium are shown as bar-plots in figure 5.2a and 5.2b respectively. Other variables are kept constant. The y-axes show the capacity in cycle 3 in percentage, while

the x-axes show the weight percentage of the changing element.

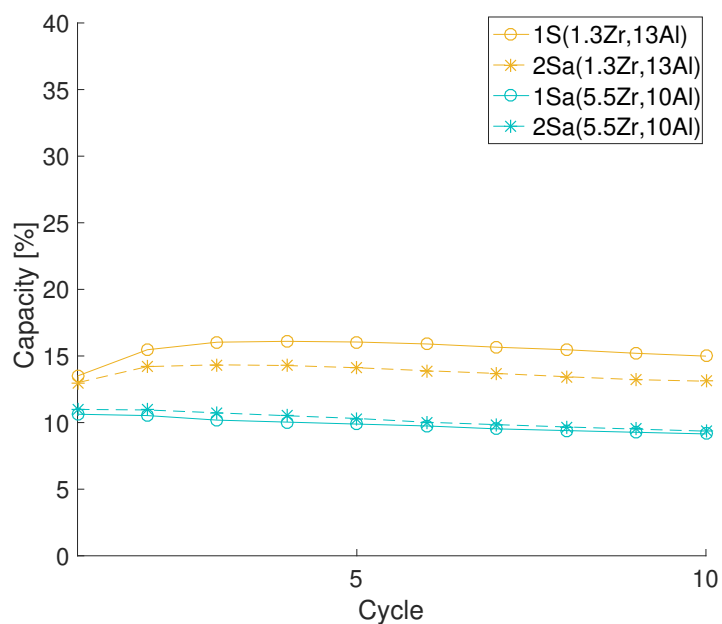
All the modified sorbents, except 1Sa(1.8Zr,6Al), have lower capturing capacities than calcined dolomite. There is a clear improvement in the performance of the modified sorbent in terms of stability compared to calcined dolomite. Calcined dolomite (black line) has a capacity loss of 16.8 % from cycle 3 to 10, and the capacity loss for the modified sorbents lies in the range of -2.1 % to 12.8 %.

As it was expected, the sorbent with the lowest content of additives, 1Sa(1.8Zr,6Al), has the highest capacity, while the sorbent with the highest amount, 1Sb(5.0Zr,13Al) the lowest capacity with cycles. The bar plots comparing the capacity losses (figure 5.2) demonstrates that both when decreasing the Aluminum content, as well as the Zirconium content, the capturing capacity decrease. The observations verify that the fraction of both modifiers in the sorbent influences its capacity.

When considering the cyclic stability, the trend between the modified sorbents is not as clear. Nevertheless, very good stability was obtained in dry conditions. The best among the sorbents tested was 1S(3.8,13Al), which showed a negative value in the capacity loss from cycle 3-10 (-2.1 %). However, it is essential to highlight the mild reaction-conditions applied. The dry conditions experiments were mostly used as a preliminary study to see if the sorbents showed an adequate performance in cyclic stability to continue further testing. For that reason, also only a short number of cycles were tested. As discussed in section 1.5, the conditions of both the carbonation and calcination impact how well the sorbents capture CO<sub>2</sub>. In the next section, experiments performed in more realistic conditions will be presented.



(a) 1S-sorbents

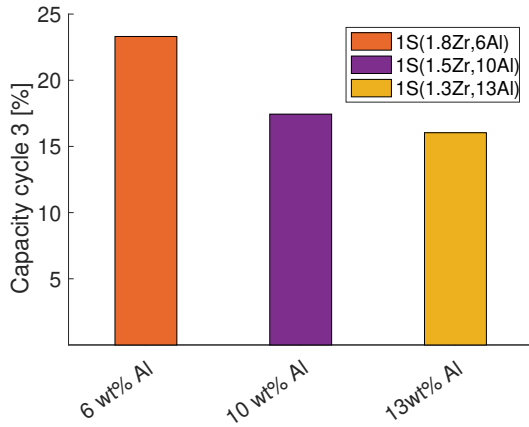


(b) 1S-sorbents vs. 2S-sorbents

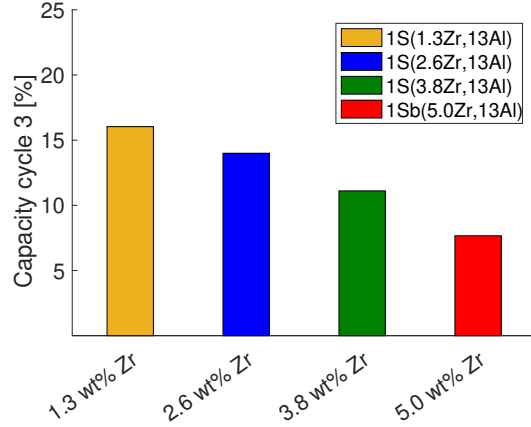
Figure 5.1: The capturing capacity of calcined dolomite and all ZrAl-based sorbents tested in dry conditions (1S(1.3Zr,13Al), 1S(2.6Zr,13Al), 1S(3.8Zr,13Al), 1Sb(5.0Zr,13Al), 1Sa(5.5Zr,10Al), 1Sa(1.5Zr,10Al), 1Sa(1.8Zr,6Al), 2Sa(1.3Zr,13Al), 2Sa(5.5Zr,10Al)). Ads: 5 % CO<sub>2</sub>, 600 °C, 30 min. Des: N<sub>2</sub>, 900 °C

Table 5.1: The capacity in different cycles ( $c_i$ ), and capacity loss ( $c_{i-j}$ ) for ZrAl-based sorbents. Calcined dolomite is included for comparison. Ads: 5% CO<sub>2</sub>, 600°C, 30 min. Des: % N<sub>2</sub>, 900°C

| Sample            | Capacity [%] |       |          | Capacity loss [%] |
|-------------------|--------------|-------|----------|-------------------|
|                   | $c_1$        | $c_3$ | $c_{10}$ | $c_{3-10}$        |
| Calcined dolomite | 22.0         | 18.4  | 14,5,3   | 16.8              |
| 1S(1.3Zr,13Al)    | 13.5         | 16.0  | 15.0     | 6.5               |
| 2Sa(1.3Zr,13Al)   | 13.0         | 14.3  | 13.1     | 7.7               |
| 1S(2.6Zr,13Al)    | 11.8         | 14.0  | 13.5     | 3.7               |
| 1S(3.8Zr,13Al)    | 9.1          | 11.1  | 11.3     | -2.1              |
| 1Sb(5.0Zr,13Al)   | 6.99         | 7.7   | 7.3      | 5.3               |
| 1Sa(5.5Zr,10Al)   | 10.6         | 10.2  | 9.1      | 10.2              |
| 2Sa(5.5Zr,10Al)   | 11.0         | 10.7  | 9.4      | 12.8              |
| 1S(1.5Zr,10Al)    | 16.1         | 17.4  | 15.8     | 7.6               |
| 1S(1.8Zr,6Al)     | 22.1         | 23.3  | 20.7     | 11.3              |



(a) Different Al content



(b) Different Zr content

Figure 5.2: Comparison of the capturing capacity in cycle 3 for similar sorbents varying the Al (a) or Zr (b) content. (1S(1.8Zr,6Al), 1S(5.5Zr,10Al), 1S(1.3Zr,13Al). 1S(2.6Zr,13Al), 1S(3.8Zr,13Al), 1S(5.0Zr,13Al) Ads: 5 % CO<sub>2</sub>, 600 °C, 30 min. Des: N<sub>2</sub>, 900 °C

### 5.1.1.2 Pellets vs. crushed sample

To see if the pellets caused any diffusional (500-850  $\mu\text{m}$ ) limitations during testing, a crushed sample was tested in dry conditions (Ads: 5 %  $\text{CO}_2$ , 600  $^\circ\text{C}$ , 30 min. Des:  $\text{N}_2$ , 900  $^\circ\text{C}$ ).

Figure 5.3 displays the capturing capacities during 10 regeneration-cycles for 2Sa(5.5Zr,10Al) in the form of pellets and crushed. Table 5.2 gives the capacities in cycle 1, 3, and 10, as well as the capacity loss from cycle 3-8 and cycle 3-10 for the three tests.

There is not any noteworthy difference in the capacity between the pellets and the crushed samples. Actually, their trends are close to identical - indicating that diffusional limitations in the pellets are not a limiting factor.

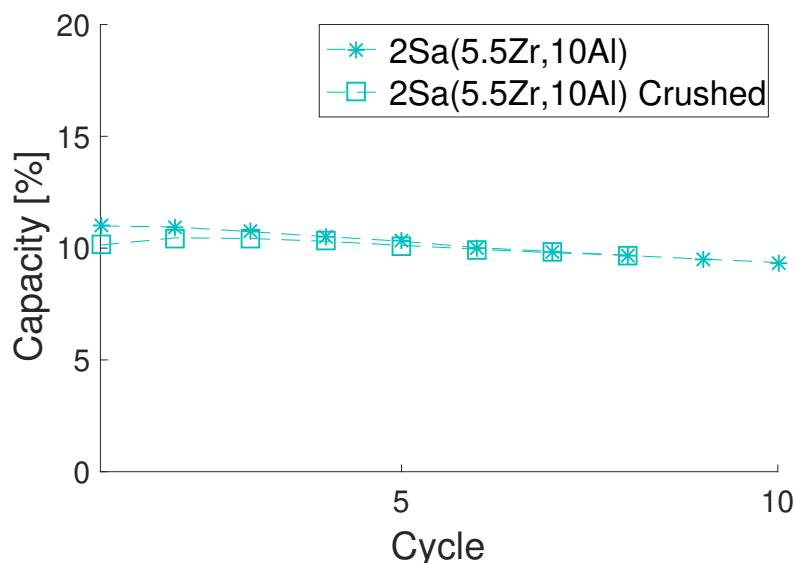


Figure 5.3: The capturing capacity of 2S(5.5Zr,10Al) as pellets (500-850  $\mu\text{m}$ ) and crushed. Ads: 5 %  $\text{CO}_2$ , 600  $^\circ\text{C}$ , 30 min. Des:  $\text{N}_2$ , 900  $^\circ\text{C}$

Table 5.2: The capacity in different cycles ( $c_i$ ) and capacity loss ( $c_{i-j}$ ) for 2S(5.5Zr,10Al) as pellets (500-850  $\mu\text{m}$ ) and crushed. Ads: 5 %  $\text{CO}_2$ , 600  $^\circ\text{C}$ , 30 min. Des: %  $\text{N}_2$ , 900  $^\circ\text{C}$

| Sample                  | Capacity [%] |       |          | Capacity loss [%] |            |
|-------------------------|--------------|-------|----------|-------------------|------------|
|                         | $c_1$        | $c_3$ | $c_{10}$ | $c_{3-8}$         | $c_{3-10}$ |
| 2Sa(5.5Zr,10Al)         | 11.0         | 10.7  | 9.4      | 9.9               | 12.8       |
| 2Sa(5.5Zr,10Al) crushed | 10.1         | 10.4  | -        | 7.1               | -          |

### 5.1.1.3 Reproducibility

In order to check the reproducibility of the synthesis method, identical sorbents were prepared in two batches. They were alike both in the ways they were prepared and the compositions of the materials. Four pairs of identical batches were produced.

Figure 5.4a presents the capturing capacity against a total number of 10 cycles for two pairs of 1S-sorbents, figure 5.4b presents the same for 2S-sorbents. "a" and "b" represent the first and second batch. All the sorbents were tested in dry conditions (Ads: 5 % CO<sub>2</sub>, 600 °C, 30 min. Des: N<sub>2</sub>, 900 °C). Table 5.3 give capacities in cycle 1,3 and 10 and the capacity loss from cycle 3-10.

The graphics demonstrate that it was possible to reproduce the sorbents. For 2S-sorbents, the tendency of the first and second batch is close to identical. However, there is a minor difference between the sorbents prepared in the first and second batch for the 1S-sorbents. For instance, 2Sa(1.3Zr,13Al) and 2Sb(1.3Zr,13Al) both have capacities close to 13 % in cycle 10, and 2Sa(5.5Zr,10Al) and 2Sb(5.5Zr,10Al) both have capacities of 9.4 %. For the two pairs of 1S-sorbents, the difference between batch one and batch two is in both cases close to 2 %. Also, the capacity loss from cycle 3-10 is noteworthy higher for 1Sa(5.5Zr,10Al) compared to 1Sb(5.5Zr,10Al) with the values of 17.2 % and 5.3 %, accordingly.

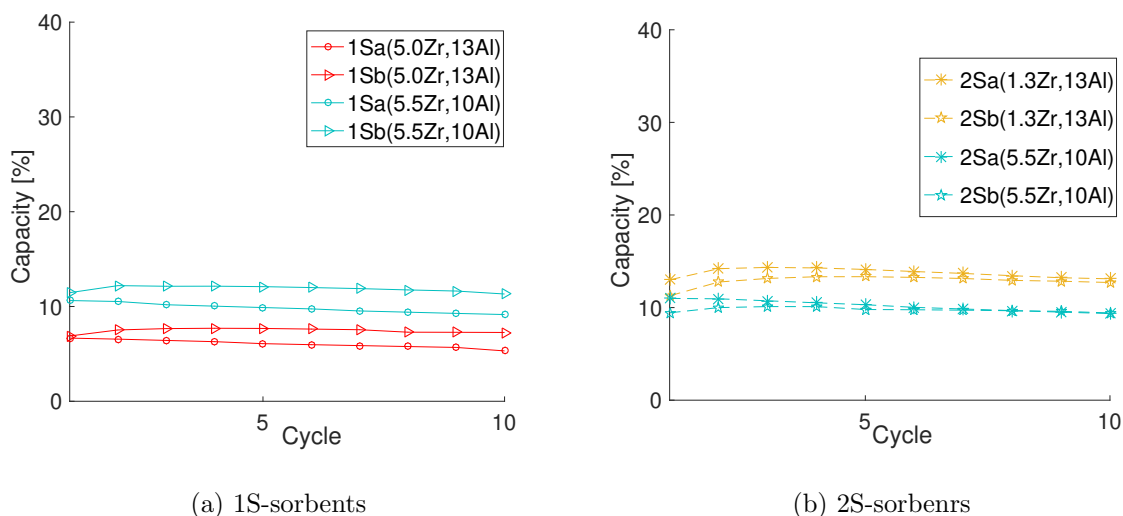


Figure 5.4: Comparing the capturing capacity of identical sorbents prepared in two batches. (1Sa(5.0Zr,13Al), 1Sb(5.0Zr,13Al), 1Sa(5.5Zr,10Al), 1Sb(5.5Zr,10Al), 2Sa(1.3Zr,13Al), 2Sb(1.3Zr,13Al), 2Sa(5.5Zr,10Al), 2Sb(5.5Zr,10Al)) Ads: 5 % CO<sub>2</sub>, 600 °C, 30 min. Des: N<sub>2</sub>, 900 °C

Table 5.3: The capacity in different cycles ( $c_i$ ) and capacity loss ( $c_{i-j}$ ) for identical pairs of ZrAl-based sorbents prepared in two batches. Ads: 5 % CO<sub>2</sub>, 600 °C, 30 min. Des: N<sub>2</sub>, 900 °C

| Sample          | Capacity [%] |       |          | Capacity loss [%] |
|-----------------|--------------|-------|----------|-------------------|
|                 | $c_1$        | $c_3$ | $c_{10}$ | $c_{3-10}$        |
| 2Sa(1.3Zr,13Al) | 13.0         | 14.3  | 13.1     | 7.7               |
| 2Sb(1.3Zr,13Al) | 11.3         | 13.1  | 12.7     | 3.4               |
| 1Sa(5.0Zr,13Al) | 6.7          | 6.4   | 5.3      | 17.2              |
| 1Sb(5.0Zr,13Al) | 7.0          | 7.7   | 7.3      | 5.3               |
| 1Sa(5.5Zr,10Al) | 10.6         | 10.2  | 9.1      | 10.2              |
| 1Sb(5.5Zr,10Al) | 11.4         | 12.1  | 11.3     | 6.7               |
| 2Sa(5.5Zr,10Al) | 11.0         | 10.7  | 9.4      | 12.8              |
| 2Sb(5.5Zr,10Al) | 9.4          | 10.1  | 9.4      | 11.7              |

The different reproducibility results can be connected to a better dispersion of Zirconium in the 1S-sorbents than the 2S-sorbents. It seems like it in the two-step method is possible to obtain similar, good dispersion. In contrast, the dispersion of Zirconium seems to vary to a greater extent when preparing in two steps. Consequently, it is harder to obtain the same capturing capacities, even for sorbents prepared following the same synthesis method. The theory will be further discussed when comparing the two different preparation methods in wet conditions (section 5.1.2.2).

### 5.1.2 Wet conditions

This section presents the results obtained from the cyclic testing in wet conditions in TGA Linseis. As described in section 4.2.2 the adsorption in wet conditions was carried out at a temperature 600°C in an atmosphere consisting of 5 % CO<sub>2</sub> and 8 % H<sub>2</sub>O in air; The desorption in 80 % CO<sub>2</sub> at 950 °C. The time of adsorption was set to 30 minutes.

It was possible to perform experiments closer to realistic conditions in wet conditions than those performed in dry conditions. In addition to the presence of steam, it was possible to have a desorption atmosphere with a high percentage of CO<sub>2</sub>. As explained in section 1.1 and 1.5 the temperature needs to be increased when increasing the partial pressure of CO<sub>2</sub> in order to reach the equilibrium pressure [18]. For that reason, the desorption temperature of the experiments carried out in wet conditions was higher than for the experiments in dry conditions.

Table 5.4 shows the capacity in cycle 3 and 10 and the capacity loss from cycle 3-10 for some of the prepared sorbents obtained in dry and wet conditions. Thus, the results are not directly comparable due to the mentioned different experimental conditions and differences



in the instruments, as explained in section 3.2.2.

Table 5.4: The capacity in different cycles ( $c_i$ ), and capacity loss ( $c_{i-j}$ ) for a selection of ZrAl-based sorbents and calcined dolomite in wet and dry conditions. Dry conditions: Ads: 5 % CO<sub>2</sub>, 600 °C, 30 min. Des: % N<sub>2</sub>, 900 °C. Wet conditions: Ads: 5 % CO<sub>2</sub>, 8 % H<sub>2</sub>O, 600 °C, 30 min. Des: 80 % CO<sub>2</sub>, 950 °C

| Sample            | Capacity [%] |          |       |          | Capacity loss [%] |            |
|-------------------|--------------|----------|-------|----------|-------------------|------------|
|                   | dry          |          | wet   |          | dry               | wet        |
|                   | $c_3$        | $c_{10}$ | $c_3$ | $c_{10}$ | $c_{3-10}$        | $c_{3-10}$ |
| Calcined dolomite | 18.4         | 14.5     | 30.8  | 19.1     | 16.8              | 37.9       |
| 1S(2.6Zr,13Al)    | 14.0         | 13.5     | 18.0  | 16.2     | 3.7               | 10.1       |
| 1S(3.8Zr,13Al)    | 11.1         | 11.3     | 16.2  | 14.3     | -2.1              | 11.6       |
| 1Sa(5.5Zr,10Al)   | 10.2         | 9.1      | 14.2  | 13.0     | 10.2              | 7.7        |
| 1S(1.8Zr,6Al)     | 23.3         | 20.7     | 29.1  | 32.4     | 11.3              | 9.4        |

Generally, the capturing capacities of the sorbents tested in wet conditions are a bit higher than for the sorbents in dry conditions, while the stability is slightly worse. For instance, the capacity of 1S(2.6Zr,13Al) in dry conditions was close to 14 % in cycle 3, while it in wet conditions was close to 18 %. The capacity loss in dry conditions was 3.7 % from cycle 3-10, while the capacity loss in wet conditions was 10.1 % from cycle 3-10.

The higher capacities in wet conditions can be related to steam during the carbonation and the increased temperature. As mentioned in section 1.5, steam presence has shown varying literature results. However, several authors observed a positive effect with the steam present in the carbonation [52, 78, 81, 83, 82, 85, 86, 87, 88]. For instance, Li et al. [83] saw that the reactivity doubled. At the same time, a higher partial pressure during the calcination, and hence a higher temperature can increase the chances of sintering [27]. The increased loss in capacities observed for some of the sorbents in wet conditions can be related to this.

### 5.1.2.1 ZrAl-based sorbents

Now follows the results for all the ZrAl-based sorbents tested in dry conditions. Figure 5.5 and 5.6 shows the cyclic stability for a total of 30 cycles for 1S-sorbents and 2S-sorbents, accordingly. Their capturing capacity in cycle 1, 3, 15 and 30, and the capacity loss from cycle 3-15, 16-30, and 3-30 are given in table 5.5 for the 1S-sorbents and 5.6 for the 2S-sorbents. In the figures and tables, calcined dolomite is included as a reference. Some of the sorbents were only tested for 15 cycles as they did not show a satisfactory performance during the cyclic testing and due to a limited time frame. The capacity loss is found from cycle 3, as the two first did not follow the same trend as the rest.

The two figures and tables clearly show that the sorbents follow the same trend as in dry conditions. The capacities obtained for calcined dolomite during cycles are higher than those obtained for all the prepared sorbents, except for 1S(1.8Zr,6Al). The difference in the cyclic stability between calcined dolomite and the modified sorbents are even more pronounced than in dry conditions; it is significantly worse for calcined dolomite. While calcined dolomite has a capacity loss of 43.9 % from cycle 3-15, the modified capacity losses of all the modified sorbents lay in the range of 5.9 % -18.5 %. The results indicate that the addition of cement and the ZrO<sub>2</sub>, indeed, could stabilize the sorbents.

Comparing the modified sorbents prepared by the one-step method (figure 5.5 and table 5.5), it is clear that increasing the amount of the additives reduced, as in dry conditions, the capturing capacity. The sorbent with the lowest number of additives, 1S(1.8Zr,6Al), has a capacity of 35.8 % in cycle 1. The other sorbents have capacities ranging from 9.2 % -18.6 % in cycle 1. However, as expected, the low amount of additives leads to low cyclic stability. 1S(1.8Zr,6Al) is also the sorbent with the highest loss in capacity being 18.5 % from cycle 3-15.

On the other hand, the sorbent with the highest amount of additives does not reach the required capturing capacity of 10 %; 1Sb(5.0Zr,13Al) only obtain a capacity of 9.2 % in cycle 3. The results observed for the sorbents with the highest and lowest amount of additives illustrate the importance of balancing the amounts of additives to obtain a good stabilizing effect but still keep a sufficient capacity.

By further investigating the capacity losses and the decline in plots, it can be observed that the sorbent with the best performance in dry conditions, 1S(3.8Zr,10Al) (green line), is still among the better sorbents. However, it suffers from some loss in capacity, with 16.9 % and 21.3 % from cycle 3-15 and 3-30, respectively. In these conditions, 1Sa(5.5Zr,10Al) (light blue line) is the sorbent prepared by the one-step method with the best stability during cycles. The sorbent only has a capacity loss of 3.7 % from cycle 16-30. However, it still has a capacity loss of 10.6 % from cycle 3-30.

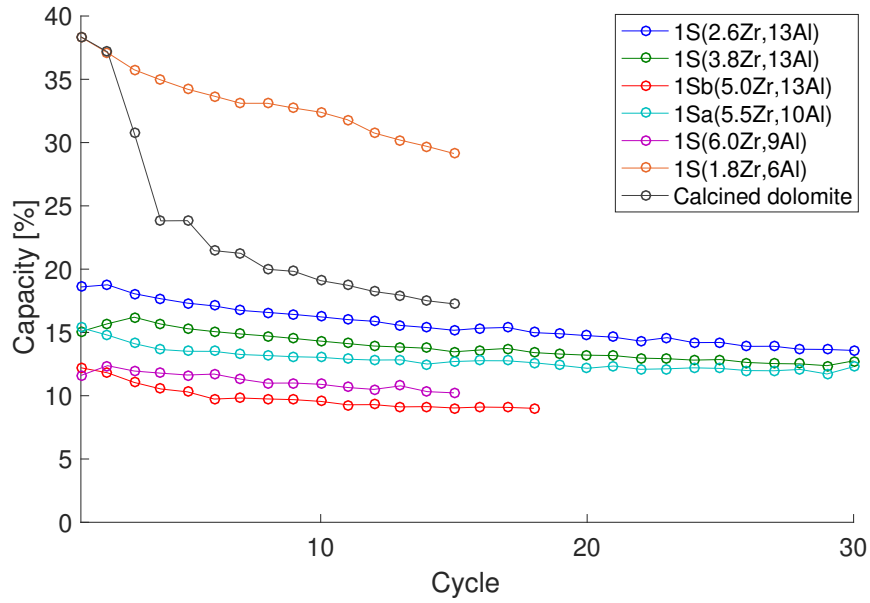


Figure 5.5: The capturing capacity of calcined dolomite and all the ZrAl-based sorbents prepared in one step. (1S(2.6Zr,10Al), 1S(3.8Zr,10Al), 1Sb(5.0Zr,13Al), 1S(5.5Zr,10Al), 1S(6.0Zr,9Al), 1S(1.8Zr,6Al)) Ads: 5 % CO<sub>2</sub>, 8 % H<sub>2</sub>O, 600 °C, 30 min. Des: 80 % CO<sub>2</sub>, 950 °C

Table 5.5: The capacity in different cycles ( $c_i$ ) and capacity loss ( $c_{i-j}$ ) for sorbents modified with cement and ZrO<sub>2</sub>. Calcined dolomite is included for comparison. Ads: 5 % CO<sub>2</sub>, 8 % H<sub>2</sub>O, 600 °C, 30 min. Des: 80 % CO<sub>2</sub>, 950 °C

| Sample            | Capacity [%] |       |          |          | Capacity loss [%] |             |            |
|-------------------|--------------|-------|----------|----------|-------------------|-------------|------------|
|                   | $c_1$        | $c_3$ | $c_{15}$ | $c_{30}$ | $c_{3-15}$        | $c_{16-30}$ | $c_{3-30}$ |
| Calcined dolomite | 38.4         | 30.8  | 17.3     | -        | 43.9              | -           | -          |
| 1S(2.6Zr,13Al)    | 18.6         | 18.0  | 15.2     | 13.6     | 16.0              | 11.5        | 24.8       |
| 1S(3.8Zr,13Al)    | 15.1         | 16.2  | 13.5     | 12.8     | 16.9              | 6.3         | 21.3       |
| 1Sa(5.0Zr,13Al)   | 9.2          | 9.4   | 8.2      | -        | 12.4              | -           | -          |
| 1Sb(5.0Zr,13Al)   | 12.1         | 11.0  | 9.0      | -        | 18.3              | -           | -          |
| 1Sa(5.5Zr,10Al)   | 15.4         | 14.2  | 12.7     | 12.3     | 10.0              | 3.7         | 12.9       |
| 1S(6Zr,9Al)       | 11.6         | 12.0  | 10.2     | -        | 14.4              | -           | -          |
| 1S(1.8Zr,6Al)     | 35.8         | 29.1  | -        | -        | 18.5              | -           | -          |

A similar tendency in the capacities for sorbents prepared by the one-step method can be observed for the sorbents prepared by the two-step method (figure 5.6 and table 5.6). 2S(5.0Zr,13Al) does not exhibit the desired activity and only have a capturing capacity of

9 % in cycle 15. The decline of 2S(2.6Zr, 13Al) (dark blue) is quite apparent, and it has a capacity loss of 17.5 % from cycle 3-15.

The behavior of 2Sa(1.3Zr,13Al), 2S(6.0Zr,9Al), and 2Sa(5.5Zr,10Al) are quite similar; however, a small difference between the sorbents can be observed. 2Sa(1.3Zr,13Al) and 2S(6.0Zr,9Al) both start with capacities of about 19 % and ends at capacities close to 14 %, respectively. 2Sa(5.5Zr,10Al), on the other hand, starts with a capacity of 18.8 % and ends at a capacity of 14.7 %. Further the capacity losses from cycle 3-15 are 27.1 % and 23.3 % for 2Sa(1.3Zr,13Al) and 2S(6.0Zr,9Al), accordingly. For 2Sa(5.5Zr,10Al), the capacity loss is only 10.6 %. The numbers make it clear that 2Sa(5.5Zr,10Al) exhibits the best performance among the sorbents prepared in two steps.

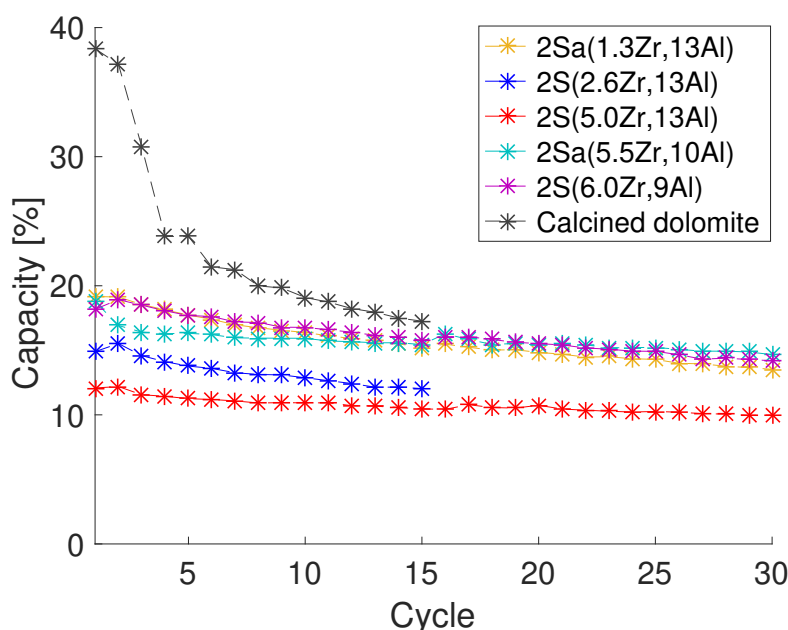


Figure 5.6: The capturing capacity of calcined dolomite and ZrAl-based sorbents prepared by the two step method. (2S(2.6Zr,10Al), 2Sa(5.0Zr,13Al), 2Sa(5.5Zr,10Al), 2S(6.0Zr,9Al)) Ads: 5 % CO<sub>2</sub>, 8 % H<sub>2</sub>O, 600 °C, 30 min. Des: 80 % CO<sub>2</sub>, 950 °C

Table 5.6: The capacity in different cycles ( $c_i$ ) and capacity loss ( $c_{i-j}$ ) for ZrAl-based sorbents prepared in by the two-step method. Calcined dolomite is included for comparison. Ads: 5 % CO<sub>2</sub>, 8 % H<sub>2</sub>O, 600 °C, 30 min. Des: 80 % CO<sub>2</sub>, 950 °C

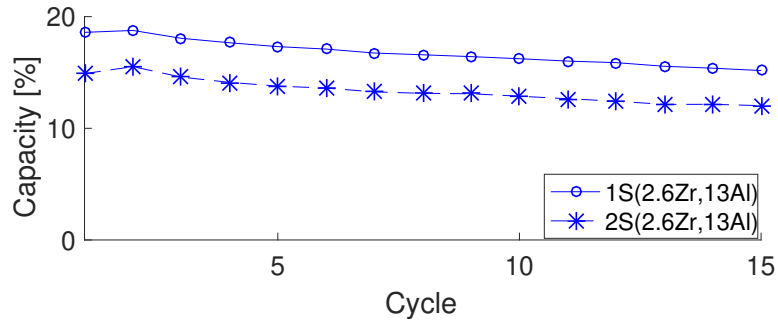
| Sample            | Capacity [%] |       |          |          |            | Capacity loss [%] |            |
|-------------------|--------------|-------|----------|----------|------------|-------------------|------------|
|                   | $c_1$        | $c_3$ | $c_{15}$ | $c_{30}$ | $c_{3-15}$ | $c_{16-30}$       | $c_{3-30}$ |
| Calcined dolomite | 38.4         | 30.8  | 17.3     | -        | 43.9       | -                 | -          |
| 2Sa(1.3Zr,13Al)   | 19.2         | 18.5  | 15.2     | 13.5     | 18.0       | 12.6              | 27.1       |
| 2S(2.6Zr, 13Al)   | 15.5         | 14.6  | 12.0     | -        | 17.5       | -                 | -          |
| 2S(5.0Zr,13Al)    | 12.2         | 11.1  | 9.0      | -        | 9.5        | 4.2               | 13.6       |
| 2Sa(5.5Zr,10Al)   | 18.8         | 16.4  | 15.5     | 14.7     | 5.9        | 9.9               | 10.6       |
| 2S(6Zr,9Al)       | 18.2         | 18.5  | 15.8     | 14.2     | 14.7       | 11.6              | 23.3       |

### 5.1.2.2 One-step method vs. two-step method

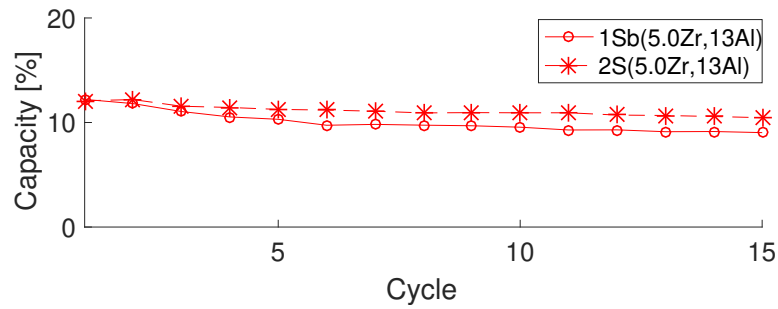
Even though the cyclic performance is similar for sorbents prepared by the one-step method and two-step method, there is a minor difference. In figure 5.7 the capturing capacity in different cycles are compared for ZrAl-based sorbents with similar compositions; each of the plots compare one step (circle) with two steps (star). The plots are given for a total of 15 cycles. Table 5.7 presents the capacities in cycle 1, 3, 15, and 30, and the loss in capacities from cycle 3-15, 16-30, and 3-30. To more clearly investigate differences in the stability, figure 5.8 illustrates the capacity losses from cycle 3-15 for the sorbents.

The trend observed is a higher capacity for sorbents prepared by the two-step method than for sorbents prepared by the one-step method. In figure 5.7 1S(2.6Zr,13Al) is the only 1S-sorbent with a capacity higher than the similar 2S-sorbent. 1S-sorbents having higher capacities are the opposite of what was expected. The expectation was that in the two-step method, it would be assured that all the ZrO<sub>2</sub> would have the possibility to react with the CaO active sites in dolomite. Consequently, it was expected that less CO<sub>2</sub> would be captured for sorbents prepared by the two-step method than the one-step method.

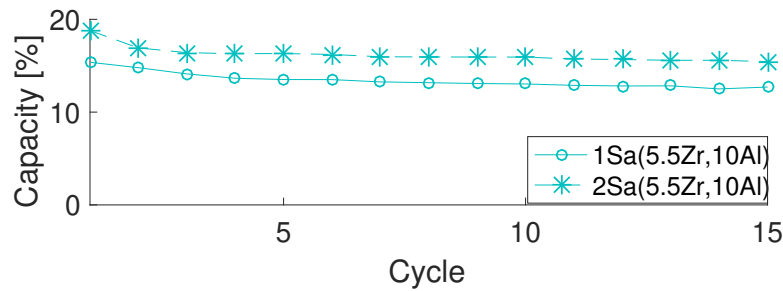
On the other hand, the stability was expected to increase for sorbents prepared by the two-step method. Overall, the stabilities in the two methods are quite similar. Nevertheless, by exploring the capacity losses both in the bar-plots (figure 5.8) and table 5.7, the capacity losses for sorbents prepared by the two-step method are mostly lower or similar to preparation in one step. From cycle, 3-15, only 1S(2.6Zr,10Al) have a somewhat lower stability than 2S(2.6Zr,13Al) with values of 16.0 % and 17.5 %, respectively.



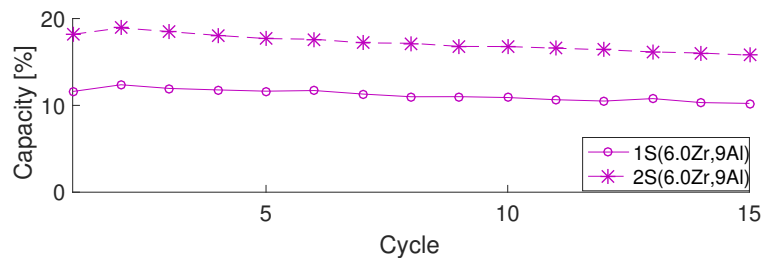
(a) 1S(2.6Zr,13Al) vs. 2S(2.6Zr,13Al)



(b) 1Sb(5.0Zr,13Al) vs. 2S(5.0Zr,13Al)



(c) 1Sa(5.5Zr,10Al) vs. 2Sa(5.5Zr,10Al)



(d) 1S(6.0Zr,9Al) vs. 2S(6.0Zr,9Al)

Figure 5.7: Comparison of the cyclic capacity of one step method vs. two-step method for different compositions of Aluminium and Zirconium. Ads: 5 % CO<sub>2</sub>, 8 % H<sub>2</sub>O, 600 °C, 30 min. Des: 80 % CO<sub>2</sub>, 950 °C

Table 5.7: Comparison of one-step method vs. two step method for ZrAl-based sorbents. The capacity in different cycles ( $c_i$ ) and capacity loss ( $c_{i-j}$ ) are presented Ads: 5 % CO<sub>2</sub>, 8 % H<sub>2</sub>O, 600 °C, 30 min. Des: 80 % CO<sub>2</sub>, 950 °C

| Sample          | Capacity [%] |       |          |          | Capacity loss [%] |             |            |
|-----------------|--------------|-------|----------|----------|-------------------|-------------|------------|
|                 | $c_1$        | $c_3$ | $c_{15}$ | $c_{30}$ | $c_{3-15}$        | $c_{16-30}$ | $c_{3-30}$ |
| 1S(2.6Zr,13Al)  | 18.6         | 18.0  | 15.2     | 13.6     | 16.0              | 11.5        | 24.8       |
| 2S(2.6Zr, 13Al) | 15.5         | 14.6  | 12.0     | -        | 17.5              | -           | -          |
| 1Sb(5.0Zr,13Al) | 12.1         | 11.0  | 9.0      | -        | 18.3              | -           | -          |
| 2S(5.0Zr,13Al)  | 12.2         | 11.1  | 9.0      | -        | 9.5               | 4.2         | 13.6       |
| 1Sa(5.5Zr,10Al) | 15.4         | 14.2  | 12.7     | 12.3     | 10.0              | 3.7         | 12.9       |
| 2Sa(5.5Zr,10Al) | 18.8         | 16.4  | 15.5     | 14.7     | 5.9               | 9.9         | 10.6       |
| 1S(6Zr,9Al)     | 11.6         | 12.0  | 10.2     | -        | 14.4              | -           | -          |
| 2S(6Zr,9Al)     | 18.2         | 18.5  | 15.8     | 14.2     | 14.7              | 11.6        | 23.3       |

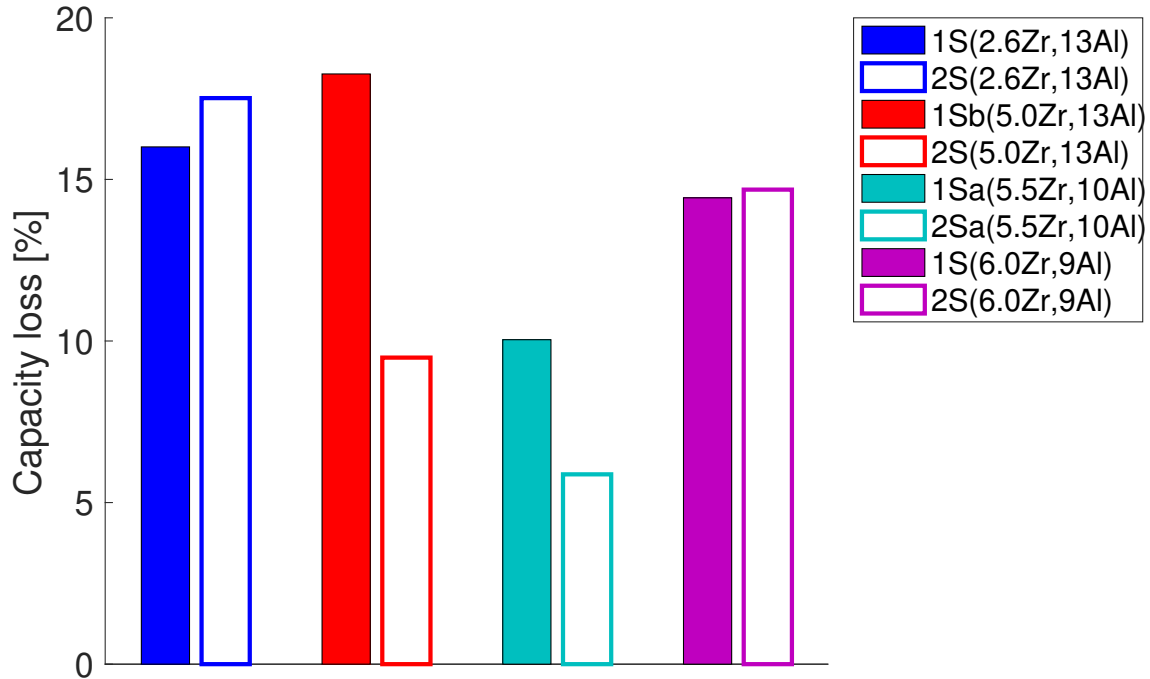


Figure 5.8: Comparison of the capacity loss of one-step method vs. two-step method for different compositions of Aluminium and Zirconium . Ads: 5 % CO<sub>2</sub>, 8 % H<sub>2</sub>O, 600 °C, 30 min. Des: 80 % CO<sub>2</sub>, 950 °C

Due to the unpredicted trend in the capturing capacities, it was speculated if the Calcium in cement had some capturing capacity. For that reason, pure cement, as well as cement mixed with the Zirconium-solution, were tested. The last was calcined, following the same calcination-procedure as for calcined dolomite (800 °C, 6 h). The sorbents were tested in dry conditions with an adsorption-atmosphere consisting of 5 % CO<sub>2</sub> in N<sub>2</sub> at 600 °C and desorption in pure Nitrogen at 900 °C. None of them were able to capture any CO<sub>2</sub> during the cycles.

A part of the explanation for the opposite trend in terms of capturing capacity might be related to the dispersion of Zirconium in the pores. When the sorbents are prepared by the two-step method, the precursor deposition might be easier to control. The theory will be investigated further in the characterization, especially in the EDS ( section 5.2.5).

Further, the difference in the capacities between sorbents prepared by the two-step method is increased with a higher cement fraction of cement. The differences can indicate that the addition of more ZrO<sub>2</sub> makes it harder to achieve a good dispersion of the modifier in the 1S-sorbents. This further can be a possible explanation for 1S(2.6Zr,13Al) having a higher capacity than 2S(2.6Zr,13Al). The sorbents have a lower weight percentage of Zirconium compared to the other sorbents presented in the figure. Hence, it was easier to obtain a good dispersion of Zirconium in 1S(2.6Zr,13Al) than in the other 1S-sorbents. A similar tendency was also observed with 1S(1.3Zr,13Al) capacities a bit over 2Sa(1.3Zr,13Al) in dry conditions (section 5.1.1).

An additional explanation for the unexpected variation in capacities might be related to CaO from dolomite reacting with cement. It is a possibility that some of the calcium-aluminates reacted with the active sites of CaO and that it was more pronounced for 1S-sorbents—hence reducing the active CaO available to capture CO<sub>2</sub>.

### 5.1.2.3 Sorbents prepared without ZrO<sub>2</sub>

ZrO<sub>2</sub> was chosen as a modifier due to its widely reported stabilizing effect [30, 32, 33, 35, 44, 47, 45, 46, 48, 49, 50, 51, 52]. However, as the results obtained in the previous sections showed a significant enhancement in the stability with an increasing amount of cement, it was decided to see the effect of cement on its own. It was also of interest to test an alternative modifier that does not form oxides with the active sites of CaO - hence expected only to impact the stability. For this CeO<sub>2</sub> was chosen, which in literature have exhibited a stabilizing effect [54, 56].

Four additional sorbents were prepared; two with CeO<sub>2</sub> as a modifier and two with only cement. They were prepared following the procedure explained in section 4.1. The two sorbents with CeO<sub>2</sub> had similar compositions as the ZrAl-based sorbents (1S(5.5Ce,10Al) and 2S(5.5Ce,10Al)). The ones with only cement were prepared with a similar (11Al) and a higher (15Al) fraction of cement.



All the sorbents were tested in wet conditions (Ads: 5 % CO<sub>2</sub>, 8 % H<sub>2</sub>O, 600 °C, 30 min. Des: 80 % CO<sub>2</sub>, 950 °C). Figure 5.9 shows the capturing capacity against a total of 30 cycles for the CeAl-based sorbents, the two best ZrAl-based sorbents, the sorbents with cement as the only modifier, and calcined dolomite. The capacity in cycle 1, 3 and 15, and the capacity loss from cycle 3-15 are given in table 5.8. The capacity loss from cycle 3-15 for the sorbents with a similar cement composition are also shown as bar-plots in figure 5.10. Here the y-axis gives the capacity loss in percentage.

An interesting observation is the similar capacities of 15Al (pink) and 1S(5.5Zr,10Al) (blue circles). However, the decline of 15Al is slightly bigger. While 15Al has a capacity loss of 16.4 % from cycle 3-15, 1S(5.5Zr,10Al) have a capacity loss of 10.0 %. Nevertheless, the observation evidences the strong stabilizing effect of cement on its own. Further investigation of this sorbent, as well as one with even more cement, is of interest. It is also needed to continue investigating the sorbents prepared with a small addition of ZrO<sub>2</sub>. Also, it is possible that the modifier affects the strength of the pellets.

The capacities of the two CeAl-based sorbents (green) are very similar. The similarities imply that mixing all together or in two steps does not affect these samples. In addition, the trend of 11Al (brown) is almost identical to 2S(5.5Ce,10Al). The capacities are of 20.0 %, and 20.4 %, in cycle 3 and 16.5 %, and 16.7 % in cycle 15, for 2S(5.5Ce,10Al) and 15Al accordingly. Both have capacity losses close to 18 % from cycle 3-15.

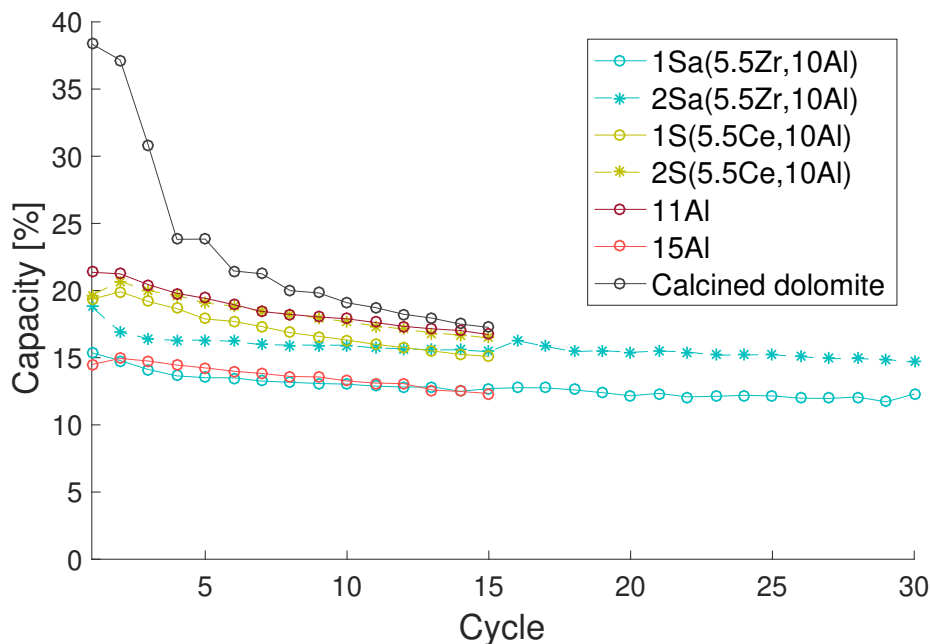


Figure 5.9: The capturing capacity of 1SA(5.5Zr,10Al), 2Sa(5.5Zr,10Al), 1S(5.Ce,10Al), 2Sa(5.5Ce,10Al), 11Al, 15Al and calacined dolomite. Ads: 5 % CO<sub>2</sub>, 8 % H<sub>2</sub>O, 600 °C, 30 min. Des: 80 % CO<sub>2</sub>, 950 °C.

Table 5.8: The capacity in different cycles ( $c_i$ ) and capacity loss ( $c_{i-j}$ ) Sa(5.5Zr,10Al), 2Sa(5.5Zr,10Al), 1Sa(5.Ce,10Al), 2Sa(5.5Ce,10Al), 15Al, 11Al and calcined dolomite. Ads: 5 % CO<sub>2</sub>, 8 % H<sub>2</sub>O, 600 °C, 30 min. Des: 80 % CO<sub>2</sub>, 950 °C.

| Sample            | Capacity [%] |       |          | Capacity loss [%] |
|-------------------|--------------|-------|----------|-------------------|
|                   | $c_1$        | $c_3$ | $c_{15}$ | $c_{3-15}$        |
| Calcined dolomite | 38.4         | 30.8  | 17.3     | 43.9              |
| 1Sa(5.5Zr,10Al)   | 15.4         | 14.2  | 12.7     | 10.0              |
| 2Sa(5.5Zr,10Al)   | 18.8         | 16.4  | 15.5     | 5.9               |
| 1S(5.5Ce 10Al)    | 19.4         | 19.2  | 15.1     | 21.3              |
| 2S(5.5Ce 10Al)    | 19.7         | 20.0  | 16.5     | 17.6              |
| 11Al              | 21.4         | 20.4  | 16.7     | 18,2              |
| 15Al              | 14.5         | 14.8  | 12.3     | 16.4              |

Further, the bar-plots in figure 5.10 clearly shows that for similar cement composition, the addition of Zirconium decreases the capacity-loss, while Cerium does not have any effect. The results indicate that the addition of CeO<sub>2</sub> does not change the cyclic performance of the sorbents; neither the capturing capacity nor the stability. Concluding, CeO<sub>2</sub> do not exhibit the expected stabilizing effect in this project.

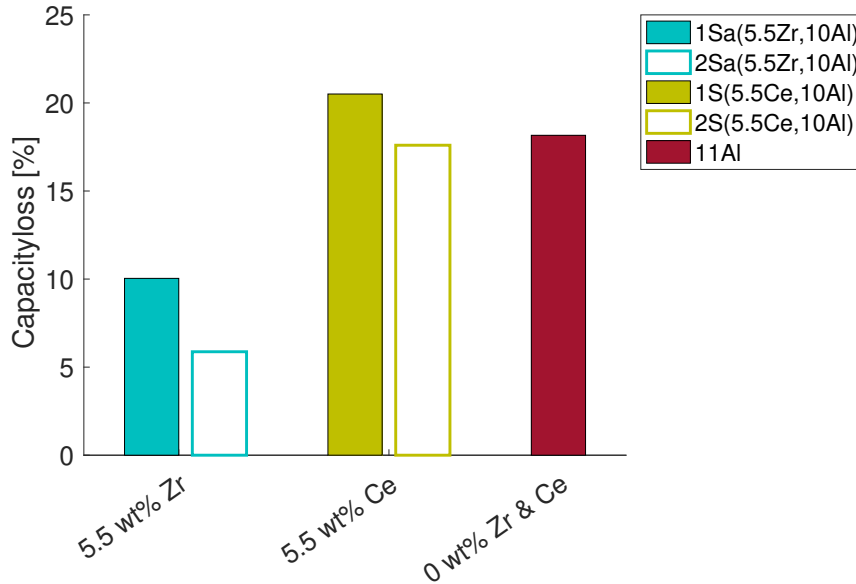


Figure 5.10: The capacity loss of 1Sa(5.5Zr,10Al), 2Sa(5.5Zr,10Al), 1S(5.5Ce,10Al), 2S(5.5Ce,10Al) and 11Al. Ads: 5 % CO<sub>2</sub>, 8 % H<sub>2</sub>O, 600 °C, 30 min. Des: 80 % CO<sub>2</sub>, 950 °C

The absence of an expected stabilizing effect for the CeAl-based sorbents is suspected to be related to the deposition of  $\text{CeO}_2$ . The reason can be related to the way the sorbents with Cerium was synthesized. However, further research is necessary to know the exact reason.

#### 5.1.2.4 Repeatability

Two samples from the same batch were tested in wet conditions in TGA Linseis. The result is shown in figure 5.11 where the capturing capacity is plotted against a total of 12 cycles. The two tests show very similar results. In addition to this, the repeatability was tested three times in dry conditions for both 15Al and 1S(1.3Zr,13Al). Both sorbents were able to obtain similar capacities in all three tests.

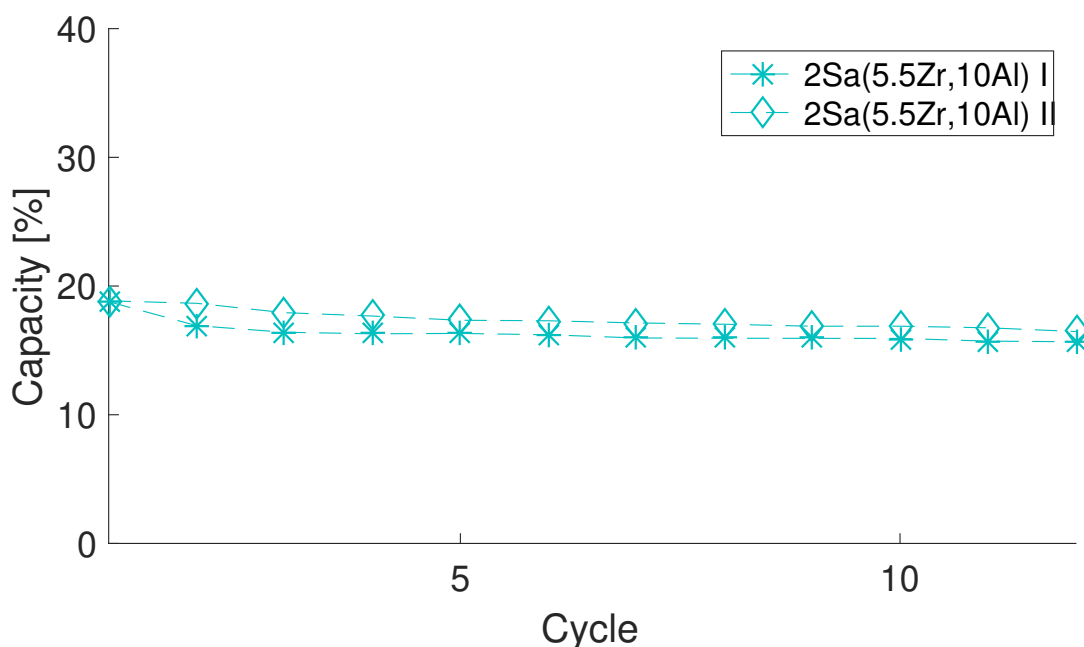


Figure 5.11: Repeatability of 2Sa(5.5Zr,10Al). Ads: 5 %  $\text{CO}_2$ , 8 %  $\text{H}_2\text{O}$  600 °C, 30 min. Des: 80 %  $\text{CO}_2$ , 950 °C

#### 5.1.2.5 Calcination effect

In sorbents whose capacities have been presented so far, two calcinations were performed during the sorbent synthesis. First, the dolomite was calcined before it was mixed with the modifiers. This calcination was performed to transform  $\text{CaCO}_3$  to active  $\text{CaO}$ . The second calcination was performed of the fresh pellets before cyclic testing. There, it was expected to obtain a degree of sintering. Thus, obtain a stable framework more resistant against sintering during the cyclic testing [28, 100]. However, the phenomena should not be too pronounced.

It is vital to find a balance between obtaining as much as possible accessible active CaO and hindering a prominent merging of the particles.

It was desired to understand more about the effect the calcination had on the sorbents. Therefore, as explained in section 4.1 one sorbent was made with uncalcined dolomite (1SUncalc(5.5Zr,10Al)) and one with intermediate calcination (2SInter(5.5Zr,10Al)).

1SUncalc(5.5Zr,10Al) was tested for four cycles in wet conditions (Ads: 5 % CO<sub>2</sub>, 8 % H<sub>2</sub>O, 600 °C, 30 min. Des: 80 % CO<sub>2</sub>, 950 °C). The sorbent was only able to capture around 3 % CO<sub>2</sub> during cycles. For comparison, the sorbent with similar composition made with calcined dolomite could capture a bit over 15 %. As the calcination of dolomite was not carried out, the carbonates in dolomite had not been transformed to their oxide form. Even though calcination was carried out in the last step, the low capturing capacity clarifies the necessity of calcining dolomite before synthesizing the pellets. The observation will be more thoroughly explained in the XRD section (5.2.2).

2SInter(5.5Zr,10Al) was tested in dry conditions (Ads: 5 % CO<sub>2</sub>, 600 °C, 30 min. Des: N<sub>2</sub>, 900 °C). Figure 5.12 displays the capturing capacities during 10 regeneration cycles for 2Sa(5.5Zr,10Al) and 2SInter(5.5Zr,10Al). Table 5.9 gives capacities in cycle 1, 3 and 10 and the capacity-loss from cycle 3-10 for the three tests.

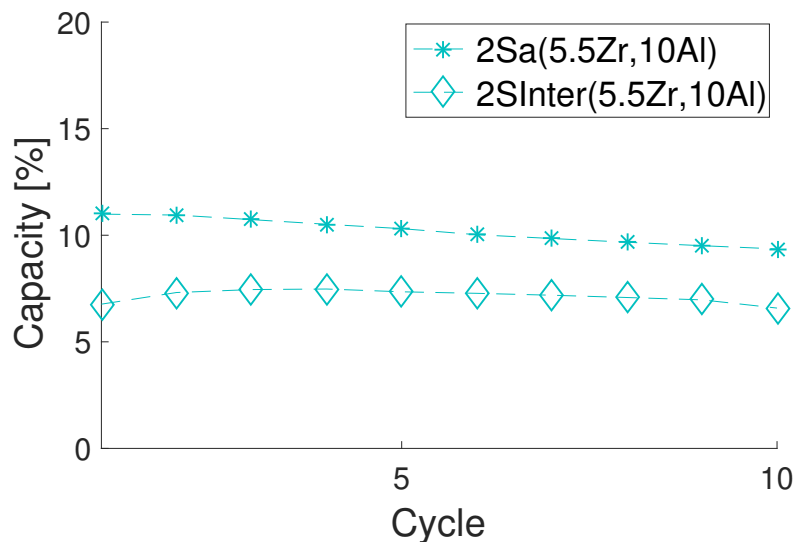


Figure 5.12: Capturing capacity of 2SInter(5.5Zr,10Al) and 2Sa(5.5Zr,10Al). Ads: 5 % CO<sub>2</sub>, 600 °C, 30 min. Des: N<sub>2</sub>, 900 °C

Table 5.9: The capacity in different cycles ( $c_i$ ) and capacity loss ( $c_{i-j}$ ) for 2SInter(5.5Zr,10Al) and(2Sa(5.5Zr,10Al). Ads: 5 % CO<sub>2</sub>, 600 °C, 30 min. Des: 100 % N<sub>2</sub>, 900 °C

| Sample              | Capacity [%] |       |          | Capacity loss [%] |            |
|---------------------|--------------|-------|----------|-------------------|------------|
|                     | $c_1$        | $c_3$ | $c_{10}$ | $c_{3-8}$         | $c_{3-10}$ |
| 2Sa(5.5Zr,10Al)     | 11.0         | 10.7  | 9.4      | 9.9               | 12.8       |
| 2SInter(5.5Zr,10Al) | 6.8          | 7.5   | 6.6      | 5.0               | 11.7       |

2SInter(5.5Zr,10Al) exhibits a low capturing capacity, only 6.8 % in cycle 1. On the other hand, 2Sa(5.5Zr,10Al) exhibited a capacity of 11 % in the same conditions. The lower capacity of 2SInter(5.5Zr,10Al) indicates more pronounced sintering of the fresh particles when additional calcination was performed. The cyclic stabilities between the two sorbents are similar with capacity loss from cycle 3-10 of 12.8 % and 11.7 % for 2Sa(5.5Zr,10Al) and 2SInter(5.5Zr,10Al), respectively. Even though the cyclic stability only was tested in dry conditions, the results indicate that preparing sorbents by the two-step method without intermediate calcination is preferable. However, the differences between the sorbents will be discussed in more detail in the characterization, section 5.2.

### 5.1.2.6 Long term stability

The sorbents exhibiting the best capturing capacities in wet conditions were further tested for a total of 60 cycles; the results are presented in figure 5.13 (Ads: 5 % CO<sub>2</sub>, 8 % H<sub>2</sub>O, 600 °C, 30 min. Des: 80 % CO<sub>2</sub>, 950 °C). The exact capacities in cycle 1, 3, 15, 30, 45, 60 and the maximum theoretical capacity for the two sorbents are given in table 5.11. Additionally, capacity losses between different cycles are given; 3-15, 15-30, 21-45, 45-60, 3-45 and 3-60. The losses are not given from cycle 16 and 46 due to small "jumps" observed in the two cycles for 2Sa(5.5Zr,10Al), which will be discuss later. The capacity losses for the first four are also presented as bar-plots in figure 5.14.

The two "jumps" observed in cycle 16 and 46 for 2Sa(5.5Zr,10Al) are probably related to how the experiments were carried out. As described in section 4.2.2 it is only possible to perform experiments with 15 cycles continuously. The raise can be related to the regeneration of the sorbent when a new set of experiment was started. Regeneration of sorbents with steam has shown to increase the capturing capacity of spent sorbents [101]. Though, further research is necessary to understand the exact cause.

The capacities of 2Sa(5.5Zr,10Al) fast go back to follow the original trend after the "jumps." Though, it is speculated that all the following capacities have a bit higher values than they would have had without the rise. Anyhow, the impact on the behavior of the sorbent is likely not significant.

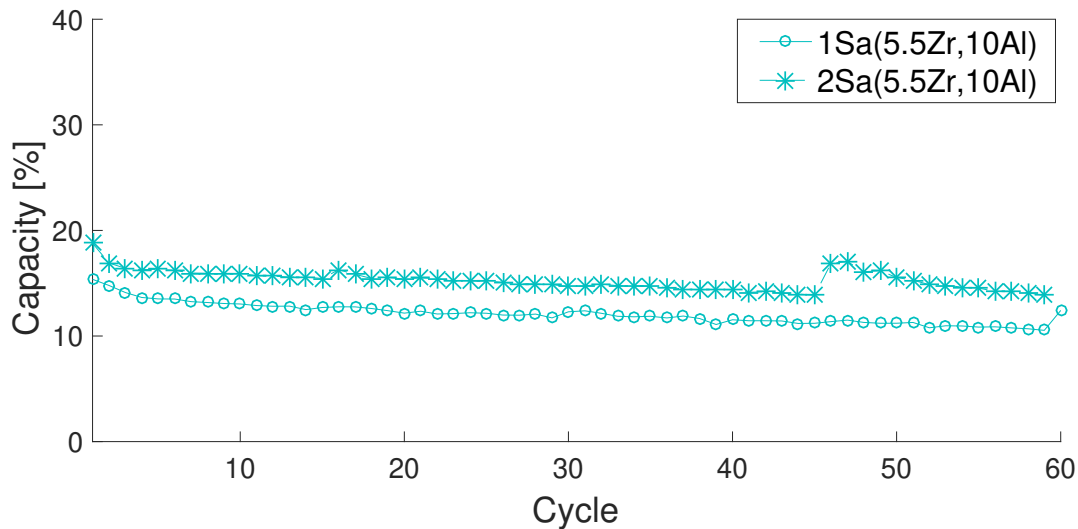


Figure 5.13: The capturing capacity of 1Sa(5.5Zr,10Al) and 2Sa(5.5Zr,10Al) during 60 regeneration-cycles. Ads: 5 % CO<sub>2</sub>, 8 % H<sub>2</sub>O, 600 °C, 30 min. Des: 80 % CO<sub>2</sub>, 950 °C

Table 5.10: The capacity in different cycles ( $c_i$ ) and capacity loss ( $c_{i-j}$ ) for 1Sa(5.5Zr,10Al) and 2Sa(5.5Zr,10Al). Total cycles: 60. Ads: 5 % CO<sub>2</sub>, 8 % H<sub>2</sub>O, 600 °C, 30 min. Des: 80 % CO<sub>2</sub>, 950 °C

| Sample          | Capacity [%] |       |          |          |          |          | Capacity loss [%] |             |             |             |            |            |
|-----------------|--------------|-------|----------|----------|----------|----------|-------------------|-------------|-------------|-------------|------------|------------|
|                 | $c_1$        | $c_3$ | $c_{15}$ | $c_{30}$ | $c_{45}$ | $c_{60}$ | $c_{3-15}$        | $c_{15-30}$ | $c_{31-45}$ | $c_{45-60}$ | $c_{3-45}$ | $c_{3-60}$ |
| 1Sa(5.5Zr,10Al) | 15.4         | 14.2  | 12.7     | 12.3     | 11.2     | 10.5     | 10.0              | 3.2         | 9.5         | 5-9         | 20.6       | 25.4       |
| 2Sa(5.5Zr,10Al) | 18.8         | 16.4  | 15.5     | 14.7     | 13.9     | 13.9     | 5.9               | 3.2         | 6.1         | 0.1         | 15.6       | 15.7       |

As already discussed, 2Sa(5.5Zr,10Al) exhibit a bit higher capacity than 1Sa(5.5Zr,10Al), while the cyclic stability is very similar. However, both the bar-plots in figure 5.14 and the capacity losses in table 5.11 show that the capacity loss for 2S-sorbents always are a bit lower than for the 1S-sorbents, except cycle 15-30, where both have capacity-losses of 3.2 %. The capacity loss from cycle 45-60 is very small, only 0.1 %. However, this can also be related to the "jump" in the capacity in cycle 46. Still, when looking at losses where there is no rise, the capacity loss for the 2S-sorbent is smaller (cycle 3-15 and 31-45). Additionally, the loss in capacity from cycle 3-60 for 2Sa(5.5Zr,10Al) is almost 10 % lower than for 1Sa(5.5Zr,10Al).

Overall, both of the sorbents show a relatively good cyclic stability over a long time, but they still suffer from deactivation. Even though very similar, it seems to be an advantage in preparing the sorbent by the two-step method, both in terms of capturing capacity as well as cyclic stability.

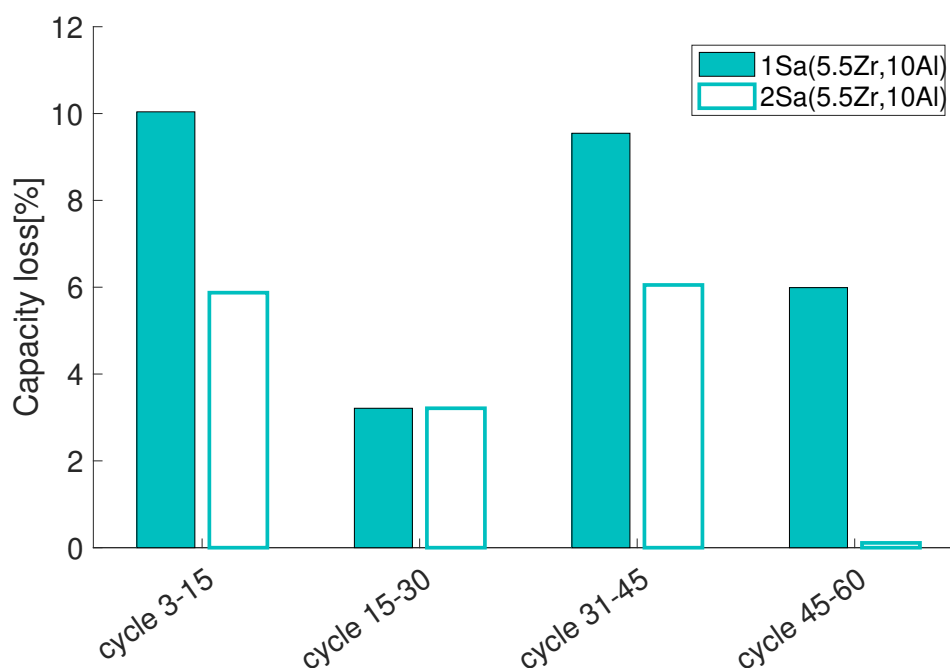


Figure 5.14: Bar plots showing the capacity loss between different cycles for 1Sa(5.5Zr,10Al) and 2Sa(5.5Zr,10Al). Ads: 5 % CO<sub>2</sub>, 8 % H<sub>2</sub>O, 600 °C, 30 min. Des: 80 % CO<sub>2</sub>, 950 °C.

### 5.1.2.7 Increase in capacity with time

Figure 5.15 presents the increase in capacity with time for 1Sa(5.5Zr,10Al) (a) and 2Sa(5.5Zr,10Al) (b) to a total of 10 minutes. In the plots cycle 3, 15, 30, 45 and 60 are represented.

In correspondence with the theory, the carbonation can be divided into two stages, as explained in section 1.3. Namely, one fast and one slow carbonation stage [24]: First, the formation of CaCO<sub>3</sub> at the surface, followed by diffusion of CO<sub>2</sub> through the layer of CaCO<sub>3</sub> in order to reach free sites of CaO. The slope in the fast reaction stages is similar in all the cycles. However, the carbonation conversion decreases during cycles.

On average, sorbents only spent a few minutes in the carbonator [24, 102]. Therefore it is desired that it takes a short time before the sorbents obtain their full capacity during cycles. 2Sa(5.5Zr,10Al) reaches the demanded capacity of 10 % fast, in most of the cycles only after a couple of minutes. In cycle 60, the capacity is reached after about 4 minutes. For 1Sa(5.5Zr,10Al), it takes some more time to reach the desired capacity. In cycle 3, it reaches the desired capacity in less than two minutes—however, reaching the capacity increases by about one minute between the cycles represented.

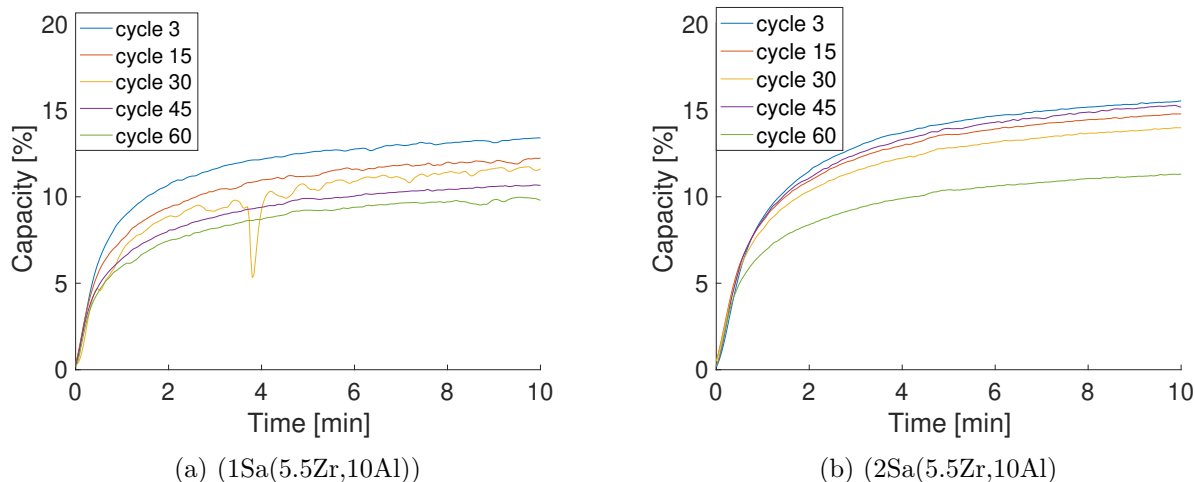


Figure 5.15: Comparison of the increase in capacities vs. time for 1Sa(5.5Zr,10Al) and 2Sa(5.5Zr,10Al). Ads: 5 % CO<sub>2</sub>, 8 % H<sub>2</sub>O, 600 °C, 30 min. Des: 80 % CO<sub>2</sub>, 950 °C.

### 5.1.2.8 Microbalance Fixed Bed Reactor

The two best sorbents were further tested in the microbalance reactor. The conditions were similar, though even more realistic than those used in TGA wet conditions. The adsorption was carried out in 5 % CO<sub>2</sub> at 600 °C for a total of 6 minutes for 1Sa(5.5Zr,10Al). The desorption was carried out in 100 % CO<sub>2</sub> at 950 °C.

Figure 5.16 presents the capturing capacities during a total of 40 regeneration-cycles for 1Sa(5.5Zr,10Al) and 2Sa(5.5Zr,10Al). Table 5.11 gives the capacity in cycle 1, 3, 15, 30 and 40 and losses in capacities from cycle 3-15, 15-30 and 3-40.

As when tested in the thermogravimetric analyzers, the 1S-sorbent exhibits a lower capturing capacity than the 2S-sorbent. At the same time, the stabilities of the two sorbents are relatively similar. However, when looking at the capacity losses, the values of the capacity losses are 35.4 % from cycle 3-40 for 1S(5.5Zr,10Al), while 13.6 % for 2S(5.5Zr,10Al). The numbers agree with earlier observations, where the 2S-sorbents tended to have marginally better stability than the 1S-sorbents.

2Sa(5.5Zr,10Al) has a capacity of 12.6 % in the first cycle, and of 11.4 % in the last cycle - hence the sorbent can keep over the required capacity of 10 % during all the tested cycles also under these harsh testing-conditions. On the other hand, 1Sa(5.5Zr, 10Al) starts at a capacity of 9.8 %, and after 15 cycles, the capturing capacity is down to 7.9.

The capturing capacities obtained in the microbalance reactor differ more from capacities obtained in the TGA with wet conditions than expected. The capacities in wet conditions in the TGA was 16.4 % for 2Sa(5.5Zr, 10Al) in cycle 3, while in the microbalance reactor,



the capacity was 11.1 %. It needs to be considered that the adsorption times were not the same, but in the figure of capacity vs. time for 2Sa(5.5Zr,10Al) (figure 5.15b), it was seen that it had almost reached full capacity after six minutes. Still, the results are not entirely comparable. As mentioned in section 3.2.2, instrumental limitations can have impacted the total capacity possible to reach. The limitations of the microbalance reactor still need to be investigated more in the future. Anyhow, the sorbents were able to keep relatively stable in both instruments, indicating their promising future.

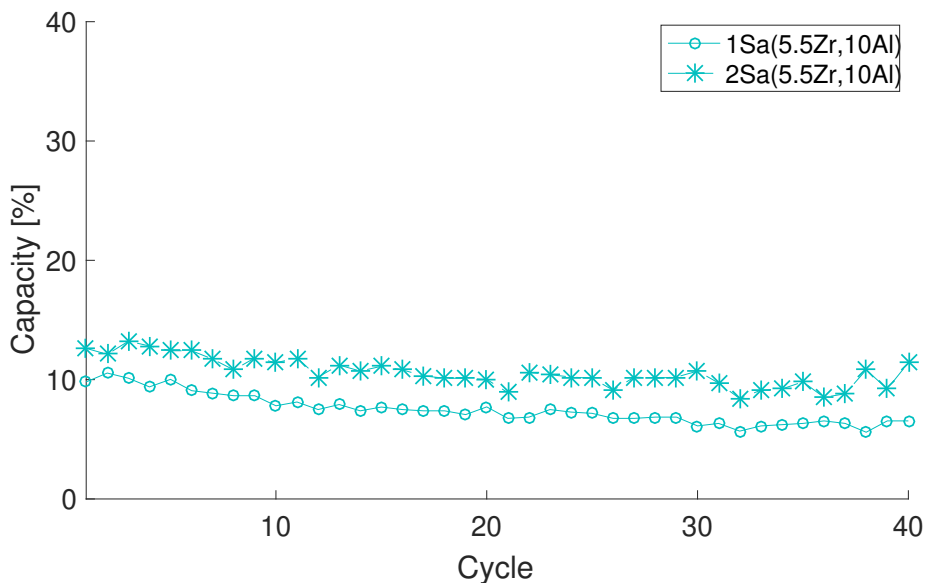


Figure 5.16: The capturing capacity of 1Sa(5.5Zr,10Al) and 2Sa(5.5Zr,10Al) during 40 regeneration-cycles tested in the microbalance-reactor. Ads: 5 % CO<sub>2</sub>, 8 % H<sub>2</sub>O, 600 °C, 6min. Des: 100 % CO<sub>2</sub>, 950 °C

Table 5.11: The maximum theoretical capacity, capacity in different cycles ( $c_i$ ) and capacity loss ( $c_{i-j}$ ) for the best sorbents modified with cement and ZrO<sub>2</sub>. Total cycles: 60. Ads: 5 % CO<sub>2</sub>, 8 % H<sub>2</sub>O, 600 °C, 6 min. Des: 100 % CO<sub>2</sub>, 950 °C

| Sample          | Capacity [%] |       |          |          |          | Capacity loss [%] |             |            |
|-----------------|--------------|-------|----------|----------|----------|-------------------|-------------|------------|
|                 | $c_1$        | $c_3$ | $c_{15}$ | $c_{30}$ | $c_{40}$ | $c_{3-15}$        | $c_{15-30}$ | $c_{3-40}$ |
| 1Sa(5.5Zr,10Al) | 9.8          | 10.1  | 7.8      | 6.1      | 6.5      | 23.9              | 20.5        | 35.4       |
| 2Sa(5.5Zr,10Al) | 12.6         | 13.2  | 11.1     | 10.8     | 11.4     | 15.9              | 3.6         | 13.6       |

## 5.2 Characterization

In order to obtain more in-depth knowledge about the sorbents, several characteristics were performed. Sorbents, both before and after testing of the cyclic stability, will be given in this section. Samples testing will be referred to as fresh, and samples after cyclic testing as spent.

### 5.2.1 X-Ray Fluorescence Spectroscopy (XRF)

In order to confirm the theoretical composition of the sorbents, X-Ray Fluorescence Spectroscopy (XRF) was performed on 1Sa(5.5Zr,10Al) and 2Sa(5.5Zr,10Al) as explained in section 3.3.1. Calcined dolomite and Cement Fondu have also analyzed as their exact composition was unknown. Five samples were analyzed for the sorbents and dolomite, four for cement. The average numbers of cement and dolomite were used to calculate the theoretical compositions in the sorbents. The calculations are given in appendix C.

Table 5.12 displays the weight percentages of oxides present in Cement Fondu, calcined dolomite, 1Sa(5.5Zr,10Al), and 2Sa(5.5Zr,10Al) obtained through XRF together with standard variations. In the case of cement, the chemical composition from the specification is included [58], and for the sorbents, the calculated theoretical values are presented.

Table 5.12: Composition of oxides obtained through XRF for Cement Fondu, calcined dolomite, 1Sa(5.5Zr,10Al) and 2Sa(5.5Zr,10Al) compared to their theoretical value. For Cement Fondu the specification ranges are included.

| Sorbent                        | CaO<br>[wt %] | MgO<br>[wt %] | Al <sub>2</sub> O <sub>3</sub><br>[wt %] | Fe <sub>2</sub> O <sub>3</sub><br>[wt %] | SiO <sub>2</sub><br>[wt %] | ZrO <sub>2</sub><br>[wt %] |
|--------------------------------|---------------|---------------|--|--|----------------------------|----------------------------|
| Cement spec.                   | 35.5-39.0     | <1.5          | 37.5-41.0                                | 13.0-17.5                                | 3.5-5.5                    | -                          |
| Cement                         | 36.7±0.8      | 1.1±0.6       | 38.6±1.6                                 | 16.3±0.7                                 | 4.8±2.6                    | -                          |
| Calc. dolomite                 | 60.6±1.0      | 36.1±0.8      | -  | -  | 2.0±1.1                    | -                          |
| (5.5Zr,10Al) <sub>theory</sub> | 48.9          | 22.6          | 11.6                                     | 4.9                                      | 2.7                        | 7.5                        |
| 1Sa(5.5Zr,10Al)                | 50.5±2.2      | 26.1±3.5      | 8.7±0.2                                  | 5.4±0.7                                  | 1.7±0.3                    | 7.0±0.5                    |
| 2Sa(5.5Zr,10Al)                | 50.3±0.5      | 26.6±0.8      | 8.3±0.3                                  | 5.0±0.2                                  | 1.8±0.1                    | 7.1±0.4                    |

The value for MgO in cement is lower than the Specification limit of 1.5 %. All the other measured values lay within the usual range. As expected, calcined dolomite mainly consists of CaO and MgO, though also, some impurities are present. These impurities were not taken into account when calculating the total weights of the sorbents.

The weight percentages of the oxides in the sorbents are close to the calculated theoretical value. The relatively small deviations might be related to differences in the calculations of the total sorbent-weights compared to the actual weight of the final sorbent, as well as inaccuracy in the instruments.

However, it is important to notice that the compositions obtained for sorbents with the same theoretical composition, synthesized in two different methods, are the same. One of the objectives of this project was to compare sorbents prepared by the one-step method with the two-step method. The similar compositions are a good indication that it was possible to prepare similar sorbents, which then are interesting to further compare.

## 5.2.2 X-Ray Diffraction (XRD)

The XRD diffractometer of several of the prepared sorbents is analyzed in this section. The phase identifications, as well as the crystallite size calculation, was performed by using DIFFRA.EVA.v5.1 as it was described in 4.3.2. In the diffractograms obtained, the y-axis of all the plots presents a normalized value of the peaks intensity, the x-axis the  $2\theta$  value in degrees from  $15^\circ$  to  $75^\circ$ . The patterns of some of the sorbents not presented in this section will be given in appendix D.

The section will start with presenting some of the phases of raw materials, and then the evolution in phases during preparation-steps will be given. Further differences in phases and crystal sizes will be investigated more in detail; for ZrAl-based sorbents, the sorbents prepared without  $\text{ZrO}_2$ , 1SUncalc(5.5Zr,10Al) and 2SInter(5.5Zr,10Al). In the end, the variation in phases before and after cycles will be presented for a selection of sorbents.

### 5.2.2.1 References

Figure 5.17 is added as a reference spectra and shows the diffractogram on Calcined dolomite and Cement Fondu after drying. The diffractogram of calcined dolomite (dark grey) shows, as expected, CaO and MgO formation. In addition two other phases are present;  $\text{CaCO}_3$  and  $\text{Ca}(\text{OH})_2$ . The presence of  $\text{CaCO}_3$  is probably related to uncompleted calcination. As explained in section 1.4.1 calcination of uncalcined dolomite ( $\text{MgCO}_3 \cdot \text{CaCO}_3$ ) happens in two steps, with the calcination of  $\text{MgCO}_3$  occurring at a lower temperature than for  $\text{CaCO}_3$ . The phase of  $\text{Ca}(\text{OH})_2$  can be related to humidity in the air.

The spectra of dry cement reveal many small peaks, where most of them represent different calcium aluminates phases; in the diffractogram, Krotite,  $\text{CaAl}_2\text{O}_4$  and  $\text{Ca}_2\text{Al}_2\text{O}_4$  are represented. Also, some of the peaks are similar to those of  $\text{Ca}_6\text{Al}_7\text{O}_{16}$ . As expected, two more phases were identified in the cement diffractograms,  $\text{Fe}_2\text{O}_3$  and  $\text{SiO}_2$ . The phases correspond to what was observed in the X-Ray Fluorescence Spectroscopy.

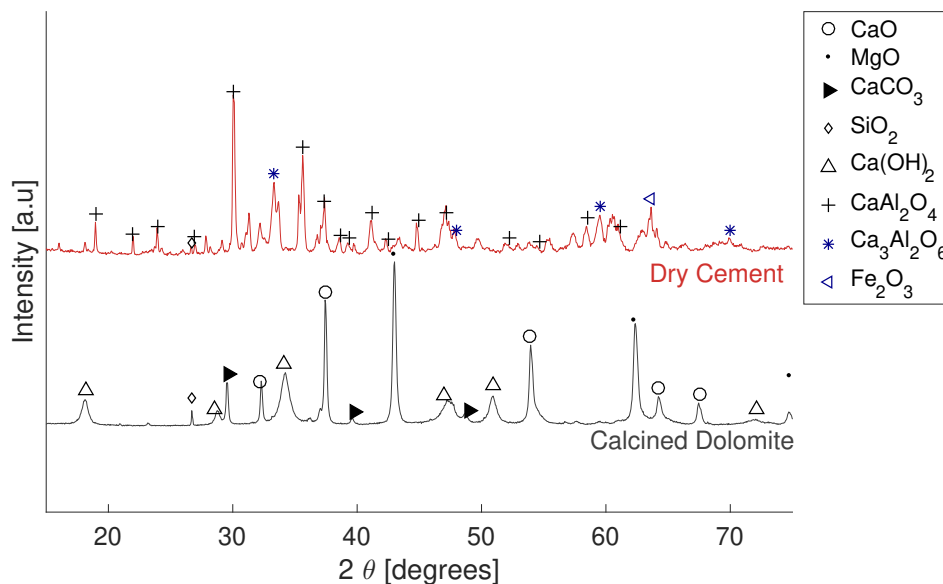


Figure 5.17: Diffraction diagram of calcined dolomite and dried cement. In  $2\theta$  range from  $15^\circ$  to  $75^\circ$ .

### 5.2.2.2 Preparation Steps

In order to see the formation of phases during the synthesis, samples were taken during preparation in a total of six steps. The diffractograms obtained for the samples from XRD are represented for 2S(6.0Zr, 9Al) in figure 5.18. The six steps are as follow;

**Step 1 (Dol + Zr)** Addition of the Zirconium-solution mixed with water to an amount close to the pore-volume of dolomite, followed by drying.

**Step 2 (+Cement)** Addition of cement.

**Step 3 (+ 1/3 H<sub>2</sub>O)** Water was added until pellets were formed. Step 3 was after 1/3 of this water was added.

**Step 4 (+ 1/3 H<sub>2</sub>O)** The next diffractogram is after 2/3 of water was added.

**Step 5 (+ 1/3 H<sub>2</sub>O)** Step 5 were when all the water was added.

**Step 6 (Calcined dolomite)** The last diffractogram represent the finished, fresh sorbent after three days of drying followed by calcination as explained in section 4.1.

The diffractogram of the first step shows peaks of Ca(OH)<sub>2</sub> and MgO. Small peaks of CaCO<sub>3</sub> and ZrO<sub>2</sub> can also be observed. The next four steps (2-5) represents the same peaks as in

the first, but in addition, different forms of calcium aluminate are observed; here marked as  $\text{CaAl}_2\text{O}_4$ . Though the peaks can also represent other calcium-aluminates similar to those observed in cement. Most of the "small" peaks in these diffractograms represent calcium aluminates. After calcination, all  $\text{CaCO}_3$  and  $\text{Ca}(\text{OH})_2$  was transformed into  $\text{CaO}$ . Further, as desired, the two stabilizing phases Mayenite ( $\text{Ca}_{12}\text{Al}_{14}\text{O}_{33}$ ) and  $\text{CaZrO}_3$  had been formed.

The formation of Mayenite during calcination when aluminates react with  $\text{CaO}$ -based sorbents at high temperatures have been observed in a wide range of studies [59, 60, 62, 66, 67]. Further, authors reported that the formation of the phase when calcium aluminate cement is introduced to  $\text{CaO}$ -based sorbents [63, 64, 65]. Also, the presence of  $\text{CaZrO}_3$  has been reported in the literature. As addressed in section 1.4.2, the phase has been reported by several authors to be formed when the  $\text{CaO}$ -based sorbent react with  $\text{ZrO}_2$  [30, 32, 33, 35, 44, 45, 46, 47, 48, 49, 50, 51, 52].

Similarly, samples were taken in a total of six steps in the preparation of a one-step sorbent 1S(6.0Zr,9Al). In that case, the first step was a mix of all the additives and the second the mixture after drying. All the diffractograms were similar to those of 2S(6.0Zr,9Al). The only difference was in the first peaks, where phases of calcium-aluminates from cement could be observed.

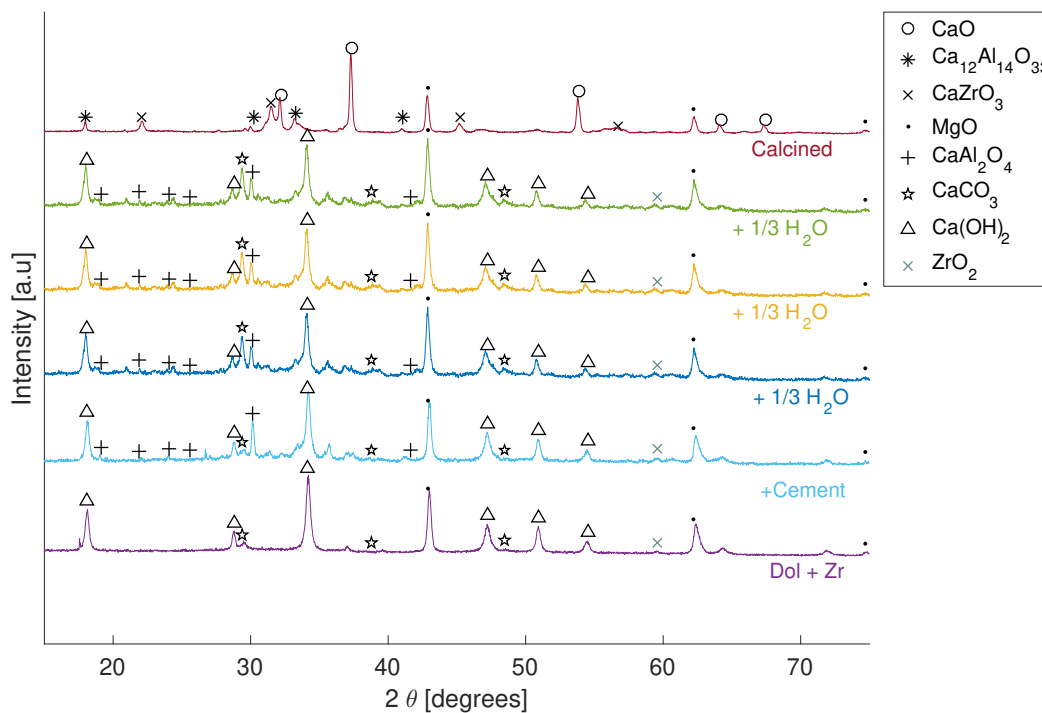


Figure 5.18: Diffraction diagram of different steps until the calcination of 2S(6.0Zr, 9Al). In  $2\theta$  range from  $15^\circ$  to  $75^\circ$ .

### 5.2.2.3 ZrAl-based sorbents

In all the prepared ZrAl based sorbents, similar phases was observed after the pre- calcination step as those seen for the calcined samle in in figure 5.18; CaO, MgO, CaZrO<sub>3</sub>, Ca(OH)<sub>2</sub> and Mayenite (Ca<sub>12</sub>Al<sub>14</sub>O<sub>33</sub>). Also, some of the diffractograms show a peak corresponding to SiO<sub>2</sub>. The next figures (figure 5.20, figure 5.19 and figure 5.21) compares differences in the ZrAl-based sorbents more in detail.

The variation in the addition of Zirconium is investigated in figure 5.19. The figure compares patterns of 1S-sorbents with a similar composition of cement and an increasing amount of Zirconium. As expected, a small increase in the peak for CaZrO<sub>3</sub> can be observed with a higher amount of Zr in the sorbents [103]. Formation of more CaZrO<sub>3</sub> was expected to give a lower capturing capacity, as more active sites of CaO in dolomite react with ZrO<sub>2</sub> according to equation 1.4. The expectation corresponds well with what was observed in the cyclic testing (section 5.1). The capacities during cycles was compared in figure 5.2b for the same three sorbents as patterns presented in figure 5.19. Their capturing capacities decreased in the same order as the peaks increases; 1S(5.5Zr,13Al) > 1S(3.38Zr,13Al) > 1S(1.3Zr,13Al).

It is clear that the formation of CaZrO<sub>3</sub> had an important effect on the stability of the sorbents. Capacity loss of sorbents with similar cement amount, with and without Zirconium was compared in figure 5.8 in section 5.1.2.3. The figure illustrated that the addition of Zirconium enhanced the stability.

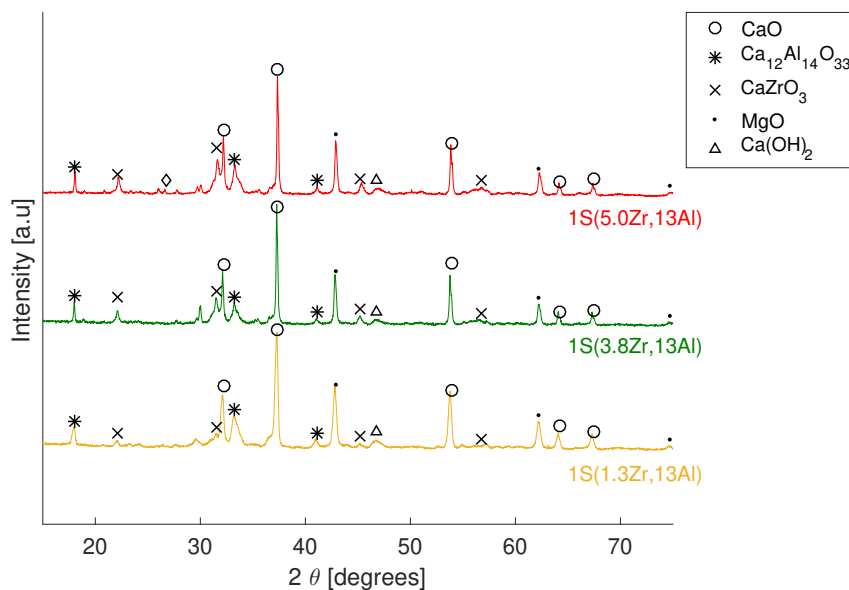


Figure 5.19: Diffraction diagram of 1S(5.0Zr,13Al), 1S(3.8Zr,13Al) and 1S(1.3Zr,13Al). In 2θ range from 15° to 75°.

Further, the variation in the patterns with cement addition is seen in figure 5.20. The

diffraction patterns are of sorbents with a similar weight percentage of Zirconium, but with a decrease in the Aluminium content. As expected, there is an increase in the Mayenite peak with a higher Aluminium amount from cement in the samples.

Also, when increasing the cement, it was observed an increase in the capturing capacities. The capturing capacities of the three sorbents presented in figure 5.20 was compared in section 5.1.1 in figure 5.2a. With the capturing capacities in decreasing orders being;  $1S(1.8Zr,6Al) > 1S(1.5Zr,10Al) > 1S(1.3Zr,13Al)$ . The reduction can be related to cement occupying more space in the pores, making diffusion of  $CO_2$  more difficult. Also, Manovic et al. [29] reported the same trend. When forming Mayenite, Calcium aluminates might need to react with some active sites in the CaO-based sorbent. Hence, the addition of cement can have led to more CaO contributing to the formation of Mayenite.

Even though the addition of the two additives showed a reduction of the capturing capacities, it is clear that the two additives could form, as desired, a stabilizing framework. The stabilities of the modified sorbents were dramatically increased compared to calcined dolomite. However, the contribution of the phases in the different sorbents will be discussed more in detail later in the report.

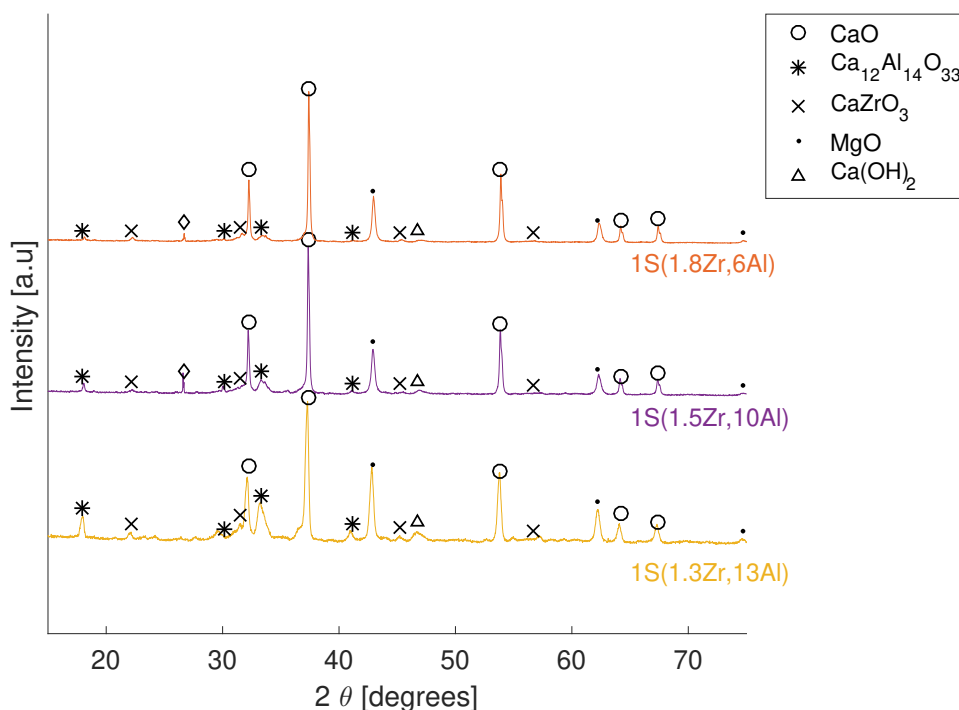


Figure 5.20: Diffraction diagram of 1S(1.8Zr,6Al), 1S(1.5Zr,10Al) and 1S(1.3Zr,13Al). In  $2\theta$  range from  $15^\circ$  to  $75^\circ$ .

To investigate differences in the one-step method and two-step method, figure 5.21a com-

compares 1Sa(5.5Zr,10Al) and 2Sa(5.5Zr,10Al) and figure 5.21b 1S(6.0Zr,9Al) and 2S(6.0Zr,9Al). There are no major differences in the patterns when comparing the two methods. However, it is important to keep in mind that it is not possible to detect what is thought to be the biggest difference between the two methods from the patterns. Namely, where in the particles the formation of  $\text{CaZrO}_3$  and  $\text{Ca}_{12}\text{Al}_{14}\text{O}_{33}$  occurred.

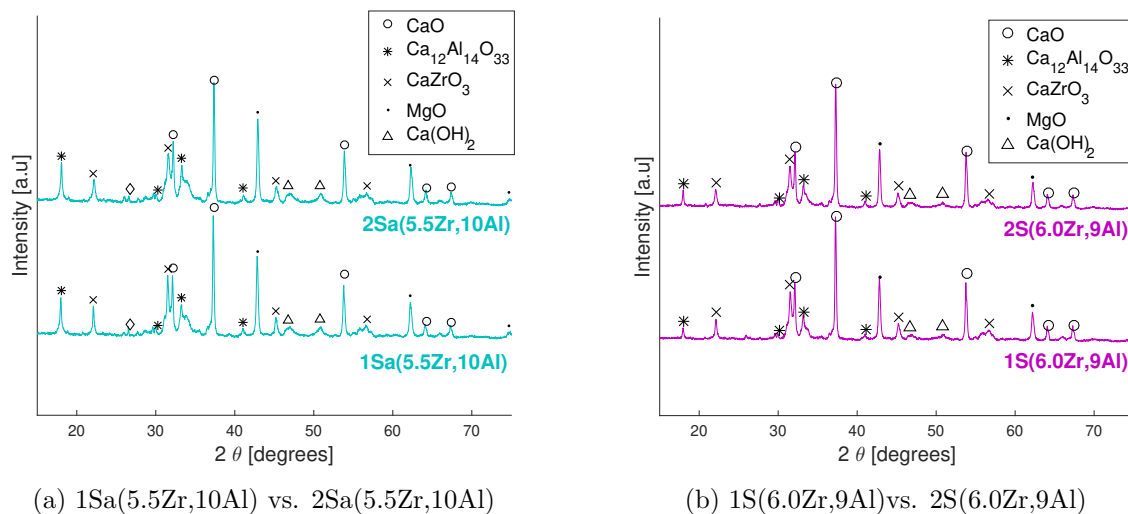


Figure 5.21: Diffraction diagram comparing one-step and two-step sorbents. In  $2\theta$  range from  $15^\circ$  to  $75^\circ$ .

Table 5.13 give crystal sizes of  $\text{CaO}$  for the ZrAl-based sorbents. Also, values for calcined dolomite are given as a reference. The values are mainly given as comparison and represent the most prominent peak of  $\text{CaO}$  (at  $2\theta \approx 37^\circ$ ). Crystal sizes were also found for  $\text{MgO}$  (at  $2\theta \approx 43^\circ$ ) and  $\text{CaZrO}_3$  (at  $2\theta \approx 22^\circ$ ), and are given in appendix ???. The same account for the rest of the crystal sizes given in this section.

In order to check the accuracy of the measurement, crystal sizes were calculated for four samples of 1Sa(5.5Zr,10Al); The value for  $\text{CaO}$  was  $47.7 \pm 0.9$ . For 1Sa(5.5Zr,10Al), the crystal size of  $\text{CaO}$  is given with the standard variation in table 5.13.

The crystal sizes of  $\text{CaO}$  all lay in the range of 40-50 nm for  $\text{CaO}$ . The crystal sizes of  $\text{MgO}$  ranged from 26-42 nm, and the crystal sizes of  $\text{CaZrO}_3$  from 24 - 40 nm. The crystal sizes of  $\text{CaO}$  in calcined dolomite and the modified sorbents are similar, with a value of 40.4 nm for calcined dolomite. A decrease in the crystal sizes of the modified sorbents compared to calcined dolomite could have been expected. However, the exposure to high temperatures in the pre-calcination probably led to a small degree of sintering. The sintering in the pre-calcination was intended, expected to form a skeleton of  $\text{CaO}$ . Which in terms can prevent further sintering of the particles during cycles.

The relatively small variation in  $\text{CaO}$  crystal sizes among the ZrAl-based sorbents does not



seem to follow any specific trend, not related to the amount of additives nor the different methods used to create them.

Table 5.13: Crystal sizes (CS) of CaO at  $2\theta \approx 37^\circ$  found from the Scherrer equation (3.2).

| <b>Sample</b>     | <b>CS CaO [nm]</b> |
|-------------------|--------------------|
| Calcined Dolomite | 40.4               |
| 1S(1.3Zr,13Al)    | 41.4               |
| 2Sb(1.3Zr,13Al)   | 47.7               |
| 1S(2.6Zr,13Al)    | 38.4               |
| 1S(3.8Zr,13Al)    | 50.2               |
| 1Sb(5.0Zr,13Al)   | 50.5               |
| 2S(5.0Zr, 13Al)   | 46.5               |
| 1Sa(5.5Zr, 10Al)  | 47.7 $\pm$ 0.9     |
| 2Sa(5.5Zr, 10Al)  | 49.0               |
| 1Sb(5.5Zr, 10Al)  | 43.8               |
| 2Sb(5.5Zr, 10Al)  | 46.5               |
| 1S(1.5Zr,10Al)    | 41.4               |
| 1S(6Zr, 9Al)      | 44.9               |
| 2S(6Zr, 9Al)      | 42.3               |
| 1S(1.8Zr,6.Al)    | 49.6               |

#### 5.2.2.4 Sorbents prepared without ZrO<sub>2</sub>

In figure 5.22 the XRD diffractograms of the sorbents made with only dolomite together with the CeAl-based sorbents are presented. In similarity with the ZrAl-based sorbents, they all consist of CaO, MgO, and Mayenite. As expected, in the diffractograms representing the CeAl-based sorbents (green) 1S(5.5Ce, 10Al) and 2S(5.5Ce, 10Al), an additional phase of CeO<sub>2</sub> was observed. The phase was as anticipated and reported in the literature when Cerium nitrate has been used as a precursor [36, 54]. The peak of 28.8 ° for 15Al could not be recognized.

The patterns of 1S(5.5Ce,10Al) and 2S(5.5Ce,10Al) are very similar. The same was observed with the capacities of the two sorbents. They did not exhibit any notable differences in their cyclic behavior between the one-step and two-step method.

It was expected that CeO<sub>2</sub> would affect not only the capturing capacity but also the stability. Unlike ZrO<sub>2</sub>, CeO<sub>2</sub> does not react with the active sites of CaO to form a mixed oxide. However, due to its high Tamann temperature CeO<sub>2</sub> can create a barrier of inert metal oxides, as explained in section 1.4 and hence reduce sintering. However, in this project, the sorbent prepared with CeO<sub>2</sub> did not show any difference in the capturing capacity, nor in

the stability compared to a sorbent only made with dolomite and cement.

As expected, the patterns of 15Al and 11Al are very similar. The only difference worth noticing is, as expected, a small increase in the peaks of Mayenite with the addition of cement. The increase corresponds with what was observed for the ZrAl-based sorbents when a higher cement amount was added. Also, 15Al had a lower capacity but slightly better capacity than 11Al. The results further strengthen the theory of cement working both as a binder and a stabilizer.

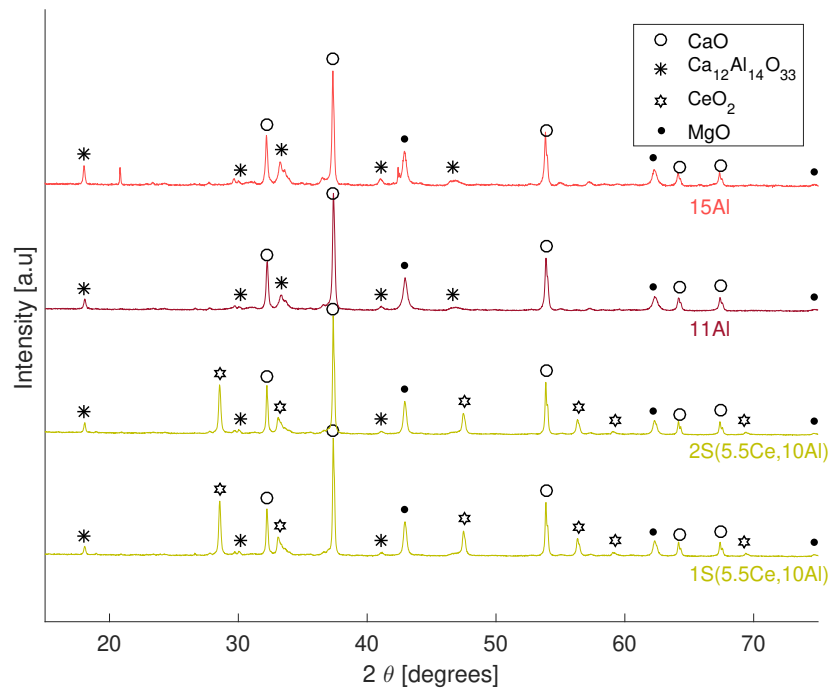


Figure 5.22: Diffraction diagram of 15Al, 11Al, 2S(5.5Ce,10Al) and 1S(5.5Ce,10Al). In  $2\theta$  range from  $15^\circ$  to  $75^\circ$ .

Table 5.14 gives crystal sizes of CaO for the sorbents prepared without ZrO<sub>2</sub>. In addition, values of calcined dolomite and the two best ZrAl-based sorbents are given as a reference. Crystal sizes of CeO<sub>2</sub> (at  $2\theta \approx 29^\circ$ ) and MgO are given in appendix D. The crystal sizes of CeO<sub>2</sub> were of about 50 nm.

In similarity, with the ZrAl-based sorbents, all the crystal sizes are relatively similar. The CeAl-based sorbents had the highest values, with 54.0 nm and 53.4 nm for 1S(5.5Ce,10Al) and 2S(5.5Ce,10Al), respectively. The values might be related to a slightly higher degree of sintering of the Cerium samples during the pre-calcination step. Nevertheless, overall there are no major differences.

Table 5.14: Crystal sizes (CS) of CaO at  $2\theta \approx 37^\circ$  found from the Scherrer equation (3.2). Sizes presented are for sorbents prepared without  $ZrO_2$  compared to the best ZrAl-based sorbents and calcined dolomite.

| Sample            | CS CaO [nm]    |
|-------------------|----------------|
| Calcined Dolomite | 40.4           |
| 1Sa(5.5Zr, 10Al)  | $47.7 \pm 0.9$ |
| 2Sa(5.5Zr, 10Al)  | 49.0           |
| 1S(5.5Ce,10Al)    | 54.0           |
| 2S(5.5Ce,10Al)    | 53.4           |
| 11Al              | 45.7           |
| 15Al              | 49.6           |

### 5.2.2.5 Calcination effect

Figure 5.23 compares the patterns of 2Sa(5.5Zr,10Al), 2SInter(5.5Zr,10Al) and 1SUncalc(5.5Zr,10Al). The patterns of 2Sa(5.5Zr,10Al), 2SInter(5.5Zr,10Al) are close to identical, both consisting of CaO, MgO,  $CaZrO_3$  and  $Ca(OH)_2$  and calcium aluminate mostly in the form of  $Ca_{12}Al_{14}O_{33}$ . 1SUncalc(5.5Zr,10Al) was found to consist of the same phases, however the calcium aluminates was mostly in the form of  $CaAl_2O_4$  and  $Ca_3Al_2O_6$ .

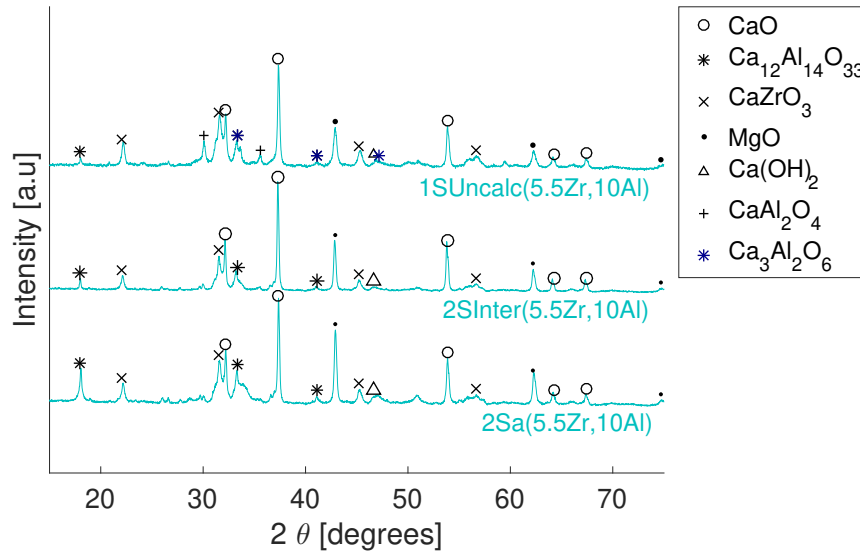


Figure 5.23: Diffraction diagram of 1Sa(5.5Zr,10Al), 2SInter(5.5Zr,10Al) and 1SUncalc(5.5Zr,10Al). In  $2\theta$  range from  $15^\circ$  to  $75^\circ$ .

Table 5.15 give crystal sizes of CaO and MgO for the sorbents represented in figure 5.23.

Also, values of 1Sa(5.5Zr,10Al) and calcined dolomite are given. The crystal sizes of all the sorbents are very similar. However, it can be noticed that the lowest value is for the sorbent made with uncalcined dolomite (39.7 nm), while the highest value is for the sorbent made with intermediate calcination (50.1 nm). This might be related to more pronounced sintering when the samples were exposed to high temperatures several times. Results obtained in the Nitrogen adsorption-desorption (section 5.2.3) and SEM (section 5.2.4) indicated that the fresh sample of 2SInter(5.5Zr,10Al) was more sintered than 1Sa(5.5Zr,10Al) and 2Sa(5.5Zr,10Al).

Table 5.15: Crystal sizes (CS) of CaO at  $2\theta \approx 37^\circ$  found from the Scherrer equation (3.2) for calcined dolomite, 1Sa(5.5Zr,10Al), 2Sa(5.5Zr,10Al), 1SUncalc(5.5Zr,10Al) and 2SInter(5.5Zr,10Al).

| Sample               | CS CaO [nm] |
|----------------------|-------------|
| Calcined Dolomite    | 40.4        |
| 1Sa(5.5Zr, 10Al)     | 47.7        |
| 2Sa(5.5Zr, 10Al)     | 49.0        |
| 1SUncalc(5.5Zr,10Al) | 39.7        |
| 2SInter(5.5Zr,10Al)  | 50.1        |

### 5.2.2.6 Fresh vs. Spent

In order to look for changes in phases and crystall sizes during cycles XRD was performed on a selection of spent sorbents, as well as calcined dolomite. The cyclic testing was performed in the microbalance reactor for 1Sa(5.5Zr,10Al) and 2Sa(5.5Zr,10Al). (Ads: 5 % CO<sub>2</sub>, 8 % H<sub>2</sub>O, 600 °C, 6min. Des: 100 % CO<sub>2</sub>, 950 °C). For the rest of the sorbents, experiments were conducted in TGA in wet conditions (Ads: 5 % CO<sub>2</sub>, 8 % H<sub>2</sub>O, 600 °C, 30min. Des: 80 % CO<sub>2</sub>, 950 °C).

In figure 5.24 diffractograms obtained for fresh and spent samples of 1Sa(5.5Zr,10Al) and 2Sa(5.5Zr,10Al) are given. The spent samples were after 40 regeneration-cycles. No new phases are observed after cycles. Both fresh and spent sorbents consist of CaO, Ca<sub>12</sub>Al<sub>14</sub>O<sub>33</sub>, CaZrO<sub>3</sub>, MgO, Ca(OH)<sub>2</sub> and SiO<sub>2</sub>. Also, the other spent samples tested obtained similar patterns as their corresponding fresh patterns.

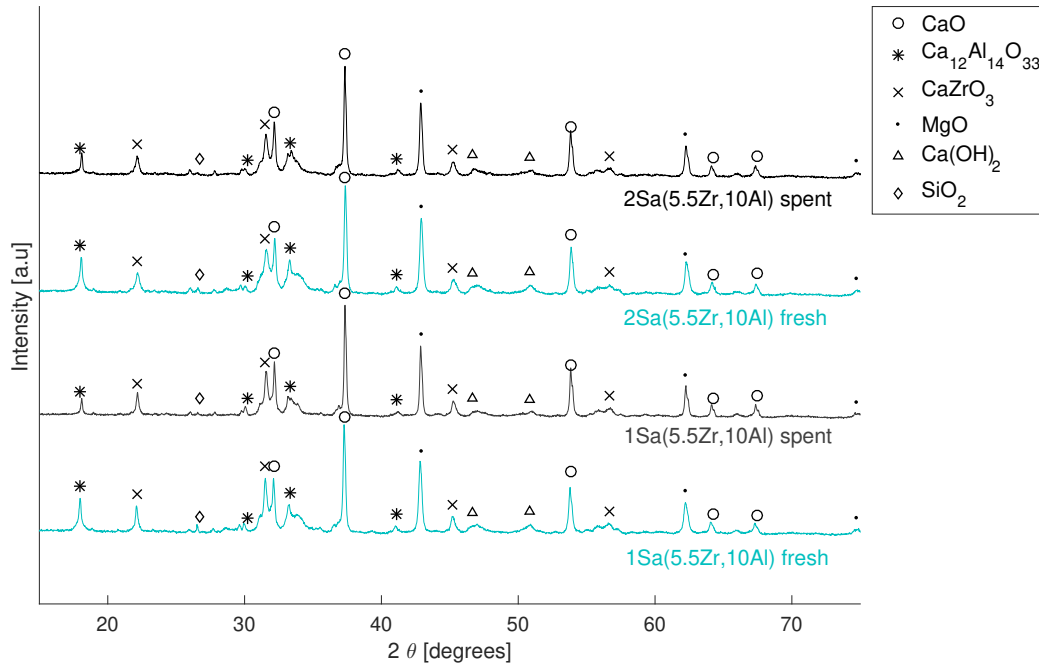


Figure 5.24: Diffraction diagram of fresh and spent 1Sa(5.5Zr,10Al) and 2Sa(5.5Zr,10Al). In  $2\theta$  range from  $15^\circ$  to  $75^\circ$ . Experiments spent: (Ads: 5 %  $\text{CO}_2$ , 8 %  $\text{H}_2\text{O}$ ,  $600^\circ\text{C}$ , 6min. Des: 100 %  $\text{CO}_2$ ,  $950^\circ\text{C}$ )

Table 5.16 presents CaO crystal sizes for the fresh and spent samples compared to calcined dolomite. The total numbers of regeneration-cycles the samples were exposed to are given in the last column.

For calcined dolomite, the crystal sizes of CaO increased somehow after 15 cycles from 40.4 nm to 47.6 nm, indicating, as anticipated, some sintering during the cycles. Despite MgO functioning as a physical barrier, sintering has widely been reported as one of the main deactivation-mechanisms of dolomite [38, 42, 104, 105, 106].

Further, the change in crystal size of 2S(5.5Zr,10Al)Uncalc is notable. Its crystal sizes increased from 39.7 nm to 47.6 nm only after four regeneration-cycles. In the sorbent XRD pattern, it was found that Mayenite had not been formed; hence, the sorbent could not form the same robust framework as the sorbents were calcined dolomite was used. When the sorbent was prepared, the dolomite was in its carbonated form, ( $\text{CaCO}_3 \cdot \text{MgCO}_3$ ). The pore-volume of uncalcined dolomite was by incipient wetness found to be very small (0.2 ml/g ). There was no surface for Zirconium to react.  $\text{CaCO}_3$  was not transformed to its calcined formed before it was exposed to high temperatures in the pre-calcination, hence after it was mixed with the additives. Consequently, the reaction between CaO and  $\text{ZrO}_2$ , and the dispersion of  $\text{CaZrO}_3$  was most likely quite deficient. Furthermore, it is a possibility that some Zirconium instead reacted with Calcium from cement.

There are no notable changes in the crystal sizes for the rest of the modified sorbents before and after cycles. The relatively small changes might be related to the inaccuracy in the measurement and non-homogeneity in the particles. The similarity in sizes before and after cycles indicates that modification of the sorbents had, as anticipated, made it possible to limit sintering during several regeneration-cycles.

Table 5.16: The crystal sizes of CaO and MgO for fresh and spent sorbents compared to calcined dolomite. Experiments spent (TGA / microbalance reactor\*) : (Ads: 5 % CO<sub>2</sub>, 8 % H<sub>2</sub>O, 600 °C, 6 / 30min. Des: 80 / 100 % CO<sub>2</sub>, 950 °C)

| Sample               | CaO [nm] |       | total cycles |
|----------------------|----------|-------|--------------|
|                      | fresh    | spent |              |
| Calcined dolomite    | 40.4     | 47.6  | 15           |
| 1S(3.8Zr,13Al)       | 50.2     | 47.1  | 30           |
| 1Sa(5.5Zr,10Al)      | 46.5     | 50.0  | 40*          |
| 2Sa(5.5Zr,10Al)      | 49.0     | 46.9  | 40*          |
| 2S(5.5Zr,10Al)Uncalc | 39.7     | 47.6  | 4            |
| 1S(1.8Zr,6Al)        | 49.6     | 46.8  | 15           |
| 1S(5.5Ce,10Al)       | 54.0     | 48.8  | 15           |

### 5.2.3 Nitrogen Adsorption-Desorption at 77 K

Nitrogen adsorption-desorption at 77 K was performed on a selection of sorbents and calcined dolomite. The experiments were performed as described in section 4.3.3. The surface area was found following the BET method, and the pore size distribution was found following the BJH-method as described in section 3.3.3. First, the results for a selection of the fresh sorbents will be given. Subsequently, the evolution in pore-size and surface area during cycles for 1Sa(5.5Zr,10Al) will be investigated. The spent samples are analyzed after performing the experiments in the microbalance due to the high amount of samples needed ( $\approx 1$  g). (Ads: 5 % CO<sub>2</sub>, 8 % H<sub>2</sub>O, 600 °C, 6min. Des: 100 % CO<sub>2</sub>, 950 °C ).

#### 5.2.3.1 Fresh sorbents

The adsorption-desorption isotherm of 2Sa(5.5Zr,10Al) obtained from the Nitrogen adsorption-desorption measurement is depicted in figure 5.25. The volume of Nitrogen adsorbed and desorbed (mmol /g) is plotted against the relative pressure ( $P/P^0$ ). Other sorbents obtained similar isotherms. The isotherm can be interpreted to be a combination of type II and IV [48, 96, 107]. For both isotherms, the use of the BET-method and BJH method is valid. Type II are typical for macropores and type IV for mesopores. The obtained isotherm might indicate that the sorbents consist of both mesopores and macropores, which will be explained more in detail later.

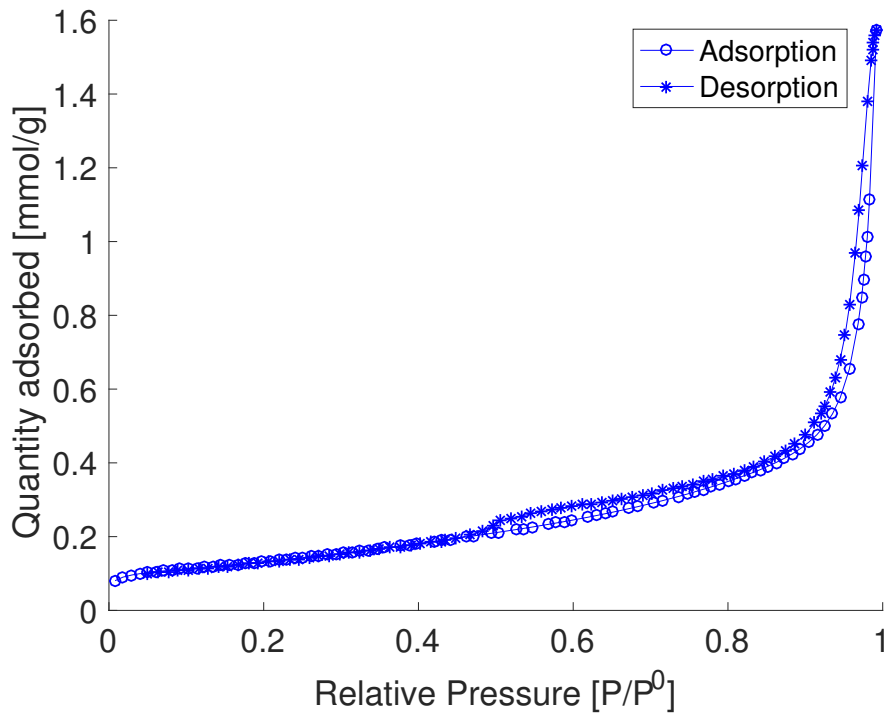


Figure 5.25: The adsorption-desorption isotherm of 2Sa(5.5Zr,10Al) obtained from Nitrogen adsorption-desorption at 77 K.

In table 5.17 the surface areas of fresh sorbents are displayed. The table includes calcined dolomite and a selection of ZrAl-based sorbents, 2S(5.5Ce,10Al), 11Al, and 15Al. Two of the sorbents were tested several times. The surface area was found to be  $8.8 \pm 0.9 \text{ m}^2/\text{g}$  for 1Sa(5.5Zr,10Al), while  $10.6 \pm 0.6 \text{ m}^2/\text{g}$  for 2Sa(5.5Zr,10Al). Experiments were performed five times and three times, respectively. The sorbents are presented with their standard variations in the table.

In general, all the sorbents obtained small surface areas, ranging from 7-18  $\text{m}^2/\text{g}$ . The calcined dolomite value is slightly higher, with a value of 21.0  $\text{m}^2/\text{g}$ . The lower surface areas of the prepared sorbents can be related to sintering during the pre-calcination step but are likely most related to the Zirconium and cement occupying area. Cement Fondu has a low porosity [58].

Among the modified sorbents, the trend is a lower surface area with a higher content of additives - this was expected, as the additives occupy more area. It can also be noticed that the sorbents with a higher surface area generally had higher initial capturing capacities. For instance, 1S(1.8Zr,10Al) with a surface area of 18.8  $\text{m}^2$  were among the sorbents exhibiting the highest capturing capacity in cycle 1 (35.8 %). At the same time, 2S(5.0Zr,13Al) with a surface area of 7.8  $\text{m}^2$  had one of the lowest capacities in cycle 1 (12.2 %). The trend is in agreement with what has been observed in literature for CaO-based sorbents [44, 68].

Table 5.17: BET surface area ( $S_{\text{BET}}$ ) for a selection of fresh sorbents compared to calcined dolomite. Obtained from Nitrogen adsorption-desorption at 77 K.

| Sample            | $S_{\text{BET}}$ [ $\text{m}^2/\text{g}$ ] |
|-------------------|--|
| Calcined Dolomite | 21.0                                       |
| 1Sb(5.0Zr,13Al)   | 8.9  |
| 2S(5.0Zr, 13Al)   | 7.8  |
| 1Sa(5.5Zr, 10Al)  | $8.8 \pm 0.9$                              |
| 2Sa(5.5Zr, 10Al)  | $10.6 \pm 0.6$                             |
| 1S(1.5Zr,10Al)    | 17.9                                       |
| 1S(6Zr, 9Al)      | 8.5  |
| 2S(6Zr, 9Al)      | 8.8  |
| 1S(1.8Zr,6.Al)    | 18.8                                       |
| 2S(5.5Ce,10Al)    | 7.2  |
| 11Al              | 15.1                                       |
| 15Al              | 11.4                                       |

Both 11Al and 15Al obtained lower surface areas than calcined dolomite. The surface area of 11Al ( $15.1 \text{ m}^2/\text{g}$ ) is higher than of 15Al ( $11.4 \text{ m}^2/\text{g}$ ). Moreover, comparing 11Al to, for instance, 1Sa(5.5Zr,10Al), the surface area of 11Al is higher ( $15.1 \text{ m}^2/\text{g}$  vs.  $8.8 \pm 0.9 \text{ m}^2/\text{g}$ ). The results clarify that both the addition of cement and Zirconium reduces the surface areas.

The pore-structure of CaO-based sorbents can have a significant impact on their performance during cycles. Chen et al. [73] found that the distribution of the pore size was more critical than the surface area. Therefore, the next part of this section will focus more on the pore-size distribution in the sorbents. However, the relationship between pore size and surface area will also be considered. In all the plots representing the pore size distribution, the x-axis gives the pore diameter ( $d_p$ ) in nm. The y-axis gives the pore volume in  $\text{cm}^3/\text{g}$ .

Figure 5.26 presents the pore-size distribution of calcined dolomite, 1Sa(5.5Zr,10Al) and 2Sa(5.5Zr,10Al). Both calcined dolomite and the two sorbents presented in figure 5.26 exhibits a bimodal distribution of the pore volumes. The sizes are at about 3-5 nm (small mesopores) and 30-150 nm (large mesopores / small macropores). The observation agrees with the isotherm interpretation, presented in figure 5.25. A bimodal distribution have also been reported in literature for CaO-based sorbents [68, 69, 108].

It is also thought that the particles consisted of larger pores. However, for that, mercury-porosimetry needs to be conducted. Even so, smaller pores (2-100 nm) contribute most to the carbonation reaction [63, 68, 70]. Wei et al. [68] found small mesopores (2-10 nm) to have enhanced the reaction control stage, while larger pores (10-100 nm) impact the diffusional controlled regime. Smaller pore sizes are also those contributing most to the surface area.

There are more mesopores with small size ( $\approx 3 \text{ nm}$ ) in calcined dolomite than in the mod-



ified sorbents. In the large pore sizes, there is no significant variation between the three samples. The larger pore-volume of calcined dolomite corresponds with its higher surface area. The larger surface area and pore volume correspond with the higher initial capturing capacity of calcined dolomite than of the modified sorbents. However, the stability was significantly worse for calcined dolomite. A similar tendency demonstrates that, despite the pre-calcination and addition of additives, the sorbents could keep a relatively good pore structure.

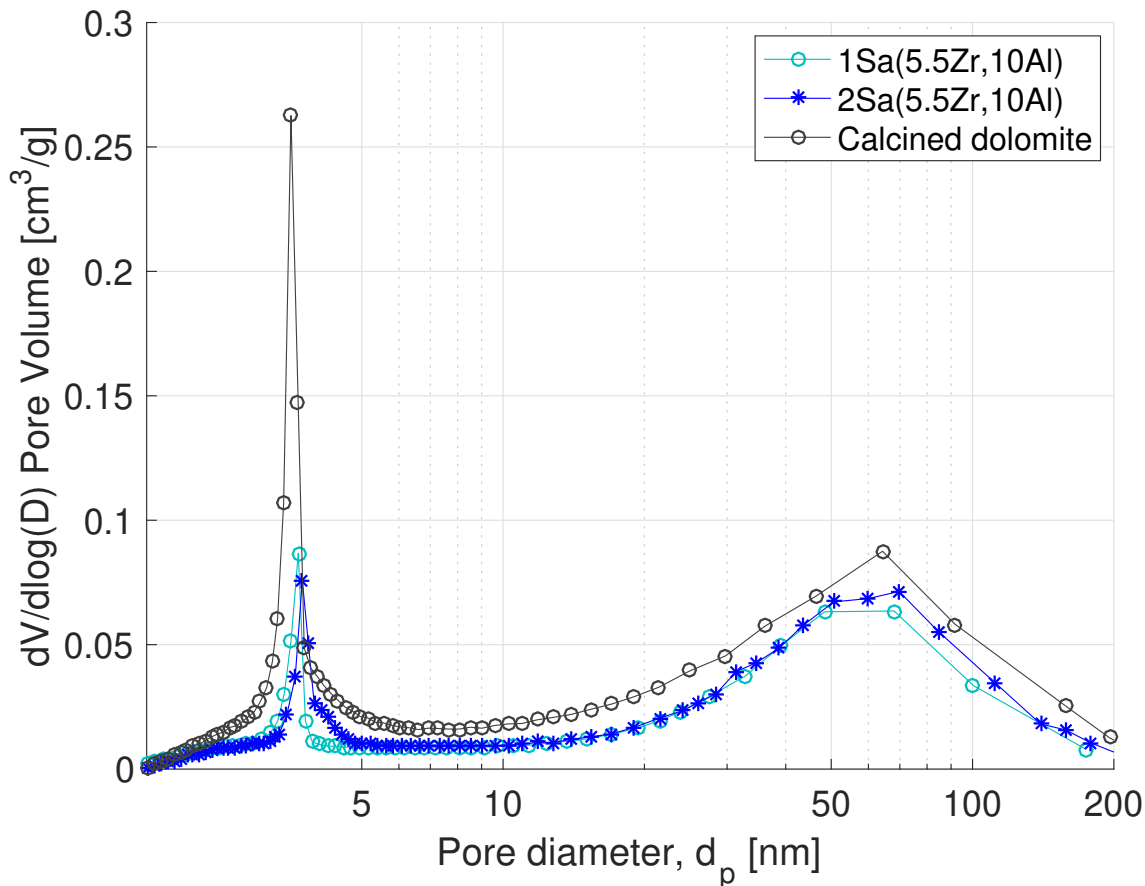


Figure 5.26: Pore volume distribution of calcined dolomite, 1Sa(5.5Zr,10Al) and 2Sa(5.5Zr,10Al) found from the desorption

In figure 5.27 the pore size-distribution of 2Sa(5.5Zr,10Al), 1SUncalac(5.5Zr,10Al) and 2SInter(5.5Zr,10Al) are compared. Their surface areas are given in table 5.18. The surface areas of 2Sa(5.5Zr,10Al) and 2Sinter(5.5Zr,10Al) are very similar ( $10.6 \text{ m}^2/\text{g}$  and  $10.7 \text{ m}^2/\text{g}$ ). In contrast, their pore-size distribution differs. 2SInter(5.5Zr,10Al) did not consist of the small mesopores. The absence of small mesopores can be related to the extra sintering during the intermediate calcination, which corresponds to its larger crystal sizes observed in section 5.2.2. The loss of small mesopores can explain why 2SInter(5.5Zr,10Al) obtained a lower

capturing capacity than 2Sa(5.5Zr,10Al). As explained earlier, small mesopores can have a positive effect on the carbonation reaction. Wei et al. [68] found a linear relationship between the increase in the uptake of CO<sub>2</sub> in the reaction controlled stage and the increase in small pores.

1SUncalc(5.5Zr,10Al) has a lower surface area (7.2 m<sup>2</sup>/g) than 2Sa(5.5Zr,10Al) and 2SInter(5.5Zr,10Al). No mesopores can be observed in the distribution, and the overall pore volume of the sorbents seems to be lower than for the two others. The use of uncalcined dolomite instead of calcined when preparing the sorbent can have had a negative effect on its porous structure, making it hard for CO<sub>2</sub> to access active CaO.

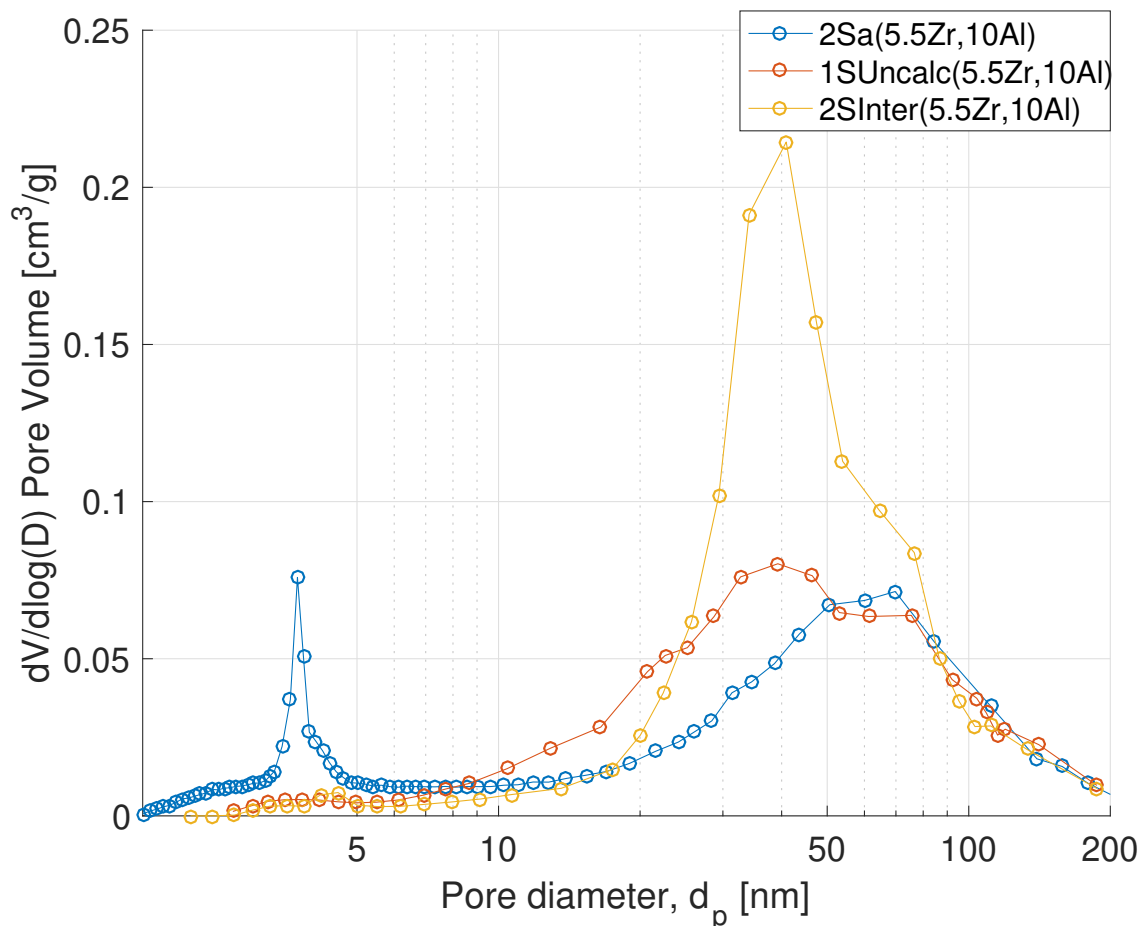


Figure 5.27: Pore volume distribution of 2Sa(5.5Zr,10Al), 2SInter(5.5Zr,10Al) and 1SUncalc(5.5Zr,10Al) found from the desorption.

Table 5.18: BET surface area ( $S_{\text{BET}}$ ) of 2Sa(5.5Zr,10Al), 1SUncalc(5.5Zr,10Al), 2Sinter(5.5Zr,10Al). Obtained from Nitrogen adsorption-desorption at 77 K.

| Sample               | $S_{\text{BET}}$ [ $\text{m}^2/\text{g}$ ] |
|----------------------|--|
| 2Sa(5.5Zr, 10Al)     | $10.6 \pm 0.6$                             |
| 1SUncalc(5.5Zr,10Al) | 7.2  |
| 2Sinter(5.5Zr,10Al)  | 10.7                                       |

### 5.2.3.2 Spent sorbents

Further, it was interesting to investigate the pore-structure of the sorbents during cycles. Literature has shown that a change in the pore-structure due to sintering and pore-collapse can significantly affect the stability [73, 63, 68, 108, 71, 70, 109, 46]. The evolution in pore size distribution and surface areas during cycles of 1S(5.5Zr,10Al) are presented in figure 5.28 and table 5.19, respectively. The fresh sorbent is compared with spent sorbent after 3 and 20 cycles.

The surface areas are very similar—however, there is a small decrease. The surface area of the fresh sorbent is  $8.8 \text{ m}^2/\text{g}$ , while the surface area after 20 cycles is  $7.6 \text{ m}^2/\text{g}$ . The pores kept their bimodal distribution, but it is shifted somewhat to the right for the spent samples. While the small sizes are closer to 3 nm in the fresh samples, they are closer to 5 nm in the spent samples—the bigger pores shifts from a peak at about 50 nm to a peak bit over 100 nm. There are also changes in the pore volumes of the sorbents after cycles. The changes in the sorbents pore-structure during cycles can indicate that a small degree of sintering and pore collapse occurred during cycles.

It can also be noted a small increase in the pore volume from cycle three to cycle 20. The changes in temperature and the sorbents continuous carbonation-decarbonation cycles can lead to a reconstruction of the pores.

Nevertheless, overall the changes in the sorbent after cycles are only minor, indicating that they very much were able to keep their porous structure through the cycles. Which evidence that modification of the sorbents could very much prevent sintering and pore-collapse in the project.

Nitrogen adsorption-desorption was not performed of spent calcined dolomite in this project due to the high amount of sample needed. However, it is expected a significant reduction in mesopores and surface-area of calcined dolomite due to sintering. Despite the presence of MgO, Naeem et al.[110] reported a reduction in the pore volume of dolomite with 87 %. Literature have shown that both the creation of  $\text{CaZrO}_3$  [46] and modification with cement [63, 108] reduced the changes in both pore volume and surface area significantly, compared to unmodified sorbents.

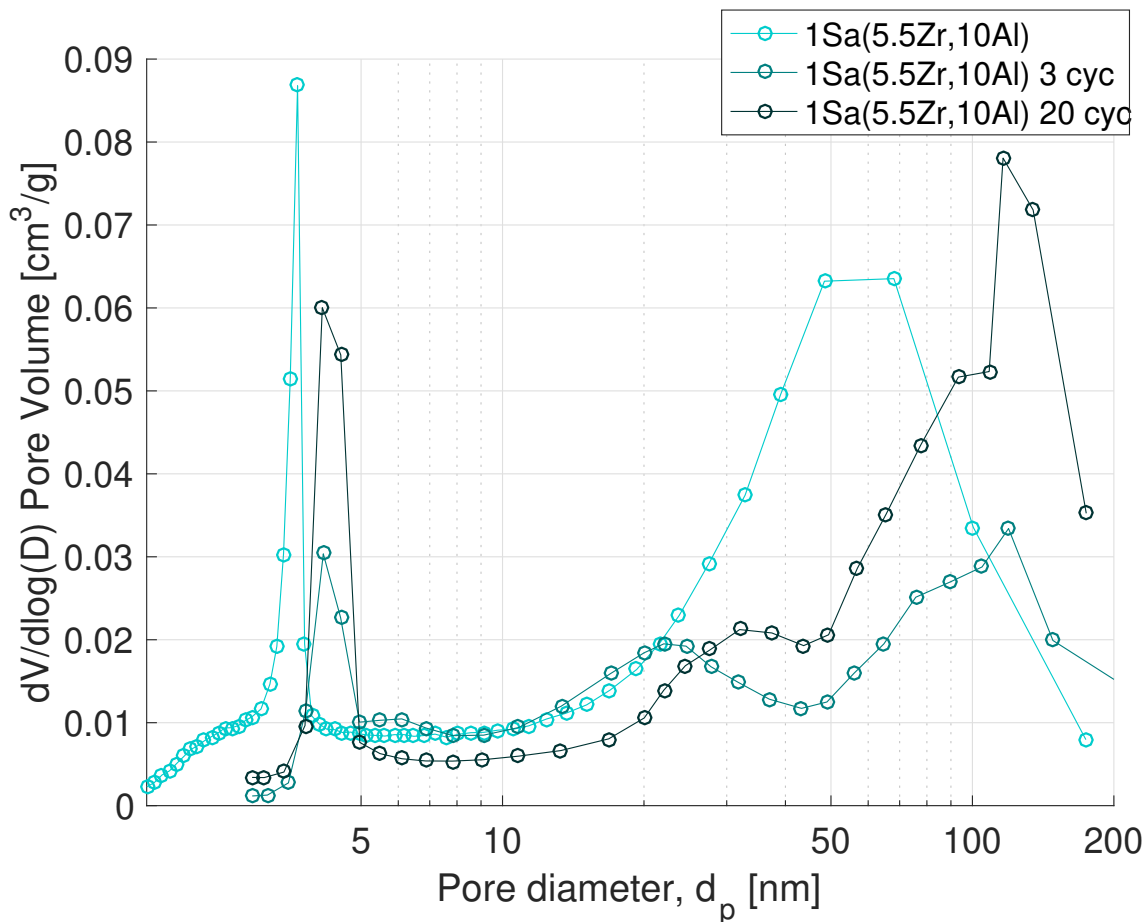


Figure 5.28: Pore volume distribution of 1Sa(5.5Zr,10Al) found from the desorption; fresh, spent after 3 cycles and spent after 20 cycles in the microbalance reactor. Ads: 5% CO<sub>2</sub>, 8% H<sub>2</sub>O, 600°C, 6 min. Des: 100% CO<sub>2</sub>

Table 5.19: The Surface area ( $S_{BET}$ ) of 1Sa(5.5Zr,10Al): fresh, spent after 3 cycles and spent after 20 cycles in the microbalance reactor. (Ads: 5 % CO<sub>2</sub>, 8 % H<sub>2</sub>O, 600 °C, 6 min. Des: 100 % CO<sub>2</sub>.) Obtained from Nitrogen adsorption-desorption at 77 K.

| Sample          | $S_{BET}$ [m <sup>2</sup> /g] |       |        |
|-----------------|-------------------------------|-------|--------|
|                 | fresh                         | 3 cyc | 20 cyc |
| 1Sa(5.5Zr,10Al) | 8.8                           | 8.4   | 7.6    |

## 5.2.4 Scanning Electron Microscopy (SEM)

To understand more about the morphology and pore structure of the sorbents, Scanning Electron Microscopy (SEM) were performed on a selection of sorbents as explained in section 4.3.4. Several pictures were taken, both at different places, particles, and different magnification. The investigations revealed that the particles are not homogeneous, though they follow a similar trend. The rest are available for the MBCL project.

First, a selection of fresh sorbents will be compared. Before a comparison between fresh and spent samples for the best ZrAl-based sorbents will be given. The spent samples were after cycles in the microbalance reactor (Ads: 5 % CO<sub>2</sub>, 8 % H<sub>2</sub>O, 600 °C, 6min. Des: 100 % CO<sub>2</sub>, 950 °C). All the pictures were taken with a voltage of 12 kV, current of 12pA, and working distance of about 4 mm.

### 5.2.4.1 Fresh Samples

Among the fresh sorbents, there were especially some sorbents that were interesting to compare. Namely, 1S-sorbents and 2S-sorbents, good and bad (1S(1.8Zr,6Al)) sorbents, the effect of performing intermediate calcination, and a sorbent prepared with only cement. Therefore figure 5.31 presents SEM-pictures of the following sorbents; 1Sa(5.5Zr,10Al), 2Sa(5.5Zr,10Al), 1S(1.8Zr,6Al) and 15Al. All the pictures were taken at a magnification of 50.000, except the 1Sa(5.5Zr,10Al) taken at a magnification of 65.000. All the sorbents show a somewhat porous structure, similar to what has been observed in the literature. [63, 64].

Figure 5.29a and 5.32a presents selected picture of 1Sa(5.5Zr,10Al) and 2Sa(5.5Zr,10Al). There are no major differences between the 1S-sorbent and 2S-sorbent. It might seem that the surface is slightly more smooth for 1Sa(5.5Zr,10Al) compared to 2Sa(5.5Zr,10Al), which can indicate a degree of sintering of the 1S-sorbent. However, the differences are not very significant. It was not observed any differences in the crystal sizes of the two sorbents in section 5.2.2.

In figure 5.29d a SEM-picture of 2SInter(5.5Zr,10Al) is presented. It is quite clear that this is the sorbent with the most compact structure. The explanation is probably related to enhanced sintering when the sorbent was exposed to intermediate calcination. The observation corresponds with what was seen in the crystal sizes, discussed in section ???. Hence it was harder for CO<sub>2</sub> to diffuse into the particle, which led to a lower capturing capacity of 2SInter(5.5Zr,10Al) compared to 2Sa(5.5Zr,10Al).

The structure of 15Al, seen in figure 5.31 shows more "flat areas" that can correspond to the skeleton created by Mayenite. The structure is similar to what has been reported earlier by Duan et al. [64]. The authors emphasized that the framework was making the pellets resistant towards attrition. Pictures were not obtained for 15Al in this project after cycles. However, it kept relatively good stability during 30 cycles. An indication that the sorbent

kept a robust framework during cycles.

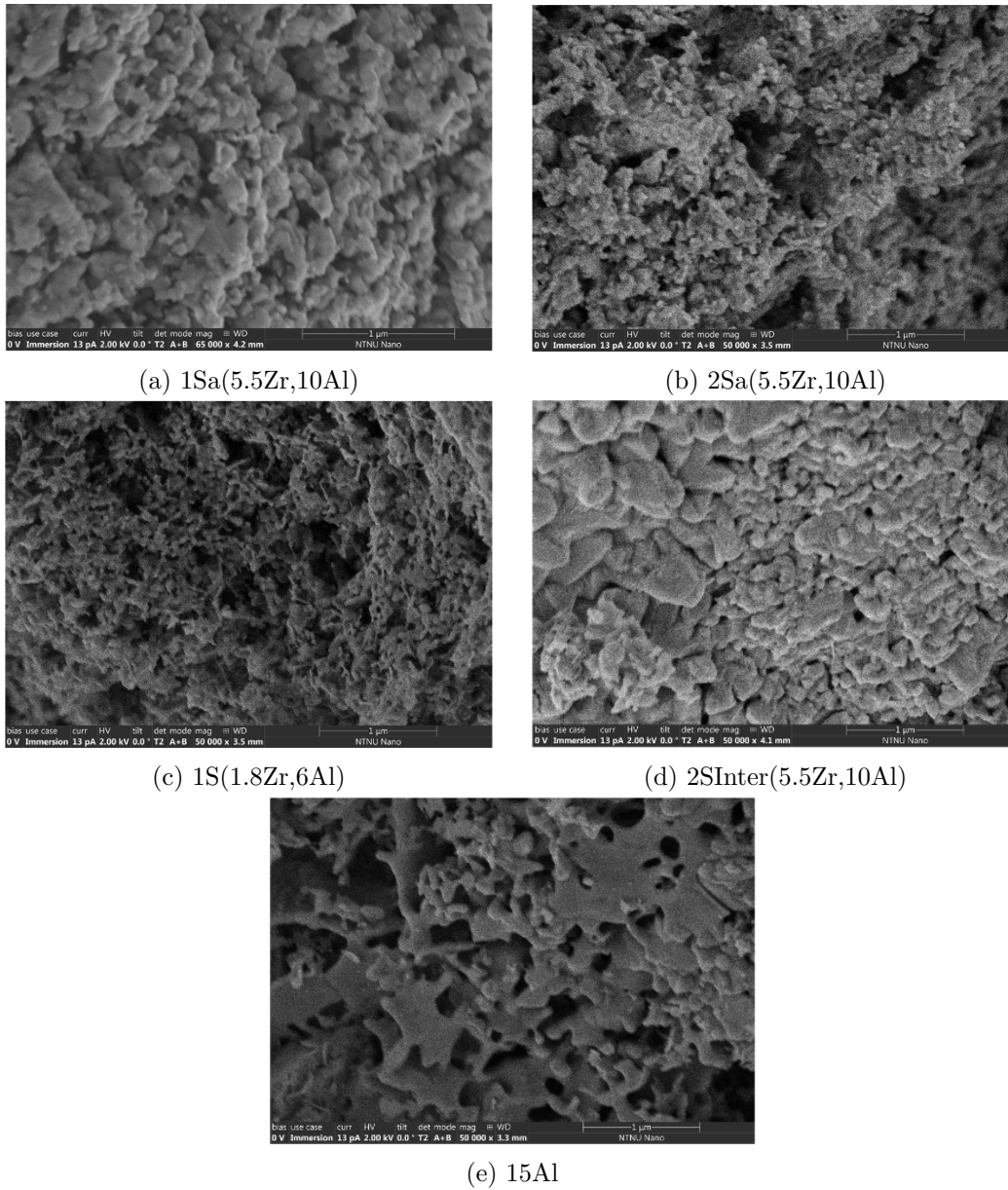


Figure 5.29: SEM pictures of a selection of fresh samples: 1Sa(5.5Zr,10Al), 2Sa(5.5Zr,10Al), 1S(1.8Zr,6Al), 2SInter(5.5Zr,10Al). Magnification: 65.000 for 1Sa(5.5Zr,10Al), 50.000 for the rest.

It is believed that all the sorbents obtained a skeleton of Mayenite, where a higher fraction of cement likely made it more robust. Though at the "flat areas," there are no pores at all. In those areas, the  $\text{CO}_2$  will face challenges diffusing into the particles and, hence, react with CaO. However, the structure can help the sorbents remain stable over a longer time

and thus prevent pore-collapse.

1S(1.8Zr,6Al) presented in figure 5.29c exhibit the most porous structure of the sorbents presented. The sorbent exhibited the highest capturing capacity of the modified sorbents and the worst stability during cycles. The open structure can have made it easier for CO<sub>2</sub> to diffuse into its pores and react with the active sites of CaO. However, worse stability, partly because 1S(1.8Zr,6Al) cannot form an equally strong skeleton of Mayenite as those made with a higher fraction of cement. And then not able to prevent pore-collapse and sintering in the same way.

#### 5.2.4.2 Fresh vs. Spent

Next, it was interesting to investigate changes between fresh and spent sorbents. Figure 5.30 presents a picture of 1S(5.5Zr,10Al) fresh, after 20 cycles and 40 cycles at a magnification of 5000. Similar pictures were also taken of all the sorbents presented in figure 5.29e, but now major differences were observed. Also, a picture was taken of 2Sa(5.5Zr,10Al) spent after 40, where the same was observed as for 1S(5.5Zr,10Al).

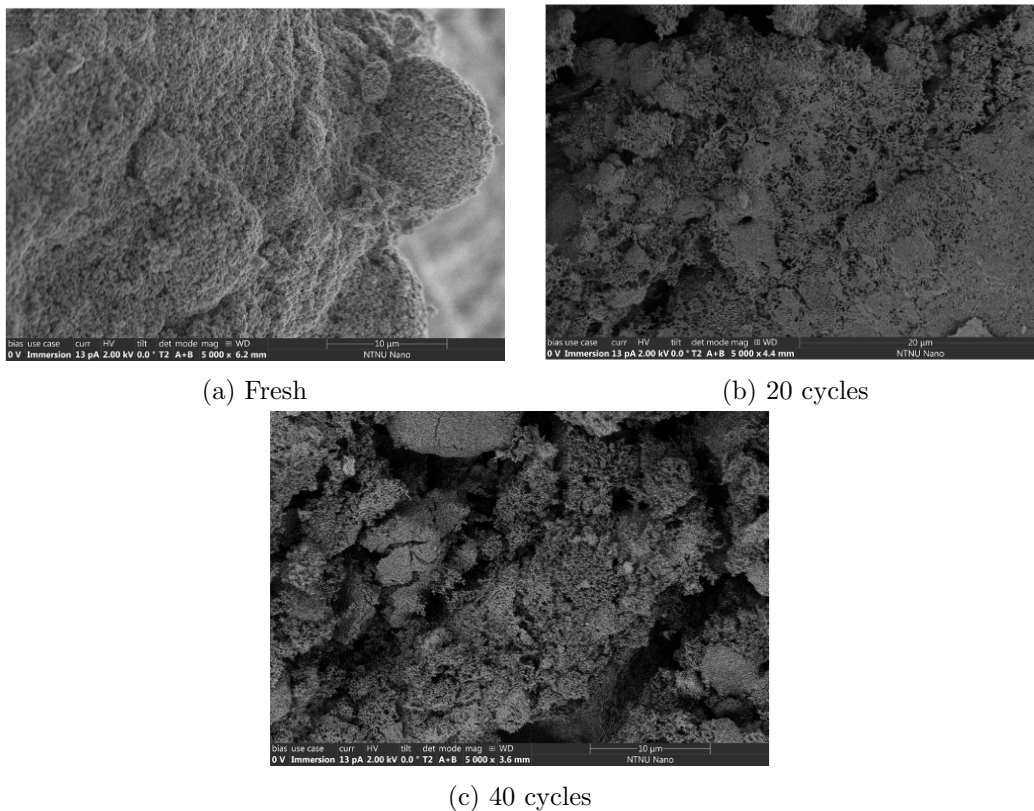


Figure 5.30: SEM pictures of 1S(5.5Zr,10Al) at 5000 Magnification. Microbalance conditions: Ads: 5 % CO<sub>2</sub>, 8 % H<sub>2</sub>O, 600 °C, 6min. Des: 100 % CO<sub>2</sub>, 950 °C

There are no significant changes that can be observed at a magnification of 5000. The only noteworthy difference is that it seems like some "cracking" have occurred after cycles. The occurrence is clearest after 40 cycles, in figure 5.30. However, it is hard to be sure if the regeneration-cycles are the only reason for the harm; it can also have been caused on the pellets journey from the reactor to the SEM-instrument. Though, it indicates that the mechanical strength of the sorbents is not very strong. Then again, it needs to be taken into account the way the sorbents were prepared. This project focused mainly on finding an optimal fraction of the additives, keeping the sorbents stable. When scaling up the procedure, the pellets will not be formed by hand but by a pelletizer, which most likely will result in a better mechanical strength of the pellets.

In figure 5.31 pictures of 1Sa(5.5Zr,10Al) fresh, after 20 cycles and after 40 cycles are presented. The two first are taken at a magnification of 65.000, while the last at a magnification of 50.000. In figure 5.32 2Sa(5.5Zr,10Al) fresh and after 40 cycles are given. Both taken at a magnification of 50.000.

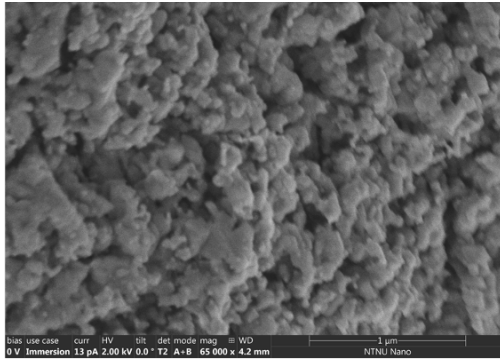
Only small changes can be observed between fresh and spent samples. In the pictures in figure 5.32, the surfaces are slightly more "smooth" in the spent samples, indicating a small degree of sintering. Nevertheless, in the crystal sizes presented in section 5.2.2, no changes in the crystal sizes after cycles was detected, which indicates that the degree of sintering was low.

Another aspect that might be noteworthy is a small change in the pore-structure during cycles. By for instance comparing 1Sa(5.5Zr,10Al) fresh and after 40 cycles, in figure 5.31a and 5.31c it seems like more larger pores have been formed. Similar, in the results from the Nitrogen adsorption-desorption presented in section 5.2.3, small changes were observed after cycles. There, especially related to the pore-volume. During the cycles, the pores are exposed to different conditions that can affect their structure. The continuous alternation between the carbonation leading to the formation of  $\text{CaCO}_3$  and the release of  $\text{CO}_2$  at high temperatures can lead to a reconstruction of the pores.

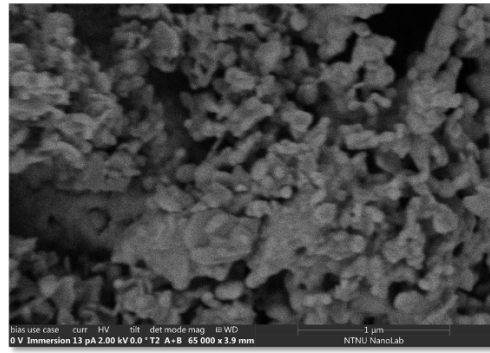
However, the most interesting observation from the figures is that there is no vital difference between fresh and spent sorbents. The results indicate that sintering and pore collapse were very much prevented in the sorbents. In literature where the phenomena have occurred to a higher degree, big differences have been detected in SEM-pictures at similar magnification. The agglomeration of particles have been significant, and pores very much blocked [63, 46, 106, 42, 55, 110]. Furthermore, doping with cement have shown that sintering is very much prevented [66, 108].

Pictures were not taken of calcined dolomite in this project. Still, despite the presence of MgO, it is expected that more pronounced sintering would have occurred in that case. It is believed that the modification of the sorbents was, as it was desired, very much able to create a robust framework in the sorbents, keeping them stable during cycles.

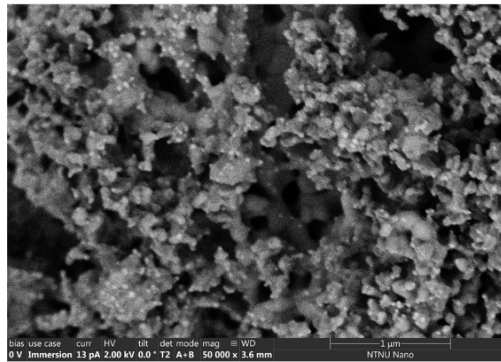




(a) Fresh

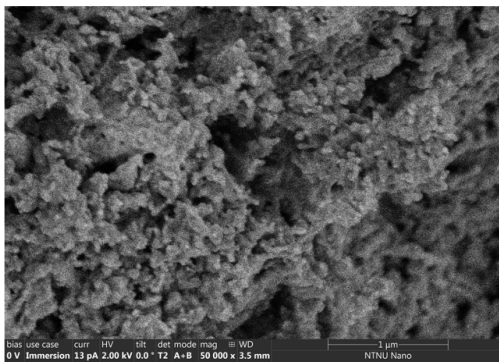


(b) 20 cycles

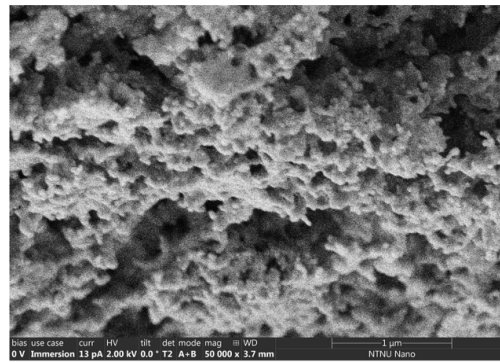


(c) 40 cycles

Figure 5.31: SEM pictures of fresh and spent 1Sa(5.5Zr,10Al). Fresh and 20 cycles at 65.000 magnification. 40 cycles at 50.000 Magnification. Experimental conditions: Ads: 5 % CO<sub>2</sub>, 8 % H<sub>2</sub>O, 600 °C, 6min. Des: 100 % CO<sub>2</sub>, 950 °C



(a) Fresh



(b) 40 cycles

Figure 5.32: SEM pictures of fresh and spent 2Sa(5.5Zr,10Al) at 50.000 magnification. Experimental conditions: Ads: 5 % CO<sub>2</sub>, 8 % H<sub>2</sub>O, 600 °C, 6min. Des: 100 % CO<sub>2</sub>, 950 °C

## 5.2.5 Energy Dispersive X-ray Spectroscopy (EDS)

In order to investigate the dispersion of the different elements, EDS mapping was performed on 1Sa(5.5Zr,10Al), 2Sa(5.5Zr,10Al), 2SInter(5.5Zr,10Al), calcined dolomite, and cement. For 1Sa(5.5Zr,10Al) and 2Sa(5.5Zr,10Al), mapping was also performed after some cycles in the microbalance reactor. (Ads: 5 % CO<sub>2</sub>, 8 % H<sub>2</sub>O, 600 °C, 6 min. Des: 100 % CO<sub>2</sub>, 950 °C). In all cases, the elemental mapping was done at a magnification of 3000. All the pictures were taken with a voltage of 10 kV, a current of 1.6 nA, and a working distance of about 10 mm. The elemental mapping was performed on several places and particles. From this, it was found that the sorbents were not homogenous, though they had similar patterns and were assumed to be comparable for all the particles. For that reason, the following discussion is assumed to be applicable for all particles belonging to the same type of sorbent.

### 5.2.5.1 Calcined dolomite

Figure 5.33 shows the elemental mapping of milled, calcined dolomite (less than 90 μm). The elements included are Calcium, Carbon, Oxygen, Magnesium, and Silisium. Probably, most of the Carbon detected correspond to the carbon-tape, where the powder was attached. The XRF revealed that the calcined dolomite also consists of small amounts of Silisium, which corresponds with the elemental mapping showing a faint, red color for this element. The pictures show that all the elements were well distributed.

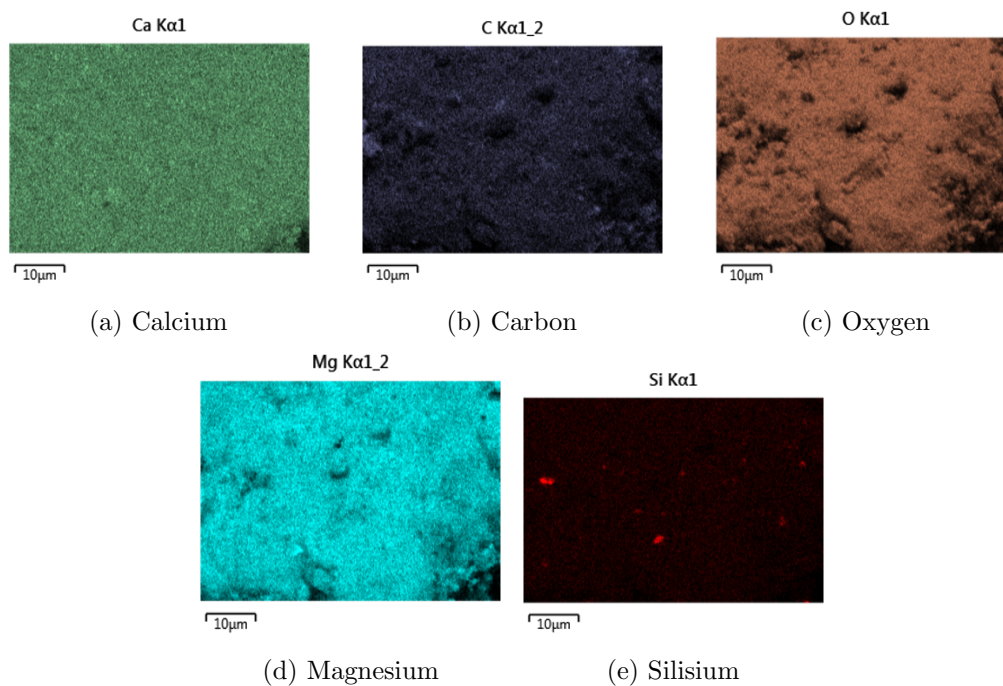


Figure 5.33: EDS mapping of calcined dolomite at magnification 3000.

### 5.2.5.2 Cement

Figure 5.34 shows the elemental mapping of cement Fondu where Calcium, Oxygen, Alumina, Silisium, and Iron are included. These are the same elements as the ones found through XRF. The elements also correspond with what was given in the product data-sheet and what was found through XRF. Also in Cement all the elements are well distributed.

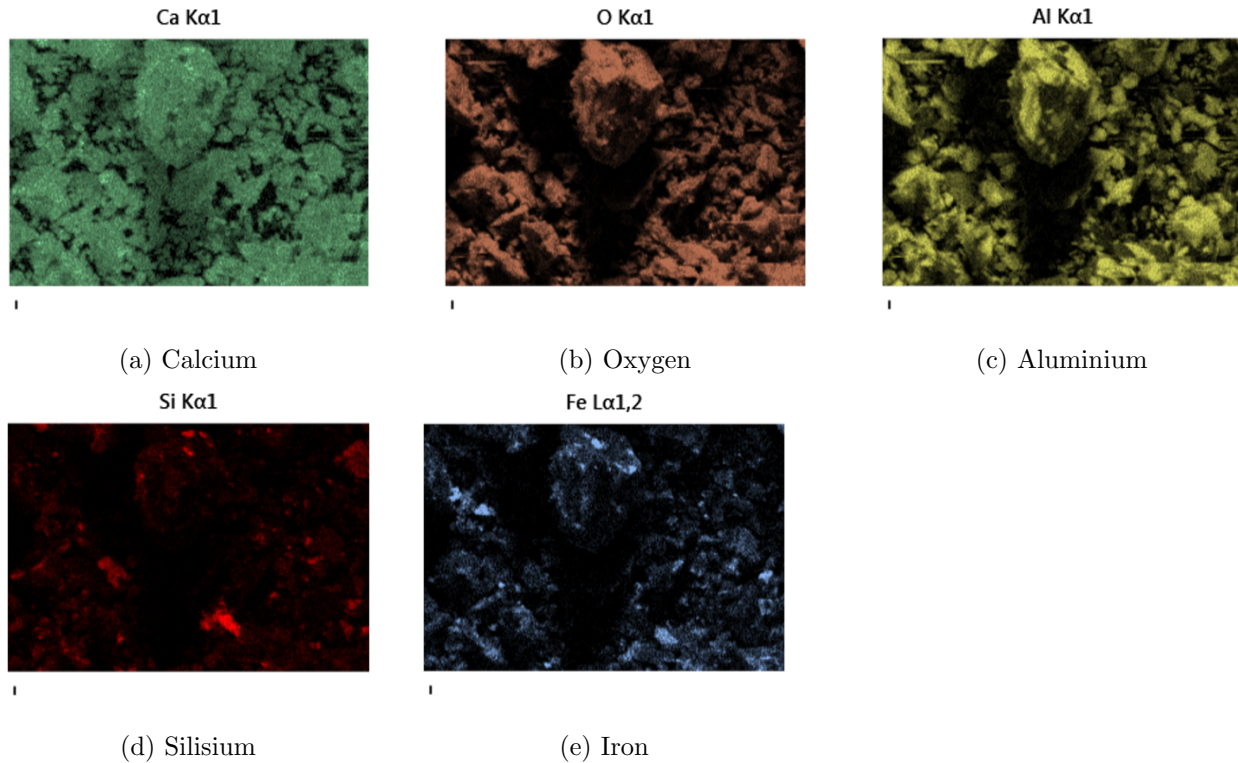


Figure 5.34: EDS mapping of cement Fondu at magnification 3000.

### 5.2.5.3 Fresh and Spent Sorbents

The next figures give the EDS mapping of prepared sorbents. The sorbents presented are 1Sa(5.5Zr,10Al) fresh (figure 5.36), 2Sa(5.5Zr,10Al) (figure 5.37) , 2SInter(5.5Zr,10Al) (figure 5.38) , 1S(5.5Zr,10Al) spent (figure 5.39) and 2Sa(5.5Zr,10Al) spent (figure 5.40 ) The spent samples are after 20 and 40 cycles, respectively. The pictures were taken of pellets in sizes  $500 \mu\text{m} - 850 \mu\text{m}$ .

The same phases are included; Calcium, Oxygen, Magnesium, Zirconium, and Aluminium. Also, to more clearly see Zirconium deposition, overlapping pictures including Calcium, Aluminum and Zirconium are given. The EDS also detected phases of Carbon, Silisium, and Iron, though they are not represented in the figures. Mapping of Carbon would only confuse, as most probably belonged to the carbon-tape. Only a small amount of Silisium and Iron is

present in the sorbents, and the colors of the two elements were weak in the mapping.

As expected, oxygen and Calcium are well distributed in all the pictures due to their existence in both cement, dolomite, and  $\text{CaZrO}_3$ . In the XRD, it was found that all the Zirconium had reacted to form  $\text{CaZrO}_3$ . Further, the deposition of Aluminium is, as expected, higher when the deposition of Magnesium is lower. Areas with more Aluminium corresponds to cement, while areas with more Magnesium to  $\text{MgO}$  from dolomite. However, the most interesting is the dispersion of Zirconium in the particles and will be discussed further in this section.

When comparing 1Sa(5.5Zr,10Al) (figure 5.36) with 2Sa(5.5Zr,10Al) (figure 5.37), there are two differences it is important to notice. 1. Where Zirconium is dispersed 2. How well Zirconium is dispersed. The distinctions can help explain the better cyclic performance observed in the two-step method compared to the one-step method. They can strengthen the hypotheses discussed in the cyclic testing, including the ZrAl-based and one-step method vs. two-step method, given in section 5.1.2 and 5.1.2.2. Literature has mentioned the importance of a good dispersion of the inert support to avoid sintering [48, 53].

Firstly, it can be noticed that for 1Sa(5.5Zr,10Al), the Zirconium is deposited both, close to the Aluminum from as well as close to dolomite, indicating that some of the Calcium in cement has reacted with the Zirconium to form  $\text{CaZrO}_3$ . When it was performed XRD of cement doped with  $\text{ZrO}_2$  the phase was observed. Secondly, it can be seen an accumulation of Zirconium at certain places in both pictures - indicating that the element is not very well dispersed. However, the dispersion is better in the 2S-sorbent than the 1S-sorbent. A worse dispersion of the Zirconium can make a structure not facilitating the carbonation reaction.

When adding Zirconium, the intention was for it to function as a barrier, preventing CaO particles from fusing - This was explained in the objective, in section 2. The illustration is again presented in figure 5.35a, while figure 5.35b illustrates a sorbent that was not able to obtain the desired distribution of Zirconium. The first will be referred to as the ideal sorbent distribution, while the second as the real sorbent distribution. In the ideal sorbent distribution, there is a good distance between the dolomite particles. The particles are kept stable both of the skeleton created by cement and good dispersion of Zirconium. All the Zirconium have reacted with active sites of CaO. In the real sorbent, the framework keeping the CaO-particles is not that perfect. The dispersion of Zirconium is not very homogeneous. In addition, some of the  $\text{ZrO}_2$  particles have reacted with the cement. The dolomite-particles are starting to get closer to each other.

Possibly, 2Sa(5.5Zr,10Al) could get closer to the ideal sorbent structure than 1Sa(5.5Zr,10Al). Likely, the small  $\text{CaZrO}_3$  particles were better distributed in the 2S-sorbent than the 1S-sorbent. Besides, some of the  $\text{CaZrO}_3$ -particles in 1Sa(5.5Zr,10Al) might instead have surrounded the cement-particles. A reduced barrier around CaO in the 1S-sorbent might have increased the chances for sintering. Hashemi et al. [44] observed an increase in the stability with a better dispersion of Zirconium in the sample.

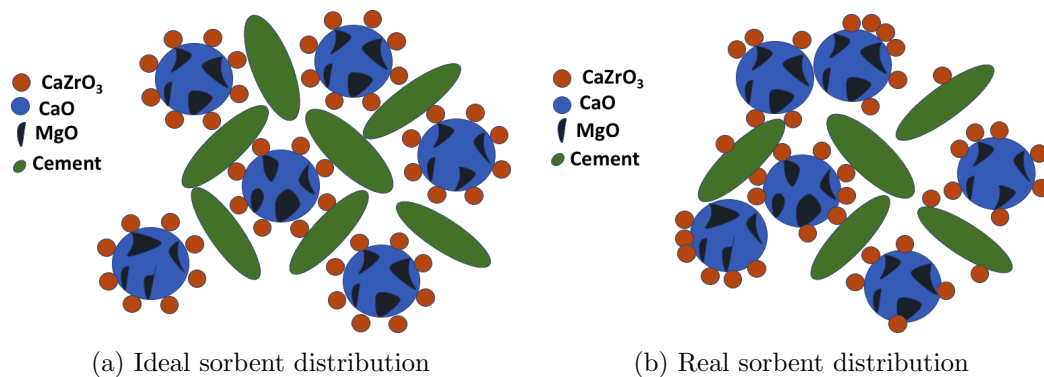


Figure 5.35: Illustration of an ideal sorbent distribution compared to a distribution close to the real sorbent distribution.

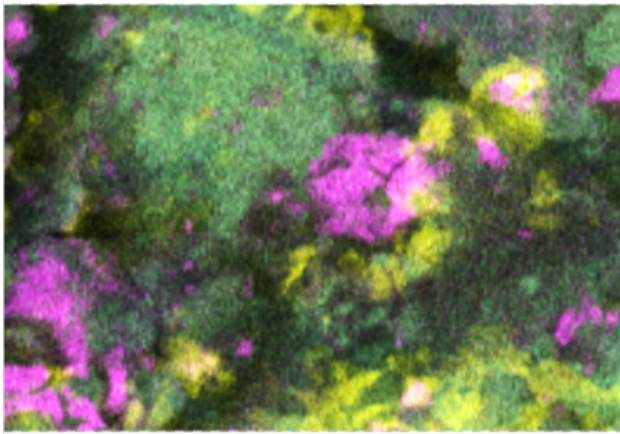
When the sorbent was prepared in two steps, the deposition of the Zirconium was more controlled. In the first step, it was controlled that the precursor was added until an amount close to the pore-volume of dolomite. Most of the Zirconium diffused into dolomites pores. When the Zirconium was added to the cement, it was harder to control its distribution. As observed in the reproducibility in section 5.1.1.3, it was easier to reproduce a sorbent made by the two-step method than the one-step method.

Further, the increasing amount of Zirconium probably increased the differences in its dispersion between the 1S-sorbents and 2S-sorbents - this can be attributed to the low surface-areas of the sorbents. It was observed that a more significant difference in the capacities between the one-step method and two-step method when a higher fraction of Zirconium was used in the sorbents.

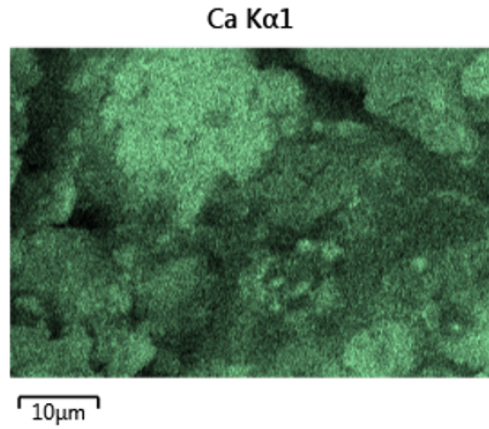
The dispersion of Zirconium is even more pronounced in 2SInter(5.5Zr,10Al) (figure 5.38). However, in the case of this sorbent, the distribution might be too pronounced. When tested in dry conditions, the sorbent exhibited a lower capturing capacity than 2S(5.5Zr,10Al). The capacity was lower than the desired 10 %. The better dispersion indicates that  $ZrO_2$  have been able to react with more of the active sites of CaO. In addition, observation in the crystal sizes in section 5.2.2 and the SEM, section 5.2.4 indicated somewhat more sintering of the fresh sorbents when intermediate calcination was done. Consequently, it might have become hard for  $CO_2$  to diffuse into the pores and react with enough active sites of CaO to obtain the required capturing capacity.

In the spent sorbents, presented in figure 5.39 and 5.40 the color of Zirconium becomes fainter. Especially this can be observed for the 1S-sorbents. The dispersion of the 2S-sorbent seems quite similar to that in the 1S-sorbent.

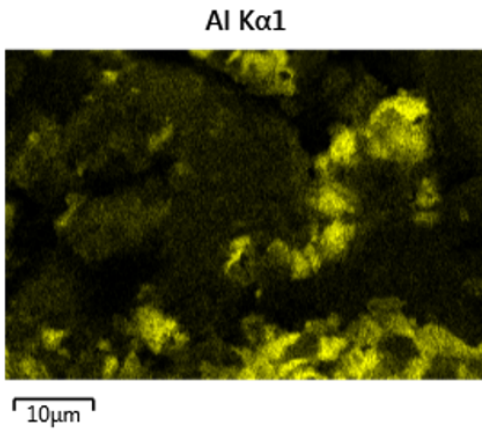




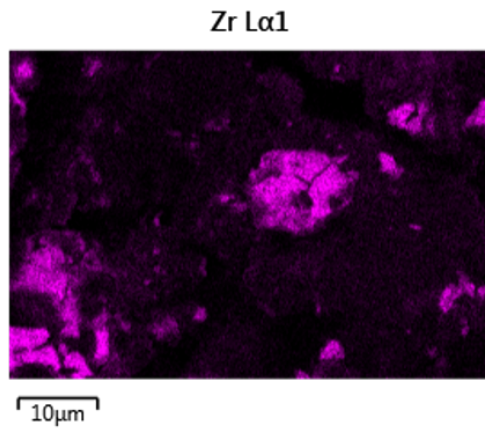
(a) Calcium, Zirconium and Aluminium



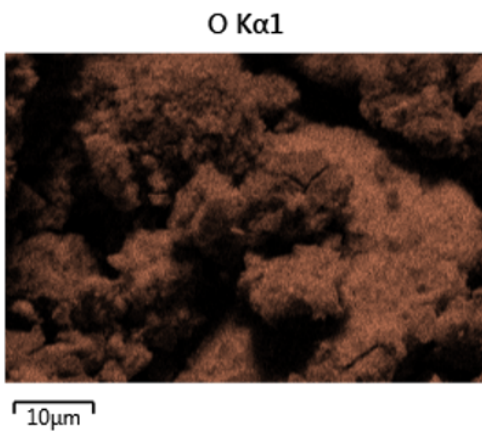
(b) Calcium



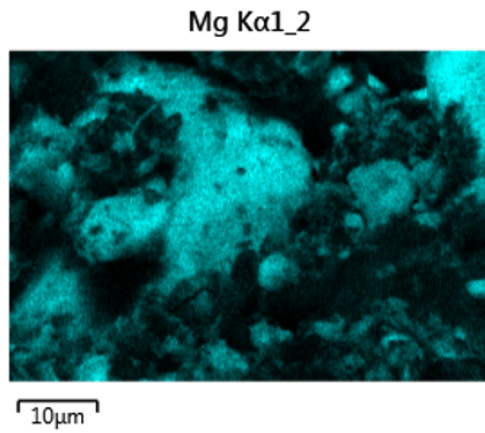
(c) Aluminium



(d) Zirconium

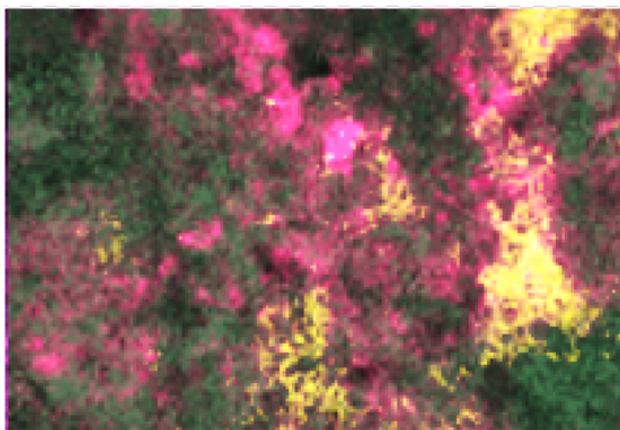


(e) Oxygen

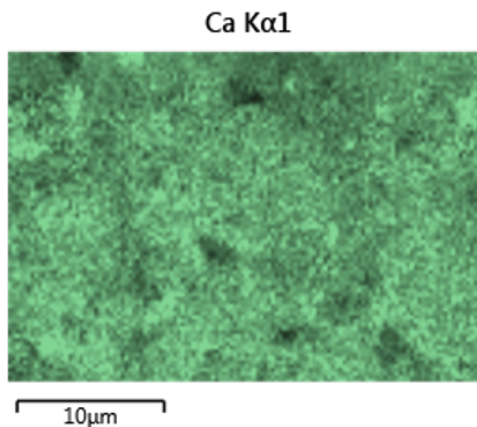


(f) Magnesium

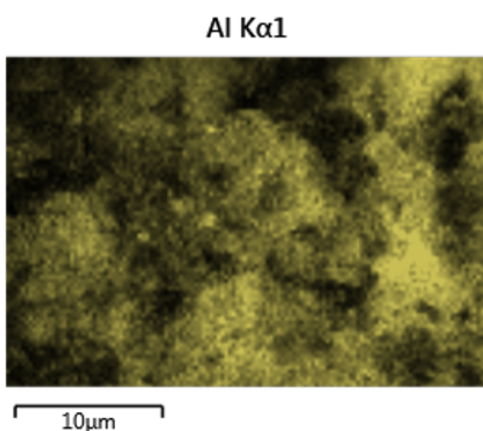
Figure 5.36: EDS mapping of 1S(5.5Zr,10Al) fresh at magnification 3000.



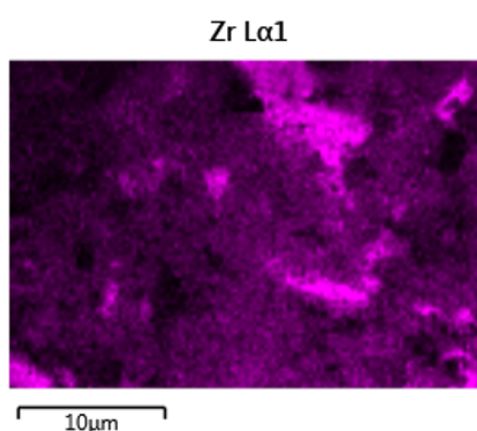
(a) Calcium, Zirconium and Aluminium



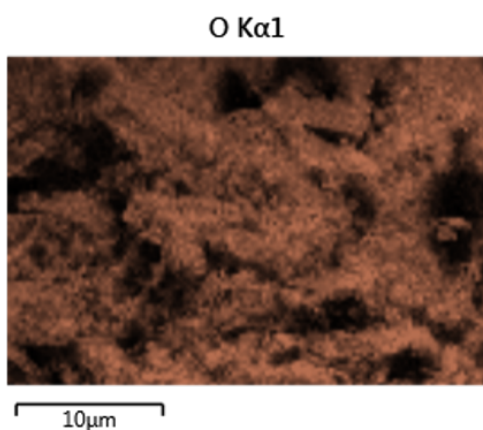
(b) Calcium



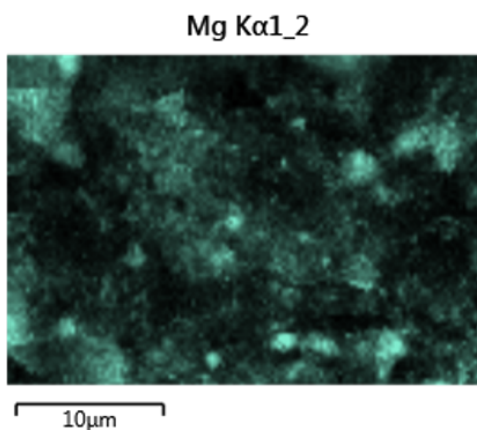
(c) Aluminium



(d) Zirconium



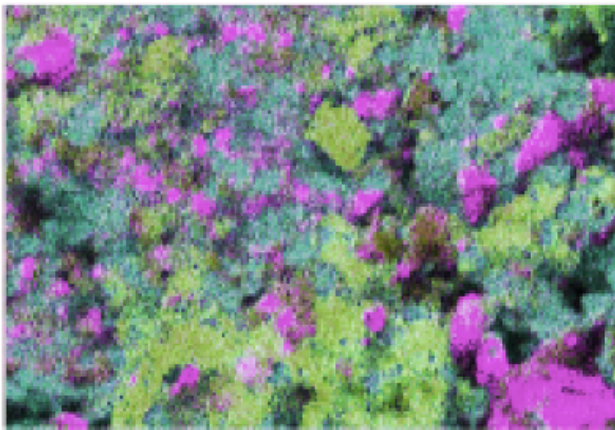
(e) Oxygen



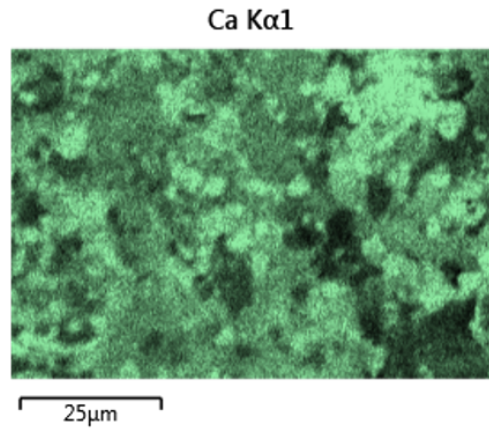
(f) Magnesium

Figure 5.37: EDS mapping of 2S(5.5Zr,10Al) fresh at magnification 3000.

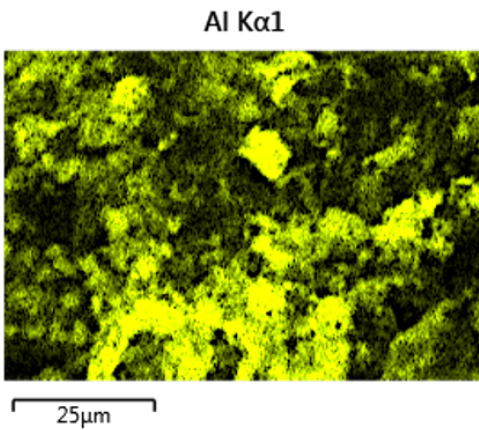




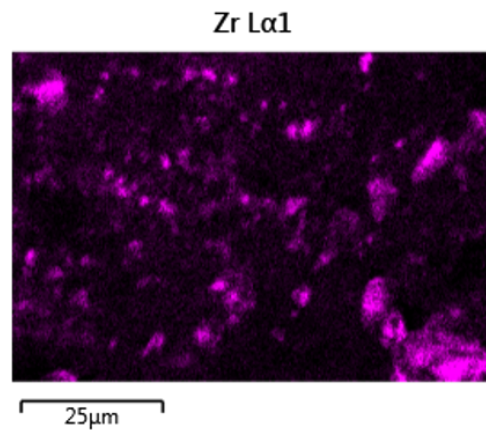
(a) Calcium, Zirconium and Aluminium



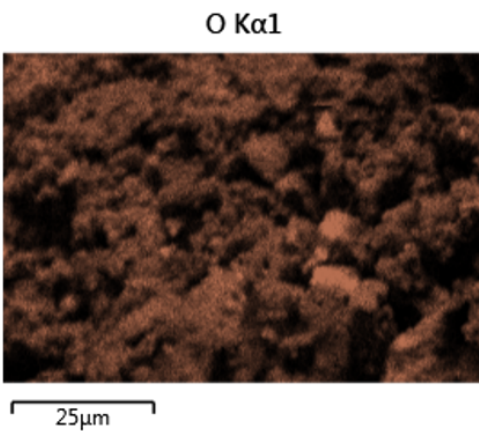
(b) Calcium



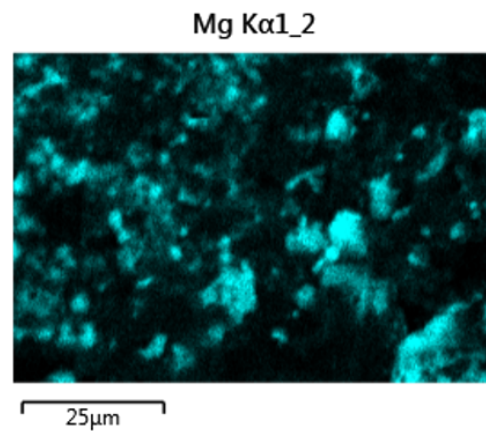
(c) Aluminium



(d) Zirconium



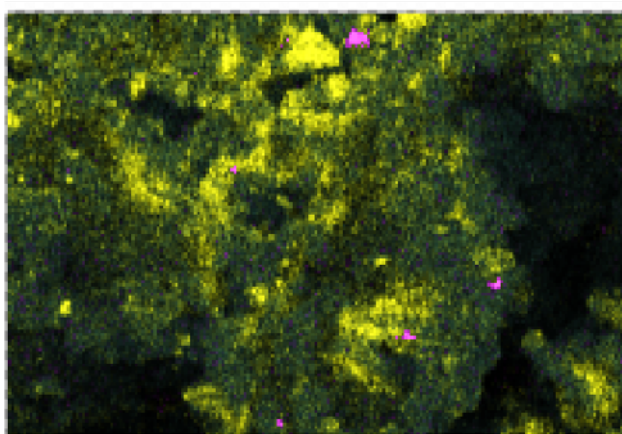
(e) Oxygen



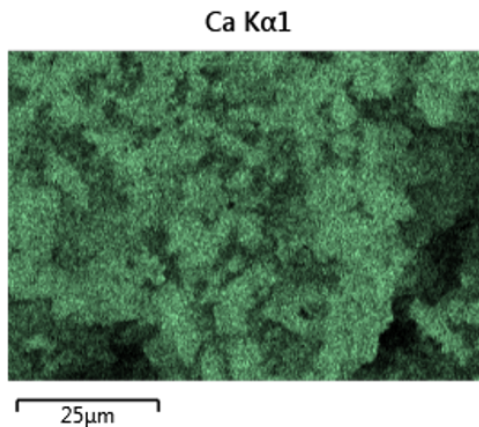
(f) Magnesium

Figure 5.38: EDS mapping of 2SInter(5.5Zr,10Al) fresh at magnification 3000. Experimental conditions: (Ads: 5 % CO<sub>2</sub>, 8 % H<sub>2</sub>O, 600 °C, 6 min. Des: 100 % CO<sub>2</sub>, 950 °C)

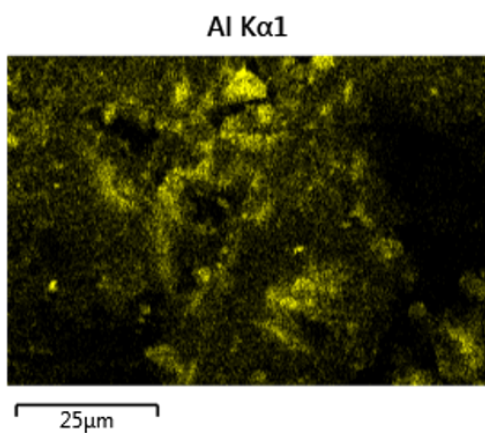




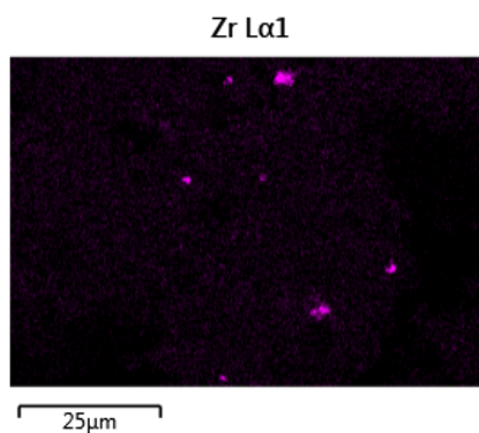
(a) Calcium, Zirconium and Aluminium



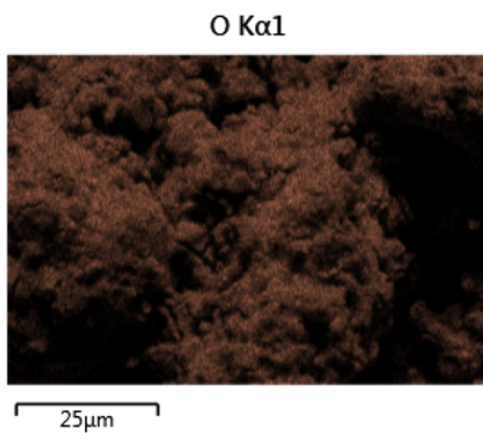
(b) Calcium



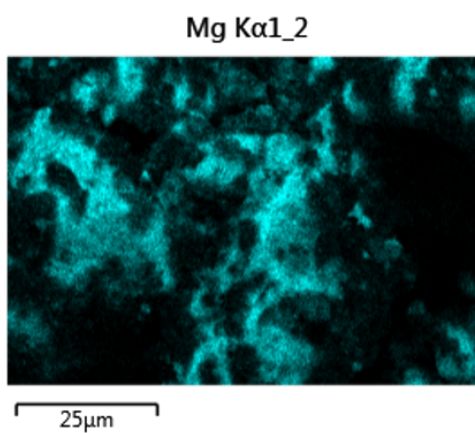
(c) Aluminium



(d) Zirconium

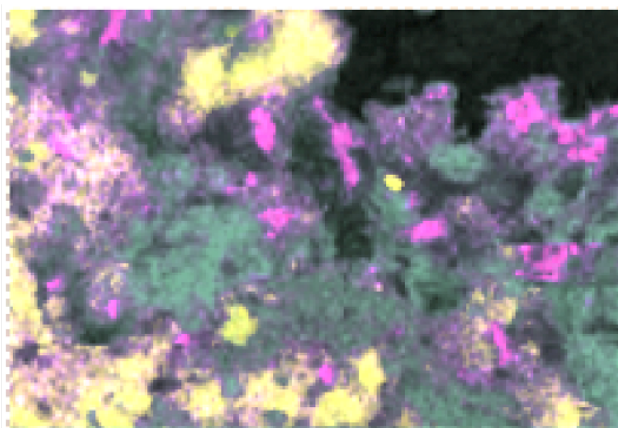


(e) Oxygen

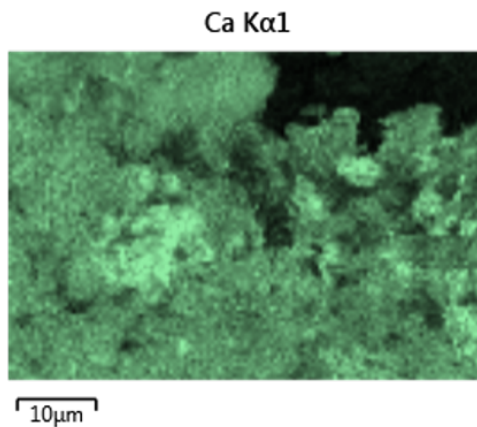


(f) Magnesium

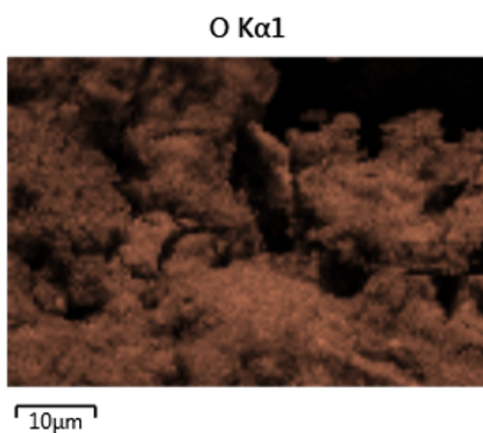
Figure 5.39: EDS mapping off 1S(5.5Zr,10Al) after 20 regeneration-cycles at magnification 3000  $\approx$  10 mm. Experimental conditions: (Ads: 5 % CO<sub>2</sub>, 8 % H<sub>2</sub>O, 600 °C, 6 min. Des: 100 % CO<sub>2</sub>, 950 °C)



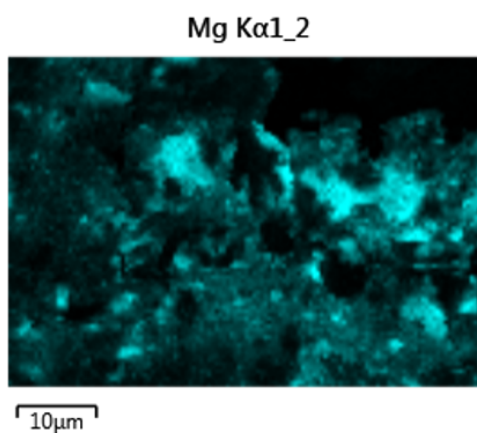
(a) Calcium, Aluminum and Zirconium



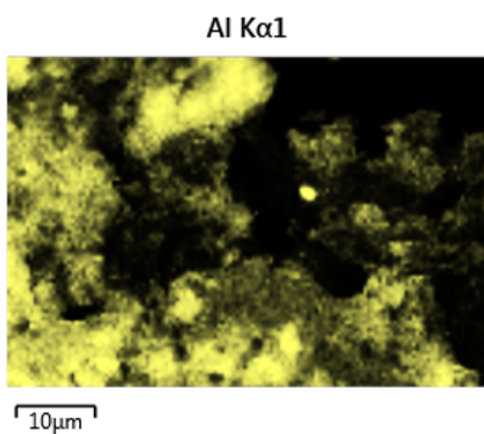
(b) Calcium



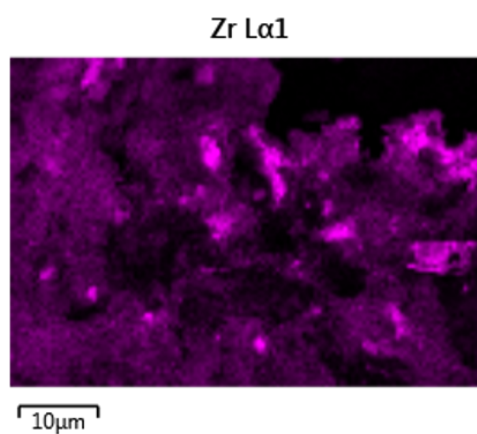
(c) Oxygen



(d) Magnesium



(e) Aluminium



(f) Zirconium

Figure 5.40: EDS mapping of 2Sa(5.5Zr,10Al) after 40 regeneration-cycles at magnification 3000. Experimental conditions: (Ads: 5 % CO<sub>2</sub>, 8 % H<sub>2</sub>O, 600 °C, 6 min. Des: 100 % CO<sub>2</sub>, 950 °C)

## 6 Conclusion

In this master project, high-temperature dolomite-based sorbents for the MBCL process were improved. Their cyclic behavior and cause of deactivation have been thoroughly investigated.

Some of the sorbents were tested in dry conditions before tested in more realistic conditions, in wet conditions. For the same type of sorbents, testing in wet conditions gave higher capacities.

Several sorbents were prepared to find the best composition additives;  $ZrO_2$  or  $CeO_2$  as a stabilizer and cement both as a stabilizer and a binder. All of the sorbents exhibited a lower capturing capacity than calcined dolomite, but their cyclic stability was considerably enhanced. Both the addition of  $ZrO_2$  and cement had a positive effect on the stability, ascribed to be due to the formation of two phases;  $CaZrO_3$  and  $Ca_{12}Al_{14}O_{33}$ . The addition of  $CeO_2$  did not improve the sorbent in this project.

The sorbents prepared by the one-pot method were made in two ways: By the one-step method (everything mixed at once) and two-step method (cement added after impregnation); Namely, 1S-sorbents, and 2S-sorbents. For the ZrAl-based sorbents, 2S-sorbents exhibited a higher capturing capacity than 1S-sorbents, which was opposite to the expected. However, as expected, the stabilities of the 2S-sorbents were generally better. The differences tended to be higher with a higher fraction of Zirconium in the samples. Further, the reproducibility of the 2S-sorbents was better than the 1S-sorbents.

From observations in EDS mapping, the cyclic behavior differences were attributed to being related to the deposition of Zirconium in the sorbents. The 2S-sorbent was able to obtain a better dispersion of  $CaZrO_3$  particles surrounding CaO than the 1S-sorbent. It seemed like some of the Zirconium had reacted with cement instead of CaO from dolomite in the 1S-sorbent. Concluding, the 2S-sorbent obtained a structure where the two additives were better distributed, which seemed to both facilitate the carbonation reaction and somehow prevented deactivation.

The best composition was found to be 5.5 wt% Zirconium and 10 wt% weight percentage Aluminium from cement. 1Sa(5.5Zr,10Al) and 2Sa(5.5Zr,10Al) exhibited among the best stabilities and was able to stay over the required capacity of 10 % during 60 cycles in wet conditions. Of these, the 2S-sorbent was considered the best. It only had a capacity loss of 5.9 % from cycle 3-15 and 15.7 % from cycle 3-60 in wet conditions. In comparison, calcined dolomite had a capacity loss of 37.9 % from cycle 3-15. 2Sa(5.5Zr,10Al) was also able to stay over a capacity of 10 % when tested for 40 cycles in more realistic conditions a microbalance reactor fixed bed reactor (cycles of 6 min) - the capacity loss from cycle 3-40 was only 13.6 %.

The stabilizing effect on cement on its own was studied more in detail. A sorbent with 15 wt% of Aluminium, 15Al exhibited a similar capacity as 1Sa(5.5Zr,10Al) during 15 cycles, with only moderately lower stability. Both had a capacity close to 15 % in cycle 3, and

their capacity losses were 16.4 % and 10.0 % from cycle 3-15 for 15Al and 1S(5.5Zr,10Al), respectively. It can be interesting to further investigate the stabilizing effect of cement in the future.

Two sorbents were prepared, with different sets of calcination than what is proposed in the one-pot method. One sorbent was prepared with uncalcined dolomite; it only obtained a capacity of about 3 % during cycles. Sintering was through XRD found to be significantly pronounced in the sample. Another sorbent was prepared with intermediate calcination (2SInter(5.5Zr,10A)). The sorbent obtained a lower capacity than the desired 10 % (dry conditions). Results from XRD, SEM, and BET indicated more pronounced sintering in the fresh sample for 2SInter(5.5Zr,10A) than those prepared without intermediate calcination. Also, from observations in EDS-mapping, it was suspected that a too high amount of the active sites of CaO had been occupied by the Zirconium.

It can be argued that by reducing the amount of Zirconium added to the sorbent, the capturing capacity could be raised sufficiently. In this project, it was intended to investigate the possibility of making sorbents by the one-pot method. Avoiding one or more steps of intermediate calcinations is preferable for scale-up. Overall, the results obtained in this project proved small differences between the sorbents made by the one-pot method and the sorbent prepared with the intermediate calcination. In conclusion, it is beneficial to prepare sorbents by the one-pot method for the aim of this project.

The sorbents prepared in this project maintained good stability during several-regeneration cycles, but still, they suffered from some deactivation. The crystal sizes of fresh and spent sorbents were similar. However, Nitrogen adsorption-desorption and SEM results revealed small changes; even though very much prevented, it seemed to be some sintering and changes in pore-structure after cycles. There could be observed small changes in the SEM-pictures of spent and fresh sorbents. The sorbents had some pores of small-size (3-5 nm), but most of the ones found through Nitrogen adsorption-desorption were in the range between large mesopores and small macropores ( $\approx$ 30-150 nm). The sizes were somewhat increased after cycles. It is speculated that improvement in the pore-structure can help prevent deactivation and should be investigated in the future.

## 7 Future Work

Overall, this project was able to optimize the dolomite-based sorbents significantly. This section provides suggestions for future work, both in terms of improving the sorbents and recommendations for future testing and characterization.

Many sorbents were prepared with different ratios of cement and  $\text{ZrO}_2$ ; it is probable that by further optimizing the ratio, the stability could have been improved even more. Furthermore, it was found that cement exhibited a remarkable stabilizing effect on its own. The sorbent prepared with the highest cement amount, 15Al, still exhibited a capturing capacity close to 15 % in cycle 1. With this result, it would be interesting to increase the amount even more.

The absence of stabilizing effect of  $\text{CeO}_2$  was speculated to be related to the preparation. For the future, it is recommended to prepare sorbents in a way it is possible to control the deposition of Cerium.

What is mostly recommended for future testing is adding a modifier that improves the porosity. Modification with biomass [64, 111], urea, polyethylene glycol, and polyvinyl alcohol [112, 113] has proven to increase the reactivity of CaO-based sorbents due to an enhanced pore structure.

In this project, some sorbents were tested both in wet and dry conditions. However, due to the limitations in the instruments, it would be interesting to perform experiments in both conditions in the same instrument. Then, it can be possible to get a better understanding of the influence of steam.

Only a few experiments were performed in the microbalance fixed bed reactor; it is desirable to do more in the future. The sorbents should be tested for many regenerations, preferably in the microbalance reactor; it does not have a limitation in the possible amount of cycles, as in the TGAs. Further, it would be interesting to see the effect of carbonation, calcination time, and different heating rates. Also, an in-depth kinetical analysis should be performed. Both impacts of temperature and pressure of  $\text{CO}_2$  and  $\text{H}_2\text{O}$ , with different amounts of steam, should be detected.

In section 5.1.2, it was shortly speculated if the sorbents had been regenerated when the cyclic testing procedures were started again. Further investigations on the possibility and effect of regenerating the sorbents are of future interest.

If more experiments are performed in the microbalance reactor, also more spent samples will be available. It is then recommended to do more characterization of spent samples to understand more about the deactivation-mechanism. For instance, more samples can be investigated through Nitrogen adsorption-desorption, both good and bad, and after different cycles.

Mercury porosimetry can be conducted in order to detect larger pores in the sorbent. However, performing the experiments are expensive, and considerations should be done before.

Further investigation of the sorbents through electron microscopy can help improve the understanding of the structure of the sorbents. Pictures were not taken of calcined dolomite after cycles but can be recommended in order to see the differences caused by sintering. In SEM APREO, it was not easy to take pictures of a lower magnification than 50.000. If good pictures had been taken at a lower scale, it could have been possible to understand even more about the pore-structure at the nanometer scale. When the master-project was performed, the STEM-instrument was broken. In the future, it could be interesting taking images with the STEM, where also transmission electron microscopy is possible.

When the optimal sorbent is found, it is desirable to scale up the synthesis method. Different types of machines should be used, in order to perform different steps, such as milling and pelletization. The sorbents should also be prepared in a way beneficial for their mechanical strength. If the performance of the sorbents is good both in terms of cyclic stability and mechanical strength, they might have a promising future for further industrial scale-up.

## References

1. Wold A. Modified dolomite-based pellets for high-temperature CO<sub>2</sub> capture. 2020
2. United Nations. Summary of the Paris Agreement. United Nations Framework Convention on Climate Change 2015 :27–52. Available from: <http://bigpicture.unfccc.int/#content-the-paris-agreemen>
3. Masson-Delmotte V, Zhai P, Pörtner H, Roberts D, Skea J, Shukla P, Pirani A, Moufouma-Okia W, Péan C, Pidcock R, Connors S, Matthews J, Chen Y, Zhou X, Gomis M, Lonnoy E, Maycock T, Tignor M, and Waterfield T. Summary for Policy-makers. In: Global Warming of 1.5°C. An IPCC Special Report on the impacts of global warming of 1.5°C above pre-industrial levels and related global greenhouse gas emission pathways, in the context of strengthening the global response to. 2018 :32. Available from: [https://report.ipcc.ch/sr15/pdf/sr15\\_spm\\_final.pdf%0Ahttp://www.ipcc.ch/report/sr15/](https://report.ipcc.ch/sr15/pdf/sr15_spm_final.pdf%0Ahttp://www.ipcc.ch/report/sr15/)
4. SaskPower. Boundary Dam Power Station. 2020
5. Institute GC. Global Status of CCS 2020. Global CCS Institute 2020. Available from: <https://www.globalccsinstitute.com/resources/global-status-report/>
6. Mathieu P. The IPCC special report on carbon dioxide capture and storage. 2006 :1611–8
7. Wang S, Yan S, Ma X, and Gong J. Recent advances in capture of carbon dioxide using alkali-metal-based oxides. *Energy and Environmental Science* 2011; 4:3805–19. DOI: 10.1039/c1ee01116b
8. Siegelman RL, Milner PJ, Kim EJ, Weston SC, and Long JR. Challenges and opportunities for adsorption-based CO<sub>2</sub> capture from natural gas combined cycle emissions. *Energy and Environmental Science* 2019; 12:2161–73. DOI: 10.1039/c9ee00505f
9. Global CCS Institute. Capturing carbon dioxide. 2018
10. Luis P. Use of monoethanolamine (MEA) for CO<sub>2</sub> capture in a global scenario: Consequences and alternatives. *Desalination* 2016; 380:93–9. DOI: 10.1016/j.desal.2015.08.004. Available from: <http://dx.doi.org/10.1016/j.desal.2015.08.004>
11. Wang J, Huang L, Yang R, Zhang Z, Wu J, Gao Y, Wang Q, O’Hare D, and Zhong Z. Recent advances in solid sorbents for CO<sub>2</sub> capture and new development trends. *Energy and Environmental Science* 2014; 7:3478–518. DOI: 10.1039/c4ee01647e. Available from: <http://dx.doi.org/10.1039/C4EE01647E>
12. Berstad D, Anantharaman R, and Jordal K. Post-combustion CO<sub>2</sub> capture from a natural gas combined cycle by CaO/CaCO<sub>3</sub> looping. *International Journal of Greenhouse Gas Control* 2012; 11:25–33. DOI: 10.1016/j.ijggc.2012.07.021. Available from: <http://dx.doi.org/10.1016/j.ijggc.2012.07.021>

13. Cormos CC. Assessment of chemical absorption/adsorption for post-combustion CO<sub>2</sub> capture from Natural Gas Combined Cycle (NGCC) power plants. *Applied Thermal Engineering* 2015; 82:120–8. DOI: 10.1016/j.applthermaleng.2015.02.054. Available from: <http://dx.doi.org/10.1016/j.applthermaleng.2015.02.054>
14. Perejón A, Romeo LM, Lara Y, Lisbona P, Martínez A, and Valverde JM. The Calcium-Looping technology for CO<sub>2</sub> capture: On the important roles of energy integration and sorbent behavior. *Applied Energy* 2016; 162:787–807. DOI: 10.1016/j.apenergy.2015.10.121
15. Berstad D, Anantharaman R, Blom R, Jordal K, and Arstad B. NGCC post-combustion CO<sub>2</sub> capture with Ca/carbonate looping: Efficiency dependency on sorbent properties, capture unit performance and process configuration. *International Journal of Greenhouse Gas Control* 2014; 24:43–53. DOI: 10.1016/j.ijggc.2014.02.015. Available from: <http://dx.doi.org/10.1016/j.ijggc.2014.02.015>
16. Subramanian ASR, Jordal K, Anantharaman R, Hagen BA, and Roussanaly S. A Comparison of Post-combustion Capture Technologies for the NGCC. 2017. DOI: 10.1016/j.egypro.2017.03.1436
17. Hanak DP, Anthony EJ, and Manovic V. A review of developments in pilot-plant testing and modelling of calcium looping process for CO<sub>2</sub> capture from power generation systems. *Energy and Environmental Science* 2015; 8:2199–249. DOI: 10.1039/c5ee01228g
18. Salaudeen SA, Acharya B, and Dutta A. CaO-based CO<sub>2</sub> sorbents: A review on screening, enhancement, cyclic stability, regeneration and kinetics modelling. *Journal of CO<sub>2</sub> Utilization* 2018; 23:179–99. DOI: 10.1016/j.jcou.2017.11.012. Available from: <https://doi.org/10.1016/j.jcou.2017.11.012>
19. Chen Z, Song HS, Portillo M, Lim CJ, Grace JR, and Anthony EJ. Long-term calcination/carbonation cycling and thermal pretreatment for CO<sub>2</sub> capture by limestone and dolomite. 2009. DOI: 10.1021/ef800779k
20. Ortiz AL and Harrison DP. Hydrogen production using sorption-enhanced reaction. *Industrial and Engineering Chemistry Research* 2001; 40:5102–9. DOI: 10.1021/ie001009c
21. Chen PD and Rout KR. Moving Bed Carbonate Looping ( MBCL ), Phase II
22. FTG / NTNU / SINTEF / 2019 / 03-05 MBCL Phase II Status Report. 2019
23. Barker R. The Reversibility of the Reaction  $\text{CaCO}_3 \rightleftharpoons \text{CaO} + \text{CO}_2$ . *Journal of Applied Chemistry and Biotechnology* 1973; 23:733–42. Available from: <http://onlinelibrary.wiley.com/doi/10.1002/jctb.5020231005/pdf>
24. Arias B, Abanades JC, and Grasa GS. An analysis of the effect of carbonation conditions on CaO deactivation curves. *Chemical Engineering Journal* 2011; 167:255–61. DOI: 10.1016/j.cej.2010.12.052. Available from: <http://dx.doi.org/10.1016/j.cej.2010.12.052>



25. Alvarez D and Carlos Abanades J. Determination of the critical product layer thickness in the reaction of CaO with CO<sub>2</sub>. *Industrial and Engineering Chemistry Research* 2005; 44:5608–15. DOI: 10.1021/ie050305s
26. Arias B, Grasa G, Abanades JC, Manovic V, and Anthony EJ. The effect of steam on the fast carbonation reaction rates of CaO. *Industrial and Engineering Chemistry Research* 2012; 51:2478–82. DOI: 10.1021/ie202648p
27. Valverde JM. Ca-based synthetic materials with enhanced CO<sub>2</sub> capture efficiency. *Journal of Materials Chemistry A* 2013; 1:447–68. DOI: 10.1039/c2ta00096b
28. Erans M, Manovic V, and Anthony EJ. Calcium looping sorbents for CO<sub>2</sub> capture. *Applied Energy* 2016; 180:722–42. DOI: 10.1016/j.apenergy.2016.07.074
29. Manovic V and Anthony EJ. CaO-based pellets supported by calcium aluminate cements for high-temperature CO<sub>2</sub> capture. *Environmental Science and Technology* 2009; 43:7117–22. DOI: 10.1021/es901258w
30. Radfarnia HR and Iliuta MC. Development of zirconium-stabilized calcium oxide absorbent for cyclic high-temperature CO<sub>2</sub> capture. 2012. DOI: 10.1021/ie301287k
31. Arstad B, Spjelkavik A, Andreassen KA, Lind A, Probst J, and Blom R. Studies of Ca-based high temperature sorbents for CO<sub>2</sub> capture. *Energy Procedia* 2013; 37:9–15. DOI: 10.1016/j.egypro.2013.05.079. Available from: <http://dx.doi.org/10.1016/j.egypro.2013.05.079>
32. Antzara A, Heracleous E, and Lemonidou AA. Development of CaO-based mixed oxides as stable sorbents for post-combustion CO<sub>2</sub> capture via carbonate looping. *Energy Procedia* 2014; 63:2160–9. DOI: 10.1016/j.egypro.2014.11.235
33. Koirala R, Reddy GK, Lee JY, and Smirniotis PG. Influence of Foreign Metal Dopants on the Durability and Performance of Zr/Ca Sorbents during High Temperature CO<sub>2</sub> Capture. *Separation Science and Technology (Philadelphia)* 2014; 49:47–54. DOI: 10.1080/01496395.2013.836672
34. Hu Y, Liu W, Chen H, Zhou Z, Wang W, Sun J, Yang X, Li X, and Xu M. Screening of inert solid supports for CaO-based sorbents for high temperature CO<sub>2</sub> capture. *Fuel* 2016; 181:199–206. DOI: 10.1016/j.fuel.2016.04.138. Available from: <http://dx.doi.org/10.1016/j.fuel.2016.04.138>
35. He X, Ji G, Liu T, and Zhao M. Effects of the Inert Materials on the Stability of Ca-Based CO<sub>2</sub> Sorbents and the Synergy with Cement Manufacture. *Energy and Fuels* 2019; 33:9996–10003. DOI: 10.1021/acs.energyfuels.9b01118
36. Chen J, Duan L, and Sun Z. Review on the Development of Sorbents for Calcium Looping. *Energy & Fuels* 2020. DOI: 10.1021/acs.energyfuels.0c00682
37. Erans M, Manovic V, and Anthony EJ. Calcium looping sorbents for CO<sub>2</sub> capture. *Applied Energy* 2016; 180:722–42. DOI: 10.1016/j.apenergy.2016.07.074

38. Li ZS, Cai NS, Huang YY, and Han HJ. Synthesis, experimental studies, and analysis of a new calcium-based carbon dioxide absorbent. *Energy and Fuels* 2005; 19:1447–52. DOI: 10.1021/ef0496799
39. Fierro V, Adánez J, and García-Labiano F. Effect of pore geometry on the sintering of Ca-based sorbents during calcination at high temperatures. *Fuel* 2004; 83:1733–42. DOI: 10.1016/j.fuel.2004.03.011
40. Lysikov AI, Salanov AN, and Okunev AG. Change of CO<sub>2</sub> carrying capacity of CaO in isothermal recarbonation-decomposition cycles. *Industrial and Engineering Chemistry Research* 2007; 46:4633–8. DOI: 10.1021/ie0702328
41. S. Zhang Lee W. *Refractories Handbook*. 2004 :215–47
42. Herce C, Stendardo S, and Cortés C. Increasing CO<sub>2</sub> carrying capacity of dolomite by means of thermal stabilization by triggered calcination. *Chemical Engineering Journal* 2015; 262:18–28. DOI: 10.1016/j.cej.2014.09.076. Available from: <http://dx.doi.org/10.1016/j.cej.2014.09.076>
43. Coppola A, Scala F, Salatino P, and Montagnaro F. Fluidized bed calcium looping cycles for CO<sub>2</sub> capture under oxy-firing calcination conditions: Part 2. Assessment of dolomite vs. limestone. *Chemical Engineering Journal* 2013; 231:544–9. DOI: 10.1016/j.cej.2013.07.112. Available from: <http://dx.doi.org/10.1016/j.cej.2013.07.112>
44. Hashemi SM, Karami D, and Mahinpey N. Solution combustion synthesis of zirconia-stabilized calcium oxide sorbents for CO<sub>2</sub> capture. *Fuel* 2020; 269:117432. DOI: 10.1016/j.fuel.2020.117432. Available from: <https://doi.org/10.1016/j.fuel.2020.117432>
45. Sultana KS, Tran DT, Walmsley JC, Rønning M, and Chen D. CaO Nanoparticles Coated by ZrO<sub>2</sub> Layers for Enhanced CO<sub>2</sub> Capture Stability. *Industrial and Engineering Chemistry Research* 2015; 54:8929–39. DOI: 10.1021/acs.iecr.5b00423
46. Broda M and Müller CR. Sol-gel-derived, CaO-based, ZrO<sub>2</sub>-stabilized CO<sub>2</sub> sorbents. *Fuel* 2014; 127:94–100. DOI: 10.1016/j.fuel.2013.08.004
47. Soleimanisalim AH, Sedghkerdar MH, Karami D, and Mahinpey N. Pelletizing and Coating of Synthetic Zirconia Stabilized Calcium-Based Sorbents for Application in Calcium Looping CO<sub>2</sub> Capture. *Industrial and Engineering Chemistry Research* 2017; 56:5395–402. DOI: 10.1021/acs.iecr.6b04771
48. Guo H, Wang S, Li C, Zhao Y, Sun Q, and Ma X. Incorporation of Zr into Calcium Oxide for CO<sub>2</sub> Capture by a Simple and Facile Sol-Gel Method. *Industrial and Engineering Chemistry Research* 2016; 55:7873–9. DOI: 10.1021/acs.iecr.5b04112
49. Hong L, Khan A, Pratsinis SE, and Smirniotis PG. Flame-made durable doped-CaO nanosorbents for CO capture. *Energy and Fuels* 2009; 23:1093–100. DOI: 10.1021/ef8007882

50. Yoon HJ and Lee KB. Introduction of chemically bonded zirconium oxide in CaO-based high-temperature CO<sub>2</sub> sorbents for enhanced cyclic sorption. *Chemical Engineering Journal* 2019; 355:850–7. DOI: 10.1016/j.cej.2018.08.148. Available from: <https://doi.org/10.1016/j.cej.2018.08.148>
51. Zhao M, He X, Ji G, Song Y, and Zhao X. Zirconia incorporated calcium looping absorbents with superior sintering resistance for carbon dioxide capture from: In situ or ex situ processes. *Sustainable Energy and Fuels* 2018; 2:2733–41. DOI: 10.1039/c8se00413g
52. Soleimanisalim AH, Sedghkerdar MH, Karami D, Mahinpey N, Antzara AN, Arregi A, Heracleous E, and Lemonidou AA. In-depth evaluation of a ZrO<sub>2</sub> promoted CaO-based CO<sub>2</sub> sorbent in fluidized bed reactor tests. *Chemical Engineering Journal* 2018; 333:5395–402. DOI: 10.1016/j.cej.2017.09.192. Available from: <https://doi.org/10.1016/j.cej.2017.09.192>
53. Hu Y, Liu W, Chen H, Zhou Z, Wang W, Sun J, Yang X, Li X, and Xu M. Screening of inert solid supports for CaO-based sorbents for high temperature CO<sub>2</sub> capture. *Fuel* 2016; 181:199–206. DOI: 10.1016/j.fuel.2016.04.138. Available from: <http://dx.doi.org/10.1016/j.fuel.2016.04.138>
54. Wang S, Fan S, Fan L, Zhao Y, and Ma X. Effect of cerium oxide doping on the performance of CaO-based sorbents during calcium looping cycles. *Environmental Science and Technology* 2015; 49:5021–7. DOI: 10.1021/es5052843
55. Guo H, Feng J, Zhao Y, Wang S, and Ma X. Effect of micro-structure and oxygen vacancy on the stability of (Zr-Ce)-additive CaO-based sorbent in CO<sub>2</sub> adsorption. *Journal of CO<sub>2</sub> Utilization* 2017; 19:165–76. DOI: 10.1016/j.jcou.2017.03.015. Available from: <http://dx.doi.org/10.1016/j.jcou.2017.03.015>
56. Hong L, Khan A, Pratsinis SE, and Smirniotis PG. Flame-made durable doped-CaO nanosorbents for CO capture. *Energy and Fuels* 2009; 23:1093–100. DOI: 10.1021/ef8007882
57. Manovic V and Anthony EJ. Screening of binders for pelletization of CaO-based sorbents for CO<sub>2</sub> capture. *Energy and Fuels* 2009; 23:4797–804. DOI: 10.1021/ef900266d
58. Characteristics G. *Ciment Fondu* (R) 1. 1:2–3
59. Li ZS, Cai NS, Huang YY, and Han HJ. Synthesis, experimental studies, and analysis of a new calcium-based carbon dioxide absorbent. *Energy and Fuels* 2005; 19:1447–52. DOI: 10.1021/ef0496799
60. Wei S, Han R, Su Y, Gao J, Zhao G, Qin Y, Stendardo S, Andersen LK, Herce C, Duan L, Su C, Erans M, Li Y, Anthony EJ, Chen H, Luo C, Zheng Y, Xu Y, Ding H, Zheng C, Qin C, Feng B, Li Z, Ouyang J, Luo G, Yao H, Zhang M, Peng Y, Sun Y, Li P, and Yu J. CO<sub>2</sub> Capture Performance Using Biomass-Templated Cement-Supported Limestone Pellets. *Industrial and Engineering Chemistry Research* 2019; 58:383–94.

DOI: 10.1016/j.fuel.2013.03.078. Available from: <http://dx.doi.org/10.1016/j.fuel.2013.03.078>  
<http://dx.doi.org/10.1016/j.cej.2013.01.045>  
<https://doi.org/10.1016/j.egypro.2019.01.641>

61. Liu W, González B, Dunstan MT, Saquib Sultan D, Pavan A, Ling CD, Grey CP, and Dennis JS. Structural evolution in synthetic, Ca-based sorbents for carbon capture. *Chemical Engineering Science* 2016; 139:15–26. DOI: 10.1016/j.ces.2015.09.016. Available from: <http://dx.doi.org/10.1016/j.ces.2015.09.016>
62. Wu SF and Jiang MZ. Formation of a Ca<sub>12</sub>Al<sub>14</sub>O<sub>33</sub> nanolayer and its effect on the attrition behavior of CO<sub>2</sub>-adsorbent microspheres composed of CaO nanoparticles. *Industrial and Engineering Chemistry Research* 2010; 49:12269–75. DOI: 10.1021/ie901561e
63. Manovic V and Anthony EJ. Long-term behavior of cao-based pellets supported by calcium aluminate cements in a long series of co<sub>2</sub> capture cycles. *Industrial and Engineering Chemistry Research* 2009; 48:8906–12. DOI: 10.1021/ie9011529
64. Duan L, Yu Z, Erans M, Li Y, Manovic V, and Anthony EJ. Attrition Study of Cement-Supported Biomass-Activated Calcium Sorbents for CO<sub>2</sub> Capture. *Industrial and Engineering Chemistry Research* 2016; 55:9476–84. DOI: 10.1021/acs.iecr.6b02393
65. Erans M, Beisheim T, Manovic V, Jeremias M, Patchigolla K, Dieter H, Duan L, and Anthony EJ. Effect of SO<sub>2</sub> and steam on CO<sub>2</sub> capture performance of biomass-templated calcium aluminate pellets. *Faraday Discussions* 2016; 192:97–111. DOI: 10.1039/c6fd00027d
66. Wei S, Han R, Su Y, Gao J, Zhao G, and Qin Y. Size effect of calcium precursor and binder on CO<sub>2</sub> capture of composite CaO-based pellets. *Energy Procedia* 2019; 158:5073–8. DOI: 10.1016/j.egypro.2019.01.641. Available from: <https://doi.org/10.1016/j.egypro.2019.01.641>
67. Li Z, Ouyang J, Luo G, and Yao H. High-Efficiency CaO-Based Sorbent Modified by Aluminate Cement and Organic Fiber through Wet Mixing Method. 2019. DOI: 10.1021/acs.iecr.9b04857
68. Wei S, Han R, Su Y, Gao J, Zhao G, and Qin Y. Pore structure modified CaO-based sorbents with different sized templates for CO<sub>2</sub> capture. 2019. DOI: 10.1021/acs.energyfuels.9b00747
69. Li ZS, Liang PT, and Cai NS. A rate equation theory for the pore size distribution of calcined CaCO<sub>3</sub> in calcium looping. *Faraday Discussions* 2016; 192:197–216. DOI: 10.1039/c6fd00019c
70. Blamey J, Anthony EJ, Wang J, and Fennell PS. The calcium looping cycle for large-scale CO<sub>2</sub> capture. *Progress in Energy and Combustion Science* 2010; 36:260–79. DOI: 10.1016/j.pecs.2009.10.001. Available from: <http://dx.doi.org/10.1016/j.pecs.2009.10.001>

71. Qiao Z, Wang Z, Zhang C, Yuan S, Zhu Y, and Wang J. PVAm-PIP/PS composite membrane with high performance for CO<sub>2</sub>/N<sub>2</sub> separation. *AIChE Journal* 2012; 59:215–28. DOI: 10.1002/aic. arXiv: 0201037v1 [physics]
72. Chen H, Zhao C, and Yang Y. Enhancement of attrition resistance and cyclic CO<sub>2</sub> capture of calcium-based sorbent pellets. *Fuel Processing Technology* 2013; 116:116–22. DOI: 10.1016/j.fuproc.2013.05.012. Available from: <http://dx.doi.org/10.1016/j.fuproc.2013.05.012>
73. Chen C, Yang ST, and Ahn WS. Calcium oxide as high temperature CO<sub>2</sub> sorbent: Effect of textural properties. *Materials Letters* 2012; 75:140–2. DOI: 10.1016/j.matlet.2012.02.015. Available from: <http://dx.doi.org/10.1016/j.matlet.2012.02.015>
74. Li L, King DL, Nie Z, and Howard C. Magnesia-stabilized calcium oxide absorbents with improved durability for high temperature CO<sub>2</sub> capture. *Industrial and Engineering Chemistry Research* 2009; 48:10604–13. DOI: 10.1021/ie901166b
75. Luo C, Zheng Y, Ding N, Wu Q, Bian G, and Zheng C. Development and performance of CaO/La<sub>2</sub>O<sub>3</sub> sorbents during calcium looping cycles for CO<sub>2</sub> capture. *Industrial and Engineering Chemistry Research* 2010; 49:11778–84. DOI: 10.1021/ie1012745
76. NTNU/SINTEF/FTG. Pellets of sorbent suitable for carbon dioxide capture
77. Xu Y, Luo C, Zheng Y, Ding H, and Zhang L. Macropore-Stabilized Limestone Sorbents Prepared by the Simultaneous Hydration-Impregnation Method for High-Temperature CO<sub>2</sub> Capture. *Energy and Fuels* 2016; 30:3219–26. DOI: 10.1021/acs.energyfuels.5b02603
78. Donat F, Florin NH, Anthony EJ, and Fennell PS. Influence of high-temperature steam on the reactivity of CaO sorbent for CO<sub>2</sub> capture. *Environmental Science and Technology* 2012; 46:1262–9. DOI: 10.1021/es202679w
79. Donat F and Müller CR. A critical assessment of the testing conditions of CaO-based CO<sub>2</sub> sorbents. *Chemical Engineering Journal* 2018; 336:544–9. DOI: 10.1016/j.cej.2017.12.050. Available from: <https://doi.org/10.1016/j.cej.2017.12.050>
80. Zhang L, Zhang B, Yang Z, and Guo M. The Role of Water on the Performance of Calcium Oxide-Based Sorbents for Carbon Dioxide Capture: A Review. *Energy Technology* 2015; 3:10–19. DOI: 10.1002/ente.201402099
81. Dunstan MT, Mauger SA, Liu W, Tucker MG, Taiwo OO, Gonzalez B, Allan PK, Gaultois MW, Shearing PR, Keen DA, Phillips AE, Dove MT, Scott SA, Dennis JS, and Grey CP. In situ studies of materials for high temperature CO<sub>2</sub> capture and storage. *Faraday Discussions* 2016; 192:217–40. DOI: 10.1039/c6fd00047a
82. Manovic V and Anthony EJ. Carbonation of CaO-based sorbents enhanced by steam addition. *Industrial and Engineering Chemistry Research* 2010; 49:9105–10. DOI: 10.1021/ie101352s

83. Li ZH, Wang Y, Xu K, Yang JZ, Niu SB, and Yao H. Effect of steam on CaO regeneration, carbonation and hydration reactions for CO<sub>2</sub> capture. *Fuel Processing Technology* 2016; 151:101–6. DOI: 10.1016/j.fuproc.2016.05.019. Available from: <http://dx.doi.org/10.1016/j.fuproc.2016.05.019>
84. Lu H, Reddy EP, and Smirniotis PG. Calcium oxide based sorbents for capture of carbon dioxide at high temperatures. *Industrial and Engineering Chemistry Research* 2006; 45:3944–9. DOI: 10.1021/ie051325x
85. Dou B, Song Y, Liu Y, and Feng C. High temperature CO<sub>2</sub> capture using calcium oxide sorbent in a fixed-bed reactor. *Journal of Hazardous Materials* 2010; 183:759–65. DOI: 10.1016/j.jhazmat.2010.07.091. Available from: <http://dx.doi.org/10.1016/j.jhazmat.2010.07.091>
86. Shaojun Y and Yunhan X. Steam catalysis in CaO carbonation under low steam partial pressure. *Industrial and Engineering Chemistry Research* 2008; 47:4043–8. DOI: 10.1021/ie8000265
87. Symonds RT, Lu DY, Hughes RW, Anthony EJ, and Macchi A. CO<sub>2</sub> capture from simulated syngas via cyclic Carbonation/Calcination for a naturally occurring limestone: Pilot-plant testing. *Industrial and Engineering Chemistry Research* 2009; 48:8431–40. DOI: 10.1021/ie900645x
88. He Z, Li Y, Ma X, Zhang W, Chi C, and Wang Z. Influence of steam in carbonation stage on CO<sub>2</sub> capture by Ca-based industrial waste during calcium looping cycles. *International Journal of Hydrogen Energy* 2016; 41:4296–304. DOI: 10.1016/j.ijhydene.2016.01.029. Available from: <http://dx.doi.org/10.1016/j.ijhydene.2016.01.029>
89. Che M, Ve JC, and Welzel EJ. Modeling and Simulation of Heterogeneous Catalytic Handbook of Heterogeneous Catalysis Neutrons and Synchrotron Radiation. 2012
90. Thermogravimetric T and Family I. Thermogravimetric Analysis ( TGA ) A Beginner ' s Guide. 1960
91. Bottom R. Thermogravimetric Analysis. Principles and Applications of Thermal Analysis 2008; 1:87–118. DOI: 10.1002/9780470697702.ch3
92. Schoff CK. Thermogravimetric analysis. 2009. DOI: 10.3139/9781569906446.010
93. MBCL Status Report. Tech. rep. FTG/NTNU/SINTEF
94. De Jong KP. Synthesis of Solid Catalysts. *Synthesis of Solid Catalysts* 2009 :1–401. DOI: 10.1002/9783527626854
95. Niemantsverdriet JCI. Concepts of Modern Catalysis and Kinetics. 2013 :129–213
96. Sing KS, Everett DH, Haul RA, Moscou L, Pierotti RA, Rouquerol J, and Siemieniowska T. Reporting Physisorption Data for Gas/Solid Systems with Special Reference to the Determination of Surface Area and Porosity. *Pure and Applied Chemistry* 1985; 57:603–19. DOI: 10.1351/pac198557040603

97. Busca G. Heterogeneous Catalytic Materials: Solid State Chemistry, Surface Chemistry and Catalytic Behaviour. 2014 :1–463. DOI: 10.1016/C2012-0-00113-5
98. Brandon D and Kaplan WD. Microstructural Characterization of Materials: 2nd Edition. 2008 :1–536. DOI: 10.1002/9780470727133
99. Mawanga M. Dolomite-based Sorbents for High Temperature Carbon dioxide capture . 2017
100. Lan P and Wu S. Mechanism for self-reactivation of nano-CaO-based CO<sub>2</sub> sorbent in calcium looping. Fuel 2015; 143:9–15. DOI: 10.1016/j.fuel.2014.11.004. Available from: <http://dx.doi.org/10.1016/j.fuel.2014.11.004>
101. Erans M, Manovic V, and Anthony EJ. Calcium looping sorbents for CO<sub>2</sub> capture. Applied Energy 2016; 180:722–42. DOI: 10.1016/j.apenergy.2016.07.074
102. Grasa G, Martínez I, Diego ME, and Abanades JC. Determination of CaO carbonation kinetics under recarbonation conditions. Energy and Fuels 2014; 28:4033–42. DOI: 10.1021/ef500331t
103. Koirala R, Gunugunuri KR, Pratsinis SE, and Smirniotis PG. Effect of zirconia doping on the structure and stability of CaO-based sorbents for CO<sub>2</sub> capture during extended operating cycles. 2011. DOI: 10.1021/jp207625c
104. De La Calle Martos A, Valverde JM, Sanchez-Jimenez PE, Perejón A, García-Garrido C, and Perez-Maqueda LA. Effect of dolomite decomposition under CO<sub>2</sub> on its multi-cycle CO<sub>2</sub> capture behaviour under calcium looping conditions. 2016. DOI: 10.1039/c6cp01149g
105. Coppola A, Scala F, Salatino P, and Montagnaro F. Fluidized bed calcium looping cycles for CO<sub>2</sub> capture under oxy-firing calcination conditions: Part 2. Assessment of dolomite vs. limestone. Chemical Engineering Journal 2013; 231:544–9. DOI: 10.1016/j.cej.2013.07.112. Available from: <http://dx.doi.org/10.1016/j.cej.2013.07.112>
106. Valverde JM, Sanchez-Jimenez PE, and Perez-Maqueda LA. Ca-looping for postcombustion CO<sub>2</sub> capture: A comparative analysis on the performances of dolomite and limestone. Applied Energy 2015; 138:202–15. DOI: 10.1016/j.apenergy.2014.10.087. Available from: <http://dx.doi.org/10.1016/j.apenergy.2014.10.087>
107. Sing KS and Williams RT. Physisorption hysteresis loops and the characterization of nanoporous materials. Adsorption Science and Technology 2004; 22:773–82. DOI: 10.1260/0263617053499032
108. Chen H, Zhao C, Yang Y, and Zhang P. CO<sub>2</sub> capture and attrition performance of CaO pellets with aluminate cement under pressurized carbonation. Applied Energy 2012; 91:334–40. DOI: 10.1016/j.apenergy.2011.09.032. Available from: <http://dx.doi.org/10.1016/j.apenergy.2011.09.032>

109. Alvarez D and Abanades JC. Pore-size and shape effects on the recarbonation performance of calcium oxide submitted to repeated calcination/recarbonation cycles. *Energy and Fuels* 2005; 19:270–8. DOI: 10.1021/ef049864m
110. Naeem MA, Armutlulu A, Imtiaz Q, Donat F, Schäublin R, Kierzkowska A, and Müller CR. Optimization of the structural characteristics of CaO and its effective stabilization yield high-capacity CO<sub>2</sub> sorbents. *Nature Communications* 2018; 9:1–11. DOI: 10.1038/s41467-018-04794-5. Available from: <http://dx.doi.org/10.1038/s41467-018-04794-5>
111. Ridha FN, Wu Y, Manovic V, Macchi A, and Anthony EJ. Enhanced CO<sub>2</sub> capture by biomass-templated Ca(OH)<sub>2</sub>-based pellets. *Chemical Engineering Journal* 2015; 274:69–75. DOI: 10.1016/j.cej.2015.03.041. Available from: <http://dx.doi.org/10.1016/j.cej.2015.03.041>
112. Tong X, Liu W, Yang Y, Sun J, Hu Y, Chen H, and Li Q. A semi-industrial preparation procedure of CaO-based pellets with high CO<sub>2</sub> uptake performance. *Fuel Processing Technology* 2019; 193:149–58. DOI: 10.1016/j.fuproc.2019.05.018. Available from: <https://doi.org/10.1016/j.fuproc.2019.05.018>
113. Wang P, Sun J, Guo Y, Zhao C, Li W, Wang G, Lei S, and Lu P. Structurally improved, urea-templated, K<sub>2</sub>CO<sub>3</sub>-based sorbent pellets for CO<sub>2</sub> capture. *Chemical Engineering Journal* 2019; 374:20–8. DOI: 10.1016/j.cej.2019.05.091. Available from: <https://doi.org/10.1016/j.cej.2019.05.091>
114. Science ML. Zirconyl nitrate solution. 2020. Available from: <https://www.sigmaaldrich.com/catalog/product/aldrich/391824?lang=en&region=NO>



# Appendices

## A Composition calculation

The desired weight-percentages of metals in the sorbents, together with a given weight of dolomite, was used in order to calculate the amount of precursor needed. This section gives an overview of the calculations.

The mass of Alumina and Zirconium,  $m_j$  was expressed according to the following equation

$$m_j = \frac{\omega_j}{100\%} \cdot m_{total} \quad (\text{A.1})$$

with  $\omega_j$  being the given weight percentage of the metal. The total mass of the sorbent,  $m_{total}$  was as follow

$$m_{total} = m_{\text{ZrO}_2} + m_{\text{calcined dolomite}} + m_{\text{cement}}. \quad (\text{A.2})$$

Here  $m_{\text{calcined dolomite}}$  is the given weight of calcined dolomite. To find the masses of  $\text{ZrO}_2$ ,  $m_{\text{ZrO}_2}$ , and cement,  $m_{\text{cement}}$ , the relationship between mole and mass was used

$$m_i = \alpha \frac{m_j}{M_j} \cdot M_i \quad (\text{A.3})$$

with  $i$  representing the masses of the oxides, and  $j$  the masses of the metals. Using the same equation the mass of Zirconyl nitrate was expressed, with  $i$  representing Zirconyl nitrate and  $j$  representing Zr.

The zirconyl nitrate solution used was diluted to 35 wt % , hence the amount of solution,  $m_{\text{Zr-Solution}}$ , to be added was

$$m_{\text{Zr-Solution}} = \frac{m_{\text{Zr-nitrate}}}{0.35} \quad (\text{A.4})$$

where  $m_{\text{Zr-nitrate}}$  corresponds to the amount of pure zirconyl nitrate.

With a given weight of dolomite of 11, 5g and desired weight percentages of Zr and Al were 1.3 % and 13.4 % accordingly, the calculations were done as follows;

$$m_{\text{Zr}} = \frac{\omega_{\text{Zr}}}{100\%} \cdot m_{total} = \frac{1.3\%}{100\%} \cdot m_{total} \quad (\text{A.5})$$

$$m_{\text{Al}} = \frac{\omega_{\text{Al}}}{100\%} \cdot m_{total} = \frac{13.4\%}{100\%} \cdot m_{total} \quad (\text{A.6})$$

$$m_{total} = m_{\text{ZrO}_2} + m_{\text{calcined dolomite}} + m_{\text{cement}} = m_{\text{ZrO}_2} + 11.5\text{g} + m_{\text{cement}}. \quad (\text{A.7})$$

$$m_{\text{ZrO}_2} = \frac{m_{\text{Zr}}}{M_{\text{Zr}}} \cdot M_{\text{ZrO}_2} = \frac{m_{\text{Zr}}}{91.22\text{g/mol}} \cdot 123.2\text{g/mol} \quad (\text{A.8})$$

$$m_{\text{Zr-nitrate}} = \frac{m_{\text{Zr}}}{M_{\text{Zr}}} \cdot M_{\text{Zr-nitrate}} = \frac{m_{\text{Zr}}}{91.22\text{g/mol}} \cdot 231.2\text{g/mol} \quad (\text{A.9})$$

$$m_{\text{cement}} = \frac{1}{2} \cdot \frac{m_{\text{Al}}}{M_{\text{Al}}} \cdot M_{\text{cement}} = \frac{1}{2} \cdot \frac{m_{\text{Al}}}{26.98\text{g/mol}} \cdot 158\text{g/mol} \quad (\text{A.10})$$

$$m_{\text{Zr-Solution}} = \frac{m_{\text{Zr-nitrate}}}{0.35} \quad (\text{A.11})$$

Solving the 7 equations, gave the 7 unknowns with the values given in table A.1.

Table A.1: Unknown values needed in order to find the right amount of precursor for a sorbent consisting of 11.5g dolomite with 13.4 wt % of Al and 1.3wt % Zr.

| Compound         | Weight [g] |
|------------------|------------|
| Zr               | 0.25       |
| ZrO <sub>2</sub> | 0.34       |
| Zr Nitrate       | 0.64       |
| Zr Solution      | 1.8        |
| Al               | 2.6        |
| Cement           | 7.6        |
| Sorbent (total)  | 19.5       |

## B Incipient Wetness method

In order to find the pore volume of calcined dolomite,  $PV_{\text{calcined dolomite}}$ , water was added to a weighted amount of the solid until it became completely wet. The volume of water added,  $V_{\text{water}}$ , was divided by the weight of solid,  $m_{\text{calcined dolomite}}$ ;

$$PV_{\text{calcined dolomite}} = \frac{V_{\text{water}}}{m_{\text{calcined dolomite}}}. \quad (\text{B.1})$$

In this project, the desired amount of Zirconium nitrate solution calculated in appendix ?? was diluted in water in order to obtain a volume close to the pore volume. From the determined amount of dolomite to use in preparation of the sorbent, the total amount of solution,  $V_{\text{solution}}$ , needed to be added was calculated

$$V_{\text{solution}} = m_{\text{calcined dolomite}} \cdot PV_{\text{calcined dolomite}}, \quad (\text{B.2})$$

As the amount Zr-solution needed was found as a mass, the volume added had to be found

$$V_{\text{Zr solution}} = \frac{m_{\text{Zr solution}}}{\rho_{\text{Zr solution}}} \quad (\text{B.3})$$

with  $\rho_{\text{Zr solution}}$  being the density of the Zr solution. Further the amount of water,  $V_{\text{water}}$  to add was found;

$$V_{\text{water}} = V_{\text{solution}} - V_{\text{Zr-solution}}. \quad (\text{B.4})$$

In the end the mass of water added was

$$m_{\text{water}} = V_{\text{water}} \cdot \rho_{\text{water}}. \quad (\text{B.5})$$

with  $\rho_{\text{water}}$  being the density of water.

From one gram of calcined dolomite, 0.7 ml of water was needed, giving

$$PV_{\text{calcined dolomite}} = \frac{0.7\text{ml}}{1\text{g}} = 0.7\text{ml/g}$$

With 11.55 g of dolomite the amount of total solution needed was:

$$V_{\text{solution}} = 11.5\text{g} \cdot 0.7\text{ml/g} = 8.05\text{ml}$$

The density of the zirconyl solution is 1.45 g/ml giving [114]. In the case 1.85 g of Zr solution needed, the corresponding volume was

$$V_{\text{Zr solution}} = \frac{1.85\text{g}}{1.45\text{g/ml}} = 1.3\text{ml}$$

Hence the volume of water needed was

$$V_{\text{water}} = 8.05\text{ml} - 1.3\text{ml} = 6.75\text{ml}$$

From the density of water, being 1.0 ml/g the amount of water,  $m_{\text{H}_2\text{O}}$ , needed was

$$m_{\text{water}} = \frac{6.75\text{ml}}{1\text{ml/g}} = 6.75\text{g}.$$

## C XRF calculation

In this section, the calculation of the theoretical values of oxides in 1Sa(5.5Zr,10Al) and 2Sa(5.5Zr,10Al) presented in section 5.2.1 will be explained. The values were calculated dividing the number of different oxides assumed to be present in the sorbents by the total weight of the sorbent. The assumed number of oxides present in the sorbents were calculated from the weight-percentages of oxides present in dolomite and cement found through XRF. The values for cement were an average of 4 samples, while the values of dolomite an average of 5 samples.

The total weight,  $m_{total}$  of the sorbents was assumed to be

$$m_{total} = m_{ZrO_2} + m_{calcined\ dolomite} + m_{cement}. \quad (C.1)$$

Here  $m_{ZrO_2}$ ,  $m_{calcined\ dolomite}$  and  $m_{cement}$  are the weights of  $ZrO_2$ , calcined dolomite and cement added when preparing the sorbents. The weight of  $ZrO_2$  was calculated from the diluted Zirconyl solution using the relationship between mole and mass, in a similar way as explained in section A.

The weight of an oxide (XO) present dolomite,  $m_{XO,dol.}$ , was calculated from the weight-percentage of the oxide,  $\omega_{XO,dol.}$  in dolomite by multiplying it with weight of dolomite in the sorbent.

$$m_{XO,dol.} = m_{calcined\ dolomite} \cdot \omega_{XO,dol.} \quad (C.2)$$

In a similar way the weight of an oxide present in cement,  $m_{XO,cem.}$  was calculated from the weight-percentage of the oxide present in cement,  $\omega_{XO,cem.}$

$$m_{XO,cem.} = m_{cement} \cdot \omega_{XO,cem.} \quad (C.3)$$

By adding the two numbers, the weight of CaO present in the sorbent,  $m_{XO,sorbent.}$  could be found.

$$m_{XO,sorbent.} = m_{XO,dol.} + m_{XO,cem.} \quad (C.4)$$

This was the used to find the weight-percentage of the oxide in the sorbent:

$$\omega_{XO,sorbent.} = \frac{m_{XO,sorbent.}}{m_{total}} \cdot 100\% \quad (C.5)$$

Following, the calculation of CaO present in the sorbent will be used as an example. The weight percentage of CaO in cement was found to be 36.7 % and the weight-percentage in dolomite 60.6 %. For 1Sa(5.5Zr,10Al) and 2Sa(5.5Zr,10Al) the weight of dolomite used was 11.5 g, the weight of cement 5.5 g and the weight of ZrO<sub>2</sub> 1.4 g. The calculations then became

$$m_{\text{total}} = 1.4 \text{ g} + 11.5 \text{ g} + 5.5 \text{ g}. \quad (\text{C.6})$$

$$m_{\text{CaO,dol.}} = 11.5 \text{ g} \cdot 60.6\% \quad (\text{C.7})$$

$$m_{\text{CaO,cem.}} = 5.5 \text{ g} \cdot 36.7\% \quad (\text{C.8})$$

$$m_{\text{CaO,sorbent.}} = m_{\text{CaO,dol.}} + m_{\text{CaO,cem.}} \quad (\text{C.9})$$

$$\omega_{\text{CaO,sorbent.}} = \frac{m_{\text{CaO,sorbent.}}}{11.5\text{g}} \cdot 100\% = 48.9\% \quad (\text{C.10})$$

In similar ways, the weight-percentages of MgO, Al<sub>2</sub>O<sub>3</sub>, SiO<sub>2</sub>, and Fe<sub>2</sub>O<sub>3</sub> present in the sorbents were calculated. Al<sub>2</sub>O<sub>3</sub> and Fe<sub>2</sub>O<sub>3</sub> were only from the cement.

## D XRD

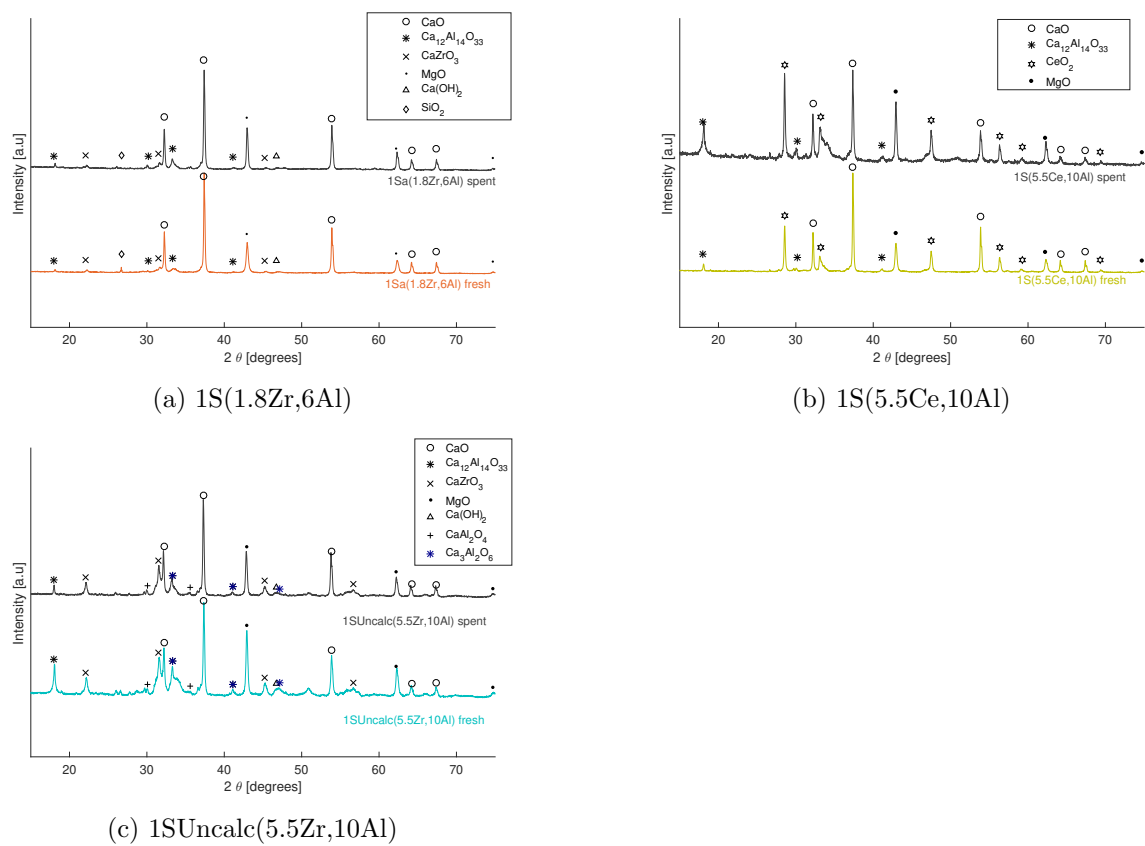
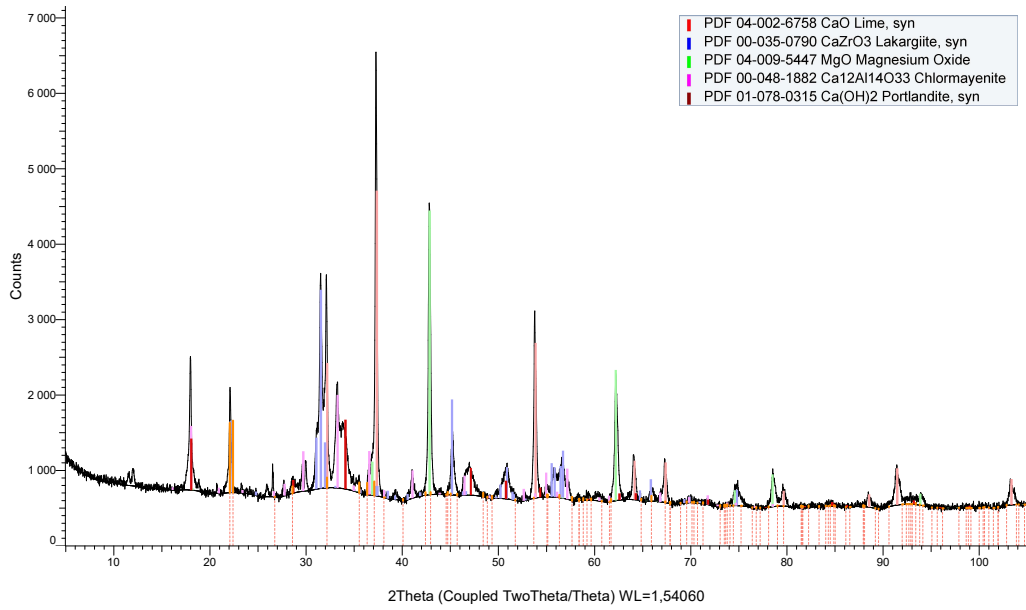


Figure D.1: Crystal phases of a selection of fresh vs. spent sorbent. In  $2\theta$  range from  $15^\circ$  to  $75^\circ$ .

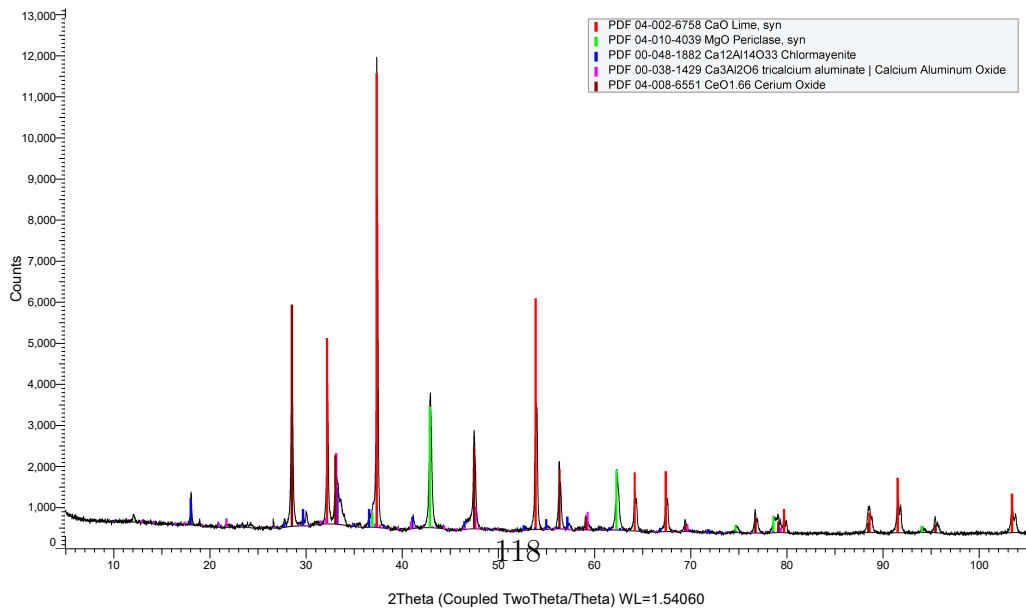
Under one XRD raw diagram for one ZrAl-based sorbent and one CeAl-based sorbent given.

### Dolomite Sorbent K (Coupled TwoTheta/Theta)



(a) 1Sa(5.5Zr,10Al)

### Tcalc (Coupled TwoTheta/Theta)



The tables gives crystal sizes found for CaO, MgO, and CaZrO<sub>3</sub> or (CeO<sub>2</sub>).

Table D.1: Crystal sizes (CS) of CaO, MgO and the stabilizing phase (CaZrO<sub>3</sub> or (CeO<sub>2</sub>).

| Sample               | CS CaO [nm] | CS MgO [nm] | CS oxide[nm] |
|----------------------|-------------|-------------|--------------|
| Calcined Dolomite    | 40.4        | 26.5        | -            |
| 1S(1.3Zr,13Al)       | 41.4        | 27.5        | 26.6         |
| 2Sb(1.3Zr,13Al)      | 47.7        | 33.6        | 39.7 / 48.1  |
| 1S(2.6Zr,13Al)       | 38.4        | 28.4        | 28.4         |
| 1S(3.8Zr,13Al)       | 50.2        | 32.8        | 36.0         |
| 1Sb(5.0Zr,13Al)      | 50.5        | 37.0        | 36.1         |
| 2S(5.0Zr, 13Al)      | 46.5        | 29.4        | 36.1         |
| 1Sa(5.5Zr, 10Al)     | 47.7 ±0.9   | 35.8±0.9    | 40.8 ±1.1    |
| 2Sa(5.5Zr, 10Al)     | 49.0        | 35.6        | 28.6         |
| 1Sb(5.5Zr, 10Al)     | 43.8        | 38.0        | 24.3         |
| 2Sb(5.5Zr, 10Al)     | 46.5        | 37.1        | 32.2         |
| 1S(1.5Zr,10Al)       | 41.4        | 41.5        | 39.9         |
| 1S(6Zr, 9Al)         | 44.9        | 31.2        | 36.5         |
| 2S(6Zr, 9Al)         | 42.3        | 33.4        | 32.7         |
| 1S(1.8Zr,6.Al)       | 49.6        | 29.4        | 32.3         |
| 1S(5.5Ce,10Al)       | 54.0        | 33.8        | 49.5         |
| 2S(5.5Ce,10Al)       | 53.4        | 33.4        | 47.9         |
| 11Al                 | 45.7        | 26.5        | -            |
| 15Al                 | 49.6        | 32.8        | -            |
| 1SUncalc(5.5Zr,10Al) | 39.7        | 25.6        | 30.8         |
| 2SInter(5.5Zr,10Al)  | 50.1        | 34.4        | 31.6         |



Table D.2: The crystal sizes of CaO and MgO for fresh and spent sorbents compared to calcined dolomite. Experiments spent (TGA / microbalance reactor\*) : (Ads: 5 % CO<sub>2</sub>, 8 % H<sub>2</sub>O, 600 °C, 6 / 30min. Des: 80 / 100 % CO<sub>2</sub>, 950 °C)

| Sample               | CaO [nm] |       | MgO [nm] |       | total cycles |
|----------------------|----------|-------|----------|-------|--------------|
|                      | fresh    | spent | fresh    | spent |              |
| Calcined dolomite    | 40.4     | 47.6  | 26.5     | 31.4  | 15           |
| 1S(3.8Zr,13Al)       | 50.2     | 47.1  | 32.8     | 38.9  | 30           |
| 1Sa(5.5Zr,10Al)      | 46.5     | 50.0  | 34.7     | 44.7  | 40*          |
| 2Sa(5.5Zr,10Al)      | 49.0     | 46.9  | 35.6     | 41.2  | 40*          |
| 2S(5.5Zr,10Al)Uncalc | 39.7     | 47.6  | 25.7     | 41.3  | 4            |
| 1S(1.8Zr,6Al)        | 49.6     | 46.8  | 29.4     | 35.6  | 15           |
| 1S(5.5Ce,10Al)       | 54.0     | 48.8  | 33.8     | 41.1  | 15           |

## E Nitrogen Adsorption-Desorption

The figure below shows a selection of obtained Hysteresis-loops.

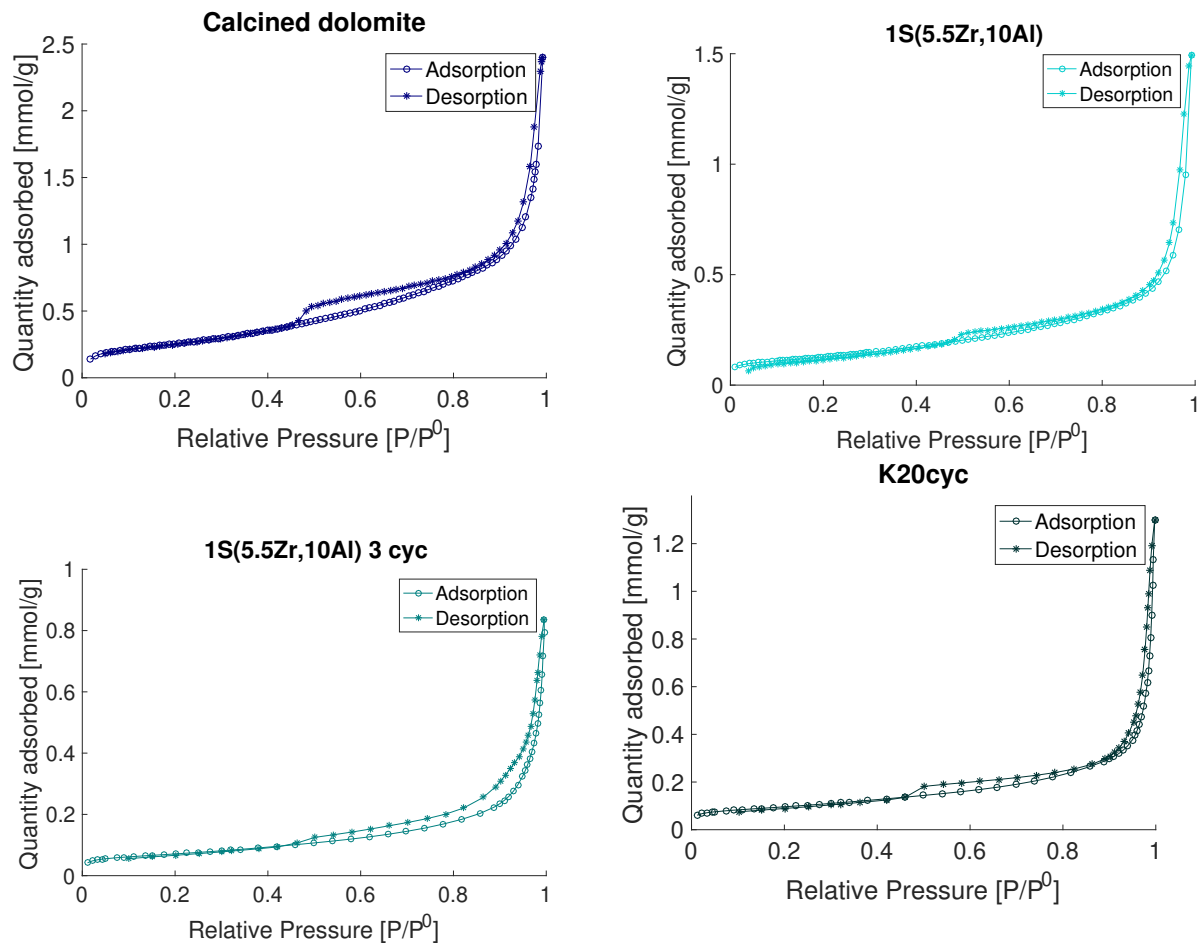


Figure E.1: Some obtained hysteresis loops.



---

|                    |  |                    |             |
|--------------------|--|--------------------|-------------|
| <b>ID</b>          | 34732  | <b>Status</b>      | <b>Date</b> |
| <b>Risk Area</b>   | Risikovurdering: Helse, miljø og sikkerhet (HMS) | Created            | 09.01.2020  |
| <b>Created by</b>  | Anne Charlotte Gusfre Wold                       | Assessment started | 09.01.2020  |
| <b>Responsible</b> | Anne Charlotte Gusfre Wold                       | Measures decided   |             |
|                    |  | Closed             |             |

**Risk Assessment:****Cat\_Master\_student\_2020\_Anne Charlotte Wold**

---

**Valid from-to date:**

1/9/2020 - 1/9/2023

**Location:**

(K5 (lab 448, 425, 447))

**Goal / purpose**

- Risk assessment for my master project project ;
- CaO-based sorbent will be prepared in the laboratory (lab 447).
  - CaO-based sorbent (based on dolomite) will be tested in
    - microbalance reactor (lab 448)
    - TGA TA (lab 441)
    - TGA Linseis (lab 420)
  - Characterisation by N2 adsorption analysis (lab 425)
  - Characterisation by XRD (lab 113)
  - Characterisation by XRF (lab 425)
  - Characterisation by SEM/TEM (nanolab)

**Background**

Preparation and Testing of sorbents for MBCL project  
Prepare CaO-based sorbent in laboratory (lab 447)

- Chemicals and gasses: Dolomite based sorbents (CaO and MgO) earlier prepared are going to be tested. Dolomite preparation (dolomite, cement, zirconyl nitrate solution and/or Cerium(III) nitrate hexahydrate )
- Preparation of sorbent: one-pot synthesis (see attached the procedure)
- Conditions: Dolomites are in different size range (0-500 mic, 500-850 mic and over 850 mic).

Test CaO-based sorbent(based on dolomite) will be tested in microbalance reactor(lab 448) and by TGA TA and TGA Linseis  
-Chemical and Gases: CO2 and N2 (sorption test), Ar (inert) and H2O. Catalyst based on dolomite prepared are going to be tested.  
-Conditions: T=500-950 oC, Patm, Total flow (max) 400mL/min.  
-Instrument for analysis: MicroGC, TGA TA, TGA Linseis

**Description and limitations**



- 
- High Temperature Furnaces): The set-up will be used when calcination of the sorbent is necessary. (Chemistry hall D).
  - One-pot Granulation: granulation method is going to use to produce sorbent pellet in a Ankarsum Original Black Diamond AKM 6230BD kitchen machine (evaporator also is needed)

Chemicals that will be used: Dolomite, Cement, ZrN2O7, Cerium(III) nitrate hexahydrate

- Microbalance reactor (used for testing) (lab 448): Will be used to test the sorbents (mainly dolomite-based). The set-up consists of a microbalance, a stainless steel reactor, a high temperature oven and the corresponding tubes and connections. Proper isolation of the system will be done in order to avoid material damages and water condensation in the tubes.

- A Micro GC is going to use in order to analyse the products.

- XRF technique will be used to find the sample-composition, boric acid will be used

Safety measures related to spread of covid19 infection:

- Avoid touching the face
- Disinfection before and after with ethanol/solvent on all surfaces I'm in contact with (door knob – card reader with code panel – screen – desk - coffee machine)
- Keep 1m distance from colleagues
- Use nitrile gloves when touching shared lab set-ups and equipment
- Wash hands as often as possible
- Update the Teams Catalysis "labs-overview" excel sheet about your weekly planning.

1.Switch off procedure for Microbalance reactor (lab 448):

- Turn off the heating oven by cooling down from the right computer and pressing the button situated in the power box manually.
- Turn off the gas flow from the right computer.
- Turn off the MS from the left computer and switch off manually following the procedure in the MS manual.
- Turn off the heating elements connected to power supply by pressing the emergency button.
- Stop the cooling water manually by turning off the tap on the left of microbalance.

#### Prerequisites, assumptions and simplifications

Assume training before the experiment starts.

#### Attachments

apparatus card.doc  
MSDS\_-\_Dolomite\_Limestone.pdf  
Synthesis procedure.docx  
Boric Acid.pdf  
Cement\_sikkerhetsDataBlad.pdf  
Nitrogen Datablad .pdf  
Zirconyl Nitrate Satey data sheet .pdf  
Cerium(III) nitrate hexahydrate.pdf

#### References

[Ingen registreringer]



## Summary, result and final evaluation

The summary presents an overview of hazards and incidents, in addition to risk result for each consequence area.

**Hazard:** Microbalance reactor gasses(CO2, N2 and Ar)

**Incident:** Gas leakage

|                          |            |                       |  |                        |  |
|--------------------------|------------|-----------------------|--|------------------------|--|
| <b>Consequence area:</b> | Helse      | Risk before measures: |  | Risiko after measures: |  |
|                          | Ytre miljø | Risk before measures: |  | Risiko after measures: |  |

**Hazard:** Heat in the Microbalance oven

**Incident:** Burns

|                          |       |                       |  |                        |  |
|--------------------------|-------|-----------------------|--|------------------------|--|
| <b>Consequence area:</b> | Helse | Risk before measures: |  | Risiko after measures: |  |
|--------------------------|-------|-----------------------|--|------------------------|--|

**Hazard:** Chemicals

**Incident:** Dolomite-Sorbent

|                          |       |                       |  |                        |  |
|--------------------------|-------|-----------------------|--|------------------------|--|
| <b>Consequence area:</b> | Helse | Risk before measures: |  | Risiko after measures: |  |
|--------------------------|-------|-----------------------|--|------------------------|--|

**Hazard:** Handling N2 adsorption set-up

**Incident:** Handling N2 liquid in BET set-up

|                          |                    |                       |  |                        |  |
|--------------------------|--------------------|-----------------------|--|------------------------|--|
| <b>Consequence area:</b> | Helse              | Risk before measures: |  | Risiko after measures: |  |
|                          | Materielle verdier | Risk before measures: |  | Risiko after measures: |  |













**Hazard:** Synthesis of sorbent

**Incident:** Use of Dolomite

|                          |       |                       |  |                        |  |
|--------------------------|-------|-----------------------|--|------------------------|--|
| <b>Consequence area:</b> | Helse | Risk before measures: |  | Risiko after measures: |  |
|--------------------------|-------|-----------------------|--|------------------------|--|



---

|                          |  |                       |  |   |
|--------------------------|--|-----------------------|--|---|
| <b>Hazard:</b>           | <b>Synthesis of sorbent</b>            |                       |  |   |
| <b>Incident:</b>         | <b>Cement</b>                          |                       |  |   |
| <b>Consequence area:</b> | Helse                                  | Risk before measures: |  Risiko after measures:   |    |
| <b>Incident:</b>         | <b>Use of Zirconyl Nitrate</b>         |                       |  |   |
| <b>Consequence area:</b> | Helse                                  | Risk before measures: |  Risiko after measures:   |    |
|                          | Ytre miljø                             | Risk before measures: |  Risiko after measures:   |    |
| <b>Incident:</b>         | <b>Cerium(III) nitrate hexahydrate</b> |                       |  |   |
| <b>Consequence area:</b> | Helse                                  | Risk before measures: |  Risiko after measures:   |    |
|                          | Ytre miljø                             | Risk before measures: |  Risiko after measures:   |    |
| <b>Hazard:</b>           | <b>Binder for XRF</b>                  |                       |  |   |
| <b>Incident:</b>         | <b>Use of Boric acid</b>               |                       |  |   |
| <b>Consequence area:</b> | Helse                                  | Risk before measures: |  Risiko after measures: |  |

**Final evaluation**

There is a low degree of risk in the microbalance reactor. The gasses and chemical products are not of big danger to the humans or to the environment.



## Organizational units and people involved

A risk assessment may apply to one or more organizational units, and involve several people. These are listed below.

### Organizational units which this risk assessment applies to

- NTNU

### Participants

Ainara Moral Larrasoana

De Chen

### Readers

Anne Hoff

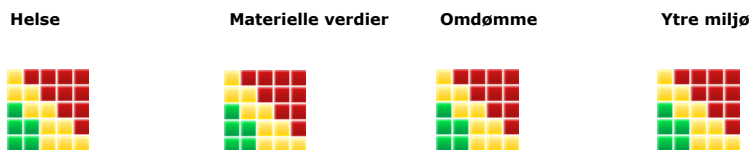
Estelle Marie M. Vanhaecke

Karin Wigger Dragsten

### Others involved/stakeholders

[Ingen registreringer]

## The following accept criteria have been decided for the risk area Risikovurdering: Helse, miljø og sikkerhet (HMS):





## Overview of existing relevant measures which have been taken into account

The table below presents existing measures which have been taken into account when assessing the likelihood and consequence of relevant incidents.

| Hazard   | Incident                                     | Measures taken into account                             |
|--|--|---|
| Microbalance reactor gasses(CO <sub>2</sub> , N <sub>2</sub> and Ar) | Gas leakage                                  | Safety equipment for Microbalance reactor               |
| Heat in the Microbalance oven  | Burns  | Safety equipment for Microbalance reactor               |
| Chemicals  | Dolomite-Sorbent                             | Fumehood  |
| Handling N <sub>2</sub> adsorption set-up                            | Handling N <sub>2</sub> liquid in BET set-up | Safety equipment for N <sub>2</sub> adsorption analysis |
| Synthesis of sorbent   | Use of Dolomite                              | Safety equipment for sorbent production                 |
|  | Use of Dolomite                              | Safety equipment for sorbent production                 |
|  | Cement                                       | Safety equipment for sorbent production                 |
|  | Cement                                       | Safety equipment for sorbent production                 |
|  | Use of Zirconyl Nitrate                      | Safety equipment for sorbent production                 |
|  | Use of Zirconyl Nitrate                      | Safety equipment for sorbent production                 |
| Binder for XRF   | Cerium(III) nitrate hexahydrate              |   |
|  | Use of Boric acid                            | Safety for XRF  |

### Existing relevant measures with descriptions:

#### Safety equipment for Microbalance reactor

- Safety Goggles
- Lab coat
- Gloves
- Isolating gloves

#### Fumehood

[Ingen registreringer]

#### Safety equipment for N<sub>2</sub> adsorption analysis

- Safety Goggles
- Lab coat
- Gloves
- Isolating gloves

#### Safety equipment for sorbent production

- Safety Goggles
- Lab coat
- Gloves
- Mask

#### Safety equipment for the HTF and calcination units

- Safety Goggles
- Lab coat
- Gloves
- Isolating gloves

#### Safety for XRF

- Gloves
- Glasses







---

## Risk analysis with evaluation of likelihood and consequence

This part of the report presents detailed documentation of hazards, incidents and causes which have been evaluated. A summary of hazards and associated incidents is listed at the beginning.

**The following hazards and incidents has been evaluated in this risk assessment:**

- **Microbalance reactor gasses(CO<sub>2</sub>, N<sub>2</sub> and Ar)**
  - Gas leakage
- **Heat in the Microbalance oven**
  - Burns
- **Chemicals**
  - Dolomite-Sorbent
- **Handling N<sub>2</sub> adsorption set-up**
  - Handling N<sub>2</sub> liquid in BET set-up
- **Synthesis of sorbent**
  - Use of Dolomite
  - Cement
  - Use of Zirconyl Nitrate
  - Cerium(III) nitrate hexahydrate
- **Binder for XRF**
  - Use of Boric acid

**Detailed view of hazards and incidents:****Hazard: Microbalance reactor gasses(CO2, N2 and Ar)**

CO2 and N2 are used as reactive gasses in the microbalance reactor for CO2 capture. Ar is used as inert gas.

**Incident: Gas leakage**

A gas leakage can occur during the gas exchange

*Cause:* Gas leakage

*Likelihood of the incident (common to all consequence areas):* **Less likely (2)**

*Kommentar:*

A gas leakage can be detected by doing a leakage-test before the experiment or it will be detected by the gas-detectors .

**Consequence area: Helse**

*Assessed consequence:* **Medium (2)**

*Comment:* No dangerous or flammable gasses.  
Gas under pressure might explode under heating

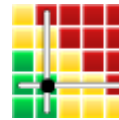
**Risk:**

**Consequence area: Ytre miljø**

*Assessed consequence:* **Medium (2)**

*Comment:* No dangerous or flammable gasses.  
Gas under pressure might explode under heating

**Risk:**





---

**Hazard: Heat in the Microbalance oven**

It is possible to be burned by the high temperatures in the oven (microbalance) due to the high temperatures used (600-900C) . There are also heated pipes with heating tape at 150-200C.

**Incident: Burns**

-----  
The microbalance reactor will reach temperatures to above 900 degrees celcius. Contact with the oven can give burns. This needs to be handled with luke-warm water.

*Cause:* Touch the furnace when it is hot

*Likelihood of the incident (common to all consequence areas):*      **Less likely (2)**

*Kommentar:*

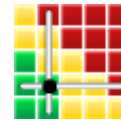
The sample should be removed when the oven is cold  
The heated pipes should not be touched and there is isolated material around the microbalance reactor  
Use of safety equipment

**Consequence area: Helse**

*Assessed consequence:* **Medium (2)**

*Comment:* Burns are not very dangerous if the work is done with care and all safety equipment

**Risk:**





---

**Hazard: Chemicals**

The sorbent will be dolomite (CaO and MgO)-based.

**Incident: Dolomite-Sorbent**

---

Although dolomite is classified as a relatively non-toxic. This product is irritating to the eyes, Respiratory Sensitizer, and skin

Likelihood of the incident (common to all consequence areas): **Less likely (2)**

*Kommentar:*

Follow good procedure and use safety equipment.  
Dolomite is not considered toxic in small amount

**Consequence area: Helse**

Assessed consequence: **Medium (2)**

*Comment:* Can cause skin, respiratory, and eye irritation.

**Risk:**





---

**Hazard: Handling N2 adsorption set-up**

The tank is filled with liquid N2 when the measurement of N2 adsorption are going to be carried out

**Incident: Handling N2 liquid in BET set-up**

---

The tank is filled with liquid N2 in each experiment, so you can be burned

*Cause:* N2 liquid handling

*Likelihood of the incident (common to all consequence areas):* **Unlikely (1)**

*Kommentar:*

Follow an good procedure and use safety equipment

**Consequence area: Helse**

*Assessed consequence:* **Large (3)**

*Comment:*

Consists of small cooled gas;  
Inneholder nedkjølt gas; might cause severe frostbite.

**Risk:**



**Consequence area: Materielle verdier**

*Assessed consequence:* **Medium (2)**

*Comment:* [Ingen registreringer]

**Risk:**





---

**Hazard: Synthesis of sorbent**

---

**Incident: Use of Dolomite**

---

Likelihood of the incident (common to all consequence areas): **Less likely (2)**

*Kommentar:*

Follow good procedure and use safety equipment.

**Consequence area: Helse**

Assessed consequence: **Medium (2)**

*Comment:*

This product is irritating to the eyes, respiratory sensitizer, and skin

**Risk:**

**Incident: Cement**

---

Likelihood of the incident (common to all consequence areas): **Unlikely (1)**

*Kommentar:*

Good procedure and use of safety equipment

Will rise with water in case of eye contact

Will rinse with water and soap in case of skin contact

In case of breathing in dust, I will get fresh air and call a doctor if necessary

**Consequence area: Helse**

Assessed consequence: **Large (3)**

*Comment:*

Causes serious eye damage.  
Causes skin irritation.  
May cause respiratory irritation

**Risk:**



**Incident: Use of Zirconyl Nitrate**

---

Likelihood of the incident (common to all consequence areas): **Less likely (2)**

*Kommentar:*

Will keep/store it away from clothing/ combustible materials.  
Will wear protective gloves/ protective clothing/ eye protection/ face  
If I get in the eyes, I will rinse cautiously with water for several minutes.

**Consequence area: Helse**

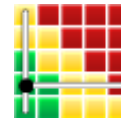
Assessed consequence: **Medium (2)**

*Comment:* Causes severe skin burns and eye damage.

**Risk:****Consequence area: Ytre miljø**

Assessed consequence: **Small (1)**

*Comment:* H272 May intensify fire; oxidizer.

**Risk:****Incident: Cerium(III) nitrate hexahydrate**

---

Likelihood of the incident (common to all consequence areas): **Less likely (2)**

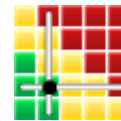
*Kommentar:*

Will keep/store it away from clothing/ combustible materials.  
Will wear protective gloves/ protective clothing/ eye protection/ face  
If I get in the eyes, I will rinse cautiously with water for several minutes.  
Only use a small amount

**Consequence area: Helse**

Assessed consequence: **Medium (2)**

*Comment:* H272, May intensify fire; oxidizer  
H318, Causes serious eye damage  
H410 Very toxic to aquatic life with long lasting effects.

**Risk:**



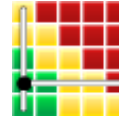


**Consequence area: Ytre miljø**

Assessed consequence: **Small (1)**

Comment: H272, May intensify fire; oxidizer

**Risk:**





---

**Hazard: Binder for XRF**

Boric acid will be used as a binder and is dangerous as it can give fertility problems

**Incident: Use of Boric acid**

---

Can give fertility problems

*Likelihood of the incident (common to all consequence areas):* **Less likely (2)**

*Kommentar:*

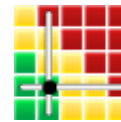
Use safety equipment and follow procedure. Rinse with water in case it gets into the eyes

**Consequence area: Helse**

*Assessed consequence:* **Medium (2)**

*Comment:* Might be dangerous in touch with sling or when swallowing. Can be give irritation to the eyes, skin and to the airways

**Risk:**



## F Matlab codes for calculating capacity

Under are matlab-codes for calculation of the capacity in each cycle in TGA TA and TGA Linseis given. Both takes everything from one excel sheet, the capacity is calculated as explained in the experimental procedure (section 4.2)

### F.1 Capacities TGA TA

```
1
2  %% CALCULATION OF CAPACITIES IN TGA TA
3  %%This codes show how the capturing capacities were calculated for
4  % experiments in TGA TA. % The files and weights used here are for
5  % 1Sa(5.5Zr,10Al). The same code could be used for all sorbents ...
6  % all followed the same procedure.
7
8  close all
9  clear all
10 clc
11 [~,sheets] = xlsfinfo('K.10cyc.stab.600-900.xlsx');
12
13
14 originalweight=13.2; %The weight of the loaded sample in mg
15
16 data= xlsread('K.10cyc.stab.600-900.xlsx', sheets{2}); %Takes in ...
17     the excel file
18
19                                     %with the data obtained from TGA TA
20
21 weight=data(2:end,3); % takes in the weight-changes
22 time= data(2:end,1); %time in minutes
23
24 %%% After all the the carbonations and calcinations, the code was
25 %%% split with a row with time = -3. In this way it was possible
26 % to split the sheet and find the beging to the end of the
27 % carbonation in each cycle.
28
29 index = [find(time == -3); size(data, 1) + 1]
30 n      = numel(index) - 1 ; % numel gives the number of of elements in ...
31     an array
32 DATASPLIT = cell(1, n);
33 for k = 1:2:n
34     DATASPLIT{k} = data(index(k)+2:index(k+1), :) ;
35
36 end
```

```

37
38
39
40 data1=DATASPLIT{1,1};
41
42
43 % Under the weight-increases in each cycle are separated.
44 time30=find(round((data1(:,1)-data1(1,1)))/30);
45 weight1=data1(1:time30(1),3);
46
47
48 data2=DATASPLIT{1,3};
49 weight2=data2(:,3);
50 data3=DATASPLIT{1,5};
51 weight3=data3(:,3);
52 data4=DATASPLIT{1,7};
53 weight4=data4(:,3);
54 data5=DATASPLIT{1,9};
55 weight5=data5(:,3);
56 data6=DATASPLIT{1,11};
57 weight6=data6(:,3);
58 data7=DATASPLIT{1,13};
59 weight7=data7(:,3);
60 data8=DATASPLIT{1,15};
61 weight8=data8(:,3);
62 data9=DATASPLIT{1,17};
63 weight9=data9(:,3);
64 data10=DATASPLIT{1,19};
65 weight10=data10(:,3);
66
67
68
69
70
71 %% The capacities in each cycle is calculated under
72
73 capacity= zeros(length(weight1),1) ;
74
75 for j = 1:length(weight1);
76     wincrease=weight1(j)-weight1(1);
77     capacity(j)=(wincrease./originalweight)*100;
78     % CapKeep=(find(capacity>0.07)); % Finds the rows where the ...
79     % capacity is bigger than 0.5
80     %newtimeL=time1(CapKeep)-time1(CapKeep(1));
81     %CapacitynewL=capacity(CapKeep);
82     % plot(newtimeL,CapacitynewL,'Color', color, 'LineStyle','-')
83 end
84 % the additional code over is in case capcity vs. time should be plotted
85
86

```

```

87     max(capacity)
88
89
90     for j = 1:length(weight2);
91         wincrease=weight2(j)-weight2(1);
92         capacity(j)=(wincrease./originalweight)*100;
93
94     end
95
96     max(capacity)
97
98
99         capacity= zeros(length(weight3),1) ;
100
101     for j = 1:length(weight3);
102         wincrease=weight3(j)-weight3(1);
103         capacity(j)=(wincrease./originalweight)*100;
104
105     end
106
107     max(capacity)
108
109         capacity= zeros(length(weight4),1) ;
110
111     for j = 1:length(weight4);
112         wincrease=weight4(j)-weight4(1);
113         capacity(j)=(wincrease./originalweight)*100;
114
115     end
116     max(capacity)
117
118         capacity= zeros(length(weight5),1) ;
119
120     for j = 1:length(weight5);
121         wincrease=weight5(j)-weight5(1);
122         capacity(j)=(wincrease./originalweight)*100;
123
124     end
125
126     max(capacity)
127
128
129         capacity= zeros(length(weight6),1) ;
130
131
132
133     for j = 1:length(weight6);
134         wincrease=weight6(j)-weight6(1);
135         capacity(j)=(wincrease./originalweight)*100;
136
137     end

```

```

138
139     max(capacity)
140
141
142         capacity= zeros(length(weight7),1) ;
143
144
145     for j = 1:length(weight7);
146         wincrease=weight7(j)-weight7(1);
147         capacity(j)=(wincrease./originalweight)*100;
148
149 end
150
151     max(capacity)
152
153
154
155         capacity= zeros(length(weight8),1) ;
156
157
158     for j = 1:length(weight8);
159         wincrease=weight8(j)-weight8(1);
160         capacity(j)=(wincrease./originalweight)*100;
161
162 end
163
164     max(capacity)
165
166
167
168         capacity= zeros(length(weight9),1) ;
169
170
171     for j = 1:length(weight9);
172         wincrease=weight9(j)-weight9(1);
173         capacity(j)=(wincrease./originalweight)*100;
174
175 end
176
177     max(capacity)
178
179
180         capacity= zeros(length(weight10),1) ;
181
182
183     for j = 1:length(weight10);
184         wincrease=weight10(j)-weight10(1);
185         capacity(j)=(wincrease./originalweight)*100;
186
187 end
188

```



## F.2 Capacities TGA Linseis

```
1
2
3 %% CALCULATION OF CAPACITIES IN LINSEIS
4 %%This codes show how the capturing capacities were calculated for
5 % experiments in TGA Linseis. % The files and weights used here are for
6 % 1Sa(5.5Zr,10Al). The same code could be used for all sorbents ...
7 % teseted, as
8 % all followed the same procedure.
9 %
10 close all
11 clear all
12 clc
13 [~,sheets] = xlsfinfo('KL3.stability.linseis') %Takes in the excel file
14 %with the data obtained from TGA Linseis
15
16 originalweight=11.2; % The weight of the loaded sample in mg. from ...
17 % cycle 31
18 % 9.4 mg
19
20 data= xlsread('KL3.stability.linseis', sheets{2});
21 %sheet 2 was for cycle 1-15, 4 for cycle 16-30, 6 for 31-45 and 8 for
22 %46-60
23
24
25
26 %% Rowstart refers to the row in the excel-sheet where the carbonation
27 % starts, and Rowend to the row in the excel-sheet when the carbonation
28 % ends. For a total of 15 cycles
29
30 Rowstart=[5404, 11121, 16837, 22554, 28270,33987, 39704, 45420,...
31 51137, 56853, 62570, 68287, 74003, 79719, 85436];
32
33 Rowend= [6305, 12005, 17701, 23398, 29095, 34793, 40490, 46187,...
34 51882, 57581, 63278, 68975, 74718, 80369, 86067];
35
36
37 for i = 1:length(Rowstart);
38
39
40 weight= data(Rowstart((i)) :Rowend(i),4);
41
42 % Column 4 is where the weight-changes in the sorbent are in the
43 % excel-sheet.
44
45
46 capacity= zeros(length(weight),1) ;
```



```
47
48     for j = 1:length(weight);
49         wincrease=weight(j)-weight(1);
50         capacity(j)=(wincrease./originalweight)*100;
51
52     end
53     % calculates all the capacities in the cycle
54
55
56     CAPACITY(i)= max(capacity); % finds the highest capacity in the cycle
57     end
58
59
60 capacities= CAPACITY
```